

REVERSIBLE ELECTRICAL BREAKDOWN IN
AMORPHOUS CHALCOGENIDES

by

A. Y. IRFAN

of

The Physics Division

Thames Polytechnic



A thesis submitted to the Council for National Academic Awards
for the Degree of Doctor of Philosophy.

December, 1974.

CONTENTS

	Page No.
Acknowledgements	(i)
Abstract	(ii)
Chapter One - Introduction	1
1.1. History	1
1.2 Reversible switching effects in solids	3
1.3 Choice of areas for investigation	11
1.4 Thesis plan	11
Chapter Two - Glasses and Switching Models	12
2.1 Disorder and classification in solids	12
2.2 Glass - its formation and structure	17
2.3 Electronic band structure	24
2.4 Electronic switching models	27
2.5 Thermal switching models	37
2.6 Phase-change models	52
Chapter Three - Experimental Techniques	58
3.1 Preparation of Amorphous Solids from the vapour phase	58
3.2 Preparation of Amorphous Solids from the liquid phase	61
3.3 Preparation of Amorphous Solids from the solid phase	62
3.4 Preparation of STAG glass alloy	63
3.5 Flash evaporation	68
3.6 Device fabrication	76
3.7 Pulse circuits and recording of I-V characteristics	96
Chapter Four - Experimental Results and Preliminary Discussion	112
4.1 Current-voltage characteristics	112
4.2 Effect of film-thickness	128
4.3 Effects of electrode materials	147
4.4 Measurement of a.c. conductance of switching devices	156
4.5 Uniaxial pressure effects	163
4.6 Effect of ambient temperature	171
4.7 Effect of electrode contact area	174
4.8 Effect of device external circuit parameters	185
4.9 Effect of pulse width and repetition rate	188
4.10 Effect of pulse polarity	189
4.11 Characteristics of devices fabricated from $\text{Si}_{12}\text{Ge}_{10}\text{As}_{30}\text{Te}_{40}\text{Tl}_8$ glass	196
4.12 Analysis of chemical composition of the thin films	196

	Page No.
Chapter Five - Discussion	
5.1 Structural changes in switching devices	199
5.2 On-state current filament	209
5.3 The multiply-branched on-state	221
Chapter Six - Summary and Conclusions	230
Appendix - Future Work	233
References	235

ACKNOWLEDGEMENTS

I am extremely and sincerely grateful to Dr. J. L. Williams, my internal supervisor, for the help and advice throughout the past three years and to Dr. J. C. Male, my industrial supervisor, for the numerous visits and many useful discussions.

I wish to thank Mr. T. Brewer for the valuable and very competent technical assistance and for his help with the drawings. My thanks are also extended to Mr. J. Malley for machining the flash evaporator and Mr. L. Guy for constructing the high voltage amplifiers.

I am indebted to Mrs. A. Hudson for typing this thesis and the various research reports.

Thanks are also due to Dr. D. L. Thomas of CERL for useful discussions, Dr. A. J. Hughes of RRE for supplying r.f. sputtered films, and Dr. E. H. Baker of Imperial College, London, for supplying the glass at early stages of this study.

Finally, I am grateful to Thames Polytechnic for the financial support which enabled me to carry out this study and I also wish to thank Mr. K. V. Hyde, Head of the School of Materials Science and Physics, and all his academic and technical staff for the pleasant and co-operative working atmosphere.

ABSTRACT

An investigation has been made of reversible electrical breakdown in amorphous chalcogenides with particular attention being paid to the on-state properties of $\text{Si}_{12}\text{Te}_{48}\text{As}_{30}\text{Ge}_{10}$ glass threshold switches.

Apparatus is described for the preparation of well-characterised materials and flash-evaporated thin-film switching devices. Measurements have been made of the current-voltage characteristics, including the effect of variation of thermal boundary conditions on the stability and form of the on-state behaviour.

All tested devices have been found to undergo a forming process which is attributed to structural changes in the device material. These structural changes have been substantiated by measurements on virgin and formed devices of (i) off-state resistance as a function of number of switching operations, (ii) off-state resistance as a function of electrode contact area, (iii) device conductance versus frequency and (v) the effect of uniaxial pressure on device off-state current. The results satisfy a model for a formed device in which there is a highly conducting and inhomogeneous filamentary region surrounded by a low-conducting glass.

It is shown that when the thermal conductivity of the device electrode material is two or three orders of magnitude greater than that of the switching glass, the magnitude of the minimum holding voltage is proportional to the square root of the thermal conductivity of the electrode material. This observation is consistent with a thermal constriction model where the minimum holding voltage is the sum of the voltage drops across the filament constrictions at electrode/glass interfaces.

The holding current is shown to be a linear function of ambient temperature and extrapolates to zero at a temperature similar to that for a threshold voltage - temperature plot.

Photographic recordings of the current-voltage characteristics of the switching devices have shown that the on-state of a formed device consists of several distinct branches depending on the switching history of the device and the electrode materials. The multiply-branched on-state is interpreted in terms of sequential forming of current channels between tellurium-crystallite clusters and the electrodes. Several mechanisms

are discussed to explain the origin of these current channels and the localized thermal breakdown mechanism is considered to be the most favourable one.

CHAPTER ONE

Introduction

1.1. History

It was pointed out by Henisch (1969) that the investigation of electrons' behaviour in solids has probably absorbed more technological man-hours than any other physical phenomenon. However, most research efforts in the past, and to a large extent at present, have been directed towards understanding and exploiting the properties of crystalline materials. In the 1930's solid-state device research was centred around the crystal diode detector and eventually culminated in the development of the transistor.

The properties of amorphous or glassy solids have only in recent years attracted the interest of solid-state scientists because (i) from a device point of view they were thought to have few, if any, commercial application except for use as insulators and (ii) theoretically, the problem posed by these amorphous materials are formidable.

A milestone in the development and progress of the theoretical aspects of the subject was Ziman's quantitative explanation of the electrical properties of liquid metals, put forward in 1960. This was a weak interaction theory and the effect of each atom was considered small. The success of Ziman's theory instigated investigation of what happens when the interaction is large as it must be when an energy gap exists. Two key points to present day understanding are the principle of Ioffe and Regel (1960) that the mean free path cannot be shorter than the distance between atoms, and Anderson's concept of localization which was introduced in his paper 'Absence of diffusion in certain random lattices' which was published in 1958. During the following years a great deal of work on electronic processes in amorphous solids was carried out by Mott (1967).

In the late 1950's and early 1960's several research workers (Ovshinsky, 1970) reported the development of novel kinds of glasses which had electrical conductivities dependent on electronic mechanisms rather than ionic processes known to be associated with conventional glasses. In addition, the conductivity of a conventional insulating glass is usually less than $10^{-8} \Omega^{-1} m^{-1}$ whereas the conductivity of these new glasses is in the range from 10^{-13} to $10^{-3} \Omega^{-1} m^{-1}$. More

important, interesting switching phenomena were observed in these glasses (Pearson et al, 1962, 1963, Ovshinsky, 1960). It was demonstrated that a rapid and sometimes reversible transition between a highly resistive and a conductive state could be achieved in these glasses by application of a sufficiently high electric field, i.e. they behaved like electrical switches.

It seems that the earliest reference to "vitreous semiconductors" was made by the Soviet scientists Gorynova and Kolomiets (1955) who, while studying various ternary semiconducting compounds, discovered that the alloy $Tl_2-Se-As_2-Se_3$ instead of having a crystalline structure, had many of the properties of a typical glass. This discovery initiated a vast programme of investigation by Soviet scientists, led by Ioffe and Kolomiets (Ioffe et al, 1960, Kolomiets, 1960), into various other similar glasses and their properties. The electrical properties of these materials were mainly investigated.

The results of the soviet team did show that the broad features of the electrical band theory of solids are preserved on transition from the crystalline state to the amorphous state, thus confirming a theory of Ioffe's that the electrical band structure of solids is determined by short range order, which should be the same in a solid whether in the crystalline or amorphous states.

The first person to exploit glassy semiconductors would appear to be S. R. Ovshinsky (1953) who produced a switching device. This device was made from an amorphous thin film of tantalum oxide deposited on a tantalum substrate which formed one electrode, while a liquid electrolyte formed a second electrode. This early switch showed repetitive switching and required a "maintaining voltage" to keep it in the high conductance state. Later, when a suitable metallized electrode was used a switch, which operated "once" only, was made. This type of switch remained in the highly conductive state regardless of whether the applied field was removed or not. This switch was first demonstrated in December, 1959, and in 1961 a patent was granted to Ovshinsky for the two types of devices.

Pearson et al (1962), of Bell Telephone Laboratories, reported that when point contacts were made to a glass such as As-Te-I switching effects were observed, but little work was done in following up this initial investigation.

In 1962 Ovshinsky applied for a second patent for a number of devices incorporating semiconducting glasses and was granted this patent in 1966. There seems to be some doubt as to when the application for the patent was made. In a sub-article published by Sideris (1966) in *Electronics* and entitled "Switch, switch, who made one first?" it was stated that the patent was applied for in 1961, a year before the report by Pearson's team. But whatever the legal situation, Ovshinsky was the only person to produce and market these devices, and until recently his group's research dominated this new field of investigation. The Soviet team mentioned above, also observed switching action (Kolomiets, 1963) in certain glasses.

Further observations on switching behaviours were made by Eaton (1964). Chopra (1965) published a report of switching action in glassy semiconducting oxides, such as those of Ta and Ti.

The "novel" glasses mentioned above are alloys of the chalcogen elements, namely, sulphur, selenium and tellurium; when produced in a glassy form they are known as chalcogenides. The electrical properties of these glasses will be discussed in other chapters, but apart from their electrical properties these glasses differ from oxide and halide glasses in a number of important respects (a) they are formed over a range of compositions and are not confined to one or two chemical compositions (Rawson, 1967), (b) the structural theories developed to explain the structures of oxide glasses are not always applicable to the chalcogenide glasses (Rawson, 1967).

From the above historical review it is clear that the recent interest in the electrical properties of non-crystalline semiconductors has been stimulated by (a) a desire for a sound theoretical understanding of electronic behaviour in such disordered materials and (b) the possible commercial applications of the fast switching phenomena which have been demonstrated in a wide range of amorphous elements and alloys.

1.2. Reversible switching effects in solids

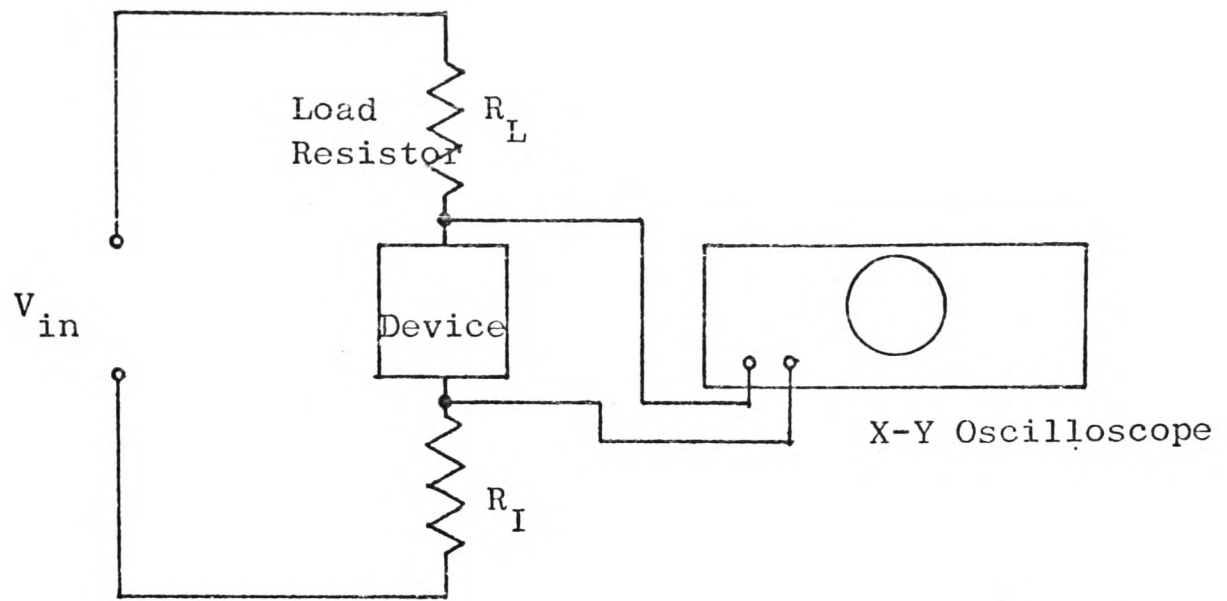
Electrical switching in solids is defined here as a transition from a high resistance state to a low resistance state under the influence of an applied electric field. The transition is reversible and non-destructive and this distinguishes switching from ordinary dielectric breakdown in solids which is destructive and irreversible. Electrical breakdown

current is generally very noisy whereas the current-voltage characteristics of a switching device are normally clean. However, it was pointed out by Bosnell (1973) that on an oscilloscope, dielectric breakdown or even air breakdown under pulse conditions can look similar to switching if the noise in the highly conductive state is suppressed. There is the possibility that breakdown in some materials has been mistaken for switching and reported accordingly.

Many materials exhibit switching effects and their characteristics can be classified broadly according to whether the performance of the device is current controlled, figure 1.2(a) or voltage controlled, figure 1.2(b), (Pamplin, 1970). In the first case the current-voltage characteristic is multivalued in voltage (S-shaped), in the second case of the voltage controlled device the current voltage characteristic is multivalued in current (N-shaped). Although both the S and N shaped characteristic conform to the above definition of switching, only the first behaviour is usually designated (and even then only in some cases) as the switching behaviour, the second type of behaviour is described as "voltage controlled negative resistance". Figure 1.1 shows a typical circuit used for displaying the I-V characteristic on an oscilloscope.

Fritzche subdivides S-shaped current-voltage characteristics into those where their working point can be stabilised in the negative differential resistance region, $\frac{dV}{dI} < 0$, and those where the device exhibits the memory action. Four groups can be distinguished as shown in figure 1.3(1) - (IV):

- (i) The negative resistance device has a I-V characteristic which is retraceable except for some hysteresis observed when the current is changed too rapidly for maintaining thermal equilibrium. With a proper device of a load resistor, R_L , this negative resistance can be stabilised at any point on the I-V curve.
- (ii) The switching device has no stable operating point between the high resistance state and conductance states. The device switches when the voltage exceeds a threshold value, V_{th} . The characteristics of this device are dealt with in some detail in a separate subsection below.
- (iii) The negative resistance devices with memory has two stable states; the first is similar to that of (i) and the second state is conductive and established at higher current and remains conductive without



Circuit used for displaying the I-V characteristics of a switching device.

Figure 1.1

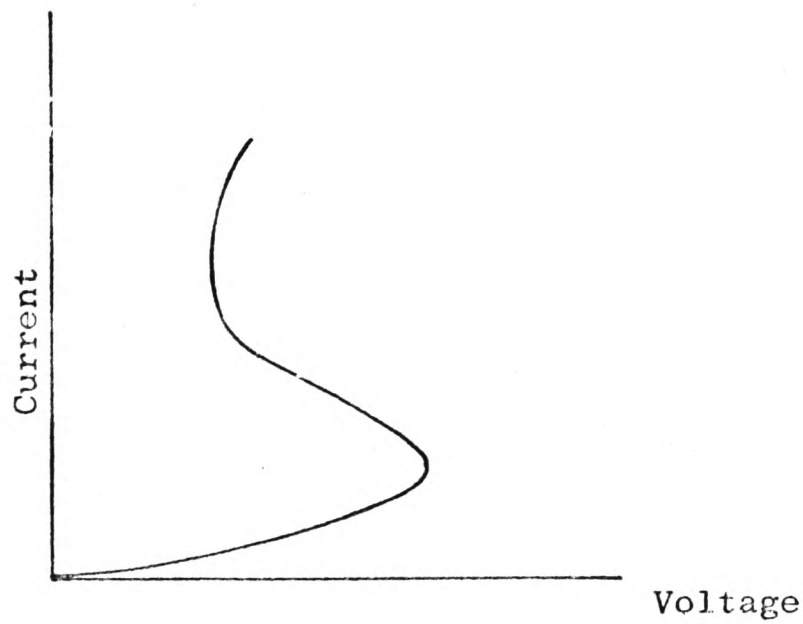


Figure 1.2(a)

S-shaped I-V characteristics

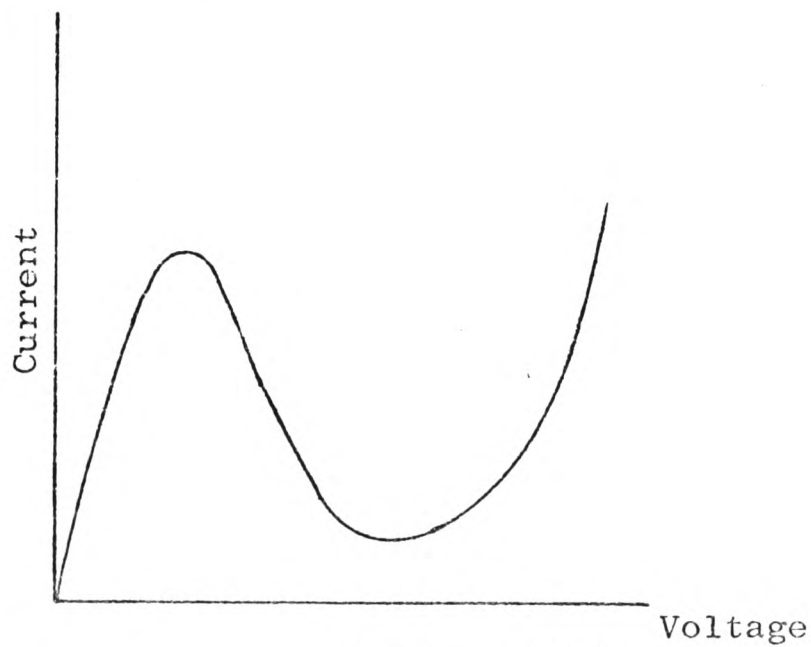
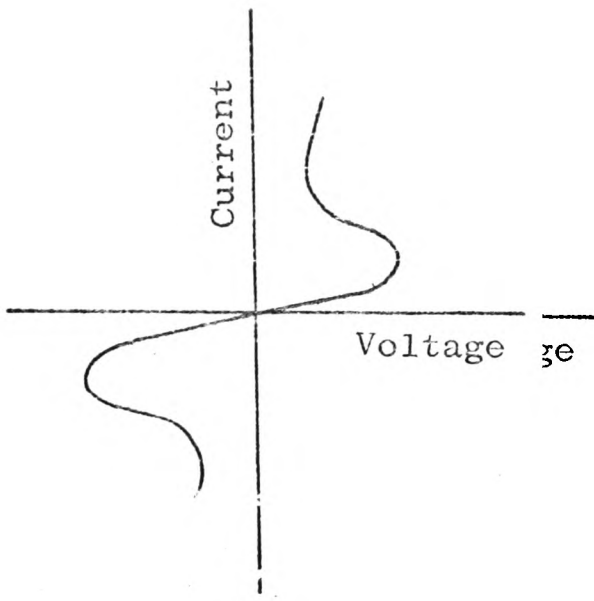


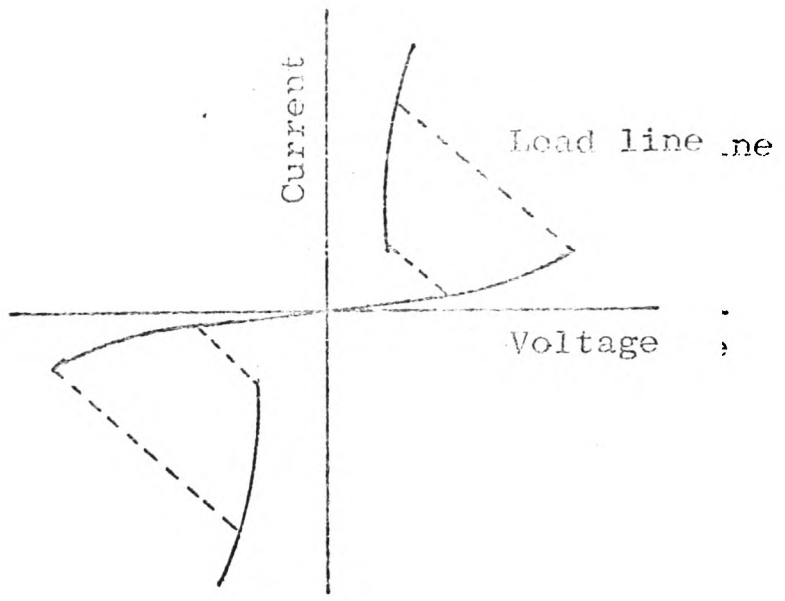
Figure 1.2(b)

N-shaped I-V characteristics



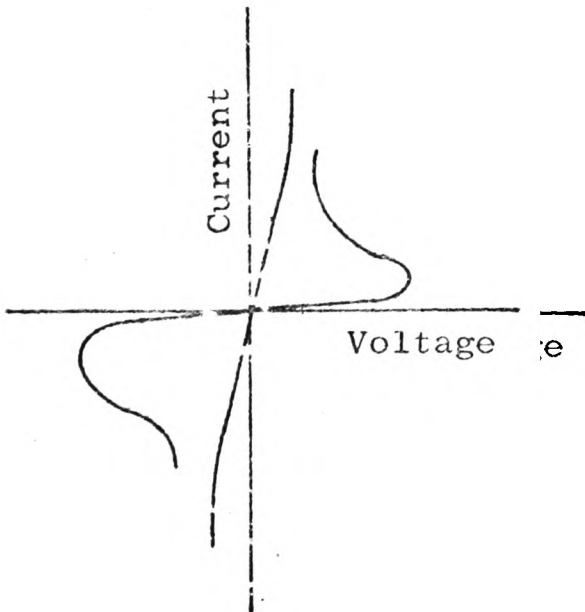
(i)

Negative resistance device



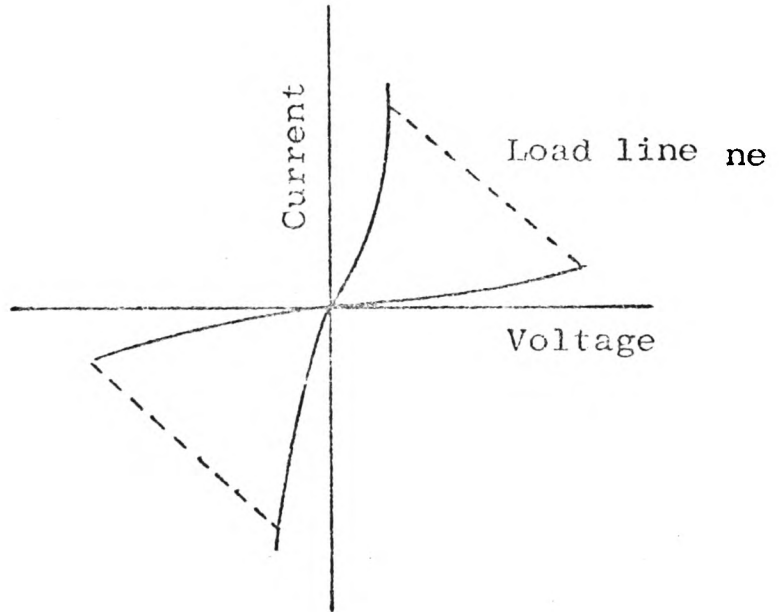
(ii)

Switching device



(iii)

Negative resistance device with memory



(iv)

Switching device with memory.

Figure 1.3

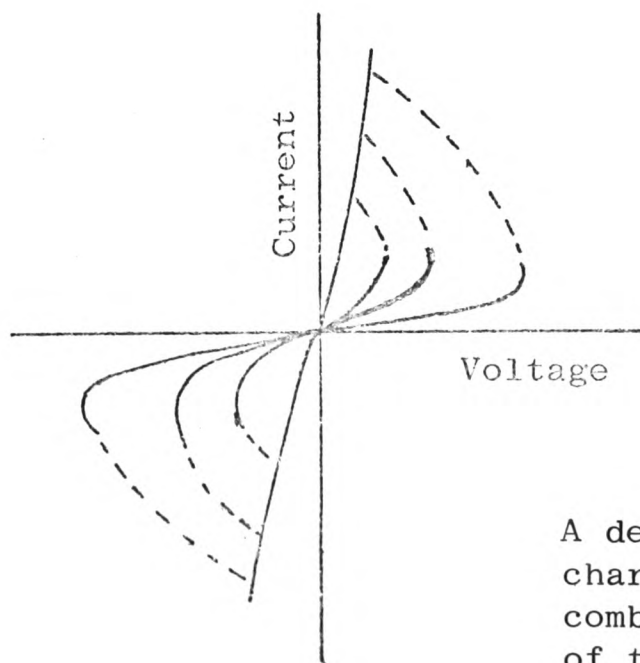


Figure 1.4

A device with electrical characteristics representing a combination of the characteristics of those of (i) and (iii) - (iv).
Drake et al (1969)

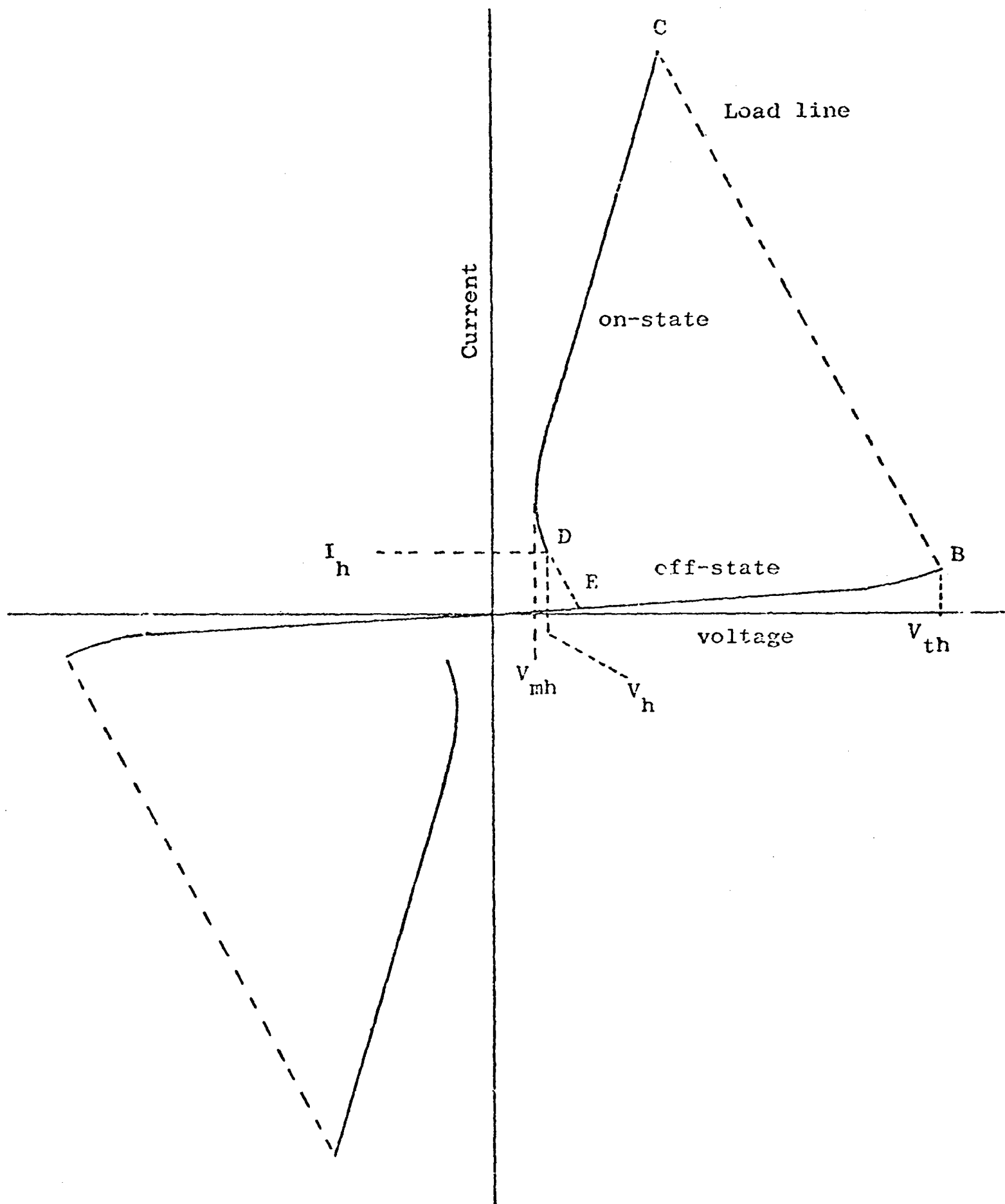


Figure 1.5.

Switching characteristics of a threshold device fabricated from chalcogenide glass.

decay. The first state can be re-established by increasing the current above a certain value and switching it off rapidly.

- (iv) The switching device with memory also has two stable states; the high-resistance state and the mode of switching are similar to those of (ii). The second state is conducting. The high resistance state can be re-established by applying a short high-current pulse.

Drake et al (1969) have added a further class of switching device, figure 1.4, with electrical characteristics representing a combination of the characteristics of those of (i) and (iii) - (iv). Effects of this kind have been found in glasses based on the $WO_3:P_2O_5$ system. The characteristics in (i) - (iv) are found in various transition metal glasses containing vanadium ions and in chalcogenide glasses.

A typical threshold switch consists of a thin films of chalcogenide glass sandwiched between two thin film metal electrodes (Bunton et al, 1972). Other types exist including the DO-7 package (Ovshinky, 1968), gap devices (Hughes et al, 1974), pore devices (Neal, 1970), and point-contact devices (Csillag and Jäger, 1970). The I-V characteristic of a threshold switch is shown in figure 1.5. This is obtained by application of a voltage pulse across the device and as the voltage is raised from zero, a high resistance 'off' state branch AB is followed until threshold is reached, value V_{th} , the device switches abruptly to a point C given by the slope of the load line, and a high conductance state CD is reached. As the supply voltage is decreased the working point moves down the on-state CD until it abruptly reverts to the off-state, point E, at the critical point D corresponding to a holding current I_h and a holding voltage V_h . The position of point E is given by the slope of the load line.

The off-state resistance exhibits an ohmic region close to the origin followed by a non-ohmic region up to the threshold voltage, V_{th} . The on-state characteristic generally shows a negative differential resistance for an on-state current of 1-3 mA and a positive differential resistance for higher current. The minimum voltage drop across a device in the region between the negative and positive differential resistance is denoted in this thesis as the minimum holding voltage V_{mh} .

The times taken for the various transitions are important parameters. When a voltage $V > V_{th}$ is applied, a voltage-dependent delay time t_d elapses before the device changes from its off-state to the on-state in a switching time t_s ($t_s \ll t_d$). The switch-off time or recovery time t_r is the transition time from the conducting on-state to the off-state

once the current drops below I_h . The recovery time is very large compared to t_s .

In a memory device, only V_{th} , t_d and t_s have any significance, the on-state parameters I_h and V_h are meaningless because the device remains in the conducting state once it is achieved. As mentioned earlier, the off-state can be re-established by a short high-current pulse.

The I-V characteristics of a threshold device are normally symmetrical in the first and third quadrants, i.e. symmetrical for applied positive and negative pulses, but there has been reports of asymmetrical characteristics (Henisch and Vendura, 1972). The behaviour of the various parameters of a threshold switch will now be considered in greater detail.

(a) Threshold Voltage V_{th}

The magnitude of the threshold voltage depends on temperature, pressure and film material composition and the electrical switching conditions such as pulse height and pulse repetition rate.

V_{th} always decreases with increasing temperature. For bulk and thick film ($>100 \mu\text{m}$) devices, the relation $V_{th} \propto (\sigma(T)/T)^{-\frac{1}{2}}$ is observed (Kolomiets et al, 1969, Warren, 1973). For thin film devices ($<10 \mu\text{m}$) the temperature dependence is much weaker (Kolomiets et al, 1969) and at low temperatures V_{th} becomes independent of temperature (Buckley and Holmberg, 1972).

Kolomiets et al (1969) have shown that the switching field is very weakly dependent on thickness in devices which are less than $10 \mu\text{m}$ thick (i.e. $V_{th} \propto d$), whereas for thicker films, the relation $V_{th} \propto d^{\frac{1}{2}}$ was observed.

The pressure dependence $V_{th}(P)$ has been measured by Walsh et al (1970) and found to vary as $\exp(P)$.

(b) Delay time t_d

There have been several reports of delay time measurements as a function of over-voltage ($V - V_{th}$), and also of film thickness. The delay time decreases rapidly as V is increased beyond V_{th} and for $V > 1.2 V_{th}$ it follows the relation (Ovshinsky, 1968, Henisch, 1969, Shanks, 1970, Lee and Henisch, 1973, Euntun and Quilliam, 1973):

$$t_d = t'_d \exp(-\alpha \cdot V)$$

where the prefactor t_d decreases with increasing temperature (Boer, Dohler and Ovshinsky, 1970) and decreasing film thickness. Lee, Henisch and Burgess (1972) studied the statistical spread in t_d and found relatively large statistical fluctuations in t_d for $(V - V_{th})/V_{th} = 0.2$ and at larger over-voltages a rather abrupt transition to a regime in which the fluctuations were less than $10^{-3} t_d$.

Values of t_d less than 10 ns have been observed in thin films and for high over-voltages but in thick films, values as high as 100 ms may be observed.

(c) Switching time t_s

After the delay time, the resistance of the device changes rapidly to a much lower value which could be 10^5 times smaller in a very short time t_s . In thin films, an upper limit of 150 ps for t_s has been measured using a sampling oscilloscope, (Neale, 1970).

(d) The on-state parameters, V_h, V_{mh}, I_h, t_r

The holding voltage V_h is normally 1-3 V in thin films and depends on electrode materials used. Much higher values have been reported by Hughes et al (1974) and they have shown that V_h in gap devices is strongly dependent on the circuit load resistor and device capacitance. In thick films ($> 100 \mu\text{m}$) the holding voltage increases with thickness. The minimum holding voltage V_{mh} has so far been largely ignored in the literature and there is almost a total absence of experimental data on its magnitude. Results obtained in this work, however, show that it has a magnitude of $\sim 0.9 - 2.5$ V depending on the electrode material used.

The recovery time t_r for thin film switches has a value of about a few μs but depends on the on-time and ambient temperature (Thomas et al. 1972). Practically, t_r is made up of two components, a fast temperature independent component and a much slower component which depends on temperature and could be several orders of magnitude longer than the first.

The holding current has typical values of 0.1 mA to 1 mA and depends on the external circuit parameters (Hughes et al, 1974). Further discussion of the on-state and its parameter is found in Chapters Two, Four and Five.

1.3. Choice of areas for investigation

This project set out primarily to investigate the nature of the on-state and characterize its parameters in thin film devices fabricated from a quaternary chalcogenide glass which had the Ovshinsky (1968) composition $\text{Si}_{12}\text{Te}_{41}\text{As}_{50}\text{Ge}_{10}$ which is frequently called STAG glass. Although during the last few years many papers have been published on the switching phenomena in chalcogenide glasses, attention has been mainly focussed on (a) the material aspects and structural changes (b) the possible conduction mechanisms in the off-state and the nature of the breakdown processes at threshold. Very little attention has been paid to the on-state of the threshold switching device and, as a result, at the time when active work started on this research project there was an absence of even a semi-quantitative theoretical model describing the on-state and a real lack of hard experimental results. Therefore, first priority was to obtain some basic and consistent results on the on-state as a function of ambient temperature, electrode material and device geometry. This programme necessitated the fabrication of well-characterized devices and the development of special testing equipment.

During the course of this research work it became very clear that structural changes played an important role in the device characteristics. To gain insight into the nature of these structural changes, measurements on the on-state were supplemented by some off-state measurements.

The development and progress of experiments are taken up in Chapter Four.

1.4. Thesis plan

Chapter Two consists of a brief review of some of the properties of amorphous materials and a survey of the various theoretical switching models.

Chapter Three describes in some detail the equipment and the special techniques used and developed for fabrication and testing of the switching devices.

In Chapter Four the results are presented with some preliminary discussion whereas the main discussion and results interpretation are given in Chapter Five.

In addition to the five chapters there is also an appendix which deals with suggestions for future work.

CHAPTER TWO

Glasses and Switching Models

Some of the properties of chalcogenide glasses were mentioned in the previous chapter. In this chapter a more detailed review, still brief, of the basic properties of these glasses is given. Also reviewed are the various switching theories developed to explain the switching phenomena in these glasses.

Although it is fairly well established that thermal runaway is mainly responsible for the switching effects in thick chalcogenide devices, there is still a good deal of controversy regarding the precise mechanisms of the switching processes in thin films: at present there are three major schools of thought (a) one which attributes switching in these devices to thermal effects, (b) a second which explains the switching phenomena in terms of purely electronic models, (c) a third which suggests that structural changes and phase changes in the material of the device play a dominant role in switching.

Any model put forward to explain the switching effect in these glasses must be able to account for a positive feedback mechanism which allows the voltage across the device to drop substantially while the current through it either remains the same or increases.

At present no single model gives an adequate and satisfactory description of a switching cycle in thin film devices. The problem of thermal switching has not been completely resolved mathematically and solution of the three-dimensional heat balance equation remains out of sight for a long time to come. The theories of electronic switching are based on the solid-state physics of amorphous materials which is not fully understood. Structural changes and phase separation are more likely to be the consequence of switching rather than the cause of it.

Although chalcogenide glasses are the primary subject of this review, some sections are applicable to any glassy material. Wherever possible, a particular reference to the switching effect in multicomponent chalcogenide glasses is made.

2.1. Disorder and classification in solids

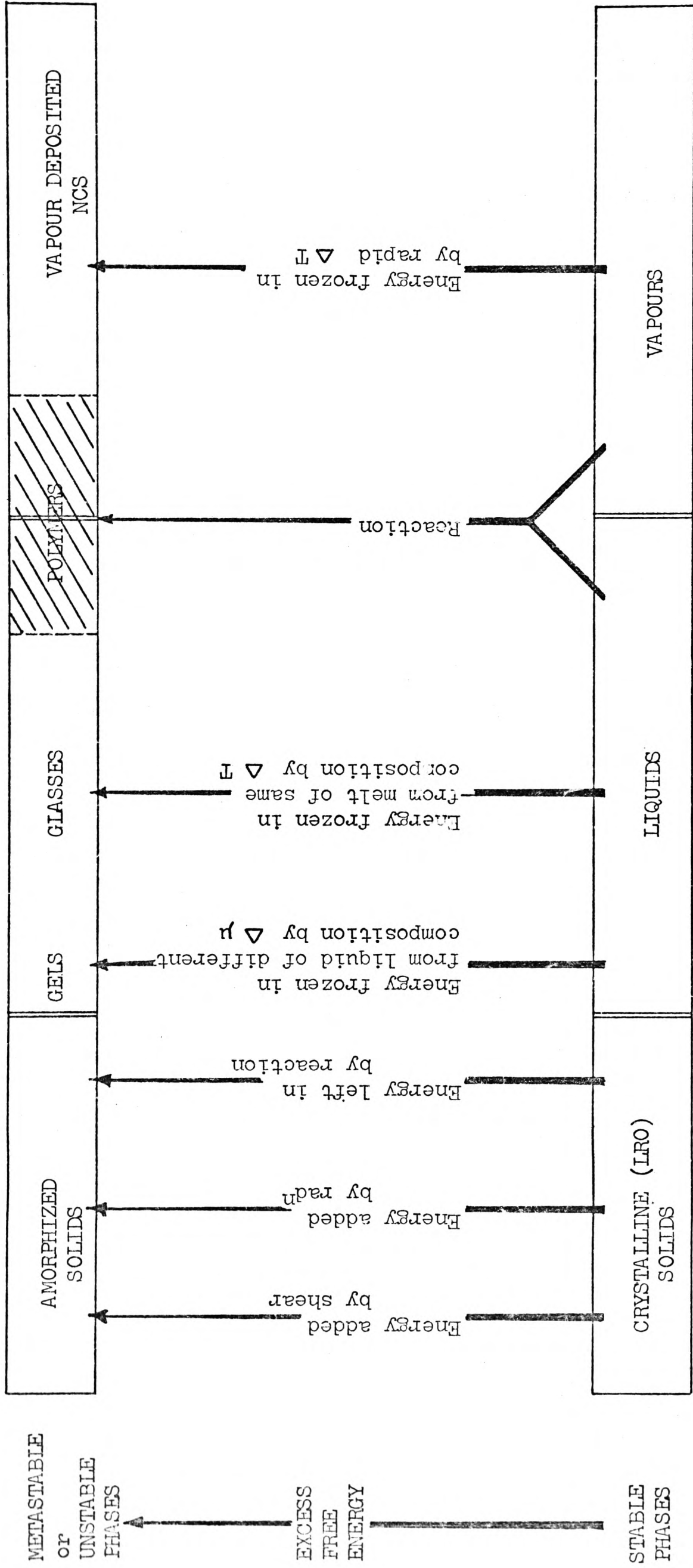
A solid can be defined as a material state which has the ability to transmit shear waves, or a state which has a minimum viscosity of 10^{15} poise. A solid thus defined can be either crystalline or non-crystalline depending upon the arrangement of the constituent atoms, ions or molecules. For a solid to be called

'crystalline' a long range periodicity, order, in the atomic arrangement must be present. There is no precise definition of non-crystallinity, but usually the absence of long range order in the atomic arrangement of a solid over distances $\sim 100 \text{ \AA}$ is taken as a condition. According to this definition a crystalline solid containing more than 10^{19} randomly distributed point defects in one cm^3 or a crystalline solid composed of small $\sim 100 \text{ \AA}$ crystallites are classed as non-crystallines. Non-crystalline solids, however, have a high degree of short range order over the first few interatomic distances.

The classification of crystalline solids based on structural studies by X-ray or electron diffraction techniques is now a well understood field which need not be mentioned any further here. Unfortunately a similar classification of non-crystalline solids is not possible at present owing to the lack of suitable analytical tools to study such aperiodic structures. A classification of non-crystalline solids has, however, been attempted by Roy (1970) using a scheme, which to quote him "is based on the fact that many basic structural features are carried over from the parent materials and the preparation process in a genetic memory which is sufficiently strong to permit the separation of non-crystalline solids into major groups." It is known that a non-crystalline material which is prepared by different methods results in different structures and this is described as polymorphism of non-crystalline solids. Figure 2.1 shows the basic outline of Roy's classification scheme. The various techniques used in preparing non-crystalline materials are outlined in Chapter 3. but it can be appreciated from figure 2.1 that Roy's classification scheme is based on the method of preparation and the origin of the material.

The non-crystalline solid formed by cooling a liquid or a melt is called a glass.

There is in the literature a widespread interchange of terms, liquid-like, glass, vitreous and amorphous which are often taken as synonymous although it is usual to define a glass as a non-crystalline solid formed by continuous solidification of a liquid. Differences between these terms have been taken account of in a scheme proposed by Stevels (1971) for the description of non-crystalline structures. He introduced the concept of repeatability numbers for non-crystalline



The relationship between the solid crystalline and true liquid and vapour phases which can be the thermodynamically stable phases. The processes by which the excess free energy is retained or pumped into the latter are indicated. Obviously not all the NCS phases have the same free energy. (Roy 1970).

Figure 2.1

structures. By starting from one (central) atom in a crystal and proceeding to the next atom, for instance, in the direction of the X-axis over a distance of the unit cell parameter, then the probability of finding the same atom again is unity if the crystal is perfect and the same applied to any number of steps. The coefficient of linear repetition in the direction of the X-axis is then defined as :

$$\text{CLR}_X = \frac{\text{number of atoms in the direction X in n steps}}{n}$$

The direction of the initial step could also be chosen to correspond with bond direction from a given atom and is not restricted to cartesian co-ordinates. In a real crystal CLR is unity for very small distances i.e. a few unit cells, from the central atom, but decreases over longer distances due to crystal imperfections. In a glass CLR is unity at very short distances but decreases rapidly at larger distances, $> 20\text{\AA}$.

The weighted average of all the CLR's (limited to a region V with one phase) in all directions i gives the average coefficient of repetition:

$$\text{ACR} = \frac{\sum_i c_i (\text{CLR})_i}{\sum_i c_i}$$

the coefficients c_i represent weighting for different directions. The magnitude of ACR has a similar value to the individual CLR's of a particular structure. From this quantity another quantity called the coefficient of repetition in space is obtained:

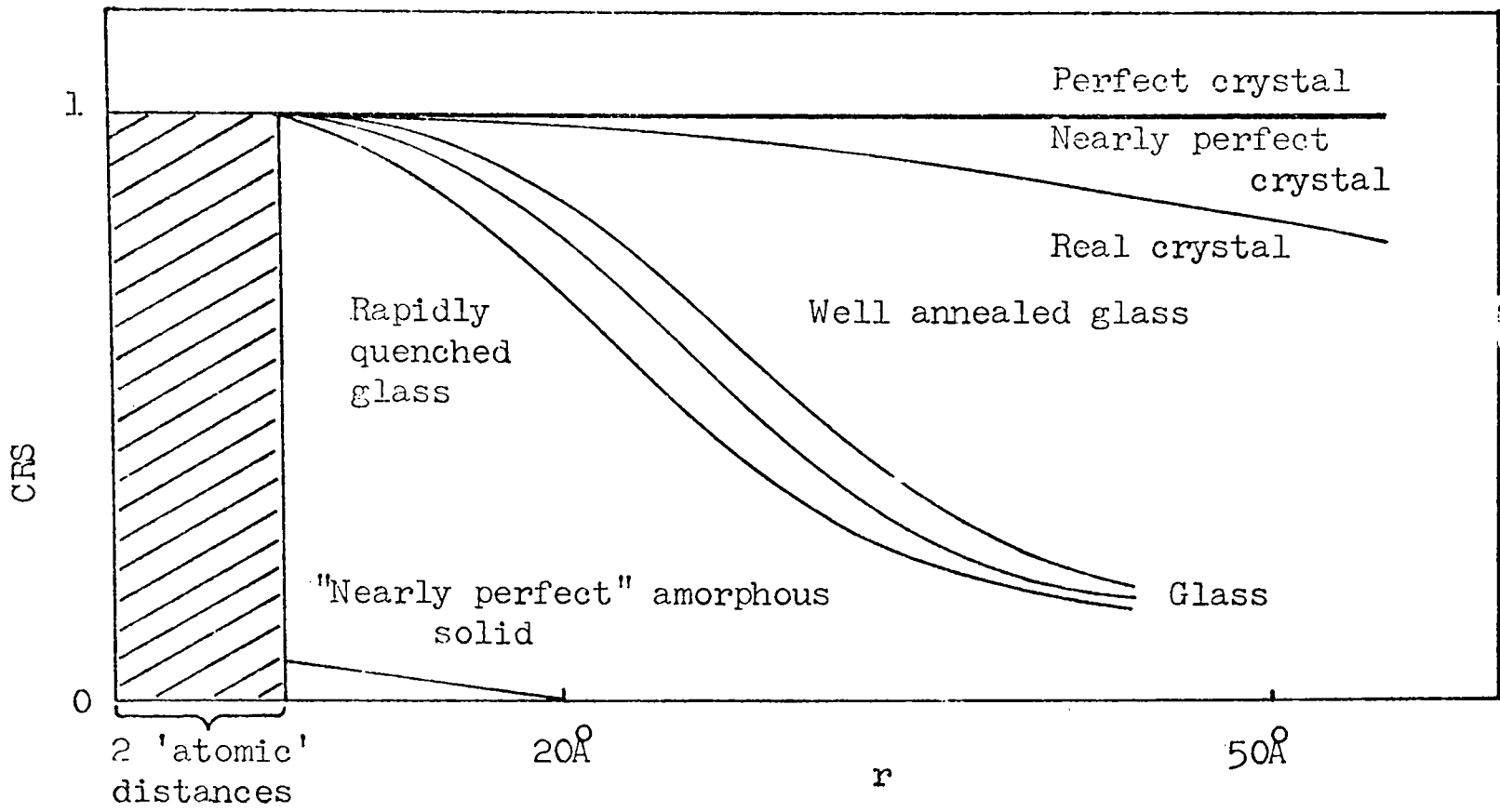
$$\text{CRS} = \frac{\sum_j N_j (\text{ACR})_j}{\sum_j N_j}$$

averaged over all the N_j atoms in a given volume. CRS is also a function of distance r . In a perfect crystal CRS is unity independent of r . For a real crystal CRS will decrease slowly with r but in glasses or amorphous solids CRS decreases very rapidly with r , and the decrease is greater in the rapidly quenched material. This is illustrated in figure 2.2(a).

The repeatability number independent of r is defined as:

$$(\text{RN})_{r_0} = \frac{1}{V_0} \int_0^{V_0} \text{CRS}(V) dV = \frac{3}{4\pi r_0^3} \int_0^{r_0} \text{CRS}(r) 4\pi r^2 dr$$

$(\text{RN})_{r_0}$ is a direct measure of the degree of order in the structure



Long range order — — — +

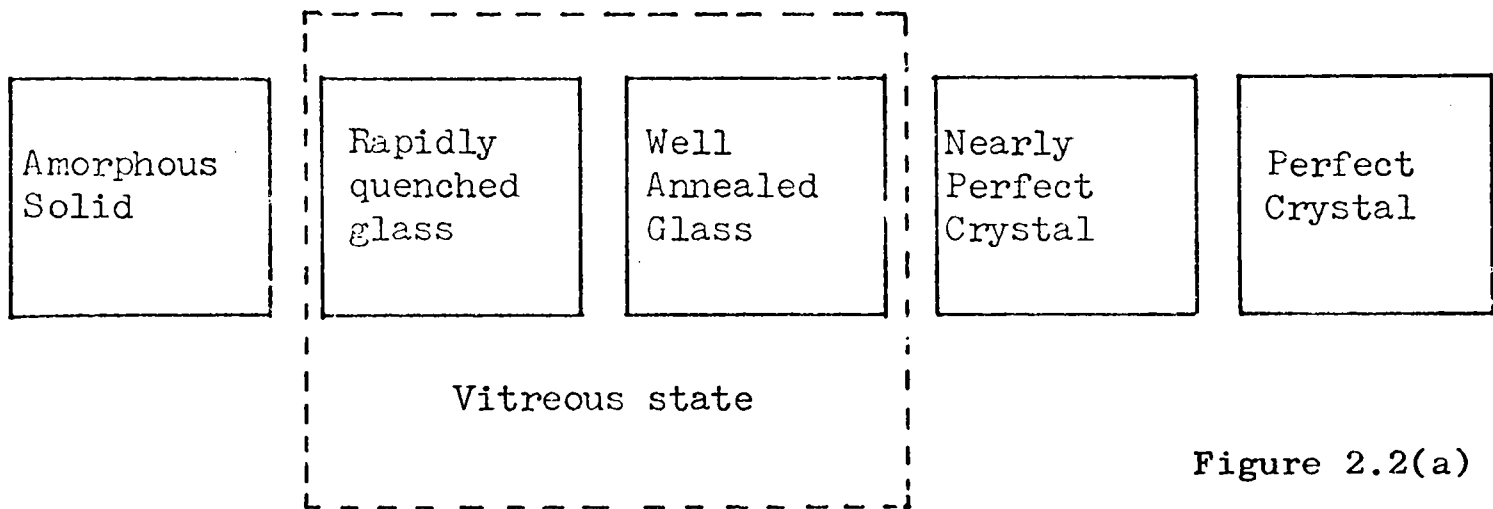
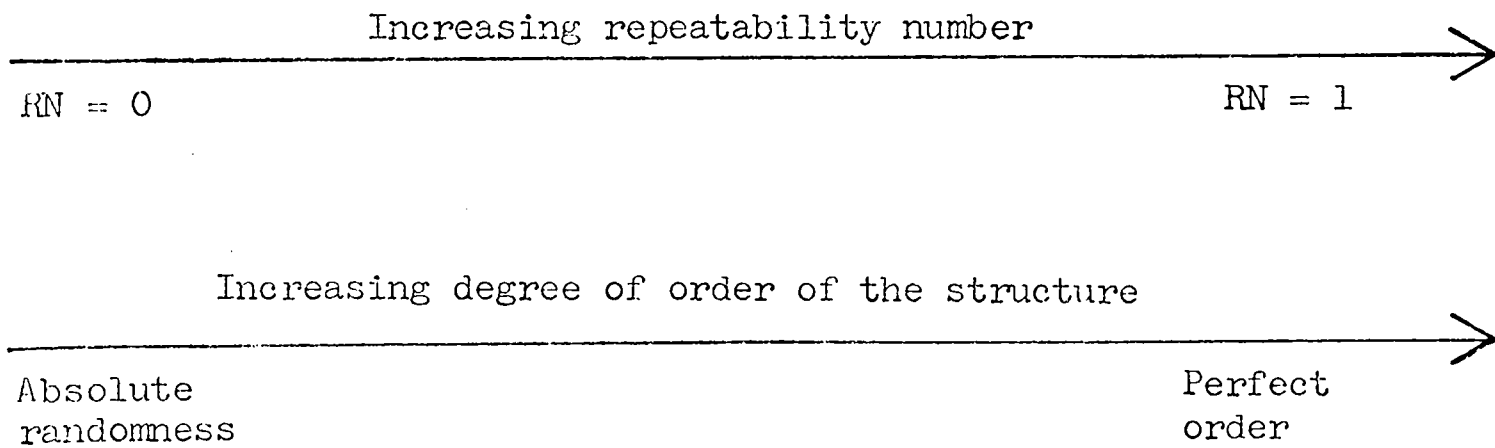


Figure 2.2(a)

Short range order — + +



(from Stevel 1971)

Figure 2.2(b)

in a limited region defined by r_0 or V_0 . In a material where the degree of order is the same everywhere, one could define a repeatability number, RN, which is a measure of the overall degree of order. If the degree of order varies then it is necessary to define a weighted average of all the local $(RN)_{r_0}^j$ s. For a perfect crystal the overall RN value is unity, for a nearly perfect crystal it is slightly less than unity, and for real crystals and vitreous systems it may be between 1 and 0. This is illustrated in figure 2.2 b). Therefore, a "perfect" amorphous solid would have an RN value equal to zero whereas vitreous and glassy solids are characterized by a finite value of RN and Stevel suggested that they should not be called amorphous solids. Owen (1973) expresses the view that a value of $RN = 0$ is more applicable to an "ideal gas" rather than to an amorphous solid.

One scheme of classifying amorphous semiconductors is in terms of the chemical bonding that is primarily responsible for cohesive energy of the solid. In crystalline solids, there are five major classes - ionic, covalent, metallic, Van der Waals and hydrogen bonded materials. Amorphous metallic alloys do exist, but these have conductivities which are comparable to the corresponding crystalline materials and do not fall into the category of semiconducting solids. Van der Waals and hydrogen bonded solids have low cohesive energies and low melting points and the corresponding amorphous solids have not been investigated to any great extent. Thus amorphous semiconductors can be broken down into ionic and covalent materials. The ionic materials include halide and oxide glasses such as V_2O_5 . Covalent semiconductors are conveniently divided into elemental and alloy semiconductors. The elemental semiconductors which include Si, Ge, Se among others are the simplest to investigate theoretically and possess only positional disorder. Covalent alloys include binary systems such as As_2Se_3 and GeTe as well as the more complex multi-component systems such as STAG glass. These alloys possess positional as well as compositional disorder and this joint disorder has a profound effect on the electronic band structure of the material as shall be seen in a later section.

2.2 Glass - its formation and structure

As stated above, a glass is a non-crystalline solid prepared

by continuous solidification of a liquid. A more informative definition was given by Jones (1956). A glass or a substance in the glassy or vitreous state, is a material which has been formed from the normal liquid state and which has shown no discontinuous changes in first-order thermodynamic properties such as volume (V), heat content (H) and entropy (S) but had become rigid (i.e. solid) through a progressive increase in its viscosity. Second order thermodynamic properties such as specific heat capacity and thermal expansivity, however, undergo discontinuous changes when a liquid is quenched or cooled to form a glass.

Some aspects of the inter-relationship between the liquid, crystalline and glassy forms of a material can be obtained from the volume-temperature diagram for a glass-forming material shown in figure 2.3. On cooling the liquid from an initial state represented by the point a the volume of the liquid decreases steadily along the line ab. If the rate of cooling is sufficiently low and nuclei are present in the melt, crystallization will take place at the freezing point, T_M . At this point there is a discontinuous change in volume represented by the line bc. On further cooling the crystalline material contracts along cd. On the other hand, if the rate of cooling is sufficiently high, crystallization does not take place at T_M . As cooling continues, the volume of the now super-cooled liquid decreases along the line be, which is a smooth continuation of ab. In the region T_g , the slope of the volume-temperature graph changes to become approximately parallel to the contraction curve of the crystalline form. The temperature, T_g , at which the bend occurs is called the glass transformation or transition temperature. At T_g the viscosity is extremely high - about 10^{13} poise (Rawson, 1967) and only below T_g it is correct to describe the material as glass. It is also at T_g that second order thermodynamic quantities such as the specific heat, C_p , expansion coefficient α and compressibility C show discontinuities as shown in figure 2.4. It must be realised that T_g is not a precisely defined temperature, i.e. the glass transition is not sharp but occurs over a temperature range. It is sometimes convenient to define the point where the liquid line and glass lines meet as a specific temperature. This temperature is called the fictive temperature in glass technology (Owen 1970).

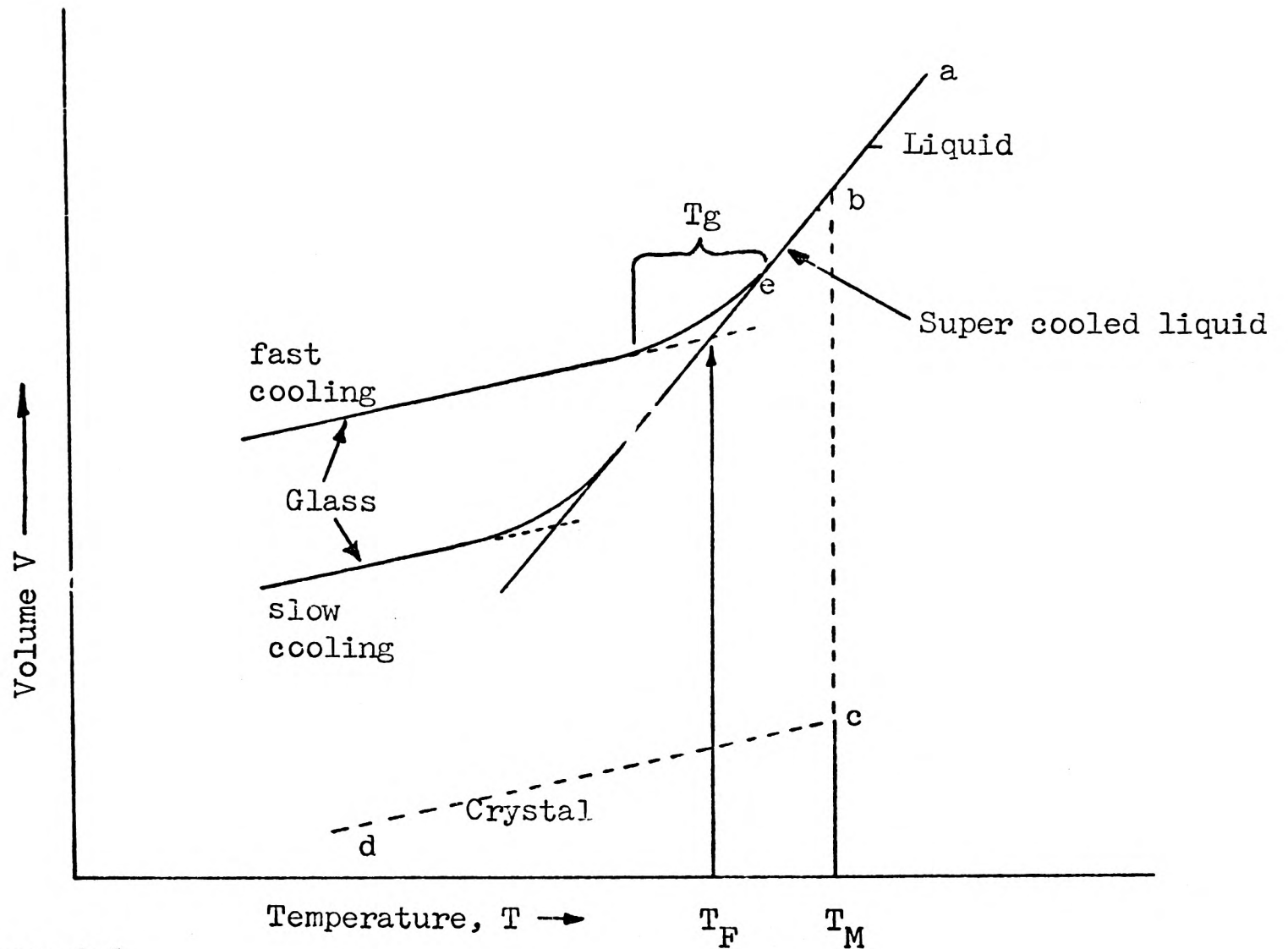


Figure 2.3

The relationship between volume and temperature for a cooling liquid.

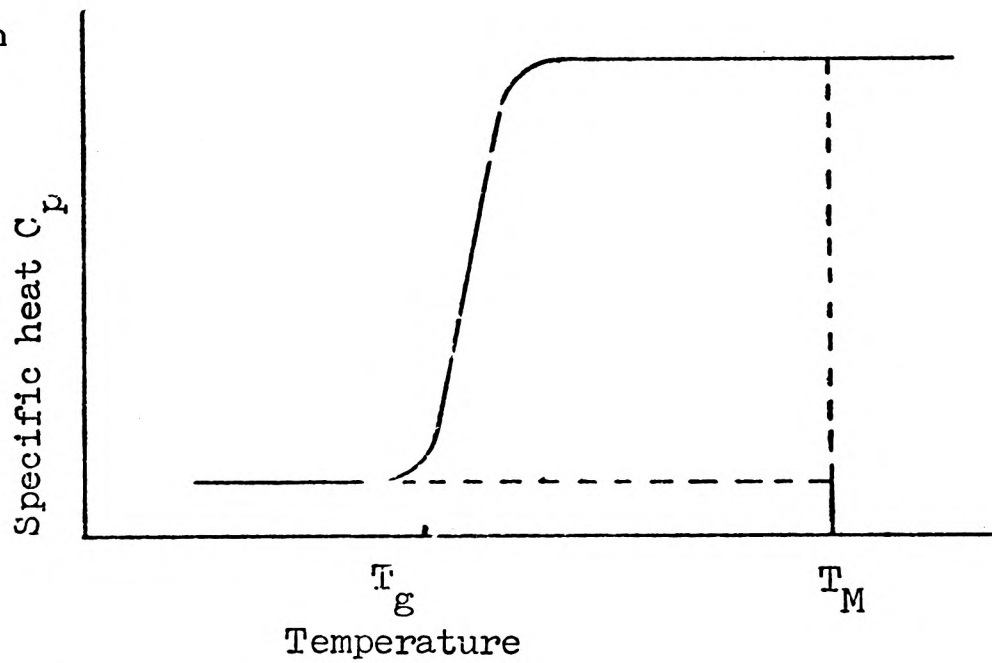


Figure 2.4

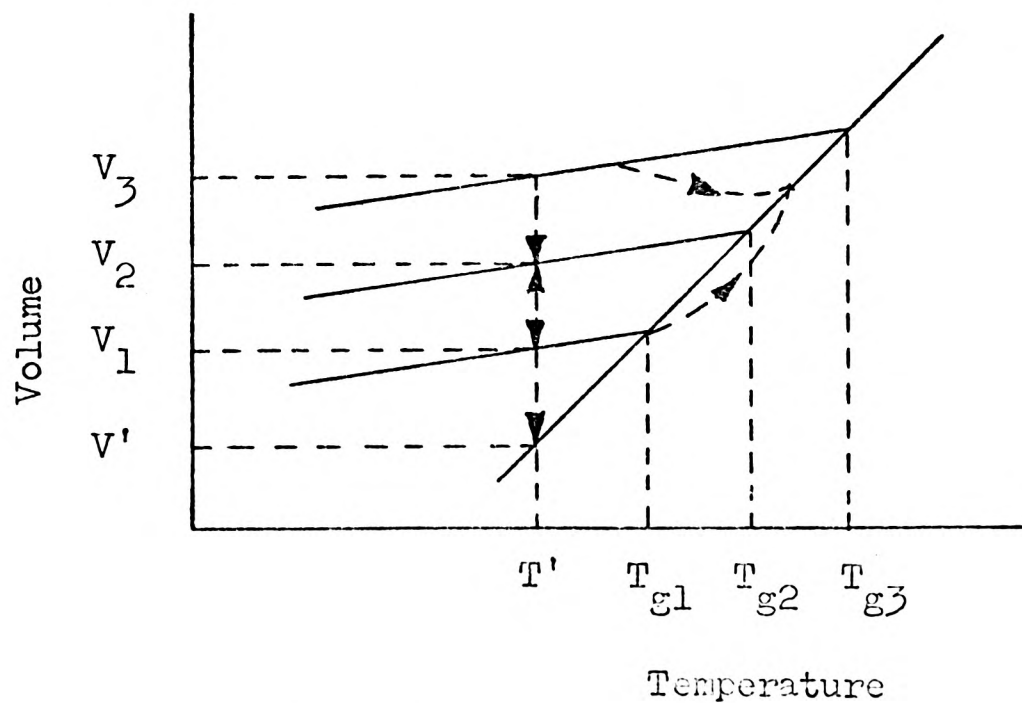


Figure 2.5

Switching in chalcogenide glasses has often been related to T_g . There have been several reports (Thomas et al, 1972) which showed that the threshold voltage temperature graphs extrapolated to zero at a temperature close to T_g . Iizima et al (1970) found that the d.c. threshold voltage in a series of related glasses increased with T_g . A relationship of the form:

$$V_{th} \propto \exp (CT_g)$$

was given. Therefore, it has been suggested that T_g plays a major role in the switching mechanism (Thomas et al, 1972) in these devices. Such predictions warrant a closer look at T_g and the behaviour of glass at temperatures below and above T_g .

The value of T_g depends upon the cooling rate, see figure 2.3, and subsequent thermal history. The greater is the cooling rate the higher is T_g . In some glasses such as As_2Se_3 (Owen, 1973, Onodera et al, 1969) the relation between T_g and the cooling rate R can be expressed in the empirical form,

$$R = R_0 \exp \left[- \frac{1}{c} \left(\frac{1}{T_g} - \frac{1}{T_m} \right) \right]$$

where R_0 and c are constants. T_g could show substantial differences of a few hundred degrees for different quenching rates.

A glass is thermodynamically unstable and when held at a temperature T' , figure 2.5, below T_g it is found that the volume, say V_3 , decreases until it eventually reached a point V' on a line which is a smooth continuation of the contraction line of the more stable supercooled liquid. Figure 2.5 also shows the volume-temperature relationships for three glasses prepared by different rates of cooling and therefore each glass has a different T_g . If the two glasses with transition temperatures T_{g1} (prepared by slow cooling) and T_{g3} (prepared by fast cooling) are held at a temperature T' , the volume of each will tend towards V' which corresponds to the volume of the supercooled liquid at that temperature. T_{g1} and T_{g3} will also change. This process, by which the glass reaches a more stable condition, is known as stabilization. The volume of the glasses and their T_g 's can also be increased by heat treatment above their T_g 's. If the two glasses with T_{g1} and T_{g3} are heated to a temperature T_{g2} , which is

the Tg of the glass prepared by the intermediate rate of cooling, and then cooled rapidly to T', the volume of glass 1 will decrease to V₂ and its Tg will decrease to Tg₂. The volume of glass 1 will increase to V₂ and its Tg will also increase to Tg₂. The rates at which the volumes and Tg's of glasses 1 and 3 increase and decrease respectively are different, the change Tg₃ - Tg₂ will be more rapid than Tg₁ - Tg₂. This shows the sensitivity of Tg and its dependence on the rate of cooling and the subsequent heat treatment of the glass. Therefore, when a differential thermal analysis is carried out to determine Tg, the rate of heating of the material must be the same as the original rate of cooling of the melt or the liquid. If the rate of heating is different, the value of Tg obtained is different from the original one. This can again be shown from figure 2.5. If glass 1 is reheated at a rate corresponding to the cooling rate of glass 2, its volume will tend to "undershoot" the supercooled liquid line as shown by the dotted line. This is because it is being heated too rapidly for attainment of equilibrium. If glass 3 is heated at a rate corresponding to the cooling rate of glass 2, its volume will tend to decrease before Tg is reached. Therefore, the original value Tg of a chalcogenide glass is obtained only when the heating rate and the original cooling rate are the same. In bulk samples such a condition may be feasible depending on the magnitude of the cooling rate. In thin films, however, the vapour quenching rate is extremely high, see next chapter, and it would be impossible to carry out a different thermal analysis experiment on the thin film material using a heating rate which is the same as the cooling or quenching rate. Therefore, it is essential that such effects are considered when interpreting data obtained from DTA experiments on thin films and particularly when relating it to the threshold voltage and threshold conditions.

The ability of a liquid to be cooled to form a glass, i.e. bypass crystallization, depends principally (Turnbull, 1969) upon (a) a set of factors such as the cooling rate R, the liquid volume V and the seed density ρ , which can be partly controlled, and (b) a set of materials constants, such as the reduced liquid-solid interfacial tension, α , the fraction of acceptor sites, f in the

crystal surface and the viscosity-reduced temperature relation which often can be characterized by the reduced glass temperature T_{rg} . The glass forming tendency increases for larger values of R , α and T_{rg} and for smaller values of v , ρ and f .

Most of the chalcogenide glasses are prepared by normal cooling, i.e. quenching at room temperature from the melt. In practice the glass formation region of a particular system is predicted by using an empirical diagram giving the glass forming region as a function of composition. Figure 2.6 shows such a diagram for the ternary glass system Ge-As-Te. These diagrams are sometimes called - conveniently but incorrectly - phase diagrams. The size of the glass forming region depends on the cooling rate such that the region of glass formation becomes larger as the rate of cooling increases. In general, memory switching devices are fabricated from alloys near the boundary of the glass forming region whilst threshold devices come from the centre of such a region.

Multicomponent chalcogenide glasses can phase separate. Information on phase separation in such alloys can be obtained from differential thermal analysis (Mackenzie, 1970) experiments on the alloys. In this technique small changes ΔQ can be detected in the heat content of a small quantity of the material as its temperature is varied slowly. These changes are associated with various structural alterations during temperature change and can be detected. Figure 2.7 (Bosnell, 1973) shows DTA traces for a glass having the chemical composition $Ge_{15}Te_{85}$ which is normally used for making memory switching devices and for a glass used for threshold switches such as STAG glass. It can be seen that although both show a glass transition temperature, T_g , only the $Ge_{15}Te_{85}$ glass exhibits any further discontinuities which in this case are a crystallization exotherm followed by a melting point endotherm.

The structure of a glassy material may be considered to be continuous with that of the liquid from which it was prepared. The problem of whether the structure of a glass is, in general, distinct and unique, or only trivially different from that of a crystalline solid has persisted for sometime now without being resolved definitely. As mentioned earlier, a glassy material is characterised by a high degree of short-range order and absence of

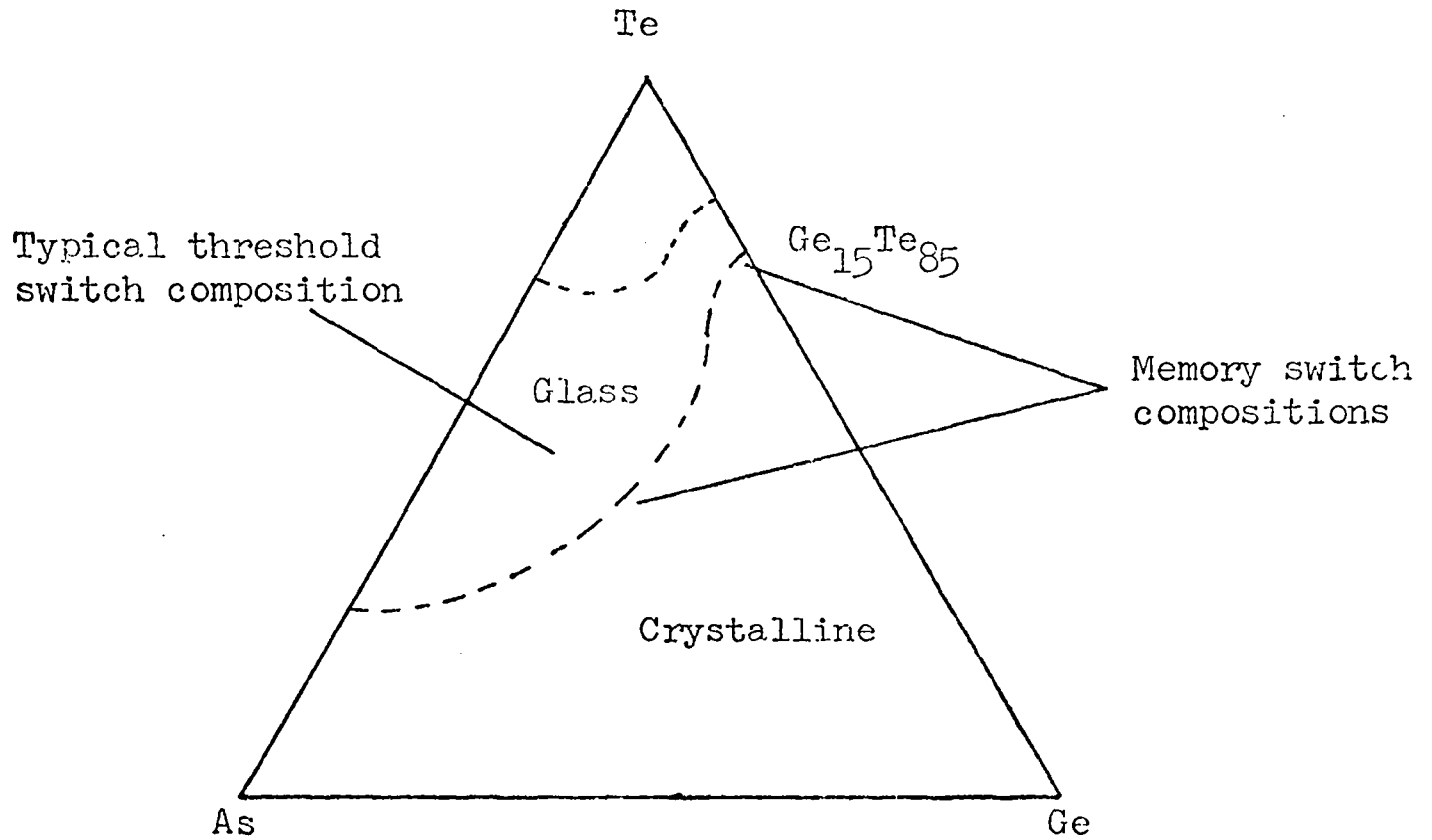


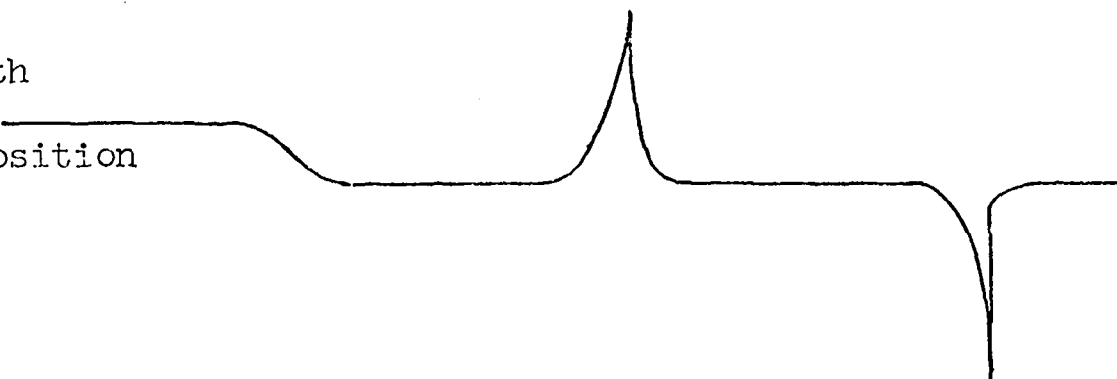
Figure 2.6

Glass formation in the system Ge-As-Te.

Material with
a typical threshold
switch
composition



Material with
a typical
memory composition



Exothermic
Endothermic

temperature

Figure 2.7

Differential thermal analysis curves of chalcogenide glasses with typical memory and threshold switch compositions.

long-range order, therefore, the structure of glass is best described by some statistical entity which gives an average of the atomic arrangement. An example of such a function is the radial distribution function which gives the probability of finding another atom in spherical shell of radius r and thickness dr around an arbitrary central atom.

Models of atomic structure of glass are based on two basic approaches (a) the random network hypothesis which was first suggested by Zachariasen (1932) to describe the structure of oxide glasses and (b) the crystallite theory of Lebedev (1926) and Porai-Kosic et al (1959) which considers the structure of a glassy material to be composed of small domains of high order bound together by regions of low order.

There have been several attempts to construct a structural model for covalent semiconductors, particularly the elemental semiconductors such as silicon and germanium (Grigorovici, 1973). However, so far as the author knows, no model exists at present which describes the structure of complex multicomponent chalcogenide alloys such as STAG glass.

2.3 Electronic band structure

Amorphous semiconductors represent systems of higher complexity than their crystalline counterpart and require for their characterization a larger number of parameters. The mathematical difficulties associated with first-principle solution of the Schrodinger equation are formidable. At present there is no rigorous quantitative theory of amorphous semiconductors, but several band models based on a semi-quantitative approach have been proposed (Mott, 1967, 1969, Cohen et al, 1969).

The simplest possible band model for an amorphous semiconductor is shown in figure 2.8(a). There is a valence band with a tail of localized states above E_v and a conduction band with a tail of localized states below E_c . Thus only a pseudogap exists between the conduction and valence bands. This simple model is based on the ideas expressed by Mott and several other research workers over the last decade. Anderson (1958) has shown that electrons in localized states cannot diffuse at $T = 0$ K. At finite temperatures they contribute to the

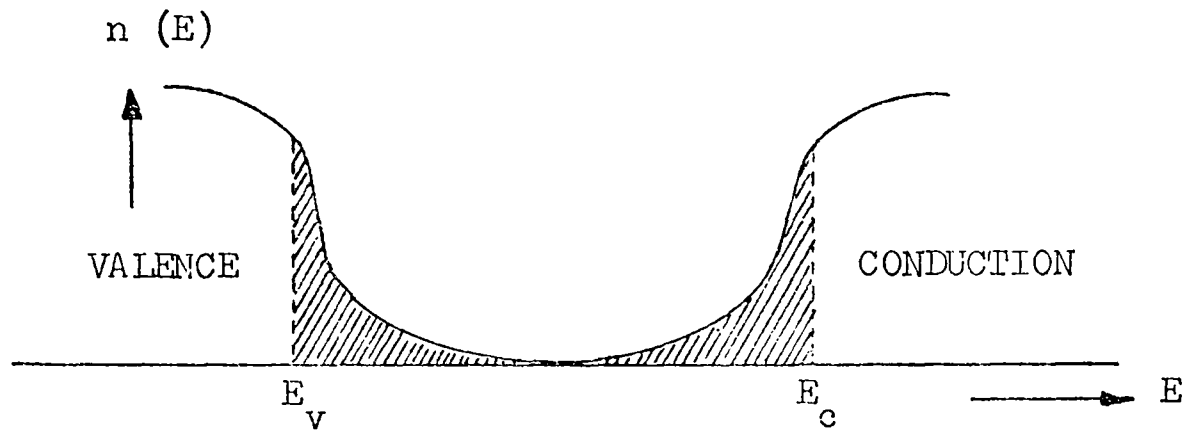


Figure 2.8(a)

A simple band model for amorphous semiconductors.

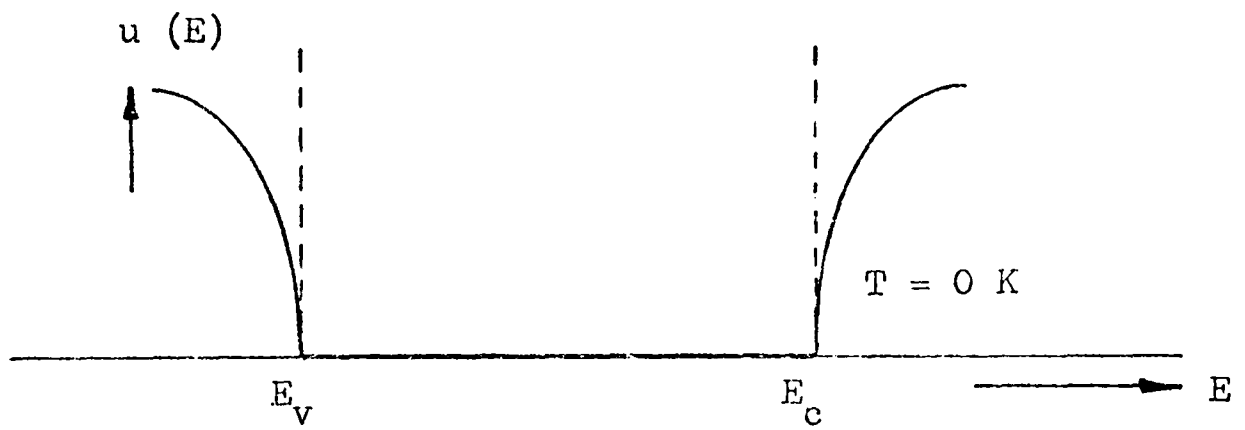


Figure 2.8(b)

The mobility gap (see text)

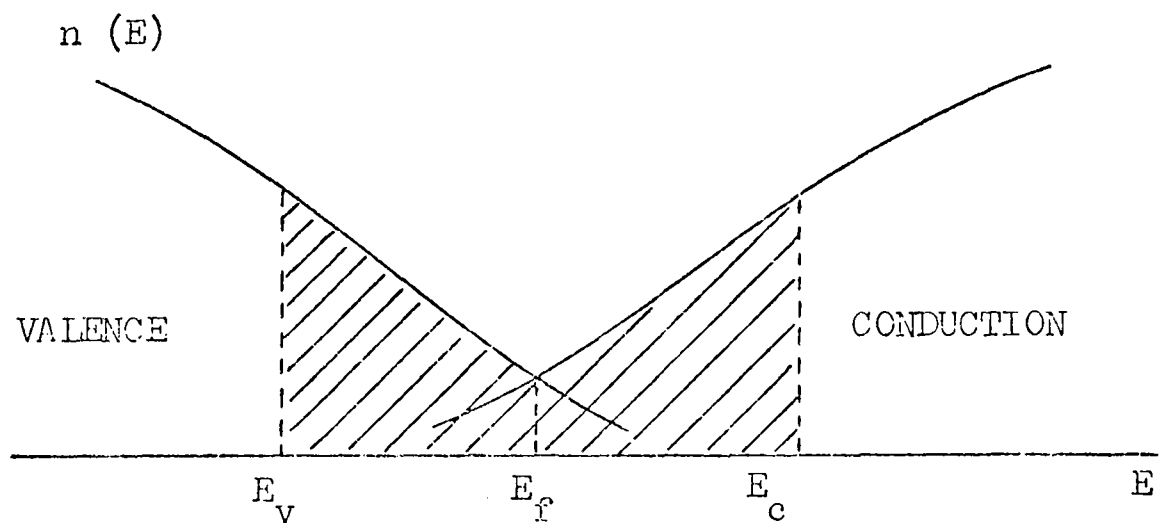


Figure 2.8(c)

The band model of Cohen, Fritzsche and Ovshinsky.

conductivity only by phonon- assisted hopping. Therefore, a fall of at least several orders of magnitude in the mobility is expected to occur near to E_v and E_c . The drop in mobility at these regions is shown in figure 2.8(b). The energies E_v and E_c are therefore mobility edges (Cohen, 1970) and these regions are called mobility shoulders (Mott, 1967). The energy range between E_v and E_c is termed the mobility gap

in view of the large differences in the nature of the various groups of amorphous semiconductors, no single model can describe the essential features of all amorphous semiconductors. As this investigation is mainly concerned with switching in multicomponent chalcogenide glasses, the rest of this section will be confined to describing a model which deals with areas of extreme disorder such as STAG glass which has positional as well as compositional disorder. Such a model was developed by Cohen, Fritzsche and Ovshinsky (1969). In this model, the increased disorder broadens the tails of the conduction and valence bands until they overlap inside the mobility gap, figure 2.8(c). This model has some unusual features. Firstly, the valence band tail states are assumed to be neutral when occupied and the conduction band tail states are neutral when empty. This places the Fermi level in the centre of the gap. Secondly, in certain regions of the material the valence band states may have higher energy than states in the conduction band. This is not an equilibrium situation and consequently electrons will fall from the top of the valence band into spatially distinct states of the lower conduction band tail. This creates positively-charged states above and negatively-charged states below the Fermi level E_f . Therefore, neutral and charged traps for electrons exist above E_f and neutral and charged-traps for holes below E_f . These trapping centres are believed to play an important part in the switching phenomena in these glasses and several electronic switching theories have been based on the CFO band model. The density of the localized states near E_f is estimated (Fritzsche, 1969) to be between 5×10^{19} and $10^{20} \text{ cm}^{-3} \text{ eV}^{-1}$. Such a large density of states will effectively pin the Fermi level and hence explain why contacts between metals and these glasses are low resistance and non-rectifying.

For a large class of multicomponent chalcogenide glasses, the d.c. electrical conductivity increases exponentially with increasing

temperature, in accordance with the normal expression for crystalline semiconductors:

$$\sigma = \text{constant} \exp\left(-\frac{E_c - E_v}{2kT}\right)$$

Often $\sigma(T)$ exhibits no discontinuity at T_g or at higher temperatures. This is interpreted as evidence of intrinsic conduction and the mobility gap is taken to be twice the activation energy $\frac{1}{2}(E_c - E_v)$. However, this is not a general result, and sharp increases in the activation energy (the slope of a plot of

$\ln \sigma$ vs. $\frac{1}{T}$), can occur at temperatures above T_g (Male, 1970, (Croitoru et al 1972a). This behaviour may be explained in terms of different conduction mechanisms being dominant at high and low temperatures. At low temperatures conduction by carrier in the extended states i.e. the states above E_c and below E_v may be less significant than the conduction by the carriers in the localized states near E_f . This latter case will have a different activation energy at very low temperatures where the argument of the exponential function will be replaced by $-\text{const } T^{1/4}$ (Mott and Davis, 1971)

2.4 Electronic Switching Models

The various possible high-field effects that could operate and made a contribution to the non-ohmic region of the off-state were discussed by Mott (1971) and reviewed critically by Owen and Robertson (1973). Attention is concentrated in this section on those mechanisms which are relevant to the threshold point and the on-state of a switch.

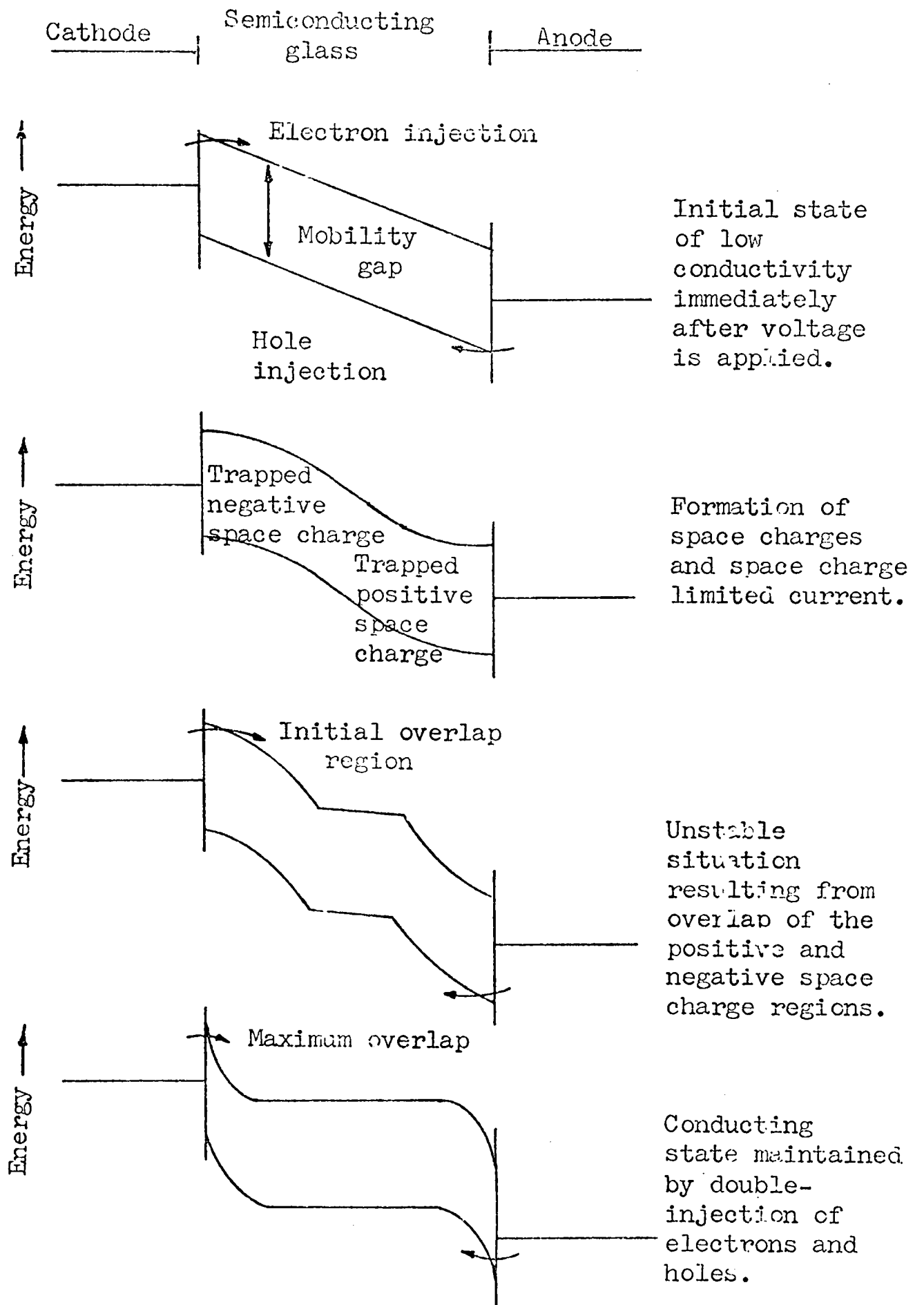
The uncertainty in the mechanism of charge transport and the inadequate understanding of the physics of amorphous semiconductors have led to the development of several electronic switching models, but the extent of elaboration in any of these models is at most semi-quantitative.

The most common class of electronic model involves the double-injection mechanism. Several authors (Mott, 1969, Henisch, Fagen and Ovshinsky, 1970, Fritzsche and Ovshinsky, 1970a, 1970b, Lucas, 1971) have proposed models in which, in the on-state, carriers are injected from both electrodes -giving a high density of carriers in the conduction and valence bands, However, the method of attainment of this state varies from one model to another and is still the subject of some controversy.

In the model proposed by Henisch (1969) and Henisch et al (1970) it is assumed that the semiconductor is described by the CFO-type band structure. The main feature of this double-injection model is the formation of a negative space charge near the cathode resulting from the immediate trapping of injected electrons by the positively-charged traps above the Fermi energy. Similarly, a positive space charge appears near the anode. The current is limited by these space charges and the internal field is also distorted resulting in an enhanced field in the bulk. At a sufficiently large value of applied field the two space-charge regions widen, spread towards each other, and eventually overlap in the centre of the bulk. In the overlap region all positive and negative traps are filled and therefore this region is neutral and highly conductive. The device is then in an unstable state and the electric field is redistributed and increased fields appear across unneutralised space charge regions. Thus injection of carriers is increased which leads to greater overlap of space charges; this represents a positive feedback loop and a collapse of device resistance followed by reversal of space-charge polarity. The conductive on-state is then sustained by double injection of both electrons and holes provided, it is postulated, the voltage across the device is larger than the mobility gap. The model is sketched in figure 2.9.

In the above model the delay time is the time required for the two space charges to overlap. In such a model it is expected that the delay time is increased if the voltage pulse polarity is reversed prior to switching, but such an effect is not observed at room temperature (Balberg, 1970, Shanks, 1970). However, Henisch et al (1971) have observed some polarity effects at low temperatures. These effects can be summarised as follows:

- (a) When a device was switched by a square pulse A, and then after a time greater than one μ s another pulse B was applied to the device, it was observed that the threshold voltage for similar delay time with pulse B was greater when A and B had the same polarity than the case when their polarities were opposed. The opposite effect was observed when a non-switching pulse A was used. Henisch et al (1971) suggested that these observations were consistent with his model's prediction that a reversal in the space-charge polarity occurred in the course of switching.



Space-charge double injection model for switching (Henisch et al, 1970).

Figure 2.9

- (b) Polar effects were observed (Henisch and Vendura, 1971) when asymmetric electrode materials were used.
- (c) The delay time increased (Henisch, 1971) when the pulse polarity was reversed before threshold conditions were reached, but the increase in delay time was smaller than expected. It is also claimed that Henisch's model (Henisch et al, 1970) is versatile enough to explain the following:
- (i) The dependence of delay time on the over voltage
 - (ii) The recovery period
 - (iii) The temperature of the threshold voltage, provided additional assumptions were made regarding the dependence of the mobility or injection ratio on temperature.
- (d) The tendency of the effective capacitance of a switching device to become negative just below the threshold voltage as reported by Vogel and Walsh (1969) and Altunyan et al (1971). This is explained in terms of dielectric polarization followed by space-charge polarization at a higher voltage. Near the threshold condition space-charge polarization is dominant and the device capacitance goes negative.

It must be recognised at this stage, that the experimentally observed dependence of threshold field on film thickness is not what is expected from a double-injection space-charge-current mechanism. Owen and Robertson (1973) pointed out that established ideas about such a mechanism in a conventional semiconductor show that the threshold field increases with film thickness, but this is not observed in chalcogenide thin films.

Lucas (1971) has pointed out that, in order to sustain the on-state by tunnelling or by double injection, the carrier lifetime must be larger than the transit time. Her model of switching is based on the assumption that beyond a critical injection current, both electron and hole traps are neutralized and the diffusion length becomes comparable with film thickness. This sharply increases the bulk conductance and the sustaining field is again concentrated at the electrodes. Lucas obtains for the critical current density an expression:

$$i_c = 2 L_u eN/\tau_o$$

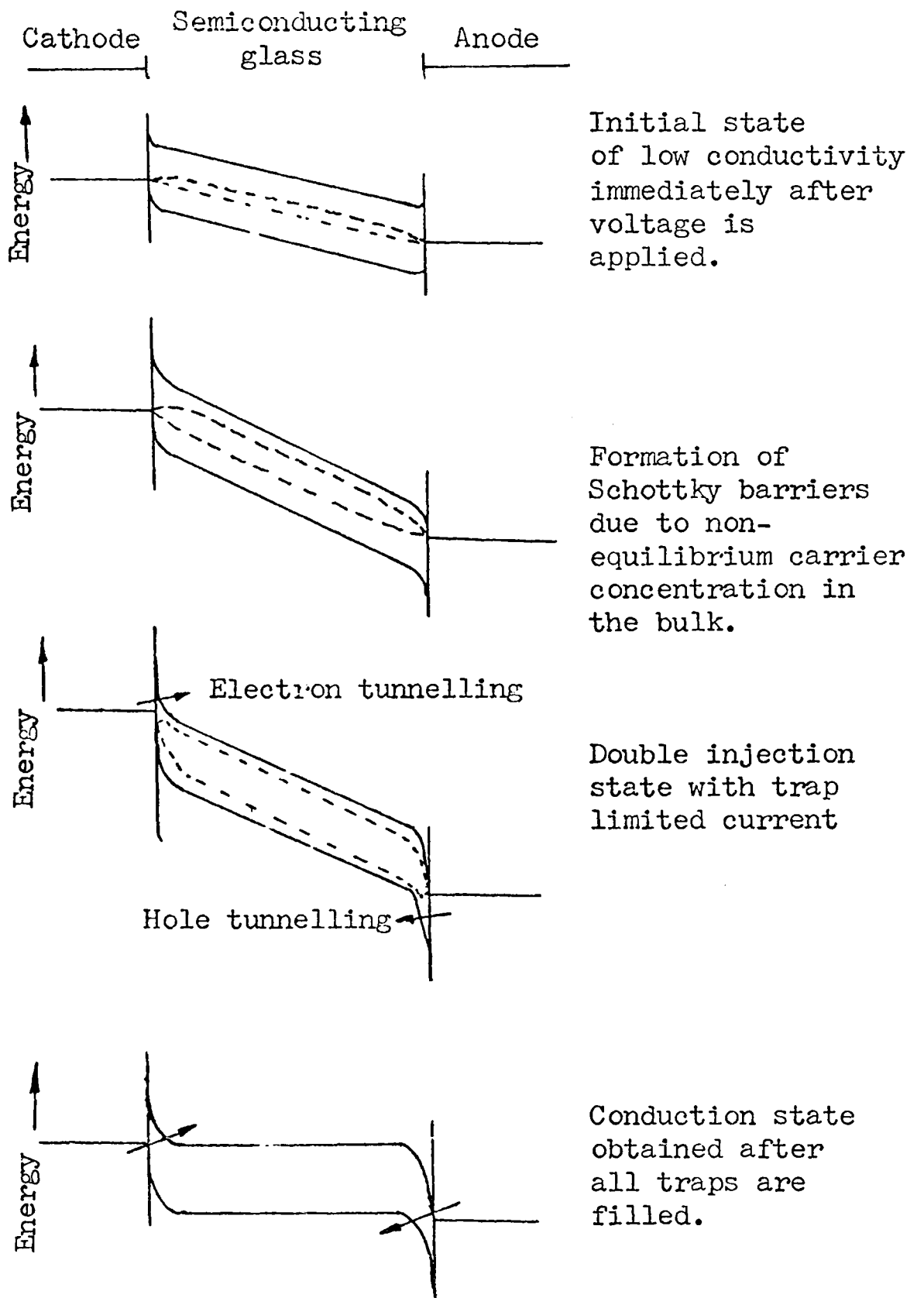
where L_u is the diffusion length and equal to electrode separation

length when switching occurs, N is the density of the recombination centres and τ_0 is the excess carrier recombination time.

The potential energy of an electron in the on-state plotted against position across the switching layer as shown in figure 2.9 was first suggested by Mott (1969). He postulated the existence of positive trapped space-charge near the cathode and a negative space-charge near the anode. The trapped charges must not be too close to the electrodes so that they could tunnel to them and also the space-charge region must not be too wide to prevent tunnelling of carriers from the electrodes. Essential features of this on-state model are that the carrier transit time is small compared with the recombination time, the holding voltage is the sum of voltage drops across the space charge regions and is larger than the mobility gap.

Fritzsche and Ovshinsky (1970) proposed a somewhat different model, sketched in figure 2.10, to that of Henisch. Their model describes a mechanism which is more likely to occur at temperatures in the vicinity of room temperature at which screening of space charge is more effective and space charges are less likely to form. In this model it is assumed that non-equilibrium carriers generated by the field cause two depletion regions to form near the electrodes. One region for electrons is formed near the cathode and one for the holes near the anode. These depletion layers are formed because the electrodes cannot supply a sufficient carrier flux to maintain the non-equilibrium current. The resulting Schottky barrier-heights grow with increasing field but their thicknesses remain in the region of 30 \AA . This allows tunnelling to take place, and trap-limited current flows until all the traps are filled. When all the traps are filled, a highly conducting state is achieved, the voltage drops, and the current increases sharply. The conductive on-state is again sustained by double injection, as long as the applied voltage exceeds the mobility gap.

In this model the delay time is primarily the time required to fill the traps in the bulk under conditions of trap-limited conduction. Such trap filling is totally independent of pulse polarity, and although the time required to set up the Schottky barriers is strongly polarity-dependent, it is much smaller than the time required to fill the traps. Therefore, the total delay time is essentially



Model of Fritzsche and Ovshinsky for switching.

Figure 2.10.

independent of pulse polarity. The recovery time must be the time required to empty the traps and it should be temperature dependent. Adler (1973), however, has reported that the recovery time and holding voltage were independent of temperature from 200 to 1.6 K. and the on-state could not be frozen in. Adler concluded that the on-state is not maintained by filled traps.

The two main models discussed so far indicate that the polarity dependence of these electronic mechanisms is governed by the ambient temperature. A transition from one mechanism to the other can occur at some temperature below room temperature when polar effects become noticeable.

Schmidlin (1970) has shown that I-V characteristics similar to those of a thin film chalcogenide switch can be obtained with a model of field-induced double injection, sustained by the build-up of charges attempting to enter the electrodes through poor contacts. In this model, electrons begin to pile up near the cathode until a steady state is reached where emission from each accumulation region just balances injection from the opposite electrode. As the field across the sample is increased the accumulation regions also increase until a critical field associated with these accumulation regions is reached and enhanced injection takes place. The additional injection results in a further increase of the accumulation regions which in turn gives rise to a negative resistance region and breakdown or transition to a highly conducting double-injection state. The threshold field in this model was calculated to be about 10^8 V/m which is greater than that observed in chalcogenide films. Moreover, this model is in no way based on the mobility gap structure for an amorphous semiconductor as described in the CFO model, and, therefore, it could be applicable to the case of crystalline semiconductors.

Although some electrode materials may form a narrow insulating layer, e.g. an oxide layer, with chalcogenide glasses, it is unlikely that all materials used in these devices do that. This model also implies a strong polarity-dependent delay time.

A switching model which assumes the presence of poor electrical contacts and a semiconducting film described by the CFO model, was proposed by Iida and Hamada (1971). In their model, carriers enter the bulk region by tunnelling through the insulating layers and fill the carrier traps present in the bulk. As the

voltage is increased, injection is increased and the resistance of the bulk decreases. This leads to an increase in the voltage drops across the insulating layers and the instability that follows is similar to the one described by Schmidlin. It is also suggested that if the injected electrons in localized states in the energy gap have a long relaxation time, the bulk region would remain in the high conductance state for a long time after the removal of the applied voltage. The device in this case would behave as a memory element which can be removed by inverting the applied pulse. However, this suggestion, and the presence of insulating layers, implies very strong polarity dependence in conflict with experimental observations. Moreover, the threshold field is again of the order of 10^8 V/m which is much larger than is observed.

Mathis (1969) developed a switching model in which the basic assumption is that the activation energy, which determines the concentration of mobile carriers, decreases with increasing concentration of carriers. Therefore, by assuming that excess carriers are generated by Zener tunnelling, an effective reduction of the mobility gap is produced. The decrease is caused by the delocalization of states near the equilibrium mobility gap due to screening by the excess carriers. Mathis was able to show that at a certain critical field the concentration of carriers is sharply increased and the I-V characteristics show a negative resistance region. This model exhibits a sharp conductivity discontinuity, at which point the mobility gap collapses and the material becomes essentially metallic. This behaviour is similar to the non-metal-metal transition in V_2O_3 (Adler et al, 1967). The independence of the minimum on-state holding voltage on film thickness is not easily explained in terms of Mathis's model.

To explain the switching process, Heywang and Haberland (1970) have used the potential fluctuation model. They stress that the injected electrons fill predominantly positive traps along the electron percolation paths and injected holes fill their respective traps along the hole percolation paths. This results in levelling and decrease of the potential fluctuation and thus an increase in mobility and a widening of the percolation paths. Double injection is facilitated and the feedback mechanism required for the high conductance on-state is thus provided. A minimum charge of the order of 10^{-10} C is required to initiate the feedback mechanism.

Zener breakdown is ruled out by Adler (1972) who holds the view that at an applied field of 10^7 V/m the Zener tunnelling rate is likely to be smaller than the recombination rate and, in addition, Zener breakdown is not usually characterized by a large negative resistance region.

Van Roosbroeck (1972) proposed a model in which he took the view that the relaxation time is long compared to the carrier lifetime, in which case a large space-charge region exists near an injecting contact. As the applied voltage is increased, the space-charge region grows out towards the other electrode, leading to a sharply increased field across the remainder of the material. Breakdown of this high-field region can induce the on-state.

Finally, hot-electron effects will now be considered. To begin with, an electric field applied across a device accelerates any free electron present in the material. If the particle acquires sufficient energy it can liberate another electron by collision with an atom and remain free. This is called impact ionization and is known to occur in crystalline semiconductors. In opposition to the occurrence of impact ionization events are recombination mechanisms which also include non-equilibrium trapping of carrier and loss of electron energy to the ion cores by phonon emission, thus preventing the electron temperature from rising above that of the material. However, when the applied field is large, $\approx 10^7$ V/m, thermalization, i.e. loss of electron energy cannot take place fast enough to keep the carrier at ion core temperature and the electrons become 'hot'. Eventually a chain reaction of impact ionization occurs resulting in avalanche breakdown.

Avalanche breakdown is likely to occur when the initial free electron density in the semiconductor is low. But when the electron density and electron-electron collision rate are sufficiently high, collective breakdown is likely to take place as a result of energy exchange in electron-electron collisions being greater than that in electron-phonon interactions.

Adler (1970) has argued that avalanche breakdown is an unlikely mechanism for switching in chalcogenide glasses. His simple calculation showed that a carrier must survive an average of 100 collisions without significant loss of energy in order for a single impact ionization to take place. However, Hindley (1970a)

has suggested that hot electrons are possible in chalcogenide glasses even at fields of 10^7 V/m, since most of the collisions that limit the mean free path are elastic. Hindley (1970a, 1970b) and Mott (1971) estimated the critical field beyond which the mobile electrons gain energy from the applied field at a rate faster than they lose it via phonon emissions. Beyond this critical field avalanche occurs resulting in a conducting plasma which can be sustained by the fields near the electrodes. The critical field is approximately given by Mott as:

$$e u F^2 = h \omega_p^2$$

where $h \omega_p$ is the energy of the phonon involved. For a phonon energy of 0.030 eV and mobility $\mu \simeq 3 \text{ cm}^2/\text{V}$, a critical field of about 3×10^7 V/m is obtained which is in very good agreement with experimental values.

The estimate of the critical field by Mott leads to a threshold field which is nearly independent of temperature. This is observed at low temperatures (Buckley and Holmberg, 1972). Mott has also pointed out that avalanche production of secondary carriers in amorphous semiconductors differs in a significant way from that in crystalline materials. The mobility of the carrier always increases with energy above the mobility edge so that an avalanche should be produced if once the rate at which the electron gains energy from the field exceeds the rate of energy loss to the phonons.

Hot-electrons effects were recently discussed in a review article by Owen and Robertson (1973). They pointed out that collective breakdown was not likely to initiate switching in chalcogenide glasses in view of the fact that the electron density in chalcogenide glasses is at the most 10^2 times greater than the low-field density as shown from the preswitching I-V characteristics. Also, Stratton's calculations (1961) show that the electron current density necessary for collective breakdown is $10^3 - 10^4$ times greater than the low-field density. However, in the case of avalanche breakdown, there are some experimental observations regarding the statistical nature of the delay time and current noise that indicate the existence of hot electrons in the vicinity of the threshold field, but comparison with well understood results obtained from work on silicon junctions indicates that they are not the main cause of switching in chalcogenide glasses.

None of the electronic switching models discussed make any quantitative predictions about the on-state parameters - the holding current and the holding voltage. In general, it is stated (Henisch et al, 1970) that the holding current is the minimum current needed to keep the traps filled, and the holding voltage provides the field that maintains the current injection process. The magnitude of the holding voltage is given as being equal or slightly greater than the mobility gap.

Electronic models have one common feature with thermal models in that they also postulate a filamentary on-state. Current filaments of electron origin have been observed in crystalline semiconductors by Barnett et al (1968), but this does not necessarily prove that current filament in chalcogenide glasses originate from electronic processes. In addition, an electronic switching mechanism can lead to a thermal on-state current filament.

Mott (1971) points out that in the case of electronic switching, the on-state current filament warms up after switching and the temperature distribution across the filament is more or less uniform. While in thermal switching, a hot thin filament is first formed at the moment of switching and then in the on-state the filament broadens and the centres cools while its outer part warms up. Mott also suggested that a measurement of the change in temperature of the hottest part of the channel with time after threshold switching could provide a test whether switching is electronic or thermal. In the author's view such a measurement does not necessarily reveal the nature of the breakdown mechanism since some authors (Boer et al, 1970) predict that electrothermal effects can lead to electronic switching and therefore cooling of the central part of the filament could occur after switching.

Owen and Robertson (1973) have estimated the diameter of the filament to be 3 - 10 μm for an on-state current between 1 mA and 1A.

2.5 Thermal Switching Models

The thermal switching model is the most popular amongst the various models developed to explain the switching phenomenon in chalcogenide glasses. Electro-thermal effects in solids have a long historical background dating back to the eighteenth century (Van Marum, 1799, Fourier, 1892). In fact, the results of some of

the calculations used at present have been known since the Franco-Prussian war.

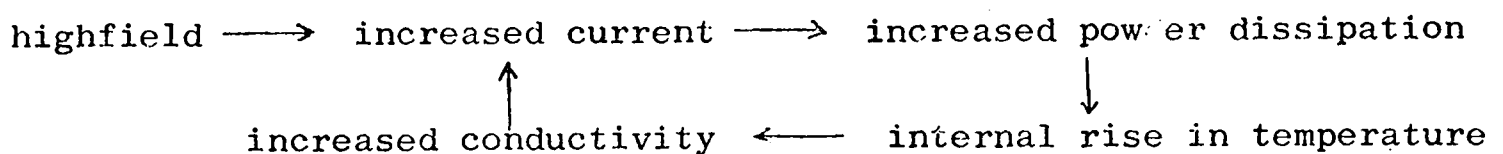
The model is essentially a quantitative one which in principle can account for the negative resistance region, delay time and filament formation in switching devices.

All thermal breakdown phenomena are governed by the heat balance equation:

$$\nabla \cdot (k \nabla T) + \sigma E^2 = C \frac{\partial T}{\partial t}$$

where T is the temperature, E is the electric field, C is the specific heat per unit volume, and k and σ are the thermal and electrical conductivities. The second term on the lefthand side of the above equation represents heat dissipation, while the first term represents cooling, and the term on the righthand side is associated with time changes in heat stored in a unit volume.

Thermal breakdown is caused by Joule self-heating of the material when the heat generation exceeds the cooling term in the above equation. This lead to an increase in the device-material temperature which in turn increases the temperature-sensitive electrical conductivity. The positive temperature coefficient of conductivity results in an increase in current and so on until breakdown occurs and a low-resistivity state is achieved. For current-controlled negative resistance to occur a feedback loop (Owen et al, 1973) must be present and this loop could be represented as follows:-



Although the physical principles of thermal breakdown are understood, mathematical solution of the heat balance equation has required the introduction of various simplifications and assumptions which have resulted in a large number of publications. Before outlining and discussing some of the proposed thermal models, it is worthwhile pointing out that:

- (a) the majority of the published and reported works have so far concentrated on the off-state behaviour and very few of them extend the calculations to cover the entire switching cycle,

(b) In all of the thermal calculations, the authors have made at least one of the following assumptions:

- (i) A uniform temperature distribution exists throughout the material. This is not an unreasonable assumption to be made for the off-state but this cannot be the case when the device is in the on-state as shall be seen in the next section where the on-state is discussed.
- (ii) The electric field is constant throughout the material. Again, if (i) is feasible during the off-state part of the switching cycle, then this assumption is also valid.
- (iii) Heat flows only parallel to the current flow. This leads to a high temperature at the centre of the device.
- (iv) Heat flows only perpendicular to the current flow. This leads to a uniform temperature along the device axis.
- (v) Terms are used in which the electrical conductivity is some function of temperature and field, or merely of the form $\sigma \propto T^n$.

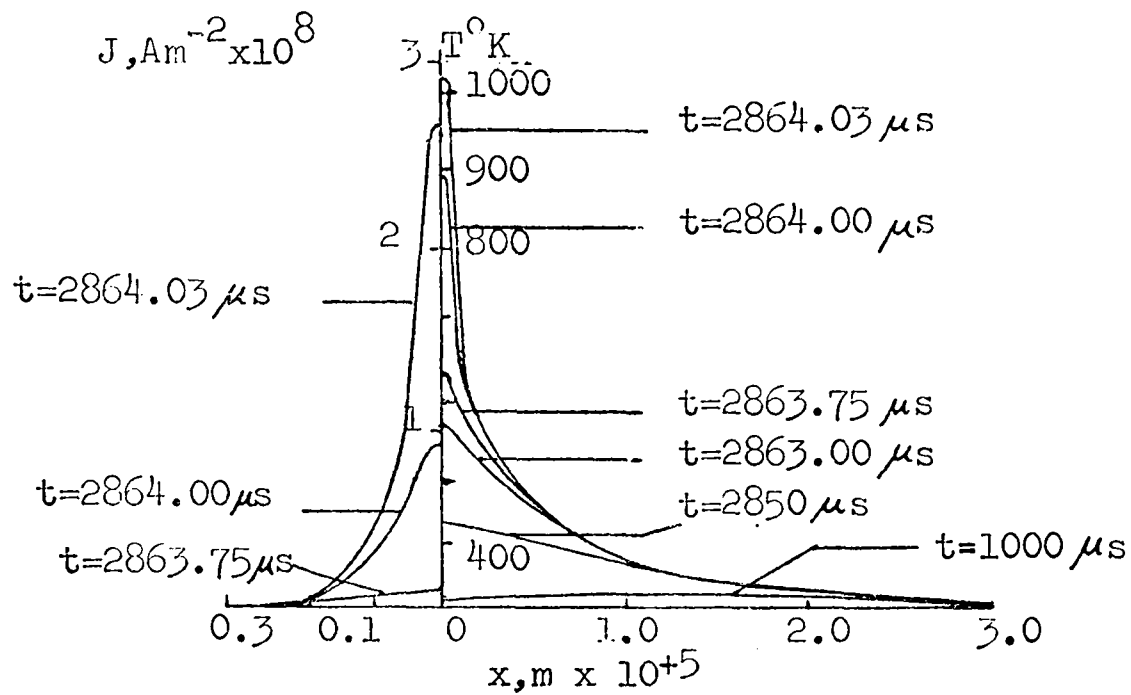
The various calculations of Warren, Male and Thomas (Warren, 1969a, 1969b, Thomas and Warren, 1970, Male, 1970, Warren and Male, 1970, Warren, 1970) will now be considered and discussed in some detail and afterwards other workers' proposals will be reviewed and compared whenever possible.

Warren (1969a) considered a slab of material with infinite Y and Z dimensions and of thickness 2a in the X-direction and having a uniform field applied in the Z-direction, the faces at $X = \pm a$ kept at fixed temperature T_a . The one-dimensional heat conduction equation is:

$$k \frac{\partial^2 T}{\partial x^2} + E^2 \sigma(T) = \rho c \frac{\partial T}{\partial t} \quad \text{--- (1.1)}$$

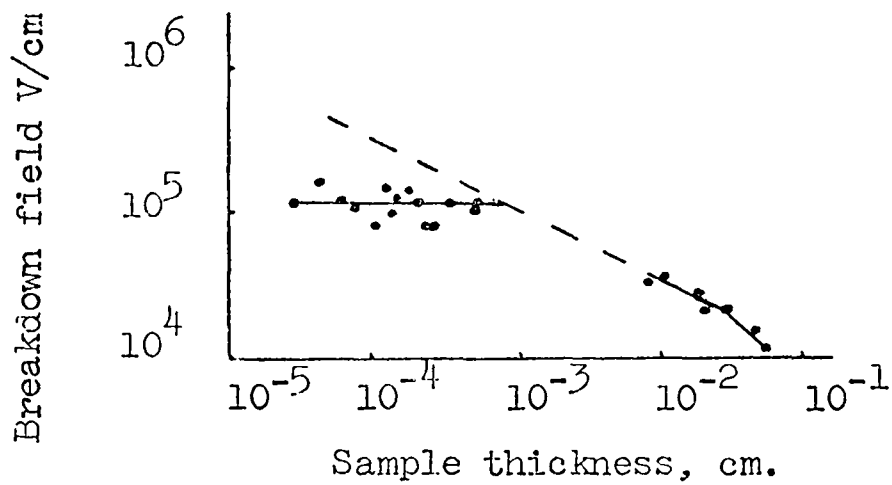
where ρ is the glass density. This equation was then solved numerically for a material with $\sigma = 1.245 \times 10^3 \exp(-u)$ where $u = \Delta E / 2kT$ and $\Delta E = 1 \text{ eV}$. The boundary conditions were $T_a = 300 \text{ K}$ and $\frac{\partial T}{\partial t} = 0$ (at $x = 0$) for all t .

Figure 2.11 shows the variation of temperature T and current density across the slab at various times after applying a field of $5.9 \times 10^7 \text{ V/m}$. From figure 2.11 and further calculations, it was shown that:



Temperature and current density within the slab at various times after the application of electric field of $5.9 \times 10^7 \text{ Vm}^{-1}$. (Warren, 1969)

Figure 2.11.



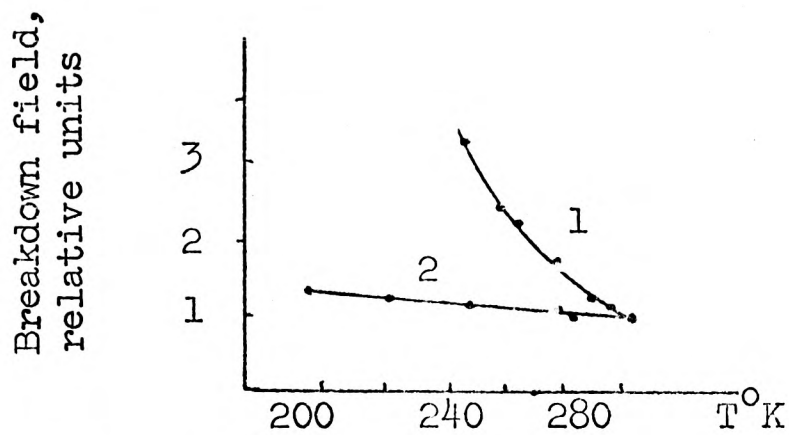
Dependence of the breakdown field on the sample thickness (Kolomiets et al, 1969).

Figure 2.12.

1. The waiting or delay time is about 2 ms.
2. The switching time is about 0.25 us.
3. After switching the current flows into a hot filament.
4. Switching occurs once the temperature of the material exceeds the ambient temperature by about 20 k.

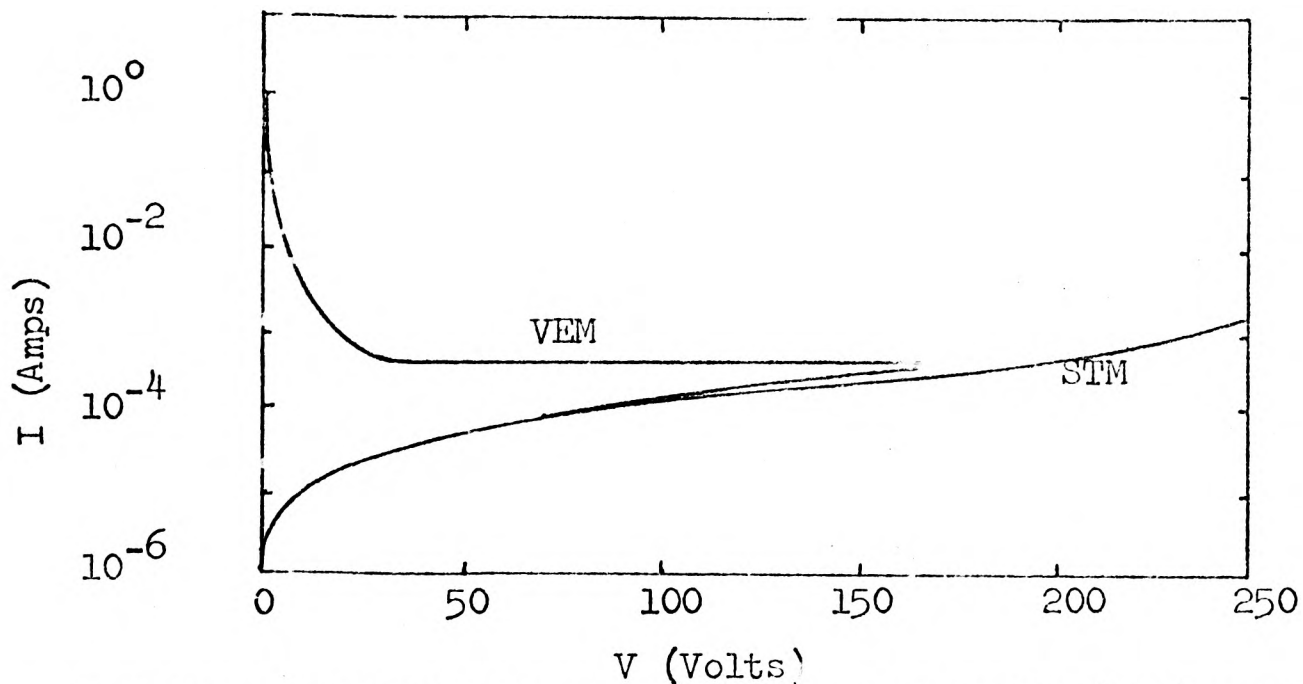
Calculation of I-V characteristics in the preswitching region were then made for two cases of heat flow (a) heat flows parallel to the current (O'Dwyer, 1964) and (b) heat flows perpendicular to the current. For case (b) the value of the breakdown voltage, ~ 16 volts, obtained was more realistic than that obtained for case (a), ~ 2900 volts, and comparable with experimental observations. It was also shown that the I-V characteristic, solved for case (b), consisted of a linear region at low fields followed by a non-linear region at higher fields. The non-linear region was terminated at lower values of applied voltage than those reported by Walsh et al (1969). This discrepancy was attributed to the cooling effect of the electrodes which was not taken into account in the calculations. However, several authors have reported certain observations in chalcogenide films which the model discussed above does not explain. Some of the observations are:

- (i) Kolomiets et al (1969) have shown from a plot of switching field against film thickness, figure 2.12, that below a certain thickness, $\sim 10 \mu\text{m}$, the threshold field was less dependent on film thickness, whereas the thermal model predicts the relationship $E_c \propto d^{-1/2}$. Differences in behaviour between thick and thin films have also been reported by Burton and Brander (1969), Stocker et al (1970) and Thomas et al (1972). Kolomiets' work has also shown that the breakdown field for thin films, figure 2.13, is weakly dependent on ambient temperature, but the thermal model predicts a temperature dependence of the form $E \propto T_a \sigma_a^{-1/2}$ which is not supported experimentally.
- (ii) The delay time was found by Csillag (1970) to be an exponential function of applied field while the thermal calculations of Collins (1970) suggest that the delay time is approximately proportional to E^{-2} .
- (iii) Experimental measurements (Walsh et al, 1969, Fagen and Fritzsche,



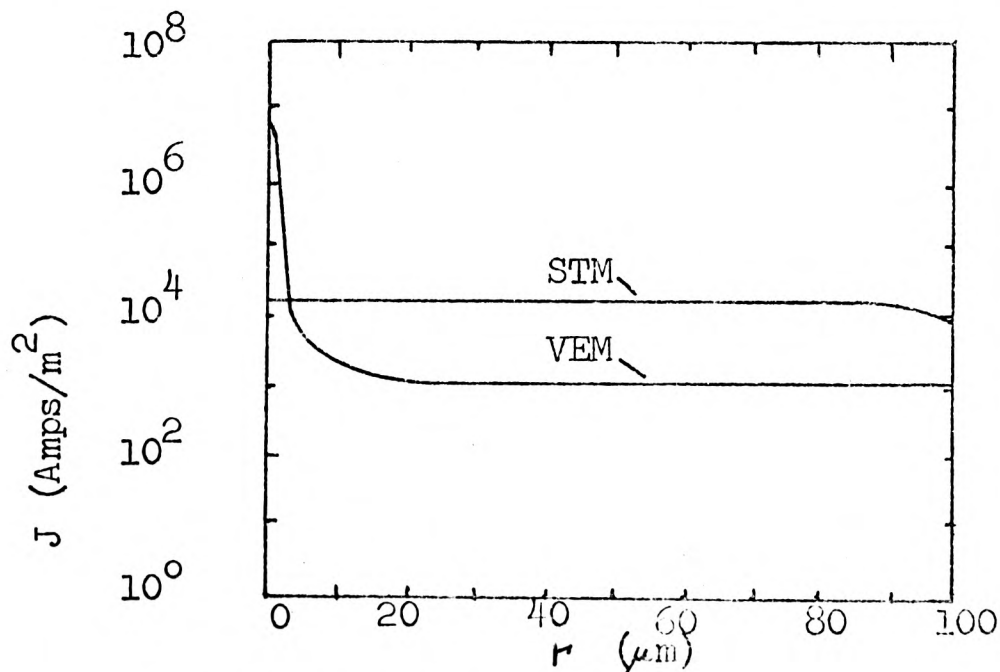
Temperature dependence of breakdown field for samples of two thicknesses d (μ); 1) 300; 2) 2. (Kolomiets et al, 1969)

Fig. 2.13



I-V Characteristics for standard thermal model (STM) and virtual-electrode model (VEM) (Kaplan and Adler, 1971).

Fig. 2.14



Current density as a function of radial distance perpendicular to the axis of a cylindrical switching device for the standard thermal model (STM) and virtual-electrode model (VEM). The VEM curve indicates filamentary current flow. (Kaplan and Adler, 1971).

1970, Hall, 1970) have shown that the preswitching non-ohmic regions consists of two distinct parts; one part which could be accounted for by thermal effects as discussed earlier, and a second part which seemed to be strongly field-dependent.

To accommodate these discrepancies, Warren and Male (1970) used the expression:

$$\sigma = \sigma_0 \exp\left(\frac{F}{F_0} - \frac{\Delta E}{2kT}\right) \quad \text{--- (1.2)}$$

for the electrical conductivity of the material where $F_0 = CT$ and $C \sim 2 \times 10^4 \text{ V m}^{-1} \text{ K}^{-1}$. In thick films, $\sim 100 \mu\text{m}$, the temperature drop is mainly in the bulk of the material, $E_c \propto d^{-1}$, and field dependence of σ is negligible. In thin films, $< 10 \mu\text{m}$, the temperature at the electrodes is comparable with that in glass and E_c then becomes proportional to $d^{-\frac{1}{2}}$.

It was also shown that under certain conditions the breakdown field became thickness independent, and a relationship for the delay time:

$$t_d \propto E^{-2} \exp\left(-\frac{E}{E_0}\right)$$

was obtained which satisfies experimental observations.

Therefore, the use of a field-dependent expression for the electrical conductivity produces solutions which are in close agreement with experimental observations.

Warren et al (1969b) maintained that a transverse heat flow was essential for current filament formation. Other calculations took the problem of a thin film with heat flowing towards the electrodes parallel to the current. An assumption of this kind has been made by Sheng and Westgate (1971) and Chen et al (1970).

Sheng and Westgate used a similar expression to equation (1.2). Their calculations were based on the existence of a critical temperature at which switching took place as postulated by Holmstrom (1969). These authors neglected the time dependence and considered only heat flow parallel to the current flow. Their results predicted a maximum temperature rise of 35 K in the glass at threshold.

In their paper, Chen and Wang (1969) calculated an expression for the threshold field, E_c . Their expression showed that:

1. At a high ambient temperature T_a , E_c is exponentially dependent

on T_a , but the dependence is linear at lower T_a .

2. E_c remains constant for thin films but decreases rapidly for increases in film thickness for thick films.

At threshold the temperature increase is about 15 K which is only a few degrees lower than that found in Warren's model. However, in the on-state their calculations give the temperature of the material to be about 480 K which is considerably lower than that predicted by Warren, Thomas and Male; but it must be pointed out that temperatures found in time dependent calculation are not those of a steady on-state, and the steady state calculations of Warren et al are unrealistic. Further differences between the types of calculations will be discussed in the section dealing with the thermal on-state but it is worthwhile mentioning here that Chen and Wang predicted a first-fire threshold voltage which is considerably larger than the subsequent threshold voltages and this is observed experimentally.

The time-dependent analysis of thermal breakdown was attempted by Burton and Brander (1969). These authors have shown experimentally that thick devices could have delay times of many seconds while thin films exhibited typical delay times of a few microseconds. Therefore, for thick samples they assumed a steady situation where heat input balances heat loss and they solved the one-dimensional heat balance equation. For thin samples, it was assumed the process is entirely adiabatic and this should result in the fastest possible thermal switching time. Their calculations for thick samples showed good agreement with experimental results, but this was not the case for thin films. They concluded that switching was possibly non-thermal in thin films.

Numerical solutions of the time-dependent heat balance equation were also obtained by Thomas and Male (1972) for STAG glass whose low-field conductivity had been experimentally determined. Their calculations included the cooling effect of the electrodes. They considered a 60 μm thick semi-infinite slab with boundaries at two sides kept at ambient temperature and an electric field applied to the slab faces. The forms of the current and temperature distributions were found to remain relatively uniform until a critical field was exceeded after which the current was channeled

into the region of the central plane. When the field was about 5.9×10^7 V/m, the current increased by two orders of magnitude in 100 psec while the central temperature rose from 750 K to 1000 K. Two-dimensional solutions were also obtained for a cylindrical block geometry where the heat flow was considered simultaneously in both parallel and transverse directions to the current flow. For a large enough field a current channel was formed with its hottest point at the centre of the block. The central hot region then split into two hot spots which grew and moved out along the axis towards the electrodes, while the channel cross-section close to the electrodes remained considerably constricted. Although their calculations show that a current filament can be formed in a very rapid time, it was suggested that field enhancement of conductivity at very high temperature may be necessary for the prediction of the very fast switching time, 0.15 μ s, observed experimentally. However, if the latest and higher values of $\sigma(T)$ of the material (Baker and Webb, 1974) are used, very high temperature and field enhancement of the conductivity are not necessary.

In addition to the temperature dependence of the material conductivity, thermal breakdown depends to a large degree on device geometry which determines the thermal boundary conditions. All the thermal calculations discussed above deal with device geometries which are essentially of the sandwich-structure type. Croitoru and Popescu (1970a, 1970b, 1972, 1973) presented calculations which deal with a co-planar or gap device and it was suggested that the expression they obtained can be applied to sandwich structures. In their early work (Croitoru et al, 1970b) they analysed switching in terms of electrical and thermal circuits and stated that the temperature of the current filament must not rise to an extent which could cause structural changes and prevent further switching; in fact, the predicted increase in temperature was given to be about 60 K above ambient, but their more recent publications consider crystallization of the material and maintain that lateral thermal instability is essential for very fast switching. They also use the concept of lateral thermal coupling and argue that a uniform current distribution may collapse into a current filament at some point on the negative resistance region of the current-voltage curve of the switching device which depends partly on the extent of lateral thermal coupling within the sample. For low

thermal coupling the channeled current may drop initially then rise again at lower voltage in the high conductance on-state.

Thermal models in which the conductivity is assumed to be a function of temperature and field are sometimes referred to as electro-thermal models. Falling in this category are also calculations which consider the preswitching region in terms of Joule heating which can initiate electronic switching. An analysis of this kind was made by Boer and Ovshinsky (1970) and Boer (1970a) where they suggested that thermal effects provoked electronic switching by double tunneling. They also considered the effect of a field-dependent conductivity on preswitching behaviour. However, they inserted the field-dependent term after solving the heat balance equation and this, as pointed out by Warren and Male (1970), does not allow a full discussion of the transition to the anomalous thin film-regime. According to their calculations the temperature of the current filament is about 1600 K at the end of the switching transition in a DO-7 device and 1000 K in the pore-type of devices. Such a high temperature was considered by them to be "too large to be maintained in the glass without destruction", therefore, it was concluded that during the switching transition the conduction mechanism underwent a change, thermal to electronic, (Boer, 1970b), resulting in a large increase in conductivity, possibly by narrowing the effective band gap. The switching branch, which follows the load line, terminates when either (a) the field drops below a critical value or (b) when the power dissipation decreases and reduces heating in the device. In the on-state the current density is about 10^6 A/cm² which requires a field of about 10^8 V/m near the electrodes to maintain current continuity by tunnelling through ~ 0.5 eV barrier. Such a high field, it is suggested, could be provided by a non-uniform temperature distribution in the glass with the temperature being highest in the centre and coolest at glass/electrode interface. Again, the temperature of the device material depends on the assumptions made for $\sigma(T)$. As pointed out earlier, temperatures of 1000 K or 1600 K may not be necessary if the latest values of $\sigma(T)$ (Baker and Webb, 1974) are considered.

The nature of the assumptions made in thermal calculations affect the predicted device behaviour in significant qualitative

ways. Kaplan and Adler (1971) have shown that, if none of the assumptions listed at the beginning of this chapter is made and no heating of the electrodes takes place, i.e. the electrodes are perfect heat sinks, solution of the steady-state problem leads to (a) the current expressed as a monotonically increasing function of the applied voltage, i.e. there is no negative resistance region, and (b) there is no current filament. These results are shown in the curve labelled STM-standard thermal model in figure 2.14. On the other hand, when a virtual-electrode model - VEM - is employed, both a negative resistance region and current filament are found as shown in figures 2.14 - 2.15. The virtual-electrode model assumes that each electrode is displaced a small distance inside the active material to produce effects equivalent to one or two possible electronic mechanisms - space-charge injection or narrow Schottky barriers. Therefore, the implication is that a pure thermal model, in the absence of electrode heating, is incapable of predicting switching behaviour unless some electronic effects are explicitly introduced.

Field-enhanced conductivity of the form

$$\sigma = \sigma_0 \exp\left(\frac{E}{E_0} - \frac{\Delta E}{kT}\right)$$

can predict negative resistance and current filament when used in pure thermal model calculations because, it is suggested, it contains electronic effects.

It is felt by the author that there is no justification for assuming that no heating of the electrodes occur. Moreover, Main (1974) has recently reported that a liquid crystal decoration technique shows that heating of electrodes does actually take place and the electrode temperature is about the same as that of the active glass. Kaplan and Adler (1971, 1972) maintain that a negative resistance region is obtained in some calculations because of the nature of the assumptions made. They consider the approximation $T_e = T_a$ as an excellent one. However, it is because of this assumption they did not obtain negative resistance in the STM and this wrong assumption has led them to the wrong conclusion. In fact, displacing the electrodes a small distance into the active material means in physical terms taking the electrodes into a hotter region and allowing their temperature to rise and this is why negative resistance region is obtained in the VEM.

2.5.1. The thermal on-state

Some of the thermal models discussed above have extended

their calculations to the postswitching region of the I-V characteristics of a chalcogenide switching device. Other models (Armitage et al, 1971) attributed the breakdown process to electronic effects resulting in a hot thermal on-state.

Turning first to Warren's calculations (1969b) integration of equation(2.1) gives the following equations of the current and electric field in the on-state:

$$I_T = 2 \sqrt{\left(\frac{\sigma_0 \Delta E k}{k}\right)} \left\{ \left[E_1(u) - \frac{e^{-u}}{u} \right]_{u_0}^{u_1} \right\}^{1/2}$$

and

$$E = \frac{1}{2a} \sqrt{\left(\frac{\Delta E k}{\sigma_0 k}\right)} \int_{u_0}^{u_1} \frac{du}{u^2 \left\{ \left[E_1(u) - \frac{e^{-u}}{u} \right]_{u_0}^{u_1} \right\}^{1/2}}$$

For a film of thickness 0.5 μm , 60 μm wide and having $\Delta E \sim 1.0$ eV, mathematical manipulation of the above equations give $I_T = 2.7$ mA and $E = 0.6$ V. In earlier work it was stated that a value of $\Delta E \geq 1$ was required for very fast switching and when a value of 1.5 eV is used, $I_T = 60$ mA and the on-state voltage across the device is 0.012 which is considerably smaller than that observed experimentally, ~ 1 V. Warren concluded that the bulk of the voltage drop in the on-state occurs near the electrodes. It is also suggested that the thermal filament (Warren, 1973) is sausage-shaped similar to that observed by Haberland and Kehrer (1970) in a chalcogenide glass. The thermal conductivity of chalcogenide glasses is much smaller than that of the electrodes material, this leads to narrowing of the channel at the channel/electrode junction resulting in a high generation of heat and the temperature of the junction becomes very high. A semi-quantitative model describing the on-state was recently proposed by Male and Thomas (1974) and will be discussed in Chapter 5.

The on-state described by Chen and Wang (1970) has somewhat different dynamics. As stated earlier, in the above models the temperature of the filament is about 1000 K while Chen and Wang give the temperature of the material in the on-state to be about 480 K. Although it is suggested that the on-state current might be channeled, it is not shown how such a channel is formed. They derived

the following expression for the holding voltage:

$$V_h = \sqrt{\frac{A R_L k_1}{d}}$$

where k_1 is a constant, A is the lateral dimension of the film, and d is the film thickness such that $A \gg d$.

This expression implies the following:

1. The holding voltage is independent of ambient temperature,
2. The holding voltage increases as the external resistor increases,
3. The holding voltage increases as film thickness decreases. This is not observed experimentally, but data on holding voltages for very thick films, $\gg 100 \mu\text{m}$, to the author's knowledge, has not been reported,
4. The holding voltage depends on the electrodes contact area with the film which again is not observed experimentally and incompatible with a filamentary on-state.

The analysis of Kroll and Cohen (1972) shows that at some point on the negative resistance region of the I-V characteristic for uniformly distributed current, the current distribution becomes unstable against collapse into a filament. In their analysis of a channeled current flow, the temperature along the axis was assumed to be uniform, a single heat transfer coefficient represented the cooling effect of the electrodes at all points within their device. Their calculations took special account of the rise of thermal conductivity of the glass with temperature. This reduced the filament axial temperature and flattened the radial temperature profiles near the axis relative to the profiles that would have been obtained had they assumed a constant thermal conductivity as other authors assumed in many cases. The rise in the channel central temperature for a current of 65 mA was about 500 K above ambient and this dropped to about 10 K at a radius of 2 μm . Considering the magnitude of this current, a temperature rise of about 500 K is rather small. In addition, their derived on-state characteristics show a qualitative as well as quantitative difference from experimentally obtained characteristics of typical thin film devices. These differences are (a) a minimum holding voltage drop of less than 0.4 V whereas in real devices this value

lies between 0.5 V and 2 V depending on the electrode material (Ovshinsky et al, 1973), (b) a differential negative resistance up to a current of 1 A, whereas real thin film sandwich devices show a positive differential resistance beyond a current of a few mA, and (c) in real devices the major part of the on-state voltage drop is found to occur near the electrodes, but in this model the field is constrained to be uniform.

2.5.2. Observations of on-state filaments

It was shown by Ridley's thermodynamic arguments (1963) that CCNR always leads to formation of current filaments. This result is frequently used to support other arguments concerning the formation of filaments in chalcogenide switching devices. Owen and Robertson (1973) point out that Ridley's model for S-type CCNR predicts the initial formation of current filament before the occurrence of switching and afterwards the filament diameter expands as the current increases until, at the end of the negative resistance region, the filament area fills the entire *actual* area. Although the initial formation of a current filament has not, as yet, been satisfactorily treated and there is still a lack of experimental evidence regarding filament formation prior to threshold conditions, it is conceivable that, if one accepts the existence of filament constrictions at the filament/electrode interface the constriction limits the spread in filament area near the devices electrodes.

A direct observation of current filament in sandwich structure type of devices is rather difficult, although liquid crystal decoration techniques, have been used by several workers (Feldman et al, 1970, Bunton, 1972) to investigate thermal effects and filaments in them. However, current filaments in gap devices have been observed and reported by several researchers. Pearson and Miller (1969) filmed evidence for liquid phase in 10 μm film of $\text{Te}_2\text{As}_2\text{Se}$. Weirauch (1970) examined a high bulk gap ($\sim 2 \mu\text{m}$) device of amorphous $\text{Se}_{50}\text{Ge}_{30}\text{As}_{20}$ with an infra-red viewer and observed a bright filament whose emitted radiation was equivalent to

a black body at 900 ~ 1100 K when the sample was switched at an ambient temperature of 548 K. Similar observations in wide-gap devices were reported by Stocker (1969, 1970). In all these observations the on-state currents were rather large and one could argue that thermal effects were caused by the relatively high currents. However, Armitage et al (1971) observed melting of the filament when the maximum current was even lower than the holding current. The investigation was carried out on a 1 μm gap sample of STAG glass with ^ascanning electron microscope and ^{an}optical microscope and melting of the gold electrodes was observed. The damage at the anode electrode was greater than that observed at the cathode and a switching model was developed by them to explain the observed phenomenon.

2.5.3. Diameter of conducting filament

This has been dealt with in the various papers of Schuoker (1971, 1972). He considered the voltage across a glass switch in the on-state to be made of three portions in series (i) the voltage across two current constrictions in the electrode which are caused by the large ratio between the diameter of the electrode and the channel (ii) the voltage drop near the electrodes that allows the injection of carriers and (iii) the voltage across the channel. By carrying out experiments on a thin film of As-Te-Ge-Si glass switch using a fast rising square current pulse applied to the switch in the on-state and measuring the initial increase and subsequent decrease in V_h and then making use of Holm's (1967) formula:

$$R = \rho_e / 2r$$

where R = constriction resistance, ρ_e is the specific resistance and r is the channel radius, Schuoker calculated a channel diameter of 2.15 μm . This author has also noted that his result was much greater than the 1 μm channel diameter at a current of 1 mA suggested by Boer et al (1970) and attributed this to the possibility that a current channel inside a hot filament may have a much smaller diameter than the filament diameter. It must be noticed that the

calculations of Schuoker were not based on a thermal on-state model.

Finally, there are several arguments against a purely thermal mechanism initiating threshold switching in chalcogenide glass switching devices. Some of these arguments are:

1. The thermal theory predicts breakdown in all semi-conducting materials which have a suitable activation energy and whose conductivities rise quickly with temperature. However, in crystalline materials the hot thermal channel could cause permanent material damage and reversible switching will not take place. This point emphasises the importance of understanding the on-state conduction mechanism which could distinguish between switching and ordinary breakdown.
2. Henisch has observed some polarity effects using asymmetric electrode materials. However, Male and Thomas (1974) have pointed out that the hot on-state filament/electrode junction could give rise to thermo-electric contribution to the energy and voltage distributions. The absence of quantitative data on the thermo-electric coefficients at high temperatures, ≥ 1000 K, makes quantitative estimates difficult to obtain. Warren (1973) suggested that the electrical conductivity may possibly be polarity dependent and some degree of ion conduction present in the material. but there is no evidence for this and the possible explanation given by Male and Thomas is more plausible.

2.6. Phase-Change Models

It is known that the electrical conductivities of chalcogenide glasses (Male, 1970, Baker et al, 1974, Fritzsche, 1971) can increase by several orders of magnitude on either heating to high temperatures or crystallization. Crystallization in switching devices is likely to take place readily when the chalcogenide glass composition corresponds to a point near the boundary of the glass forming region in the phase diagram.

Several authors have attributed switching to structural or

phase changes in chalcogenide switching devices. An early report on the observation of structural changes was made by Eaton (1964). He showed that during the operation of a device joule heating was sufficient to allow a phase change to take place in As-Te-I glass, producing regions of high-conductivity material between the electrodes. The transformation from one resistance state to another in a switch was the result of the thermal breakdown of the material, where either a high-resistance glass phase or low resistance crystalline phase could be obtained by rapid or slow cooling.

Switching caused by a phase change or structural change implies a mass transport process which has to be extremely fast to explain the very fast switching times which have been observed. Pearson, (1969, 1970) has suggested that the fastest speed with which a phase change can travel through a material is the speed of sound in that material. Pearson suggested that a figure of 4000 m sec^{-1} was not unreasonable. Therefore, for a chalcogenide film of one micron thickness, a calculated time of 250 psec could be obtained for a phase-change front to travel through the sample from one electrode to the other. However, if the phase change fronts grew simultaneously from many nuclei already present in the glass then this could have the effect of considerably reducing the calculated switching time.

Stocker (1970) proposed a model to explain fast threshold switches which can be summarized as follows:

- (a) After the application of an electric field, local devitrification was produced by heating and once nucleation took place the new phase front then travelled very rapidly with the speed of sound and produced a filamentary path of devitrified material.
- (b) The current then increased further until it was limited by the load resistor or the resistance of the structure. The filament in the on-state consisted of molten glass at high temperature.
- (c) At switch-off, the molten filament cooled very rapidly so that a transformation occurred to a glassy rather than a phase separated state. This model explained forming, i.e. the reduction in threshold voltage of a device that was operated several times, in terms of the occurrence of crystallization at the electrodes after switch-off. Also, memory effects resulted from the slow cooling of the molten filament. It is

not clear why cooling in memory devices should be slower than in threshold devices since it is expected that threshold and memory devices, of similar geometry, have similar thermal properties, i.e. similar thermal conductivities and heat capacities. In addition, one would expect the cooling rate to be fastest at the electrodes and it is not made clear why crystallization in this case should occur near the electrodes and not in the centre of the device.

Pinto (1971) has found that heat treatment of certain chalcogenide glasses, in the Ge-As-Se system, did not cause crystallization of the glass. His heat treatment included heating the glass to a temperature of 550°C. Differential thermal analysis of these glasses did not show crystallization peaks (Pinto et al, 1971). Therefore these observations led this author to the conclusion that memory action in chalcogenide devices was caused by a field-induced phase transition possibly of the Mott type of insulator-metal transition (Mott and Davies, 1968) or the type proposed by Mathis (1969).

It is difficult to see why in the above model the combined effect of field and temperature on phase-changes was not considered. The effect of electric field on phase separation in oxide glasses has been demonstrated by De Vekey et al (1970) and Andreeva et al (1971). De Vekey found that when two similar cast slabs of a $\text{CaO-SiO}_2\text{-Al}_2\text{O}_3\text{-MgO-TiO}_2$ glass were placed in a furnace and an electric field applied across one slab and the temperature raised to just below the transition point of the material, the sample with the applied electric field showed a concentration of well formed nuclei of moderate size on examination, while the other sample showed only a few sporadic discontinuities.

Theoretical considerations of the effect of electric field on nucleation kinetics have been published by Kashchiev (1972). It was predicted that if a spherical cluster was formed in a spherical system which was much larger in volume than the cluster, then the electric field either stimulated or inhibited the cluster formation depending on whether the cluster's dielectric permeability was smaller or larger than that of the surrounding system. If the permeability of the newly formed phase, or cluster, was less than that of the older phase of the system, the electric field stimulated the nucleation while in the converse case it inhibited the process.

Another publication which suggested that switching in chalcogenide glass may be associated with a field-influenced dielectric phase transition is due to Walsh et al (1969). These authors showed that threshold voltage of a chalcogenide switching device extrapolated to zero at a temperature in the vicinity of 500 K for films made from Te-As-Ge-Si-Ga glass. They predicted that in a given film there was one transition temperature which played a central role in the conduction and switching mechanisms. When the material was at a temperature below this transition temperature the material was in a high resistive state and above it in a high conductive state. The reduction in threshold voltage with temperature increase was interpreted as due to a decrease of the transition temperature caused by the electric field. This field-influenced reduction was about $1.4 \text{ K v}^{-1} \text{ cm}^{-1}$ when the contact loading on the film was about 70 gm. The phase transition involved could be a dielectric phase transition.

The transition temperature of the thin films was found to coincide within experimental error, with the glass-transition temperature (500 K) of the bulk material from which the films were prepared.

Perhaps the most detailed study of structural changes in chalcogenide switching devices has been the research work of Bosnell et al (1972a, 1972b, 1973) who also proposed a qualitative switching model based on the structural changes observed by them. They stated that breakdown stabilization in thin chalcogenide films was only attained in earlier thermal calculations (Bosnell, 1973) because the conductivity of the chalcogenide glass reached a plateau, i.e. saturated, at temperatures in excesses of 1000 K (Male, 1970). Their model involved a two-stage process consisting of thermal runaway followed by the precipitation of a conducting thermodynamically-unstable channel from the region of the hot filament. This stabilized the runaway and high temperatures were no longer necessary. A virgin, unswitched, device exhibited a forming process, i.e. a drop in threshold voltage to about one third of that of the first-fire threshold voltage after several operations, and it was suggested that during the forming process phase separation (Thomas et al, 1972) was encouraged resulting in the precipitation

of a filament of substantially different composition from its surroundings in a formed device as was shown by sophisticated electron-microscope examination of formed devices. The filament diameter was less than 5 μm and embedded in the filament were large single tellurium crystallites with their major crystallographic axes aligned in the direction of the applied electric field. The forming process was believed to have the same effect on thin films as heat treatment since phase separation was also observed after heating and annealing films. A switching device was permanently locked in the on-state when the crystallites interconnected and formed a permanent high conductance path between the electrodes. The existence of a continuous tellurium filament between the electrodes was also reported by Sie Dugan and Moss (1971). The major difference between switching and dielectric breakdown was that in the case of a switching device a highly-conducting filament of different composition was precipitated out of the material at a "well defined" temperature such as T_g .

Amorphous elemental semiconductors (Bosnell et al, 1972b, Bosnell 1973) and amorphous alloys outside the glass forming region in the phase diagram of an alloy were found to "switch" only once and the high-resistance state could not be recovered. This effect was interpreted in terms of the above model where the precipitation of the conducting phase at a critical temperature coincided with the crystallization temperature which also depended on the electrode material of the device.

Finally, one main feature of the outcome of the above investigations was the conclusion that there was no basic difference between memory and threshold switching. It was only the relative stability of the threshold material that made repetitive switching in threshold switches possible and therefore a longer on-state time was required before a threshold switch turned memory, i.e. permanently locked in the on-state.

It is felt that far too much emphasis was placed on the importance of T_g in switching devices. Calella et al (1970) carried out investigations on several chalcogenide switching devices of different but unspecified compositions to determine whether there was a direct correlation between the measured T_g and the transition

temperature obtained by extrapolation of threshold voltage-temperature graphs. No correlation was found between these two temperatures although several compositions showed a coincidence within experimental error of the two temperatures, but other materials showed a wide divergence of the two temperatures and any connection between T_g and the switching transition temperature was described as "at best indirect".

CHAPTER THREE

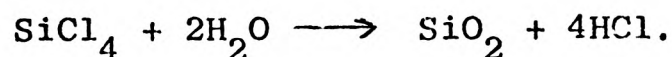
EXPERIMENTAL TECHNIQUES

In this chapter amorphous or non-crystalline solids will be used as general terms to include all solids which have no long range periodicity in the lattice which implies one or two diffuse rings in electron and X-ray diffraction. Amorphous solids can be prepared from the solid, liquid or vapour phase by processes "which essentially cause an excess of free energy or chemical potential to be more or less temporarily frozen-in to the system", (Owen, 1973). Therefore, the basic goal in preparing amorphous materials is to freeze them into a metastable state characterized by the absence of long range order. In the next paragraph the various methods, common and uncommon, for the preparation of inorganic amorphous materials will be briefly discussed.

3.1. Preparation of Amorphous Solids from the Vapour Phase

(a) Vapour phase-hydrolysis

This method represents a chemical reaction involving one or more materials in the vapour phase (Secrist and Mackenzie, 1964). The most widely known example of this method is the commercial preparation of high-purity silica glass by the vapour hydrolysis of silicon tetrachloride (Dalton, 1963). Pure SiCl_4 is made to react with water vapour formed during the combustion of an oxy-hydrogen flame and hydrolysis takes place according to reaction.



Thermal decompositions which produce glassy thin films can also be included in this method. An example of this is the decomposition of buthylborate at 700° to 900°C in vacuum to produce B_2O_3 amorphous films.

(b) Glow-discharge decomposition

Decomposition is reported (Owen, 1973) to occur at comparatively low temperature, Chittick et al (1969) described the use of radio-frequency glow discharge to deposit films of amorphous silicon from silane gas onto substrates at 25° - 650°C . The deposition rate was a few microns per hour at a

pressure of about 0.1 torr.

Mixtures of gases, e.g. silane and nitrous oxide may also be used to give SiO_2 .

(c) Thermal evaporation

This is the most commonly used technique for the production of amorphous thin films and has been reviewed in numerous articles and books on thin film preparation (Holland, 1963, Chopra, 1969, Maissel et al, 1970).

Thermal evaporation is normally carried out in a vacuum chamber at high or ultra-high vacuum and the material is heated either by an electric filament or in a boat, or by electron-beam bombardment or using an r.f. induction coil. The vapour is deposited on to a substrate whose temperature is controlled.

All evaporation plants consist of several basic elements: a vacuum chamber which is sometimes made from stainless steel in ultra-high vacuum systems, a source of material to be evaporated, a substrate, and associated monitoring equipment to control film thickness and rate of evaporation etc. Most pumping systems, except sorption and getter ion pumps, introduce some foreign materials such as hydro-carbons and mercury vapour. These contaminants, in addition^{to} atmospheric residuals, affect the purity of the deposited film and make control difficult. Moreover, systems vary in their pumping speeds for various atmospheric gases, in effect concentrating certain species which may get incorporated in the deposited thin film. There are also other deposition parameters which are not always easily controlled in thermal evaporation, viz. filament temperature, substrate temperature, size of source material.

Thermal evaporation is not generally suitable for preparation of thin films from multi-component alloys, or components, because of differential evaporation of constituents. However, a variant of thermal evaporation, known as flash evaporation may be used to give better composition control. This technique was used in the present work to prepare amorphous

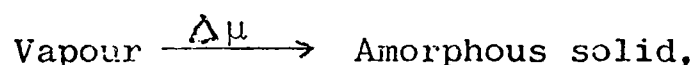
chalcogenide thin films and will be described in a later section.

(d) Sputtering

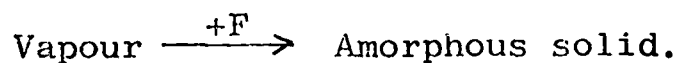
This method is frequently used to prepare commercial amorphous chalcogenide devices (Neale, 1970). The surface of the material to be deposited acts as a target which is bombarded by energetic ions. The ions can be chemically inert, or may combine chemically with the target material to give a compound deposit. For example, oxygen gas is used with a vanadium metal target to prepare vanadium oxide films.

Sputtering can be either r.f. or d.c., but d.c. sputtering is not normally used when the target material is a poor conductor or a dielectric. Most of the amorphous semiconductors being used are not sufficiently conducting for d.c. methods and r.f. sputtering is therefore normally used. Sputtered films prepared from STAG glass usually show a small increase in Te content and a loss in Si content relative to the target source material (Bosnell et al, 1972a). In addition, films from the same target material can have different compositions for different thicknesses. To compensate for the loss of Si, target materials initially richer in silicon have been used (Allison, 1972).

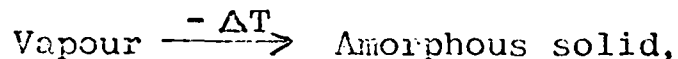
In methods (a) and (b), amorphous films are produced directly from the vapour phase. Methods (c) and (d) produce amorphous films from the vapour phase also but the starting materials are solids, which in method (c) may go through the liquid phase unless the solid sublimes. In reactive sputtering and methods (a) and (b), the thin films are produced as a result of a chemical reaction and, therefore, a change in the chemical potential (Owen, 1973). These processes can be represented by the expression:



where $\Delta\mu$ is the change in chemical potential. Non-reactive sputtering is a process where free energy is injected into the system and can be represented as:



Method (c) is simply represented as:



where F is the free energy and ΔT is temperature change.

3.2. Preparation of amorphous solids from the liquid phase

(a) Quenching of melts

The amorphous solid obtained from quenching a melt is commonly known as glass. In this method the melt is cooled at such a rate so as to bypass crystallization and form an amorphous solid. Whether or not the melt of a given material forms a glass is determined by many factors such as the cooling rate and viscosity (Turnbull, 1969). Some of the thermodynamic aspects of this method were discussed in Chapter Two.

The number and variety of materials that have been prepared in a glassy form have been greatly increased by sophistication of techniques. Melt quenching rates extend from $\sim 10^{-2}$ deg/s in an annealing furnace (Serjeant and Roy, 1968), to $10^3 - 10^4$ deg/s in strip furnaces, to $10^5 - 10^7$ deg by the most complex splat cooling techniques (Duwez, 1963, Chen and Miller, 1970). Vapour quenching rates are much higher than rates of melt quenching and rates as high as 10^{15} deg/s have been reported (Nowick, 1969).

(b) Chemical reaction and precipitation from solution

An example of this method is the precipitation of amorphous As_2S_3 from a solution of As_2O_3 in dilute hydrochloric acid by passing hydrogen sulphide gas. Amorphous As_2S_3 prepared by this method is reported to have a similar T_g to that observed in samples prepared by method (a).

(c) Electrolytic deposition from solution

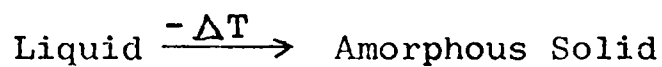
Tauc et al (1970) have reported the deposition of thick amorphous films of germanium on a copper cathode by the electrolysis of GeCl_4 in glycol.

(d) Dessicating gels

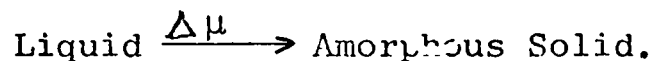
Amorphous silica can be prepared by low temperature

dehydration of silicic acid solution. Complete dehydration is obtained by baking at high temperature ($\sim 1270\text{K}$) (Owen, 1973).

Method (3.1a) is similar to (3.1b) and can be represented by:



Methods (b) - (d) are best represented as:



3.3 Preparation of amorphous solids from the solid phase

(a) Reaction amorphized solids

(i) Anodic Oxidation

Amorphous thin film oxides of several materials and elements such as Si, Al and Ge can be prepared by anodic oxidation using either an aqueous or non-aqueous electrolyte (Owen, 1973).

(ii) Loss of volatile constituent

In this process a volatile component in a solid compound is lost leaving an amorphous solid behind it.

(b) Irradiation

Crystalline quartz can be transformed into an amorphous solid by bombardment with fast neutrons. A dosage of about 1.5×10^{23} neutron/cm² has been reported (Wittels, 1954, Primak, 1958, Secrist and Mackenzie, 1964).

Similarly, a thin amorphous layer can be formed on a single crystal of germanium by bombardment with 100 KeV oxygen ions. The dosage is about 10^{15} ions/cm² (Parsons, 1965).

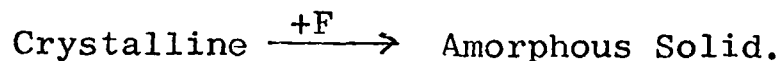
(c) Shock wave treatment

The transformation of crystalline quartz into an amorphous phase can take place under high shock pressures at relatively low temperature. This transformation may be regarded as due to the introduction of a high concentration of defects into the crystal lattice, but the exact mechanism is unknown. The properties of the amorphous SiO₂ prepared by this method are identical to fused silica.

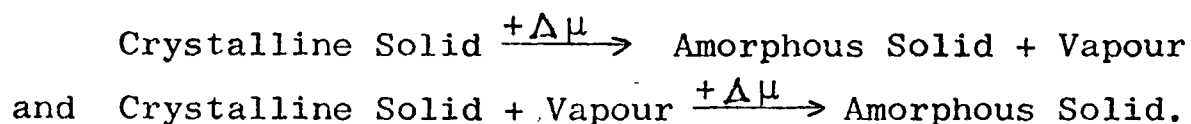
(d) Shear-amorphized layers

Amorphous surfaces can be produced on some crystals, e.g. quartz and cristobalite by the shearing stresses produced by grinding or comminution (Owen, 1973), but the number of materials that have been prepared by this method is not very large (Roy, 1970).

In methods (b) - (d) free energy is injected into the crystalline solid, i.e.



Methods (i) and (ii) in (a) are best represented in terms of chemical potential addition to the systems, i.e.



In order to prepare well-characterized chalcogenide switching devices for examination, it was first necessary to acquire, prepare or construct the following:-

- (a) High purity grade elemental constituents of the glass alloy,
- (b) a rocking furnace and quartz ampoules,
- (c) a vacuum plant with a suitable flash evaporator for depositing the thin films,
- (d) suitable glass substrates and electrode materials,
- (e) out-of-contact masks prepared from thin sheets of Mo by conventional photoetching techniques,
- (f) liquid nitrogen/water-cooled substrate holder.

Various electronic pulse circuits were then designed to examine the characteristics of the devices.

Details of the major techniques and equipment that were developed are given in the following sections.

3.4 Preparation of STAG glass alloy

The glass used in this work was prepared from Specpure grade As, Te, Ge, Si. The constituents of the STAG glass were weighed out and put into a clean quartz ampoule. The cleaning of the ampoule involving soaking it first in a solution of chromium trioxide then rinsing it with distilled water. Iso-propyl alcohol was then poured into it and the ampoule was then put in an ultrasonic cleaner

for two minutes to dislodge any particles stuck on the inner walls. After that, the alcohol was poured away and the ampoule was allowed to dry in a hot oven.

The quartz ampoule containing the glass constituents, which were usually crushed in the form of coarser powder, was connected to a vacuum plant, see fig. 3.1, which could be pumped down to a pressure of 10^{-6} torr.

To ensure that the powdered material inside the ampoule was well outgassed, the ampoule was usually pumped out for more than three days and then sealed with an oxygen-propane flame. It was then placed in the rocking furnace, drawn schematically in fig. 3.2. This rocking furnace was constructed from an ordinary high-temperature tube furnace which was fixed on a pivoted platform. The platform was made to rock by the rotary action of the electric motor which was translated into a resprécating motion with ^{the}aid of one arm connected to the motor shaft, and another connected to the platform via a ball joint as shown in figure 3.2.

The temperature of the furnace was raised in steps so that the vapour pressures of As and Te would be reduced through slow reactions with the two other elements and high pressures would not occur inside the ampoule. Accordingly, the temperature was first raised to 500°C , approximately 50°C above the melting point of Te, and held for three hours. It was then raised to about 600°C , which is the boiling point of As and held for two hours, finally, the temperature was raised to about 950°C and maintained for 48 hours with occasional rocking of the furnace. At the end of this period the ampoule was taken out and air quenched. The surface of the prepared alloy was usually smooth and glossy. However, if the temperature of the furnace was raised to about 1050°C and maintained at this temperature for 24 hours or more, the alloy surface was found to be dull, and signs of reaction between the glass alloy and the inner surface of the silica ampoule were visible.

The method described above for the preparation of chalcogenide glass is the most common technique and has been reported by several workers (Pearson et al, 1963, Deis et al, 1970, Hilton, 1970 and Savage, 1970).

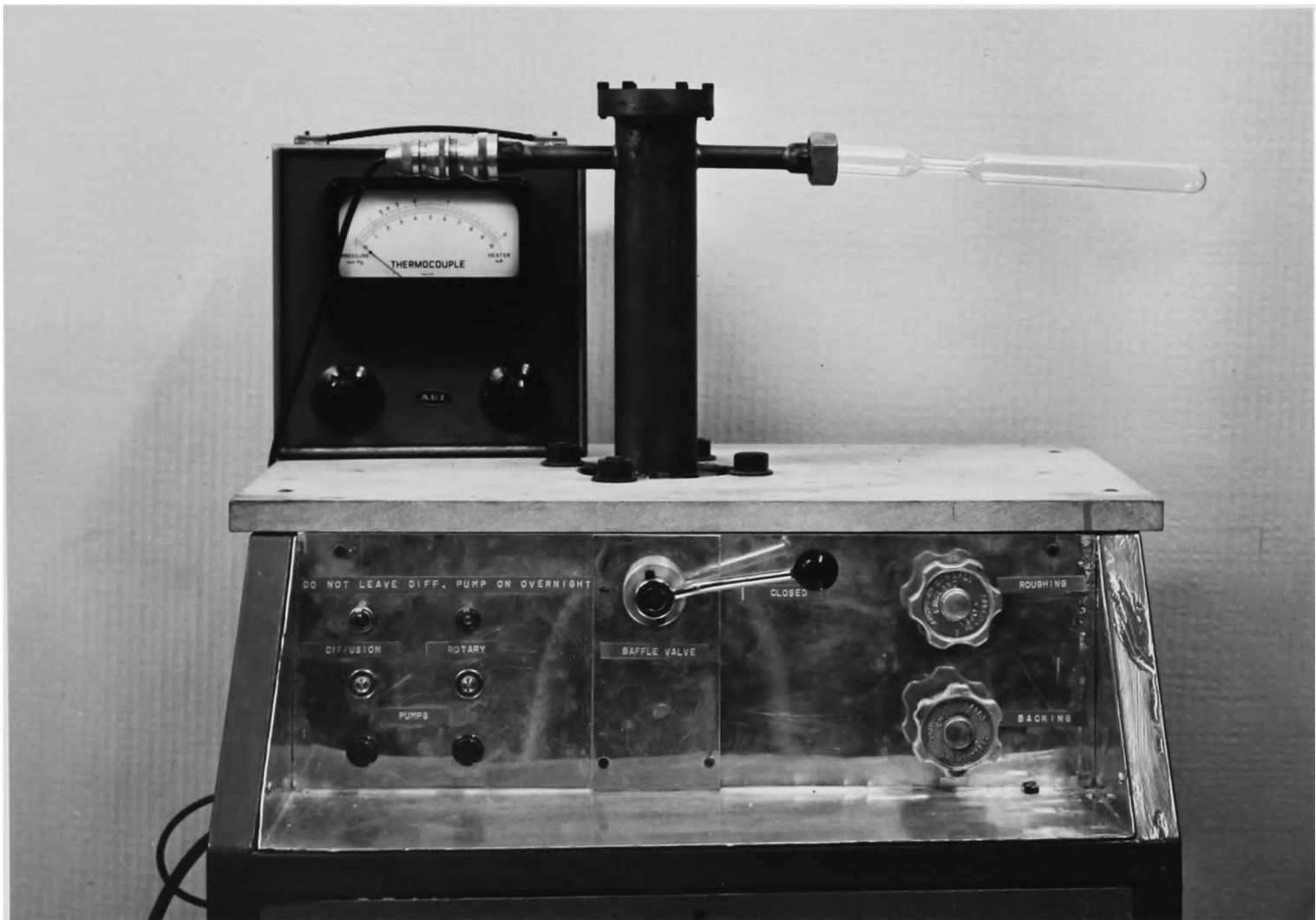
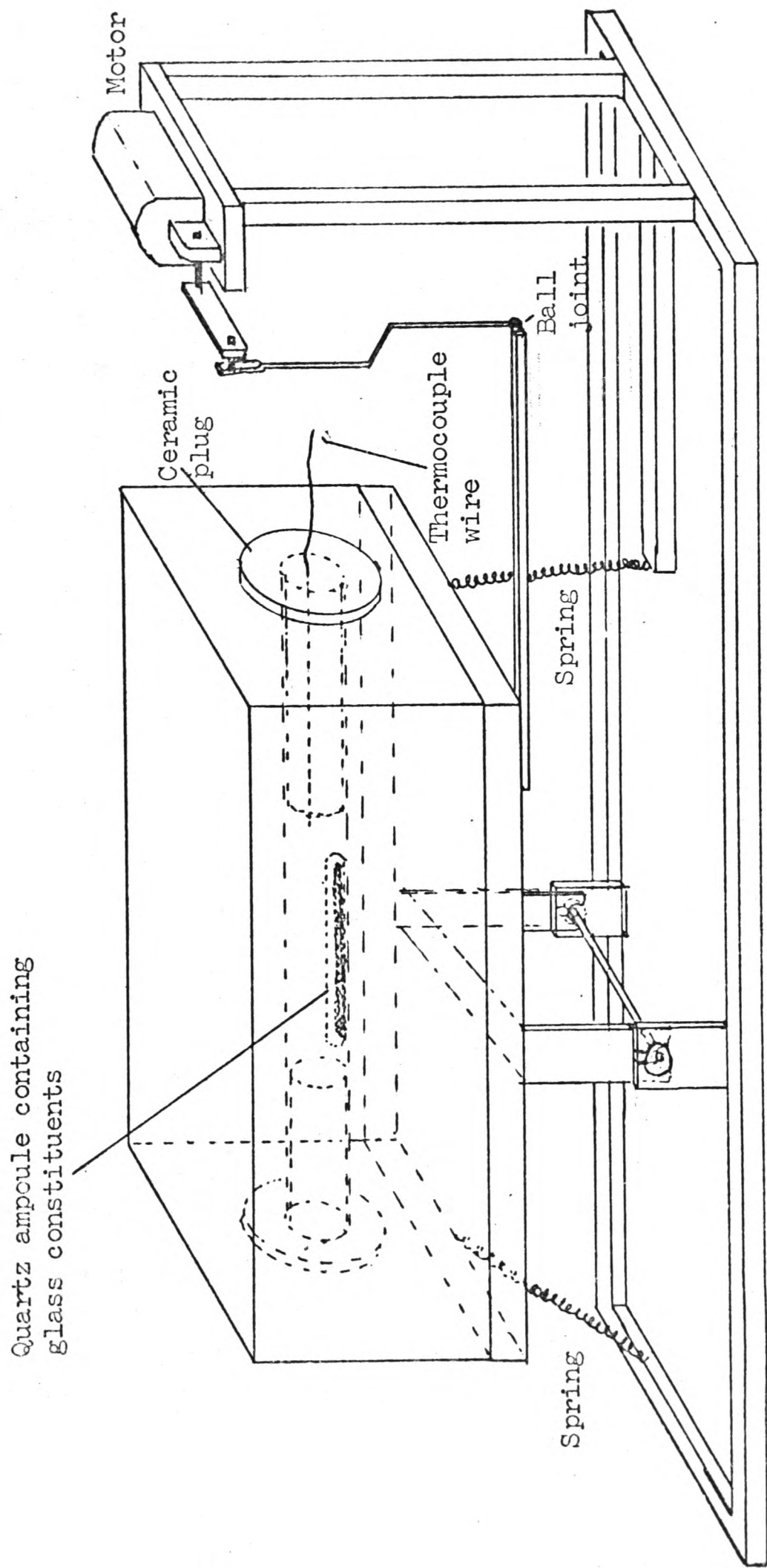


Fig 3.1.



THE ROCKING FURNACE

FIG. 3.2

At early stages of this work STAG glass was supplied by The Royal Radar Establishment and by Dr. E.H. Baker of Imperial College, London. The preparative technique used by Baker was somewhat different to the one just discussed. The glass constituents were put into an unsealed ampoule which was then placed in a high pressure furnace. The furnace was made from a section of a naval gun barrel and pure argon pumped into it to a pressure of 50 atmospheres. The temperature was then raised to above the melting point of Si and maintained for one hour, then cooled to 500°C. The sample was then quenched in a jet of argon gas. This method had the advantage of preparing large quantities of STAG glass in a matter of two hours.

The table below shows some of the properties of the elemental constituents of STAG glass and the amounts involved in preparing 50 grams of the alloy.

Element	At. No.	At. Weight	M.P. (°C)	Vap. pressure at 1000°C (atm)	B.P. (°C)	Amount in grams per 50 grams of STAG
As	33	74.92	814	75		11.908
Si	14	28.18	1420	Negligible	2355	1.786
Te	52	127.60	450	1.2	990	32.458
Ge	32	72.59	937	Negligible	2830	3.847

The alloy was made in batches of 45 grams, and this quantity occupied about one third the volume of the sealed quartz ampoule after quenching.

3.4.1. Characterization and examination of prepared glass samples

As a working definition, it was taken that "characterization describes those features of the composition and structure (including defects) of a material that are significant for a particular preparation, study of properties, or use, and suffice for the production of the material" (MAB, 1967). Complete characterization, if at all possible, of any amorphous material is time consuming and demanding in equipment. Therefore, it was decided to carry out a few basic examinations on the prepared glass and compare the results with those obtained for an RRE sample. These examinations included optical microscopy, X-rays and differential thermal analysis.

X-ray examination of a powdered sample and microscopic examination of a polished sample showed no signs of crystallinity in either the glass prepared by the author or the sample supplied by RRE.

DTA on the STAG glass was carried out in a Stanton Differential Thermal Analyser System 67 incorporating module 18 which had a temperature range -150 to +500°C. The reference material was alumina of B.D.H. analytical reagent quality. The amount of alumina used was 0.12 gm and this gave a good thermal match to 0.38 gm of STAG glass. The experiment was carried out with pure nitrogen gas flowing through the sample chamber at a rate of 10 ml/minute. The temperature was raised from ambient to 500°C at a heating rate of 20°/minute.

The value of T_g was found to be 225°C and no crystallization peaks were recorded beyond this temperature, see section 2.3. These results were in good agreement with those of Bosnell and Savage (1972).

3.5. Flash Evaporation

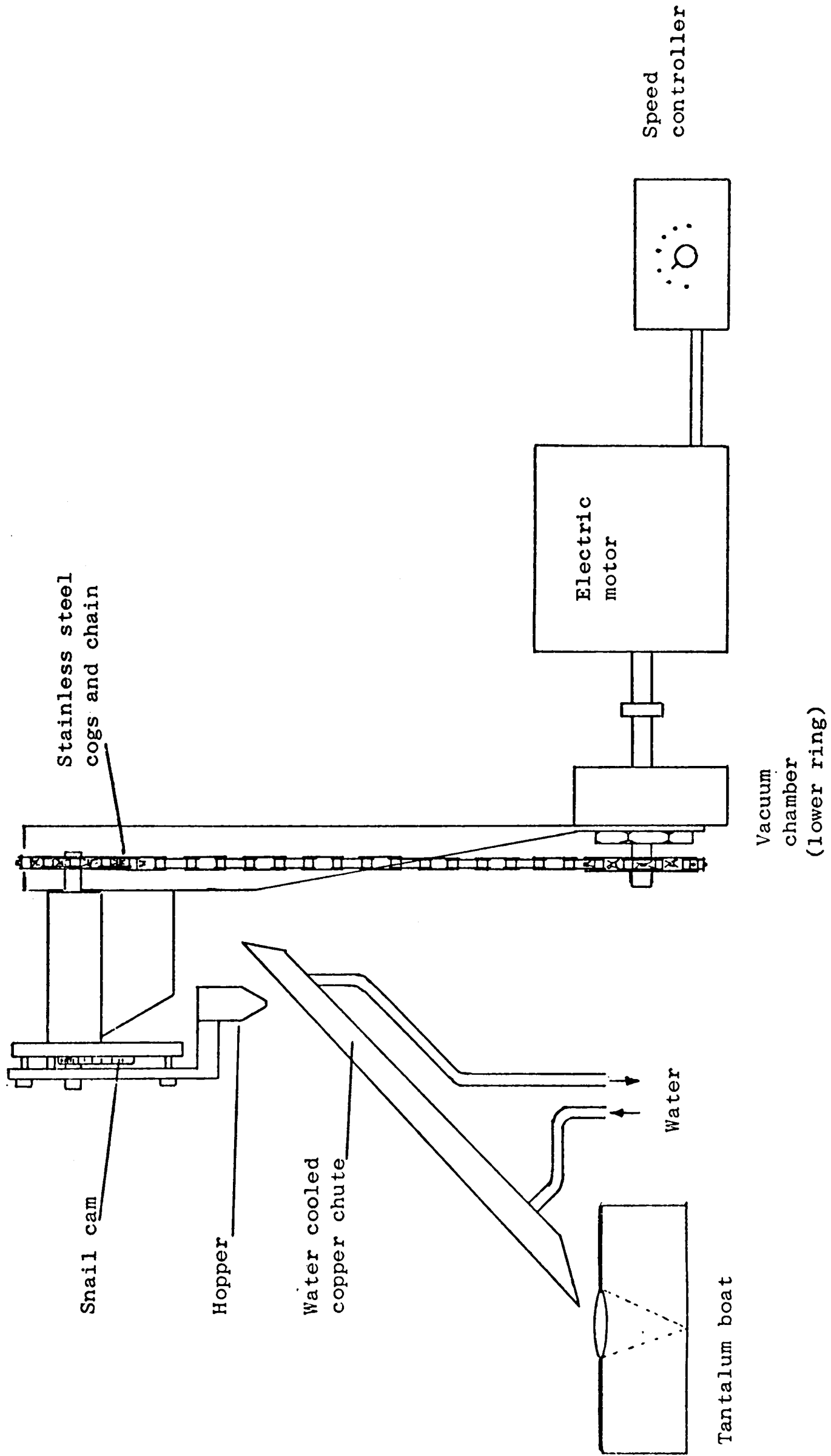
Flash evaporation was described as a variant of thermal evaporation used for the deposition of thin films from multi-component alloys or compounds. Evaporation of some alloys by conventional techniques results in differential evaporation of alloy constituents, and deposited films show considerable deviation from the original composition. These alloys usually possess a wide disparity in the vapour pressures of their elemental constituents, and this is the case in STAG glass.

In the flash evaporation method, powder particles are dropped on to a very hot ribbon or boat usually made from refractory metal sheet. The technique was first introduced by Seigel and Harris (1948) who used it to evaporate brass and other metal alloys. There are certain problems associated with this technique such as (i) the technological difficulties involved in handling and dispensing of the powdered material; and (ii) the compositional errors involved as a result of mechanical loss of some particles as soon as they touch the

hot surface. This loss is a result of (a) the adsorbed gasses in the powder particle causing the particle to be violently ejected from the boat's hot surface and this is likely to happen if the system is not well outgassed, and (b) the boat being far too hot, i.e. the particle can be driven out by its own vapour. However, flash evaporation has been used successfully to evaporate many alloys and compounds (Beam and Takahashi, 1964, Richards, 1966, Ellis, 1967) and several powder-dispensing techniques have been developed. Some systems have used a clockwork motor-driven belt (Seigel and Harris, 1948) and others used a vibrating hopper or positive-displacement feed mechanism such as an Archimedean screw (Beckman, 1962). Glang et al (1967) have described an elaborate system for flash evaporating presintered Cr-SiO pellets. Theoretical considerations of flash evaporation have been discussed by Ellis (1967). He also suggested that two conditions would have to be met in this method: (1) The complete evaporation of one particle should deposit not more than one monolayer at the substrate for if each particle fractionates and gives a thick layer then the final film will be stratified (in the absence of sufficient diffusion). (2) Each particle should evaporate to completion before the arrival of the next. In practice, none of these conditions is fully met.

No suitable flash evaporation equipment was available at the start of the project and thus it was necessary to design and construct a system for evaporating STAG glass. Early attempts to construct such a system included the use of a V-shaped chute made to vibrate by a small magnet and an a.c. coil as in a loudspeaker, or a small hopper, made to vibrate by an electric bell mechanism, but neither of these proved satisfactory as a powder dispenser. The system finally used is described below.

The flash evaporator system is shown in figure 3.3. It consisted of a small hopper, which could take up to 10 grams of powdered glass, machined from Al block and operated by a snail cam mechanism. The snail cam was in turn operated



THE FLASH EVAPORATOR

Fig. 3.3.



Figure 3.4

The STAG glass ingot obtained after breaking the sealed quartz ampoule.

by a speed-controlled electric motor, fitted outside the vacuum chamber, via a high-speed Birvac rotary shaft, stainless steel cogged wheel, and a stainless steel chain. When the motor shaft turned the hopper was lifted then dropped onto a stop releasing an amount of glass powder onto a machined upper chute. The powder then slid in the chute grooves and dropped into a conically shaped Ta, or Mo, evaporator made from 0.001" thick sheet supplied by Goodfellow Metals Ltd. The cone had a diameter of 2 cm and a depth of 7 cm. It was maintained at a temperature of 350°C (measured by an optical pyrometer), by passing about 150 amp through it. Evaporators of different shapes were initially tried out, but as far as limiting the ejection of powder particles from the evaporator was concerned, the conical evaporator proved to be the most satisfactory one.

Because of the relatively low softening point of the glass (about 300°C) (Armitage et al, 1972), the chute was water cooled to prevent the powder from agglomerating and clogging in the chute groove.

A suitable powder particle size was found to be -60 + 100 mesh, i.e. 251-152 µm. Finer powders flowed less readily on the chute and coarser powders, although they minimised the problem of ejection from the evaporator, were considered too large in particle size for flash evaporation.

The powder was obtained by grinding the prepared glass ingot, obtained by breaking the silica ampoule described earlier, see figure 3.4, in a hard ceramic pestle and mortar with liquid nitrogen added during the grinding to prevent local heating which could cause oxidation of the glass particle (Bunton et al, 1972). The powder was then sieved using standard 60 and 100 mesh Endecoths sieves which were thoroughly cleaned to avoid contaminating the powder.

The powder flow rate from the hopper could be varied by (a) controlling the motor speed, and (b) using a hopper of a different aperture. Three hoppers of different hole sizes were machined. The hole sizes were 1000, 700 and 350 µm.

and made with standard workshop drills Nos. 60, 70 and 50 respectively.

To assess the uniformity of the powder flow rate from the hopper, the evaporator was removed and a clean glass beaker was put in its place. The motor was then turned on and the amounts of powder collected in the beaker after 1, 5, 10, 15, 20 and 30 minutes were weighed out and recorded. Figure 3.5 shows a plot of weight of powder collected in grams versus time and indicates a reasonably uniform powder flow rate. These results were taken using the hopper with a hole size of 1000 μm and a motor speed of 80 revolution/sec. The flow rate could be improved by precision control of the motor speed and by using powder in a finer range, say 152-200 μm , but this would have produced more powder waste and besides, the fluctuations in the flow rate as shown in figure 3.5 were quite small and acceptable.

The vacuum unit in which the flash evaporator was fitted was basically an Edwards 12E3 plant, having a model E150 rotary pump and a type 403 diffusion pump. The original bell-jar work chamber was replaced by a 12 in. diameter, 16 in. high Pyrex glass cylinder with a stainless steel top plate, see figure 3.6. The top plate was fitted with a substrate holder, a rotary shaft and electrical feed-in unit. The glass cylinder rested on a stainless steel ring (2 $\frac{1}{2}$ in high, $\frac{5}{8}$ in. thick, 12 in. inside diameter) having 8 'portholes' equally spaced around its circumference for the attachment of additional feed-ins and gauges etc. A standard plug was fitted to one of these ports and had two holes drilled in it to take the two $\frac{1}{4}$ in. copper pipes which delivered the cooling water to and from the copper chute. An I.G.2 ionization gauge (Edwards) was fitted to another port. The rest of the ports were blocked with standard plugs. A Viton 'O' ring seated in a square section groove in the stainless steel ring sealed the ring to the base plate of 12.E.3 coating unit. L section Viton seals were used between the glass cylinder and the stainless steel top plate and between the glass cylinder and the stainless steel ring. The base plate of the unit had

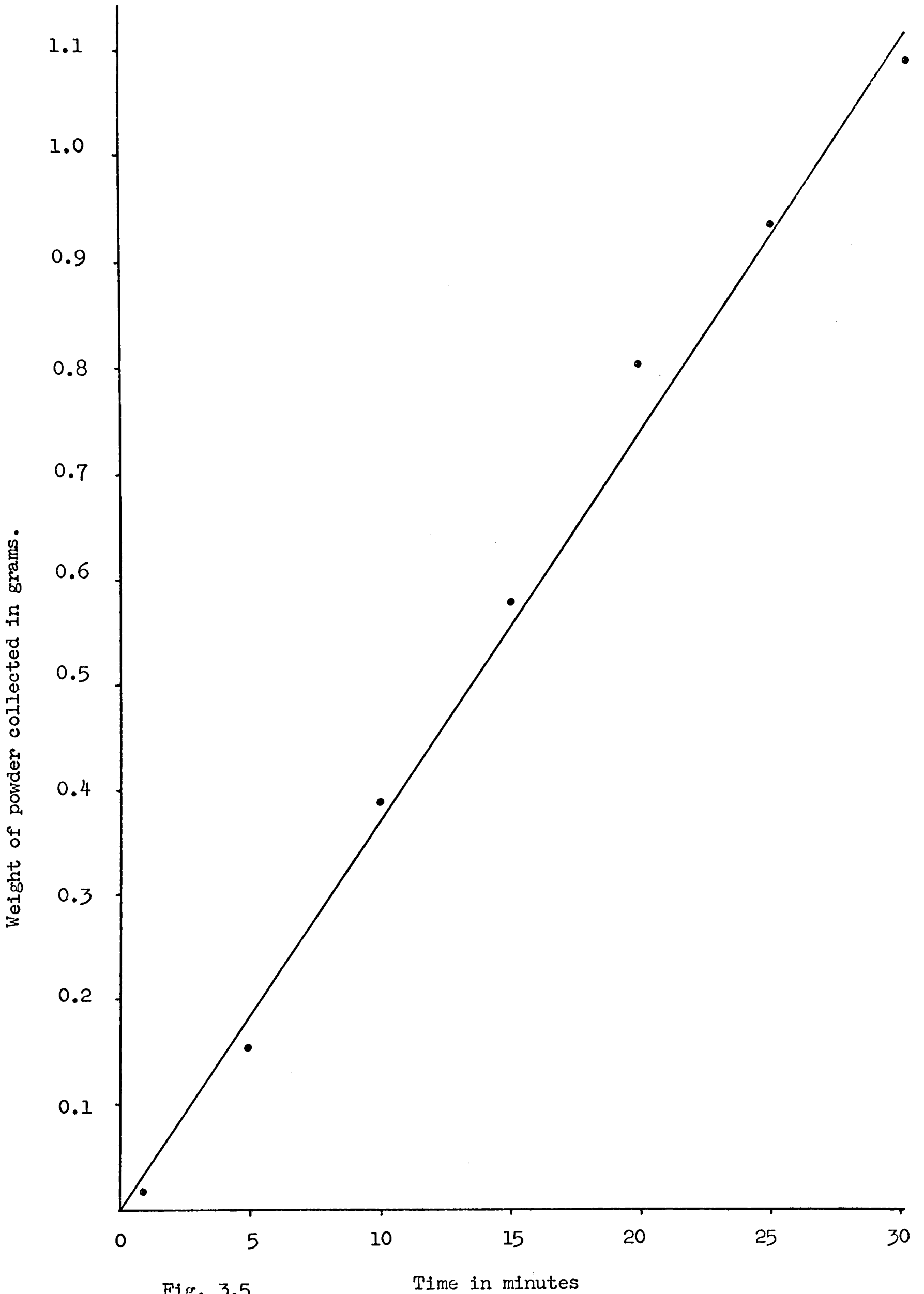


Fig. 3.5



Figure 3.6

The equipment used for preparing the thin films from STAG glass.



Figure 3.7

View of the base plate and lower part of the vacuum chamber.

facilities for feed-in electrodes and the high current Edwards feed-through units were connected to it via these facilities. The outer parts of these feed-through units were connected to the secondary of a heavy-current, (200 amps), transformer. The primary of the transformer was supplied from a 10 A variable auto-transformer mains Variac. The current feed-through units were connected inside the vacuum chamber to copper rods, each 4 ins. long and 1 in. in diameter. The other ends of these rods held the evaporator, see photograph 3.7.

To improve the vacuum, an Edwards, type N.T.M.4A liquid nitrogen cooled vapour trap was fitted between the oil diffusion pump and the lower surface of the base plate. In addition, a foreline-trap was fitted between the rotary and diffusion pump side and a flexible coupling on the rotary pump side. The flexible coupling relieved any unnecessary stresses because of the relative position of the trap and the rotary pump.

In addition to the pressure ionization gauge mentioned earlier, the plant had Pirani and Penning gauge heads with their associated units for monitoring the pressure inside the vacuum chamber. A vacuum better than 10^{-5} torr could be obtained after one hour of pumping, but this dropped down to 3×10^{-5} torr during deposition.

3.6 Device Fabrication

The devices made in this project were of the sandwich, gap and point-contact type geometries. The fabrication of each individual type will be discussed in later paragraphs, but processes that were common to the preparation of all or two types of device will be dealt with first. These processes are substrate cleaning, preparation of out-of-contact masks, monitoring of film thickness and deposition of metal electrodes.

3.6.1. Substrate Cleaning

Corning 7059 fire-polished 2 x 3 x 0.075 cm borosilicate glass substrates were used. The choice of this substrate material was made in accordance with the description of device preparation and requirements given by Neale (1970). Prior to the deposition of the film, each substrate was subjected to the following treatment:

1. 5 minute wash in 1 part Teepol and 1 part distilled water.
2. Rinse and wash in distilled water.
3. Agitation for 5 minutes in an ultrasonic bath filled with acetone.
4. Half an hour degrease in iso-propyl alcohol vapour.

The transfer of a substrate from one cleaning stage to the next was carried out using a pair of tweezers. The vapour degreasing was carried out in the apparatus shown in figure 3.8. It was possible to obtain a liquid-free vapour on correct adjustment of the flow of water through the cooling condenser and the applied heat rate. The substrate, when removed from the degreaser, looked clean and dry.

The cleanliness of the substrate surface has a decisive influence on film properties and adhesion. Films, metallic or amorphous chalcogenide, deposited on substrates cleaned by the procedure described above exhibit good adhesion to the substrate surface and showed no pinholes.

3.6.2. Preparation of Masks

It is sometimes necessary for the deposited films to have a certain shape or pattern of specific dimensions. This is the case in microelectronics and in other cases where the substrate contains more than one device on it. The generation of a particular film pattern can be achieved by the use of deposition masks. These masks are of two kinds, in-contact and out-of-contact masks. The in-contact type was not used in this work and need not be described. The preparation of out-of-contact masked is described below.

The mask shape was first drawn with eight times the required dimensions on millimetre graph paper. A thin glass sheet was then placed on top of the drawing and printed circuit tape, supplied by Bradley Co., was stuck on the upper surface of the

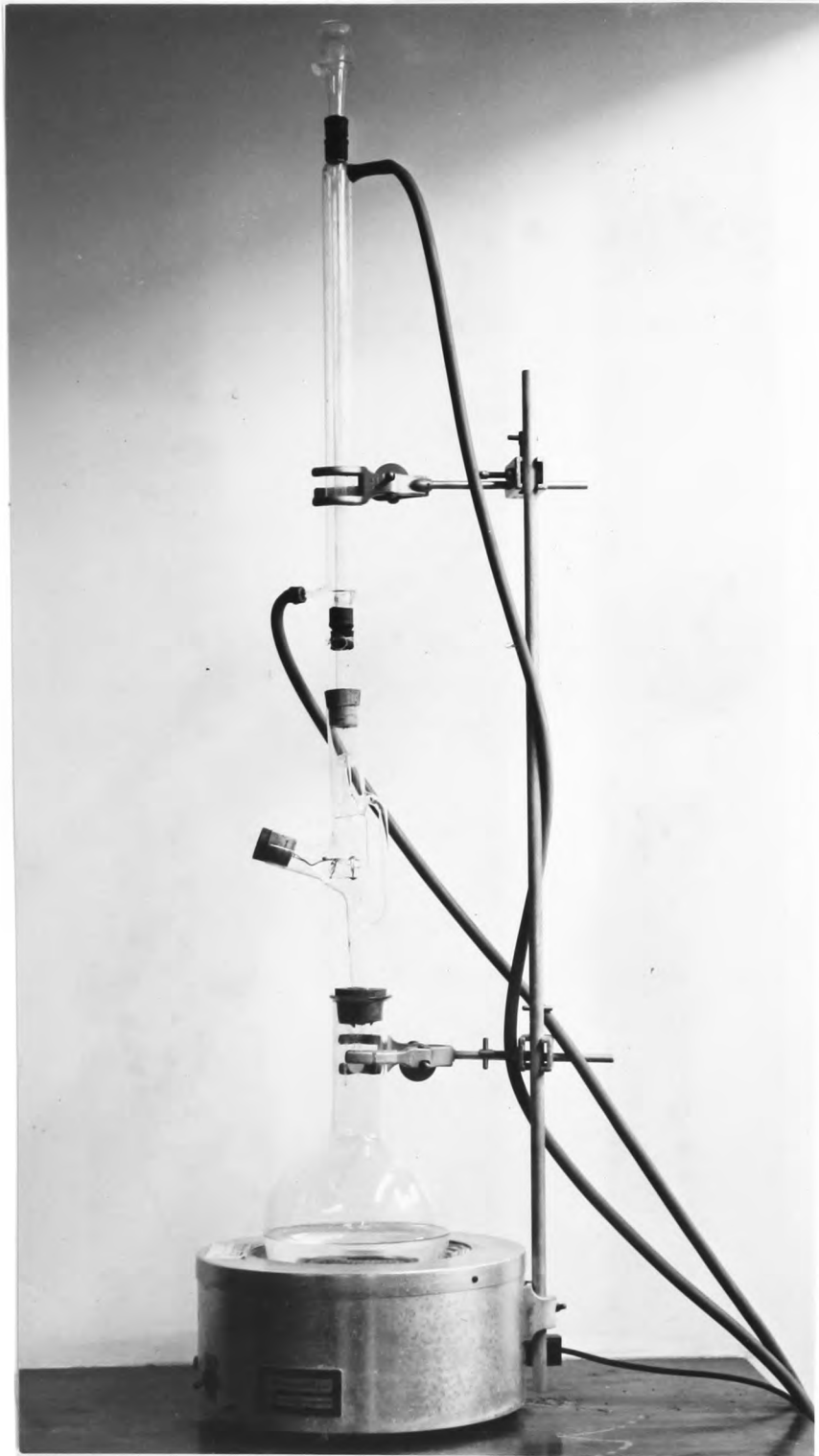


Fig.3.8

The vapour degreasing plant.

glass to form an identical pattern as the drawing. Utmost care was taken to ensure that the dimensions of the pattern were identical to the original drawing. The pattern was then photographically reduced in size by a factor of eight, and a 'positive' i.e. black outline on a clear background was produced. The photographing was carried out using a camera set-up especially designed by the Physics Division Electronics Workshop for making printed circuit boards. The positive was then used to make another identical positive and this was done using photographic contact paper. The two positives were then placed on top of one another and adjusted until the patterns on them coincided. Three edges of the positive were joined together using 'sellotape' leaving a fourth side into which a molybdenum sheet could be slid.

The sheet was cut into 4 x 4 cm pieces from a large 0.002" thick sheet supplied by the Tungsten Manufacturing Co. Ltd. Molybdenum was used because it does not deform at high temperatures and has a small temperature coefficient of expansion.

The sheets were then thoroughly cleaned and scrubbed using commercial scouring powder which helped to improve the keying and then washed in carbon tetrachloride, then acetone to remove any grease. The sheets were handled only with tweezers.

When dry, the sheets were coated with "Kodak Printed Circuit Resist". The coating was carried out by pouring a small drop of resist on one corner and allowing it to flow over the whole sheet. This was repeated on the other side, and the sheet drained and hung up to dry at a temperature of 80°C inside an oven. The coating and drying was carried out in a room where no fluorescent lighting was used because the photo resist is sensitive to ultra-violet light. To produce a mask, a dry coated sheet was placed centrally inside the envelope formed by the two positives. The envelope and the sheet were sellotaped

together to prevent the sheet from moving position. One side of the envelope was then exposed to ultraviolet light from a high-pressure mercury lamp, for approximately 4 minutes. The plate was then turned over and the other side exposed for the same period of time. The sheet was then taken out and developed in Kodak Printed Circuit Resist Dye Developer. The mask shape outline was then etched away. The etchant solution comprised:

1 part concentrated H_2SO_4
1 part concentrated HNO_3
3 parts distilled water

and was freshly made when required. Another suitable etchant was a solution of concentrated hydrochloric acid in H_2O_2 , one volume of HCl added to one volume of H_2O_2 , but because H_2O_2 decomposes when stored for prolonged periods, this etchant was not normally used.

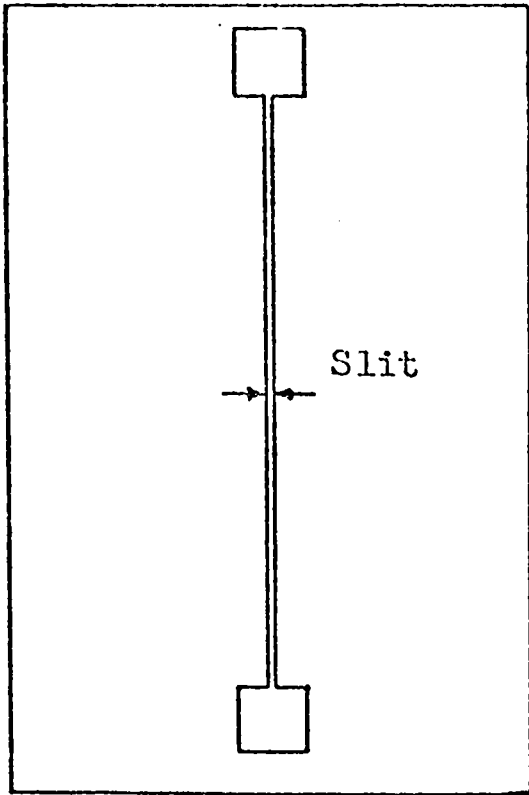
The overall dimensions of the mask sheet were cut to 2 x 3 cm, also by etching, so that it was the same size as the glass substrate and fitted easily into the substrate holder jig. The developed resist on the etched sheet was removed with Kodak Printed Circuit Resist Thinner and the masks were then washed with acetone and allowed to dry.

Figure 3.9 shows five masks fabricated from molybdenum sheet. Masks (a) - (c) were used for making sandwich type devices, (d) and (e) were used for making gap devices. The exact dimensions of the slits will be discussed later.

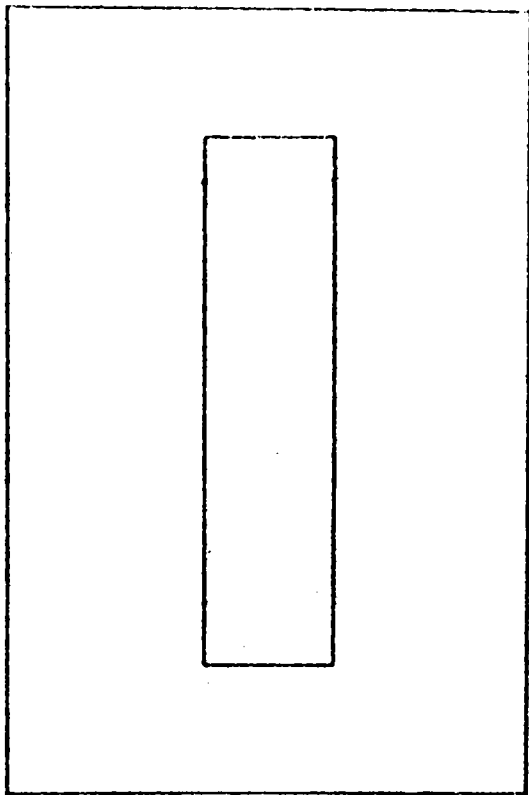
3.6.3. Film thickness measurement

Three different methods were initially used to measure film thickness. These included an optical interference technique, the use of a quartz crystal monitor and the stylus (Talysurf) method.

Measurements by the optical interference method were carried out with a Hilger and Watts Thin Film Measuring Interference Microscope N.130. This instrument measures the thicknesses of thin films to an accuracy of $\pm 25 \text{ \AA}$. This accuracy is obtained by measuring the difference between the optical path

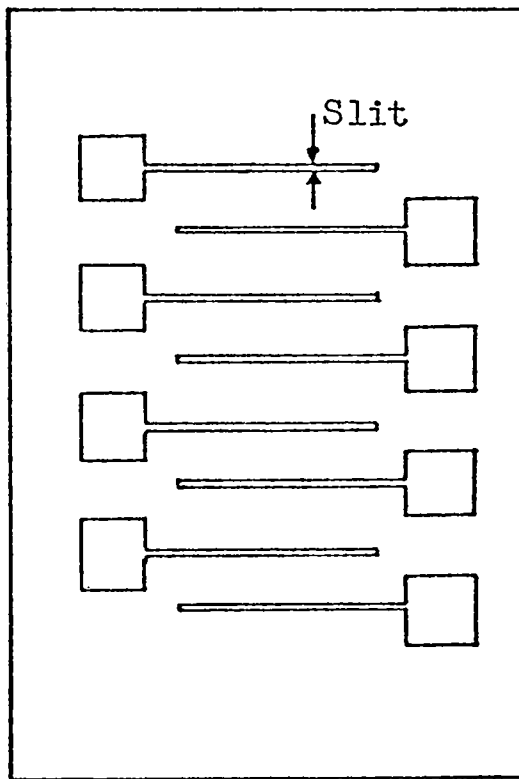


(a)

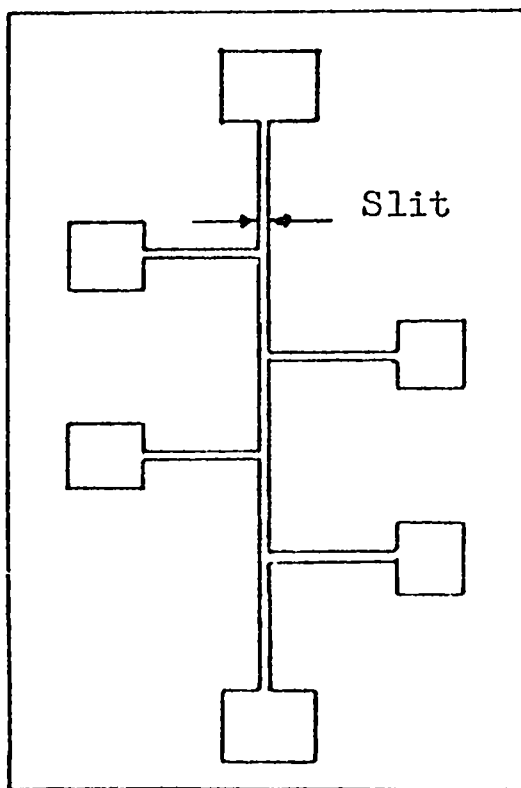


(b)

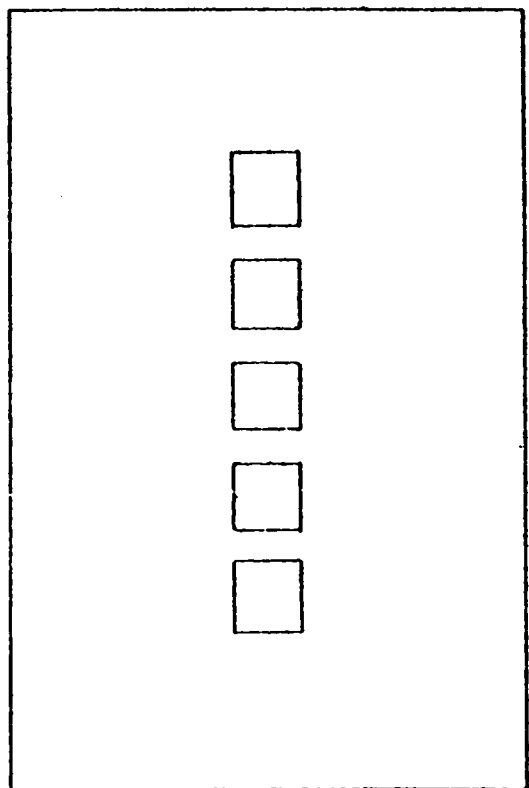
The masks used in fabricating sandwich and gap devices.



(c)



(d)



(e)

length of light reflected from the coating and that from the adjacent backing substrate. If the film material is not a very good reflector of light, like STAG glass it is an advantage if the film, or part of it near one side, and the uncoated area of the backing substrate, are coated with a thin film of aluminium, see figure 3.10(a).

Incident light is split by a semi-reflecting optical flat placed with its reflecting surface in contact with the sample. The resultant multiple beam interference fringes are viewed and measured with a wavelength spectrometer.

The sample was illuminated by a parallel beam of white light and the image of the surface step was focused on the slit of the spectrometer. Discontinuous dark fringes, resulting from the surface break between the coating and the backing material, were seen against a continuous spectrum of white light in the eyepiece of the spectrometer as shown in figure 3.10(b).

Referring to figures 3.10(a) and (b), the difference $t = (d' - d)$ is the film thickness to be measured and corresponds to the change Δd in the wavelength from position A to position a.

For two adjacent fringes, say n and $n + 1$, having the wavelength λ_1 and λ_2 , d' and d are given by the expressions:

$$d' = \frac{n}{2} (\lambda + \Delta \lambda)$$

$$d = \frac{n}{2} (\Delta \lambda)$$

$$\text{where } n = \frac{\lambda_2}{\lambda_1 - \lambda_2} .$$

Hence by measuring only three values, λ_1 and λ_2 to find the value of n , and then $\Delta \lambda_1$, the film thickness is obtained.

The actual film thickness measurement using this apparatus was not carried out on the film intended for device fabrication but on a film evaporated on a substrate held next to the device substrate during

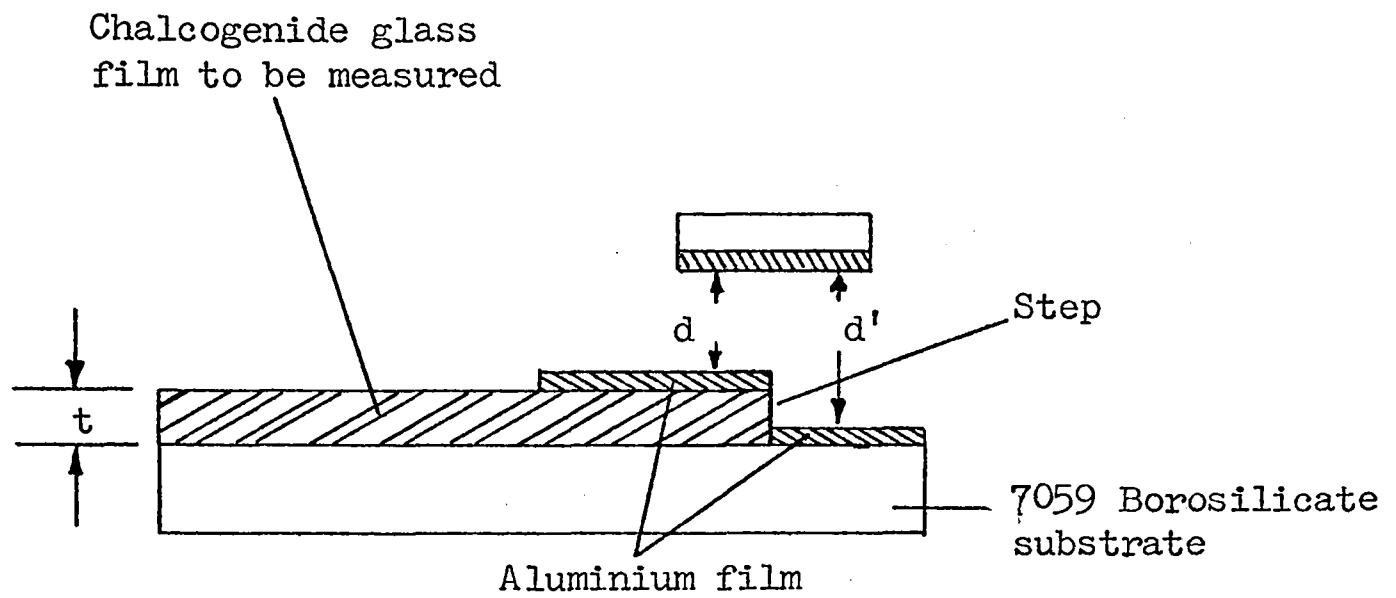


Fig. 3.10(a)
Semireflecting optical flat with film sample including step for multiple beam interferometric measurement of film thickness.

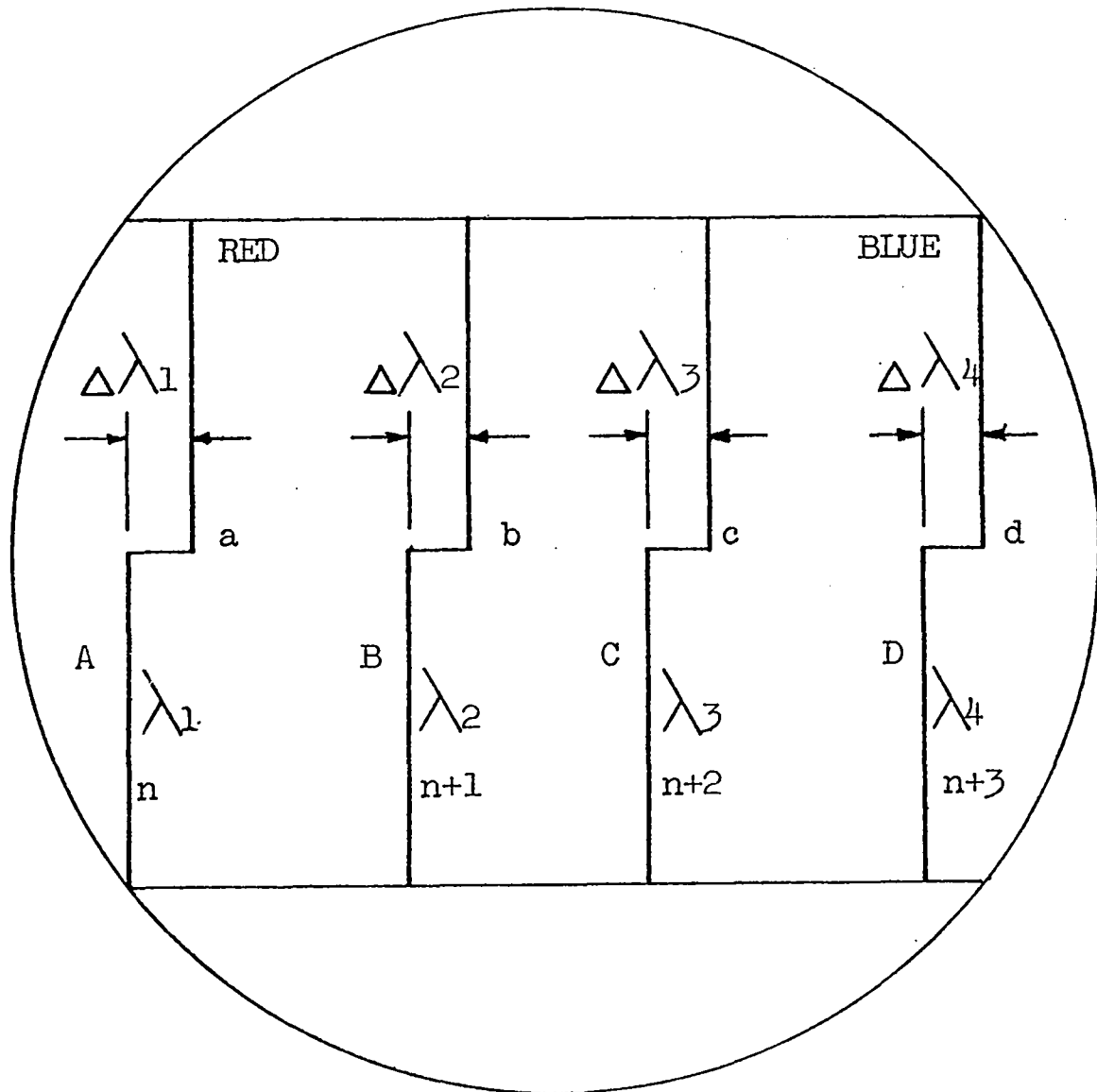


Fig. 3.10(b)
The interference fringes as viewed by the spectrometer eyepiece.

the deposition of the chalcogenide glass film. This was done to avoid having to coat the device substrate, with the STAG glass film on it, with an aluminium film.

In the stylus method of measuring film thickness, a mechanical stylus is made to trace the surface of the thin film and its vertical displacement is amplified electronically to record step heights and surface irregularities. The system used in this project was a Taylor-Hobson Talysurf 4 shown in figure 3.11. The stylus in this system was a diamond with a rounded tip ($\sim 1\mu$ diameter) and the pick-up arm to which it was attached was delicately balanced so that the load on the stylus was extremely small. The vertical measurement of the stylus was detected with a transducer, amplified by several order of magnitude, and then displayed on a recorder. The stylus always left a trace on the film and for this reason the measurement was always carried out on a second substrate as in the case of the optical method.

Figure 3.12 shows a typical stylus trace on the recorder chart. The film was on flash evaporated chalcogenide glass. The vertical movement was amplified 50,000 times. Hence, the film thickness was about $0.28 \mu\text{m}$.

The table below gives the thickness of three thin films as measured by the Talysurf and the Hilger and Watts interference microscope.

Films	Thickness (A°) Talysurf	Thickness (A°) Hilger and Watts Int.
1	2800	2870
2	5670	5675
3	13200	13190

The two methods just described for measuring film thickness are sufficiently accurate for determining final film thickness, but not suitable for monitoring the thickness during film deposition. Although the powder flow rate from the chute was reasonably constant,

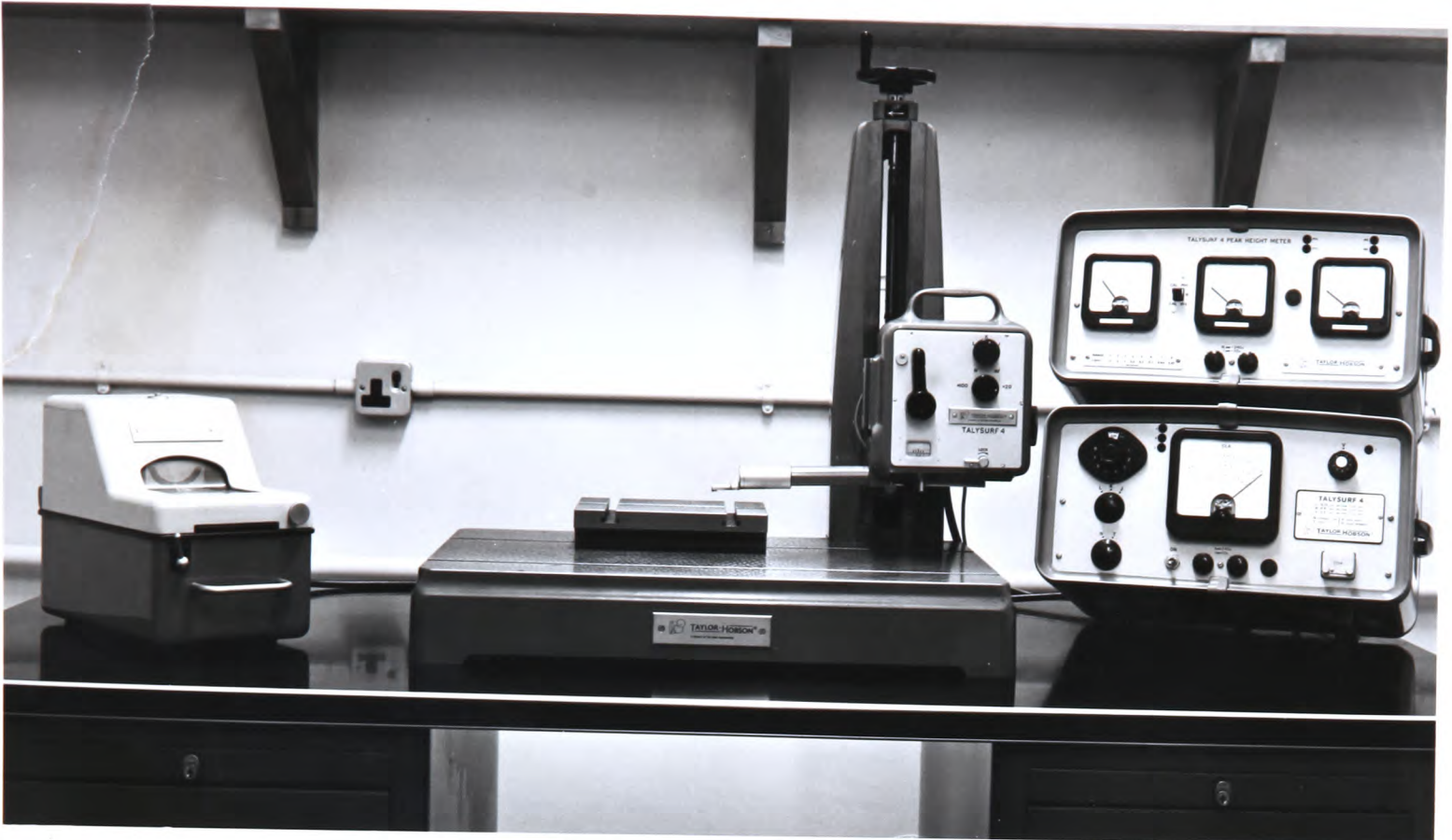


Figure 3.11

The Talysurf used for measuring film thickness.



Figure 3.12

A Talysurf stylus trace.

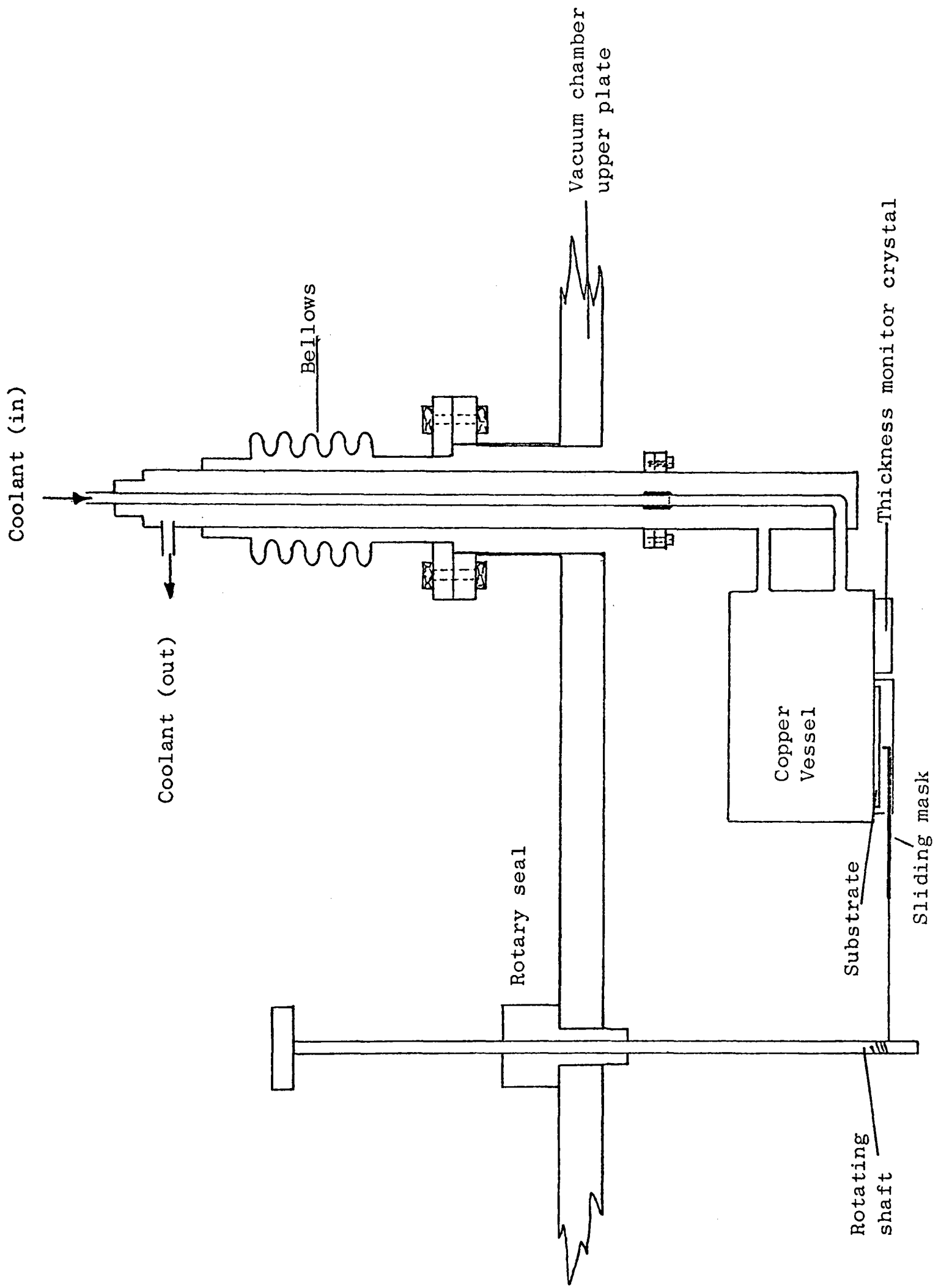
it was not always possible to produce a film of a desired thickness by simply timing the film deposition period. This difficulty arose from the fact that some powder particles were not evaporated completely, and the extent of this problem varied from one deposition to another. To monitor the thickness during film deposition an Edwards quartz crystal monitor was used.

The monitor crystal was mounted on the substrate cooling block so that vapour was deposited simultaneously on the substrate and on an area of the crystal surface defined by drilling a $\frac{1}{4}$ " hole in its containing can, Fig.3.13 Both thickness of the film and its rate of deposition on the crystal face were displayed on conventional meters.

The monitor was calibrated by evaporating a film and comparing the resulting shift in the crystal's natural resonant frequency with subsequent Talysurf measurements of film thickness. This process was repeated for several films of different thicknesses, obtained by varying the deposition times from about twenty minutes to two hours by keeping the flow rate constant. Results are shown in figure 3.14.

To obtain a film of particular thickness, the corresponding frequency-shift was first read from the calibration plot and deposition of the film was continued until the frequency-shift meter showed the desired reading. The deposition process was then terminated first by switching the flash evaporator motor off and then turning off the evaporator current.

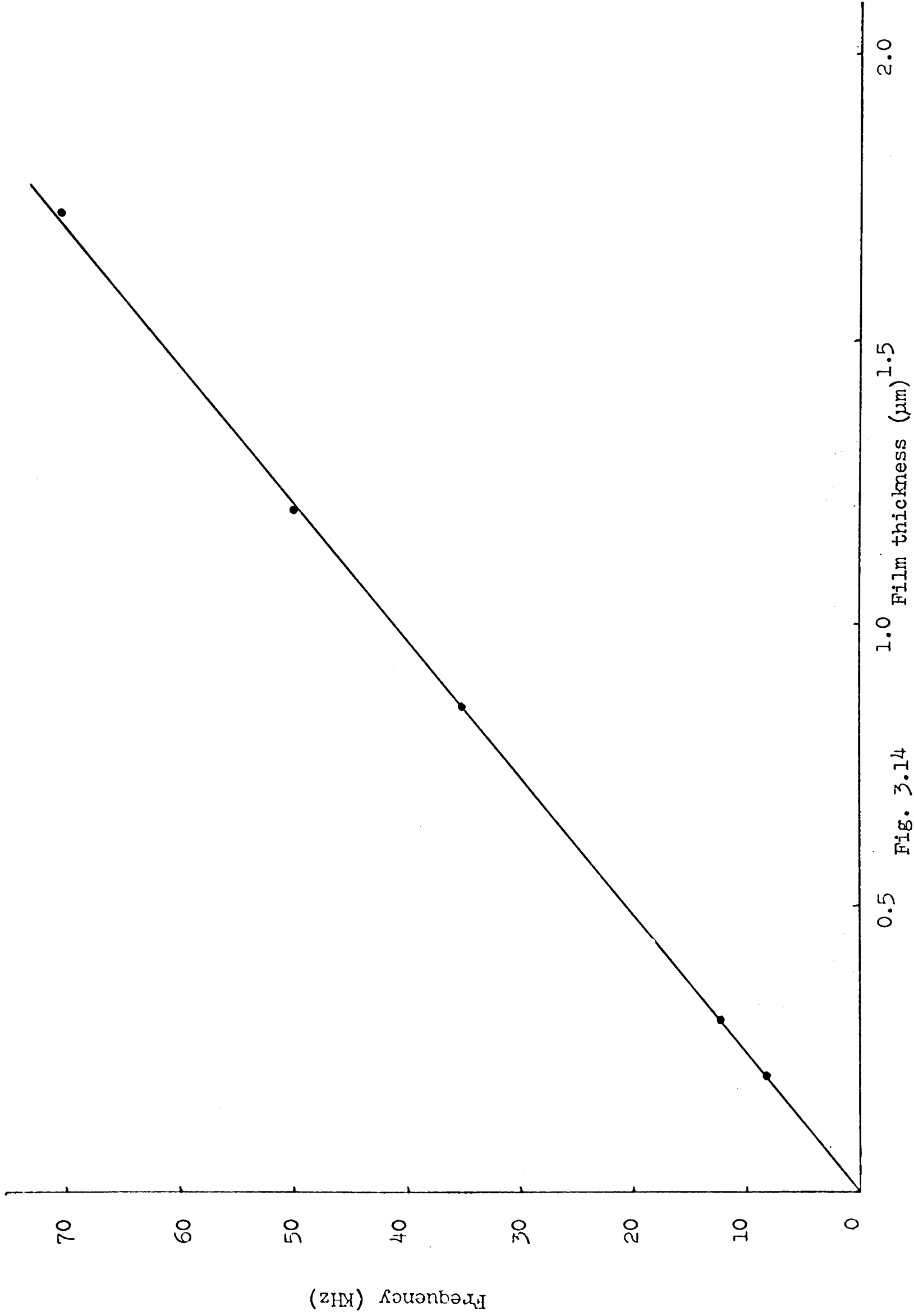
The quartz crystal method of measuring film thicknesses is very sensitive to temperature and, therefore, it was necessary to keep the monitor crystal temperature constant during calibration. This was achieved by running tap water through the cooling block, see figure 3.13. Any further use of the calibration



THE SUBSTRATE HOLDER

Fig. 3.13

Calibration Curve of Film Thickness Monitor



curve was carried out under the same temperature conditions.

3.6.4. Deposition of metal electrodes

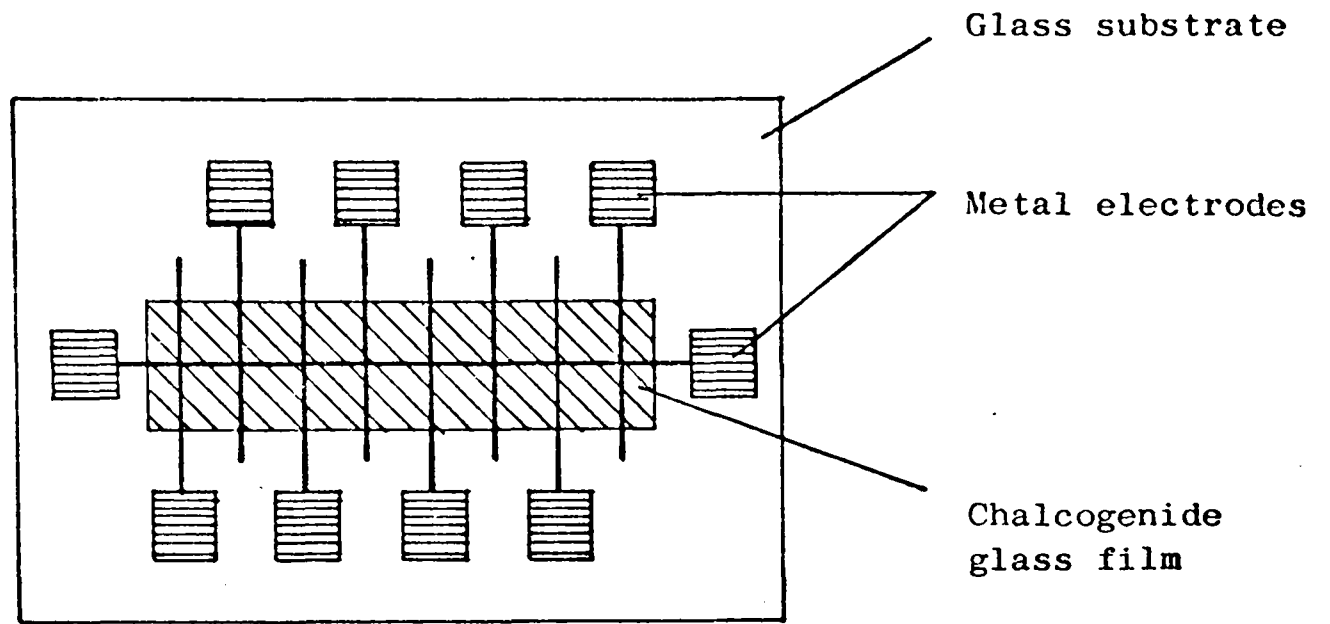
The deposition of metal electrodes, see figure 3.15(a) and (b), was carried out in a separate vacuum plant. This was another Edwards 12E1 vacuum system but had no liquid nitrogen cold trap or a foreline trap. The base plate was fitted with a Birvac (type RG2) electron beam bombardment ring gun with its H.T and L.T supply electrodes, figure 3.16(a). Some electrode materials, e.g. Mo, Ta and W, were difficult to evaporate even by electron beam bombardment. Mo films deposited by electron beam bombardment were extremely porous; Ta and W could not be evaporated because of their high boiling points (5300° and 5900° C). Aluminium, chromium and gold were easily evaporated up to thicknesses of 3 μ m. The film thicknesses were estimated from deposition rates for each material which were given by the electron-beam gun manufacturer.

The ultimate vacuum inside the vacuum chamber prior to the electrode deposition was about 6×10^{-5} torr and this dropped to 3×10^{-4} torr during the evaporation of the electrode material.

Having described the various processes that were common to the fabrication of the various types of chalcogenide switching devices, the description of each individual type of device is given below.

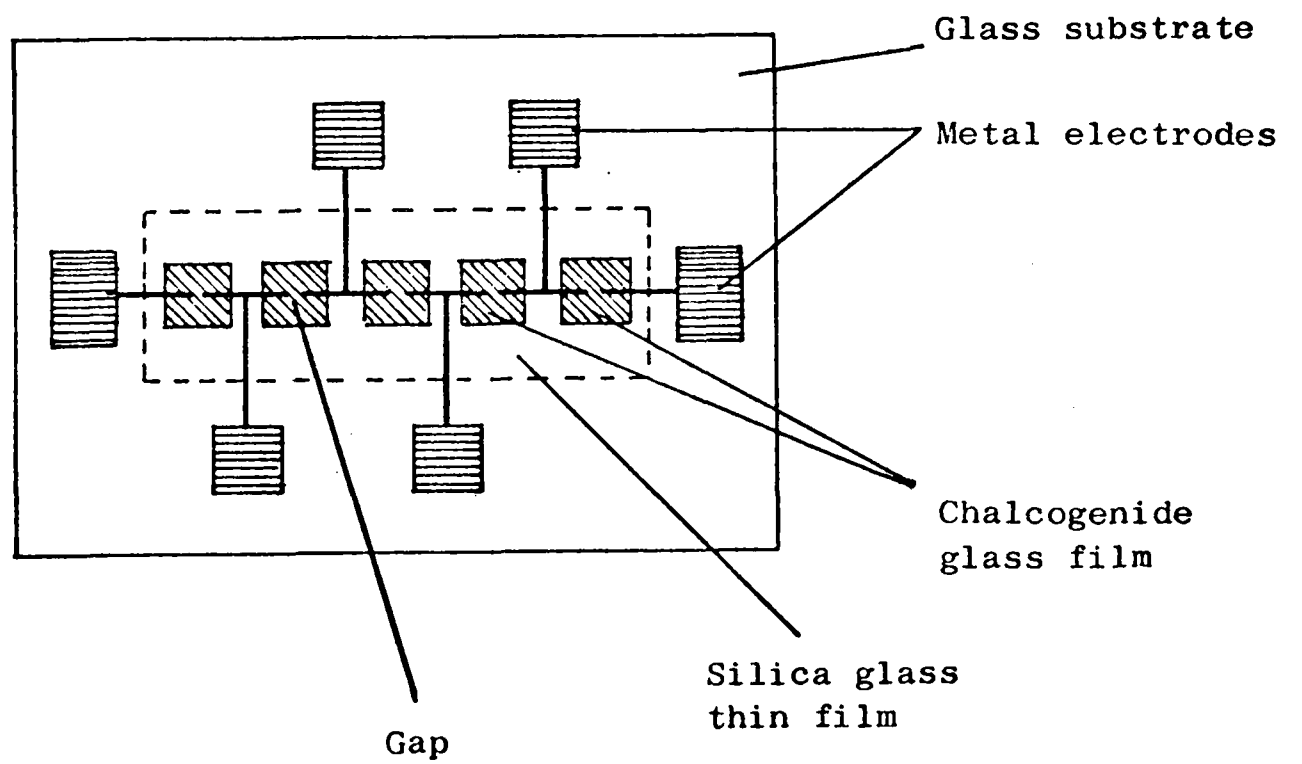
3.6.5. Sandwich Devices

A sandwich type switching device was prepared by first cleaning the glass substrate and then mounting it on the top of mask (a), see figure 3.9., which itself was mounted in the slot of a jig. The jig was simply a rectangular piece of aluminium, $\frac{1}{4}$ " thick, which had a rectangular hole of 2.8 x 1.8 cm. On the surface of one side, near the edges of the hole there was a square



AN ARRAY OF EIGHT SANDWICH DEVICES

Fig. 3.15(a)



AN ARRAY OF FIVE GAP DEVICES

Fig. 3.15(b)

groove 0.25 mm deep and 1 mm wide so that the mask and the substrate matched correctly. The jig was screwed to the cooling block via tapped holes in the bottom surface of the copper block, see figure 3.13.

The substrate holder, with the substrate and mask fitted to it, was transferred to the electrode-deposition plant which was then pumped out and the electrodes were deposited by electron-beam bombardment. The thickness of the metal film was usually in the range 2-3 μm . After this, the substrate was taken out and mask (a) was replaced by mask (b), see figure 3.9, and the substrate transferred to the flash evaporation plant. The plant was pumped out for more than 24 hours. The substrate was normally held about 25 cm above the source but this distance could be varied by compressing or stretching the bellows shown in figure 3.13. The deposition of the chalcogenide film was carried out at a rate of 0.6 $\mu\text{m}/\text{hour}$ using a motor speed of about 50 rev/sec and a hopper with a hole size of 1000 μm .

Water cooling was used during the deposition and preliminary temperature measurements with a chromel/alumel thermocouple showed that the temperature of the substrate rose only by a few degrees above room temperature even when the deposition time exceeded two hours. Liquid N_2 cooling was used initially, but to improve the outgassing of the substrate this was replaced by water cooling.

After depositing a chalcogenide glass film of a desired thickness, the substrate was taken out and the top metal electrode was deposited using mask (c).

3.6.6. Point-Contact devices

Point-contact devices did not require the use of deposition masks. A thin film of Al/Cr was first deposited over the entire surface of the substrate and on top of this a chalcogenide glass film was deposited. The Al/Cr thin film acted as the lower electrode and the top contact was a molybdenum rod with the contact end hemispherically shaped, ~ 3 mm diameter, and polished with diamond paste to give it a fine finish.



Figure 3.16(a)
The electron-gun vacuum plant.

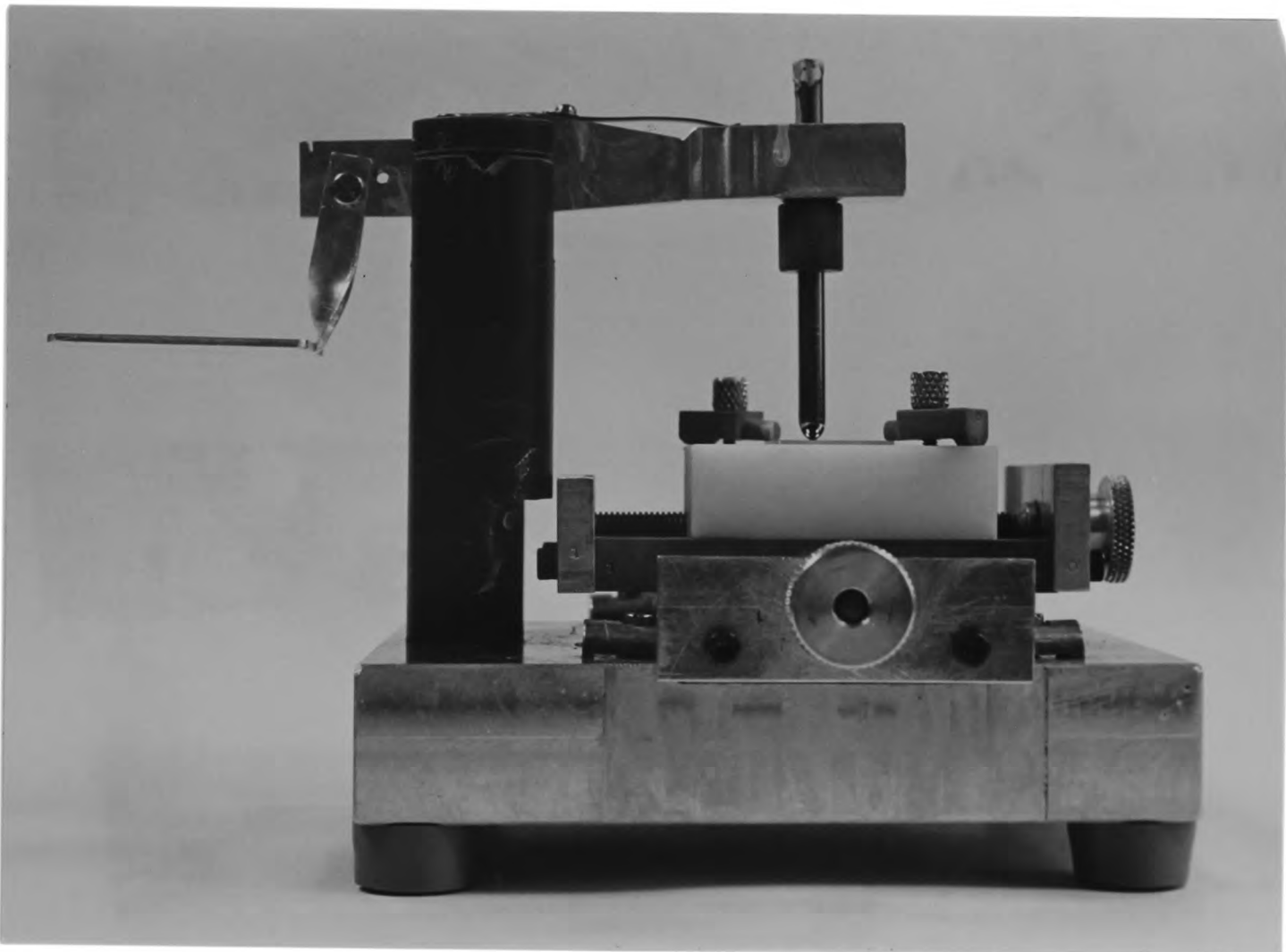


Figure 3.16(b)
The point-contact device jig.

The top contact was mounted on the cantilever arrangement of the point-contact device jig shown in figure 3.16(b) and thus provided constant pressure on the surface of the chalcogenide film. The film substrate was horizontally mounted on the X-Y platform of the jig.

It was not possible to measure the probe contact area accurately, but it was estimated to be comparable with the contact area in a D07 device (Neale, 1970). The diameters of the graphite hemispherical tips in a D07 device were found to be about 5 mm. They were measured by projecting a magnified image of a D07 device on a screen. The projector is shown in photograph 3.17 and was of the type used by mechanical engineers for comparing profiles of small machined objects.

3.6.7. Gap Devices

Gap devices, figure 3.15(b), were fabricated using masks (d) and (e), figure 3.9. In the absence of precision etching facilities, the gap was produced using a thread-masking technique (Weimer et al, 1964). In this technique, wires or threads were placed across the substrate surface on which the metal film was to be deposited. Mask (d) was then placed on the substrate surface and the two mounted on the substrate jig and screwed to the substrate holder. The masking threads used were either 2 μm thick diameter platinum wire (Wcolaston Wire, supplied by Johnson and Matthey) or adhesive threads. The latter were produced by pouring a small quantity of a viscous adhesive such as Evostick on the tips of two glass rods held very close to one another and then moving the rods apart until an extremely fine thread was drawn (Schuöcker, 1973). The thread was then laid across the substrate surface and left to dry before the application of the film deposition mask (d). After deposition of the thin film the thread was

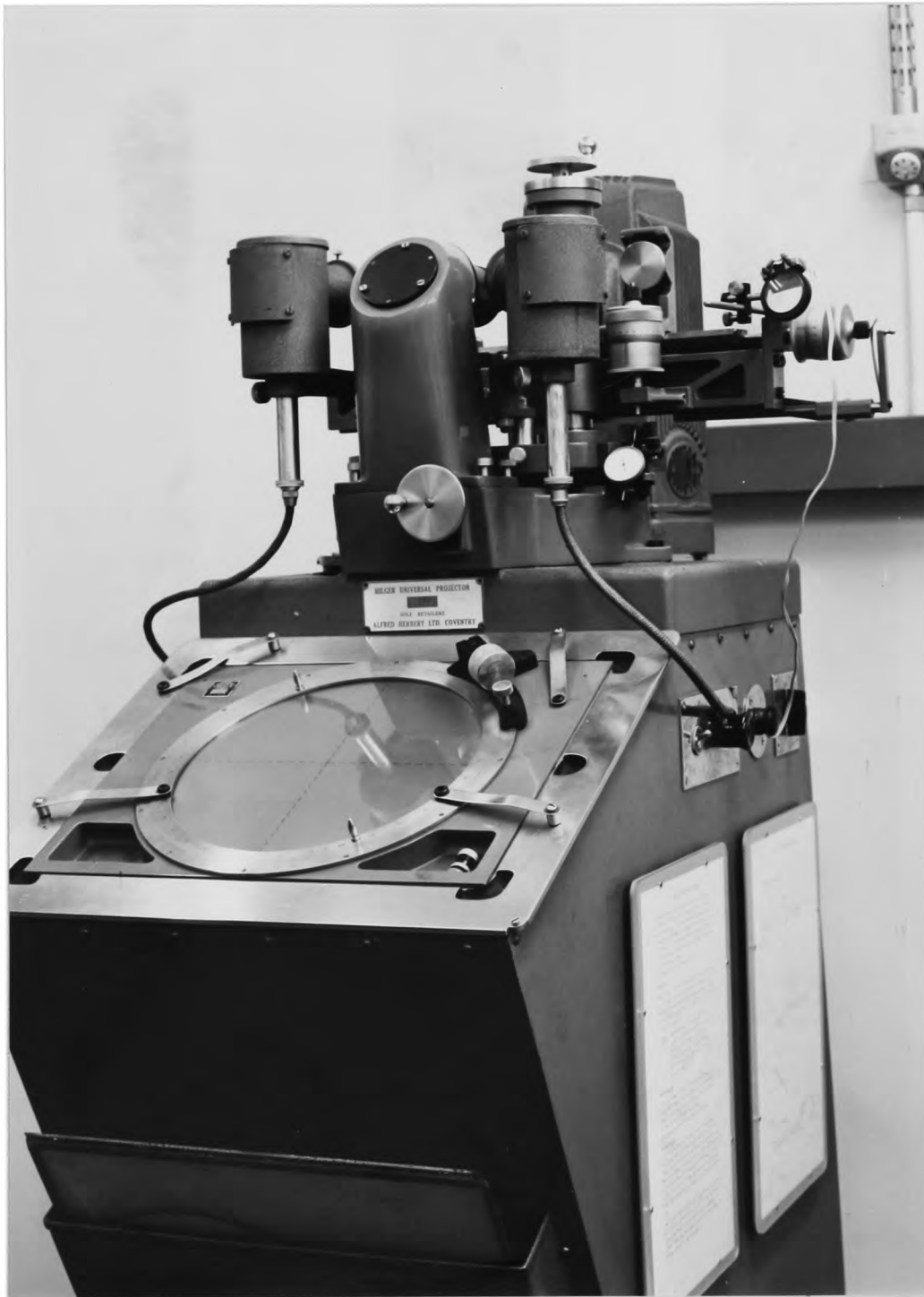


Figure 3.17

The projector used for examining the detailed geometry of a DO-7 device.

washed away with acetone.

The gaps made using the 2 μm wire were 1.6 μm wide and could be accurately reproduced, but the width of those gaps made by the adhesive thread method were difficult to control. Therefore, actual measurements were carried out on the well-characterised devices made using Woolaston-Wire masking.

In addition to thin film gap devices, "bulk" gap devices were also made by evaporating the metal electrodes on a polished surface of a 3 mm thick chalcogenide glass disc. These devices were similar to those described by Armitage et al (1972), but razor-blade scratching of the electrodes was not used to make the gap. The gap was made by wire-masking as described above. To reduce the possibility of a conductive "skin" (Green et al, 1972; Cohen, 1973) forming on the surface of the chalcogenide glass, gap devices were coated with a thin layer of fused silica by electron-beam bombardment, see figure 3.15(b).

3.6.8. Device capacitance

The capacitance of a sandwich device is given approximately by the expression:

$$C = \frac{k_r k_o}{d} A \text{ farads}$$

where K_r is the dielectric constant and equal to 16 (Bosnell et al, 1972), d is the film thickness, A is the active or crossover area, and k_o is the absolute permittivity and numerically equal to 8.855×10^{-12} farads/meter. For a device with a film thickness of 2 μm and a self-capacitance of 2 pf, an active area of $\sim 70 \times 10^{-6} \text{ cm}^2$ is required. If the top and bottom electrodes have the same width, then the active area is a square with side-length equal to 0.0084 cm. In fact, the slits in masks (a) and (c) were originally designed to have such widths, but after etching were found to be several times larger. As a result, the capacitances of sandwich devices were in the range

5-10 pf. The capacitances were measured with a Marconi Circuit Magnification Meter type TF1245. Connections to the thin film metal electrodes were made with 0.002" diameter tinned copper wires using an air-drying silver dag.

3.7. Pulse circuits and recording of device I-V Characteristics

Figure 3.18 shows the arrangement of pulse circuits used for examining the current-voltage characteristics of the devices. The practical arrangement is shown in figure 3.19. With the exception of the pulse generator and oscilloscopes, the circuits were specially designed and constructed for the present work. In addition, an X-Y plug-in unit was purchased and fitted to the Solartron oscilloscope. The devices were switched by voltage pulses taken from the pulse generator and amplified to a sufficient level. The descriptions of the individual circuits and the operation of the network are given below.

Voltage pulses were supplied by a Farnell modular double-pulse generator with single shot facilities. It had two separate outputs with independent control of pulse width, delay, amplitude and polarity. One output was from a variable slope module which controlled the pulse rise and fall times. The second output delivered rectangular pulses. The pulse repetition frequencies were in the range 0.01 Hz to 10 MHz and the rise time was approximately 10 ns.

The operational amplifier circuit, figure 3.20, was designed using a Fairchild 709 integrated circuit unit. It had two inputs, one inverting and the second non-inverting. When the inverting input S_1 was open S_2 was closed and vice versa. The gain of the amplifier was variable and numerically equal to the ratio of the feedback resistor to the input resistor. Thus the maximum gain was ten.

The high voltage power amplifier was initially constructed using an E184 valve in the circuit shown in figure 3.21(a). The circuit had a voltage gain of about 13 and was capable of delivering pulses up to 120 volt peak height. The output of this circuit was connected to the input of a cathode follower, figure 3.21(b), with an output impedance of 150Ω . The two circuits were fitted in one box to make a unit with a single-ended input

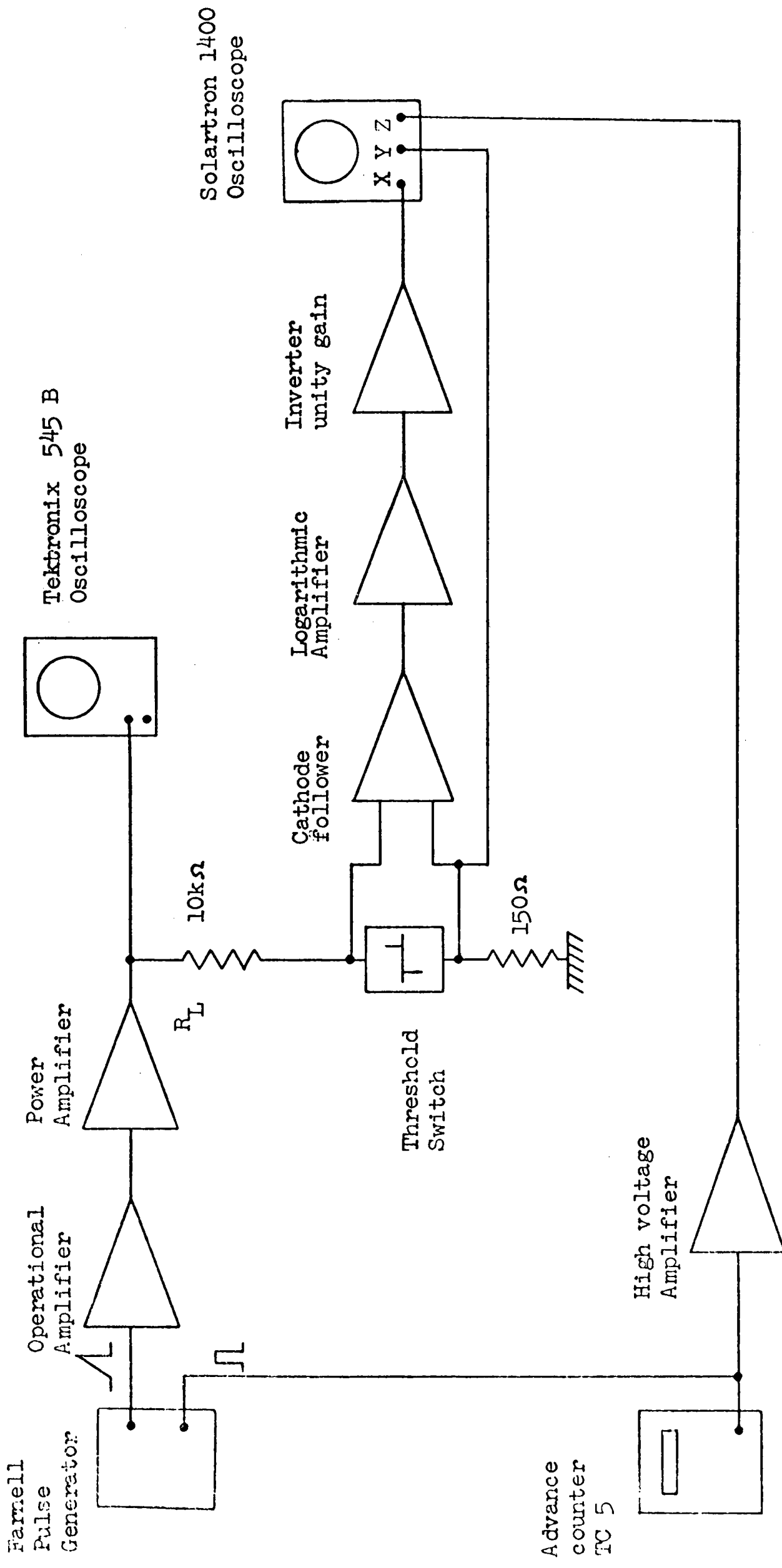


FIG. 3.18 SCHEMATIC DIAGRAM OF DEVICE - EXAMINATION NETWORK.

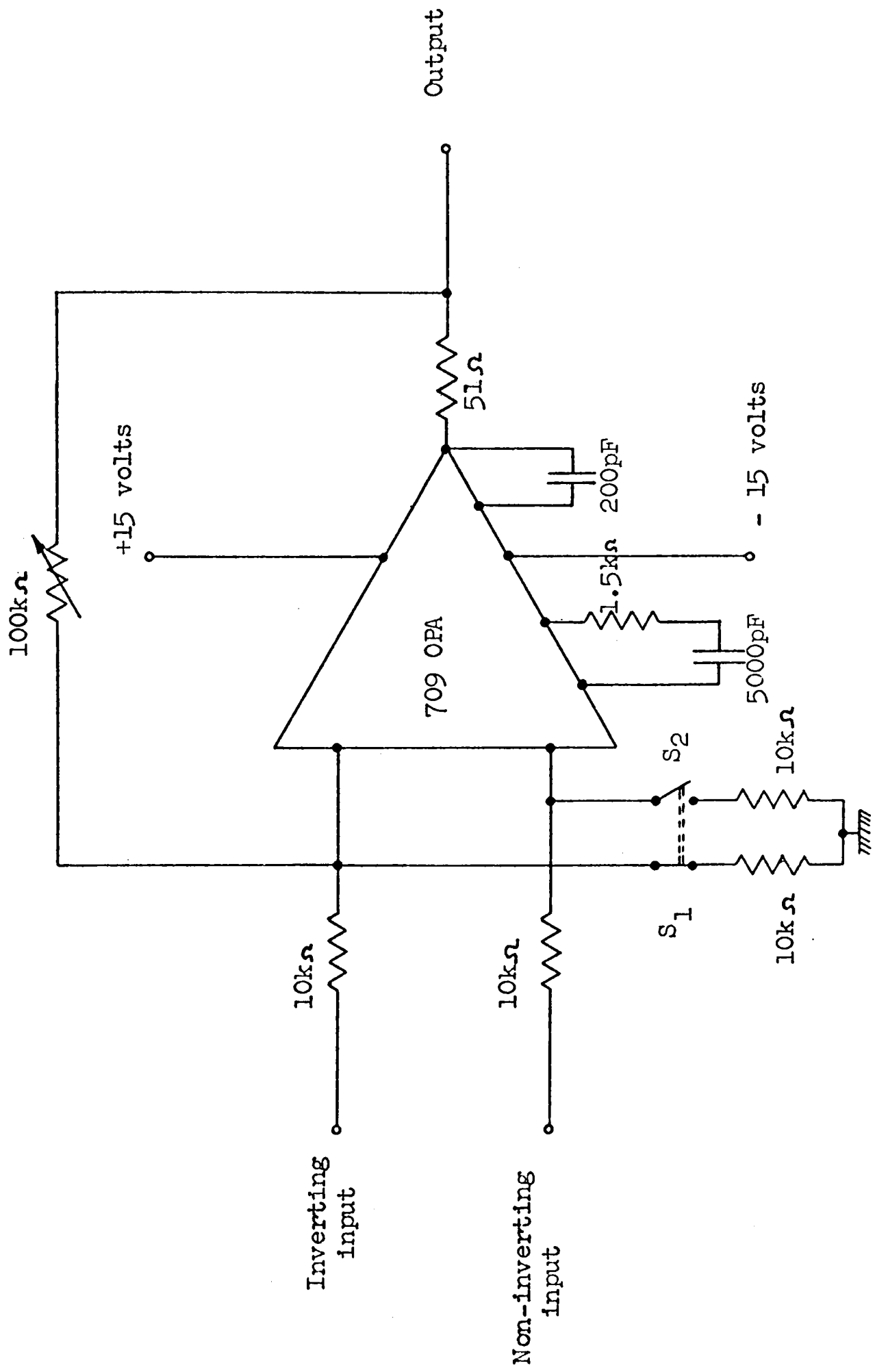
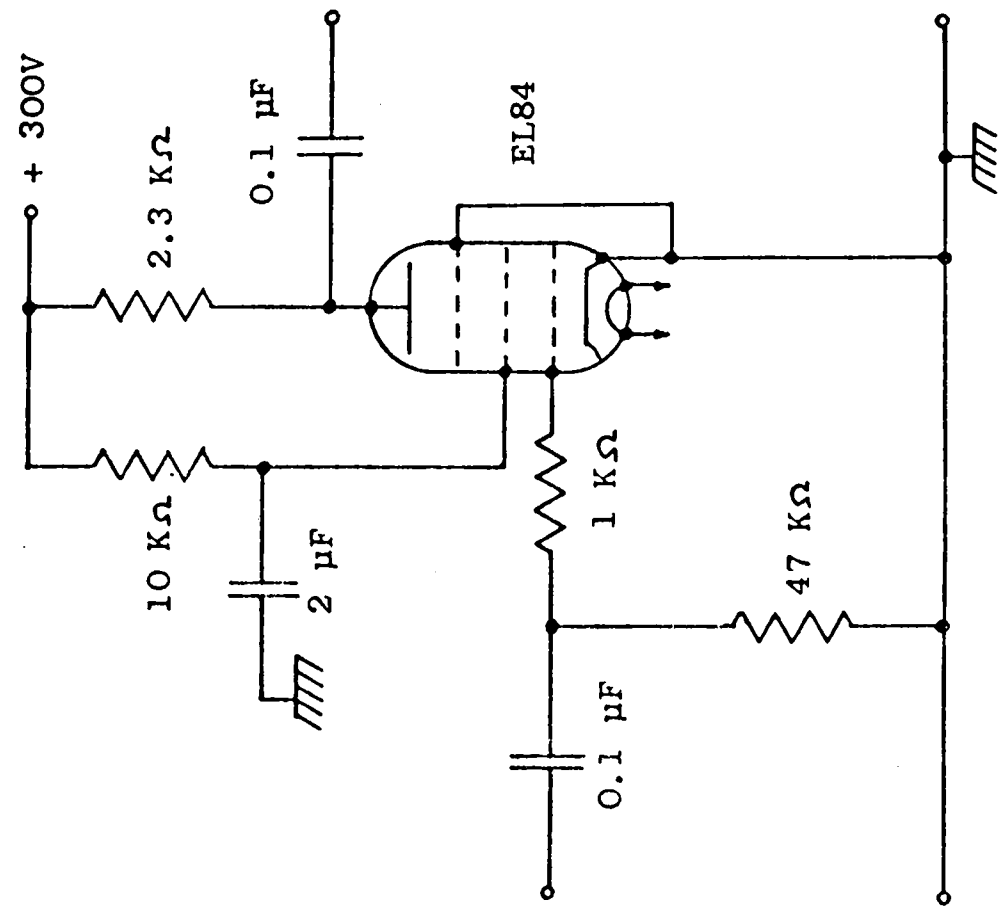
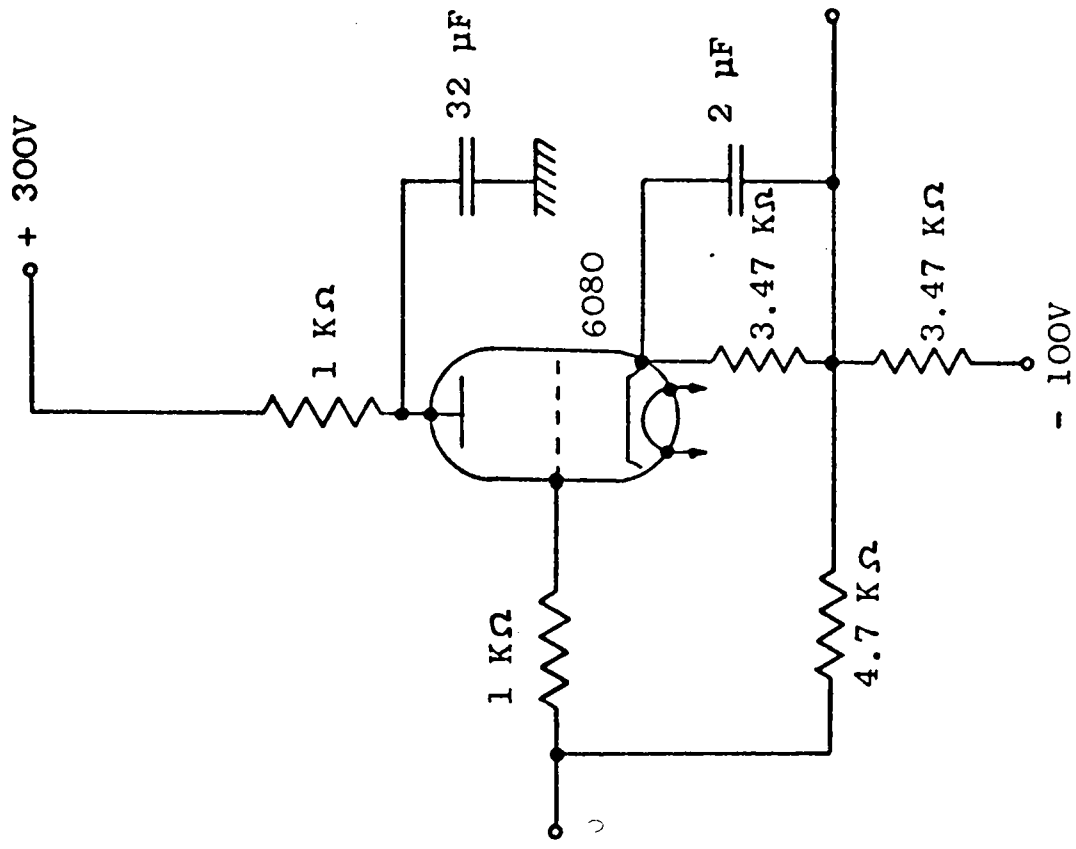


Fig. 3.20

709 OPERATIONAL AMPLIFIER CIRCUIT.



HIGH VOLTAGE AMPLIFIER
Fig. 3.21(a)



CATHODE FOLLOWER
Fig. 3.21(b)

and output. This unit was later replaced by the circuits shown in figures 3.22 and 3.23. The circuits in figure 3.22 drawn with its power supply, was used to amplify positive-going pulses, while the circuit in figure 3.23 was used for negative-going pulses. Each of these amplifiers had a voltage gain of about ten and was capable of delivering pulses up to 100 volt peak height at a current of 10 mA.

Two amplifiers of each circuit were built and the four fitted with their power supplies, inside one single box, but each amplifier had its own separate input and output sockets fitted on the front panel of the box.

The logarithmic amplifier circuit, figure 3.24, was especially designed to take fast pulses. It converted the horizontal X-scale of the I-V characteristics of the device into a logarithmic one so that the sensitivity for the horizontal-axis could be increased for low voltages and the fine details of the low-voltage on-state of a device displayed while also keeping the full off-state characteristics on the oscilloscope screen.

As the logarithmic amplifier had an input impedance of 10 K Ω which was considerably lower than the off-state resistance of the switching device, a cathode follower with a high input impedance was connected between the logarithmic amplifier and the device. The cathode follower was identical to the one shown in figure 3.21(b).

The logarithmic amplifier had an inverting input which made it necessary to follow it by an inverting operational amplifier of unity gain, see figure 3.20.

Figure 3.25 is a calibration curve for input versus output voltage of the logarithmic amplifier. The calibration was carried out using a ramp pulse of 1.3 ms at a repetition rate of 100 pulse/sec. This pulse was chosen because it was representative of the pulses used to examine the devices.

All the circuits designed were constructed on printed circuit boards, with each board especially made for every circuit. Connections between the various electronic units were made via 50 Ω BNC sockets and plugs and high frequency coaxial cables.

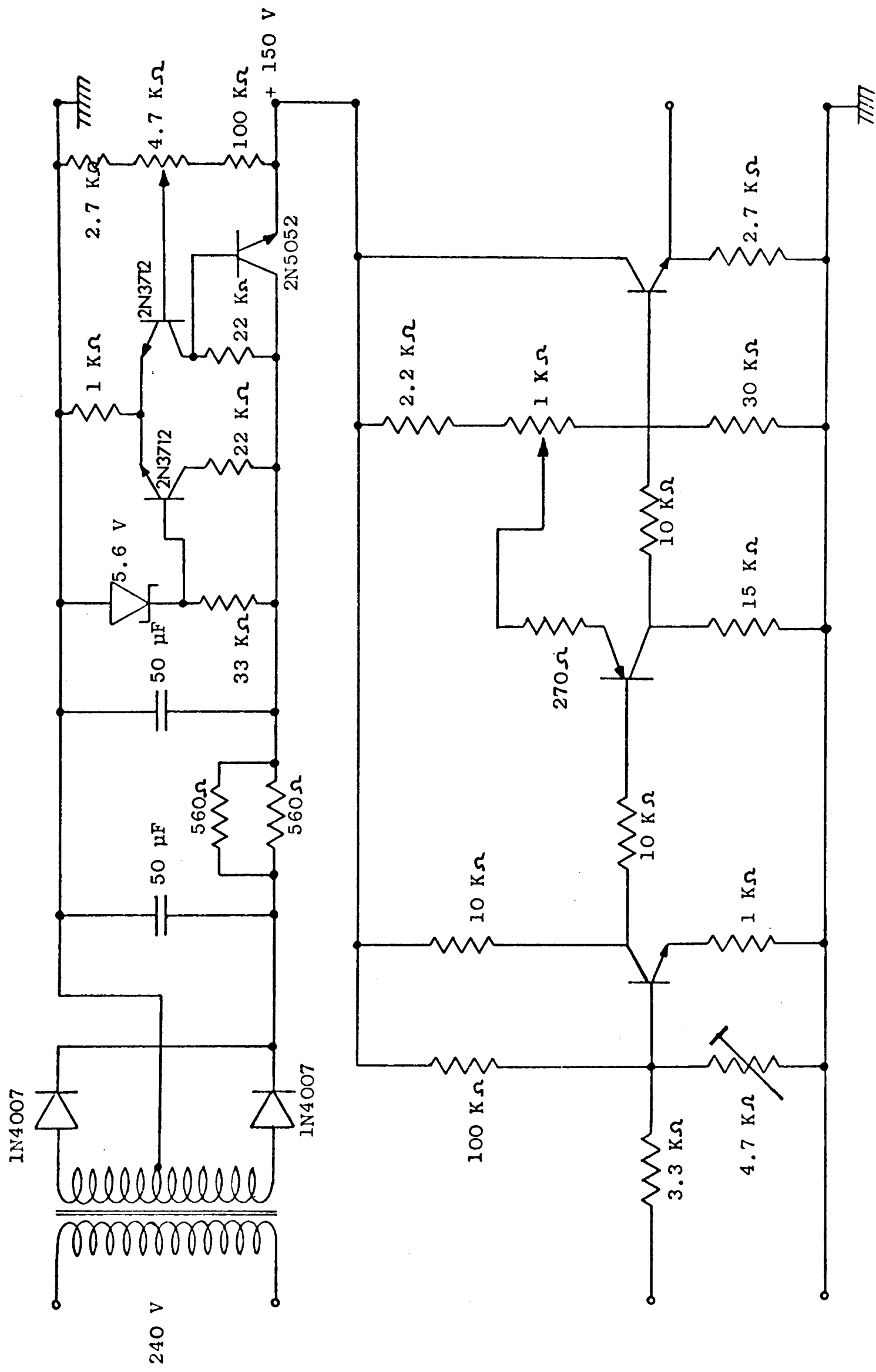


FIG. 3.22 TRANSISTORISED HIGH VOLTAGE AMPLIFIER WITH POWER SUPPLY

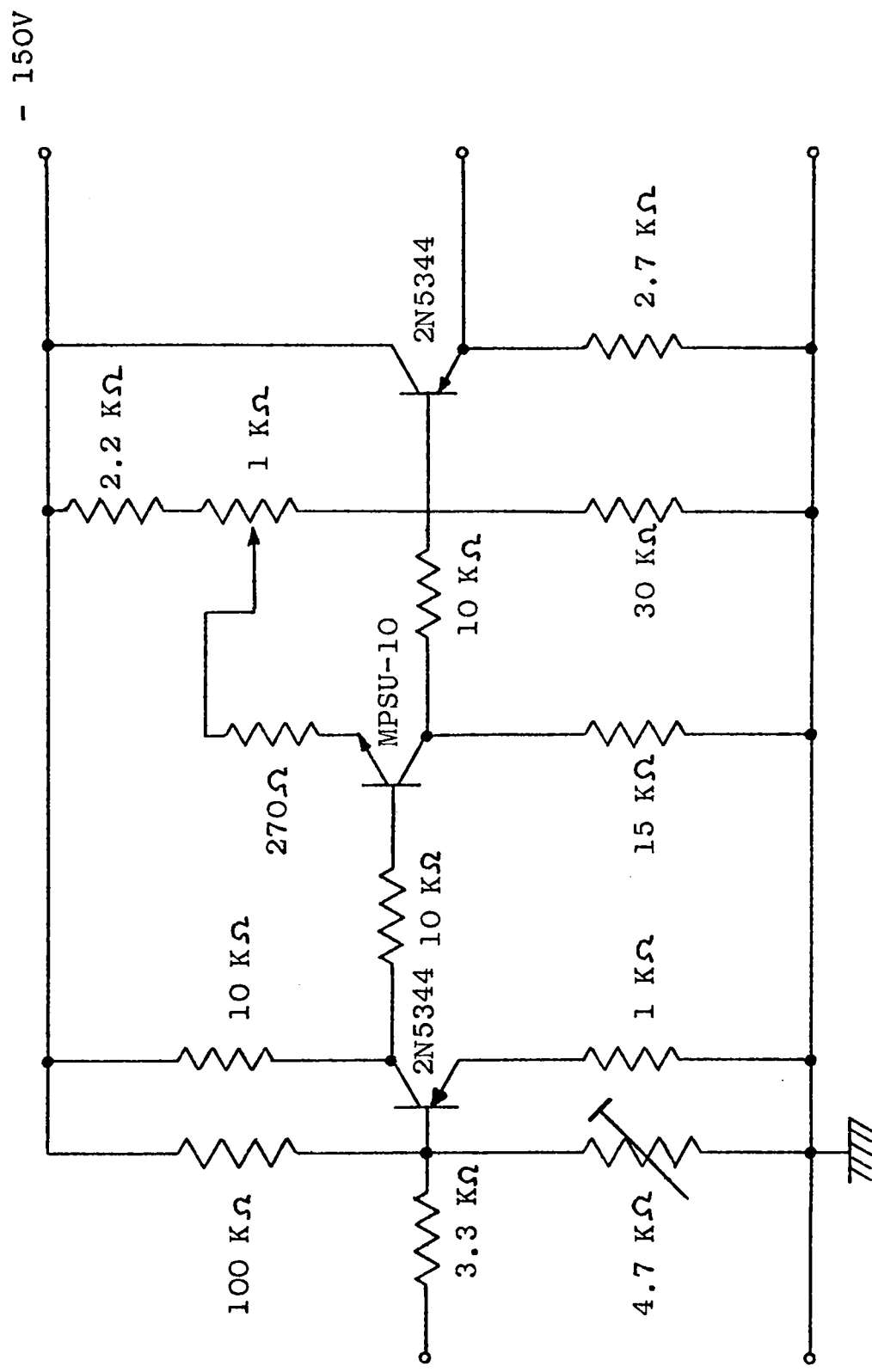
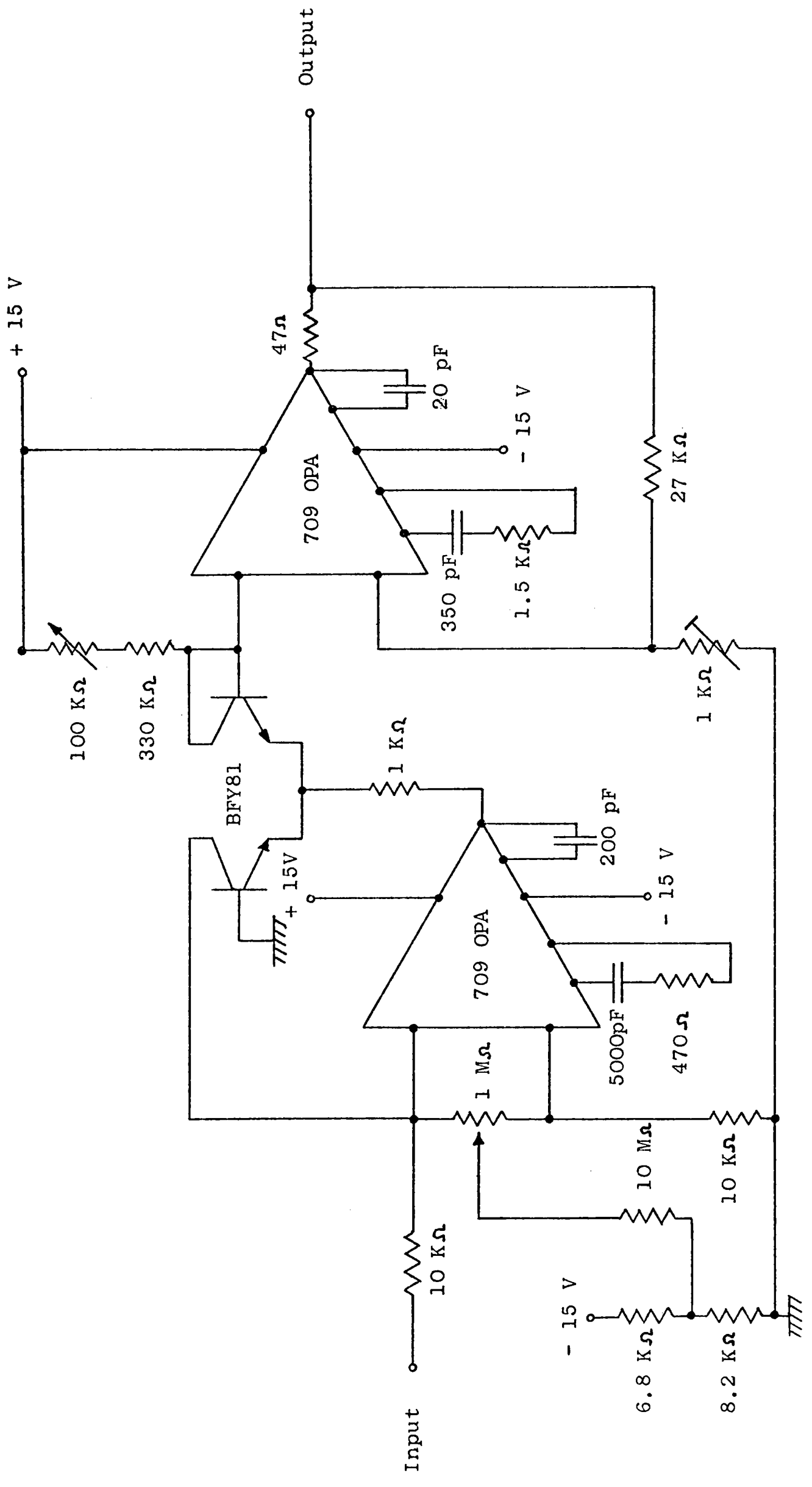


Fig. 3.22 TRANSISTORISED HIGH VOLTAGE AMPLIFIER



LOGARITHMIC AMPLIFIER

Fig. 3.24

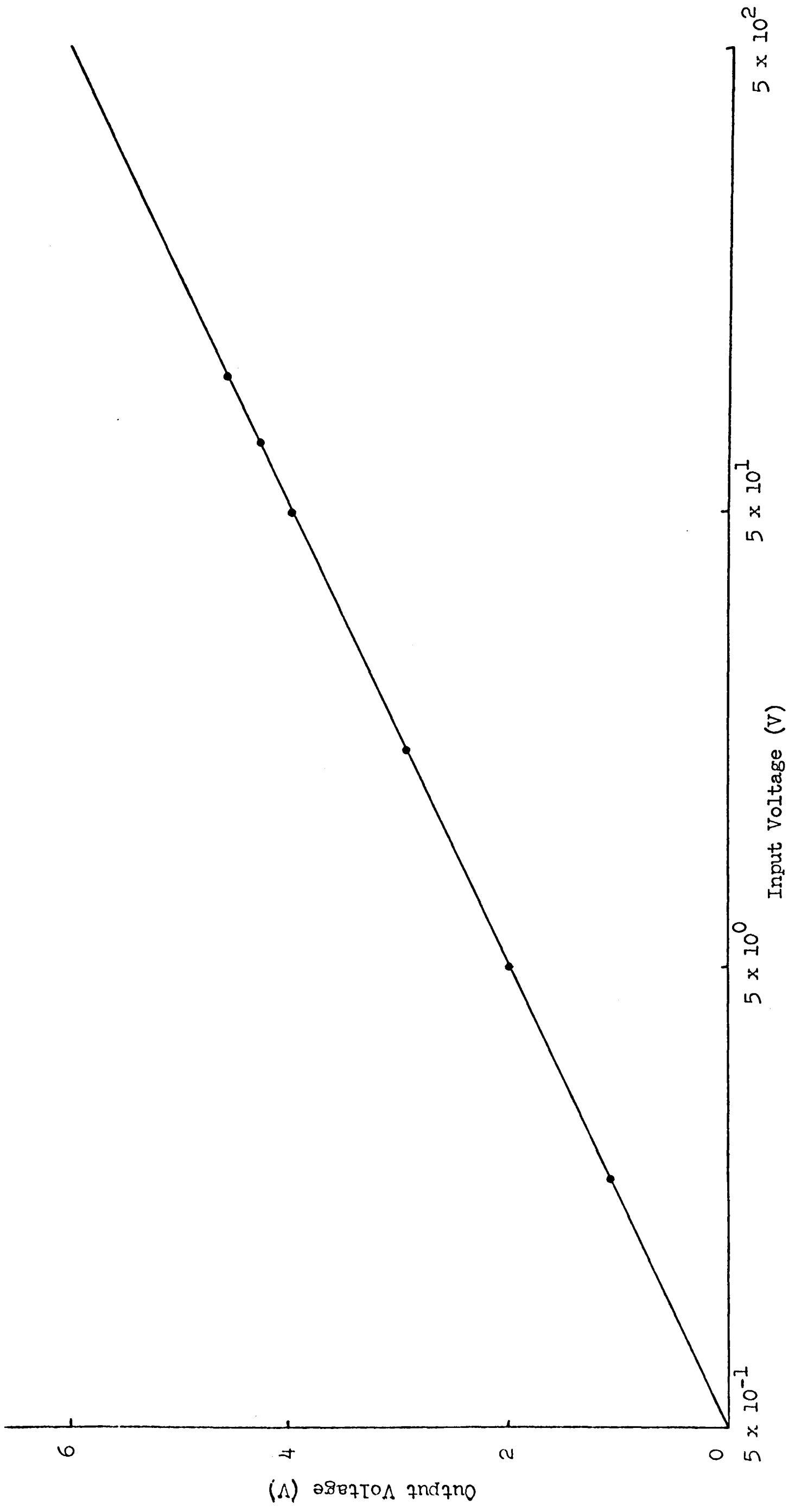


FIG. 3.25

CALIBRATION CURVE FOR LOGARITHMIC AMPLIFIER

When examining a device, a 9 V ramp pulse, of specific width and repetition rate, was taken from the variable slope module of the pulse generator and fed into the appropriate input of the variable gain operational amplifier circuit. The output of the operational amplifier was then fed into the power amplifier. The output of the power amplifier was connected via a "T" connector to (i) one input of a double-beam Tektronix Oscilloscope type 545B, and the gain of the operational amplifier was adjusted until the pulse height displayed on the oscilloscope screen was 80 volts, (ii) the device test circuit which consisted of the thin film switching device, a load resistor R_L which was $10\text{ k}\Omega$, and a 150Ω resistor which was used for measuring the current through the device. The device circuit was placed in a Mu-metal box for shielding purposes. The voltage across the device was fed to the horizontal X-input of the X-Y oscilloscope via the cathode follower and the logarithmic amplifier. The voltage across the 150Ω resistor was directly fed to the vertical Y-input of the oscilloscope. The I-V characteristics of the device were then photographed on a Polaroid film. For good photographic recording the pulse generator was operated in the single-shot mode and brightness modulation was required. This was achieved by first turning the screen spot brightness down until it became invisible and then taking a positive square pulse from the second output of the pulse generator and amplifying it to 50 volts before feeding it to the Z-axis input of the X-Y oscilloscope. The square pulse had the same width as the device test pulse and was synchronised with it, so that when the camera shutter was opened the spot was visible only for a period equal to device pulse duration time.

The brightness modulation pulse was also fed to the input of an Advance TC5 pulse counter, see figure 3.18. This unit counted the pulse that was applied to the device circuit and also the switching operations.

When the logarithmic amplifier was not used the cathode follower was replaced by the high input impedance differential amplifier shown in figure 3.26. The Ancom 15B₂ operational amplifier used in this circuit had an f.e.t. input and a fixed gain of 100, but as the output of the Ancom 15B₂ unit could

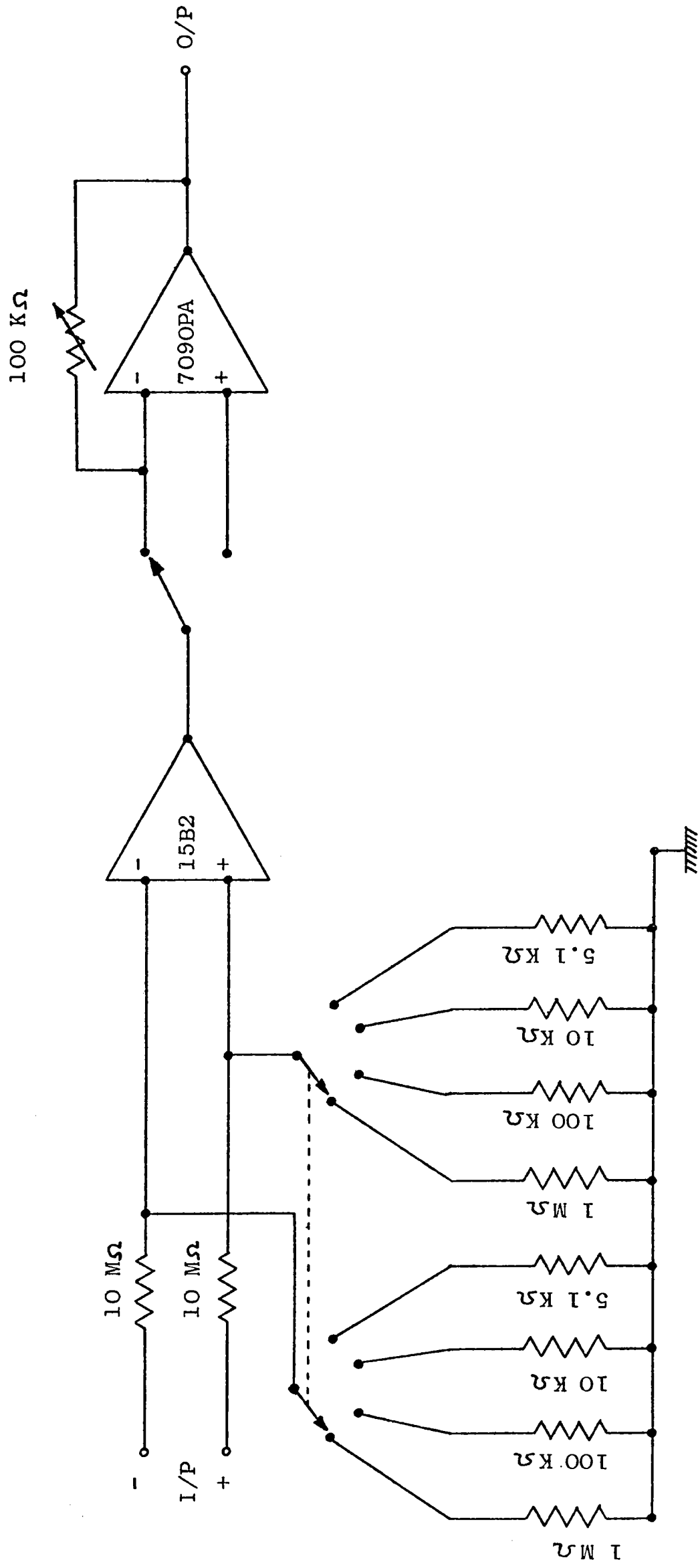


Fig. 3.26 HIGH INPUT IMPEDANCE DIFFERENTIAL AMPLIFIER

deliver a maximum of 10 volts the input signal had to be drastically attenuated. The extent of the attenuation was determined by the magnitude of the input signal and was made variable by providing a potential divider consisting of several resistors as shown in figure 3.26. The input had also two sockets, one for negative pulses and a second for positive pulses. The output of the differential amplifier was fed to the input of a variable gain 709 operational amplifier to provide an extra control over the magnitude of the output signal. Because of the relatively low output voltage, this circuit was not suitable for use with the logarithmic amplifier which was mainly intended to take high input voltages.

In addition to the use of ramp pulses, the devices were switched with a slow rise-time pulse without the sharp corners of a ramp pulse. This pulse was chosen because it did not have the high frequencies associated with a ramp pulse. The pulse shape is shown in figure 3.27 and looks approximately like a half-sine pulse. It was generated by the circuit shown in figure 3.28 by feeding a square pulse, 2 V high and

10 ms wide, from the Farnell pulse generator into its input. The tuned circuit was shock-excited and produced a damped oscillation. The damping was imposed by the diode and the emitter follower. In the absence of the damping effect of the diode and the emitter-follower circuit "ringing" oscillations were observed on each side of the pulse. The damped pulse, or oscillation, at the output of the emitter follower had a width of 0.3 ms and an amplitude of 0.8 volts. To increase the pulse height, the output of the emitter follower was connected to the input of a variable gain 709 operational amplifier.

The circuit described above is the transistorised version of a somewhat similar valve circuit described by Puckle (1955). Although half-sine pulses could be obtained by simply rectifying a sinusoidal voltage waveform, obtaining a single-shot half-sine pulse is a far more complicated matter and it was more convenient to use the circuit just described.

Finally, the linearity of the system used for examining the

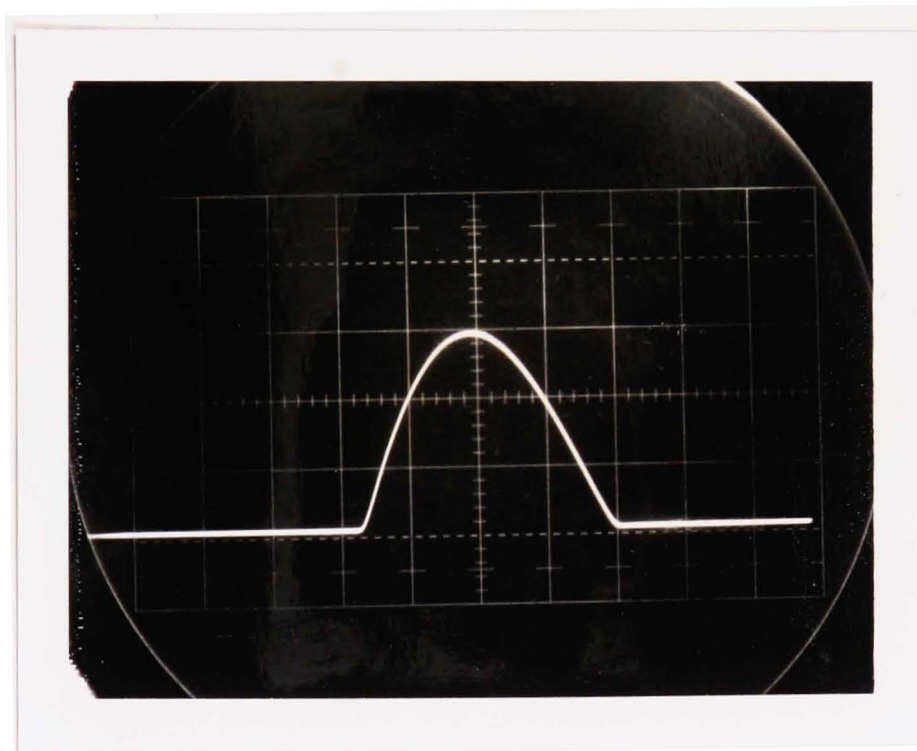


Figure 3.27

The output pulse generated by the circuit shown in figure 3.28.

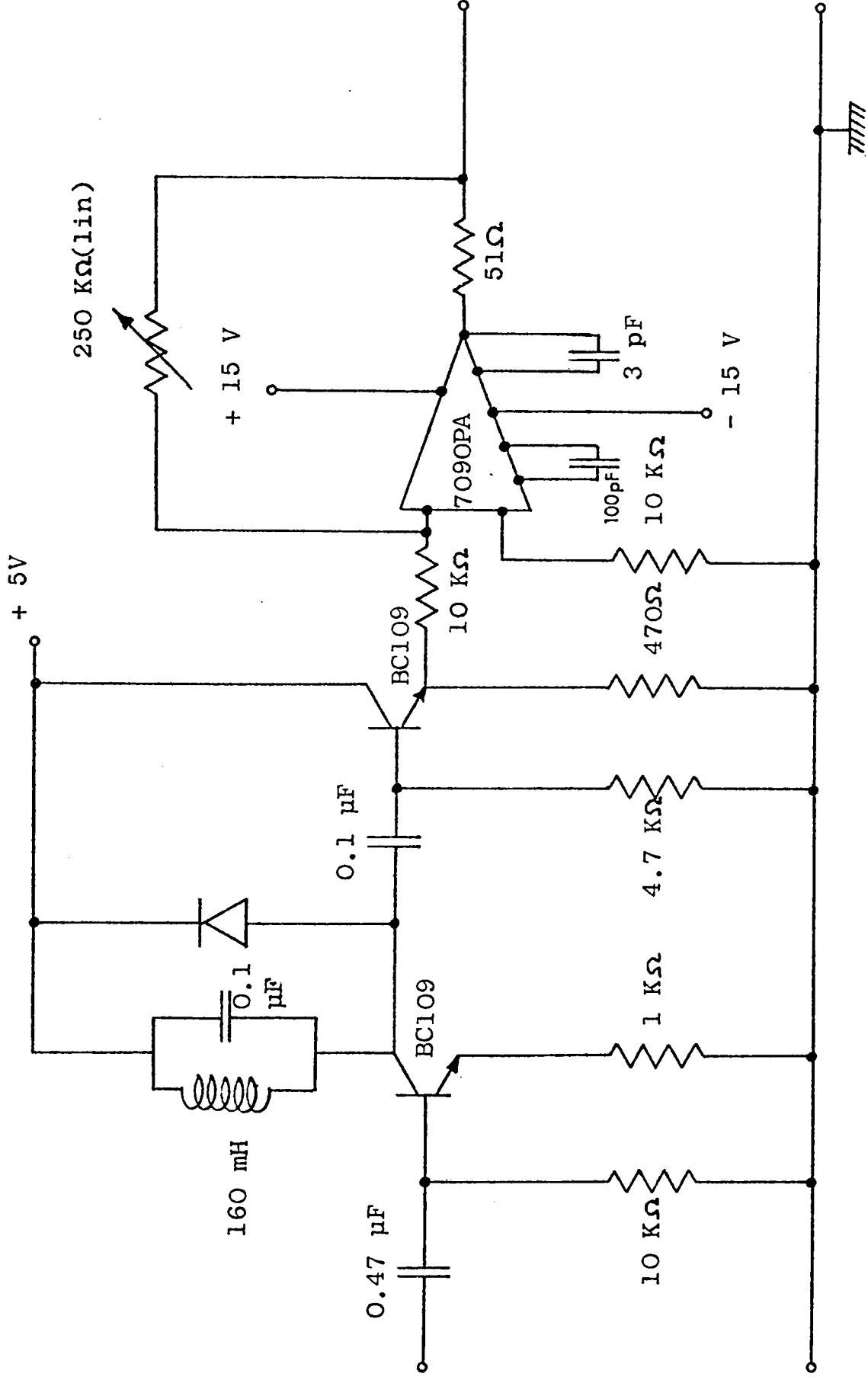


Fig. 3.28 SINGLE SHOT HALF-SINE PULSE GENERATOR

characteristics
current-voltage of the switching devices, figure 3.18,
was examined by replacing the switching device with a 1 M Ω
resistor and then applying the various pulses and frequencies
used for switching these devices. These pulses are mentioned
in Chapter Four. No phase shift could be detected for any
of the pulses and frequencies used.

CHAPTER FOUR

Experimental Results and Preliminary Discussion

4.1 Current- voltage characteristics

Figure 4.5 shows a typical current-voltage characteristic of a chalcogenide glass switching device. Attention in this section will be confined to the threshold voltage and the on-state characteristic.

(a) Threshold voltage

Ramp pulses of 1.3 ms width at repetition rates of (i) 1 pulse/sec and (ii) 100 pulse/sec were initially used for switching the devices. The pulse width was very large compared to the widths of 2-5 μ s used by other workers (Hensch et al, 1971) for examining similar devices. However, for a clear display of the current-voltage characteristic of a switching device it proved necessary to use pulses of slow rise time. The current through the device was limited by a 10 K Ω series resistor unless stated otherwise.

Of \sim 110 virgin devices tested, all were found to undergo a forming or first-fire process, after which the threshold voltage dropped considerably. Figure 4.1 shows a plot of threshold voltage versus number of switching operations for a typical point-contact device, 1.6 μ m thickness, with Al/Cr film as bottom electrode and Mo probe as top contact. It can be seen that the first-fire voltage, 50 V, dropped to about 13 V after a few switching operations. When the device attained a steady threshold voltage it was said to be formed. In some cases this process was found to take at least 10^3 operations. In general, the threshold voltages of formed devices showed very small fluctuations for at least 10^4 operations before a noticeable decrease was observed. Finally, after about 10^7 operations switching ceased when the device became permanently locked in the on-state. All tested devices - provided they had similar geometry, thickness and were tested under similar electrical conditions - which were fabricated from the same film had the same first-fire threshold voltage and similar threshold voltage versus number of operations behaviour as can be seen from figures 4.1 and 4.2 which were obtained for devices on the same substrate. This indicated that the thin film had a uniform composition across its surface.

Point-Contact Device (Cr-Mo Electrodes)

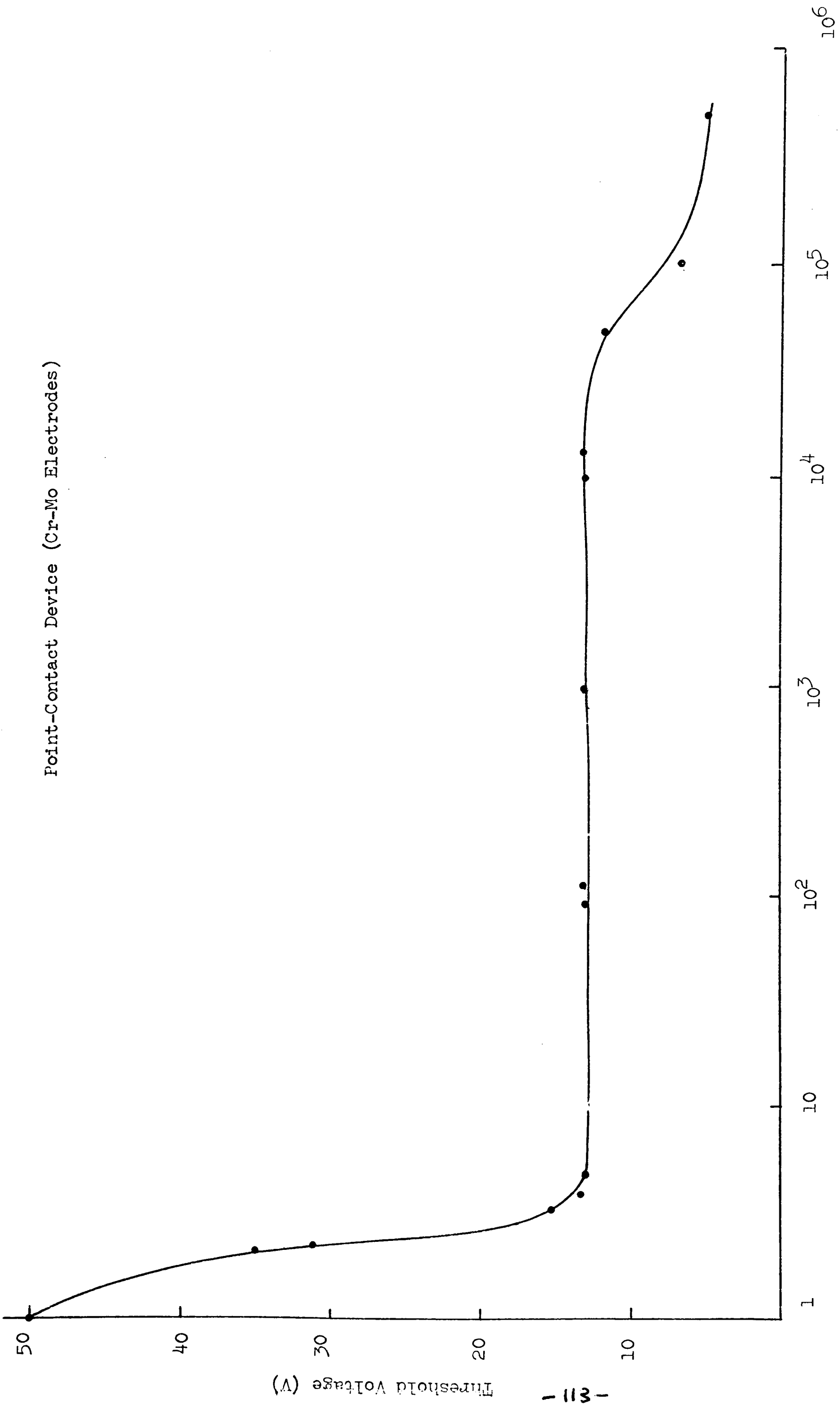


Fig. 4.1

Figure 4.3 shows the number of switching operations versus threshold voltage for a sandwich device of film thickness of about $0.6 \mu\text{m}$ and with Al/Cr cross-over electrodes. The first-fire voltage was 15 volts which dropped to about half this value after 4×10^2 operations. The fluctuations in threshold voltage of sandwich devices were much greater than in point-contact devices. Forming in thick sandwich devices, $\sim 2 \mu\text{m}$, was achieved after one or two operations but the threshold voltage of a formed device behaved in a rather erratic manner compared with that of a point-contact device. This erratic behaviour is believed to be due to the large crossover area and associated large self-capacitance of a sandwich device. This gives rise to a large capacitive energy which is discharged in the active material on switching and could have serious effects on the stability of the glass alloy composition and also cause some electrode damage.

The effect of different pulse repetition rates on device performance can be appreciated by comparing figures 4.1 and 4.2 with figure 4.4. In figures 4.1 and 4.2 the pulse repetition rate was 1 pulse/sec while the pulse repetition rate was 100/sec in figure 4.4. It can be seen that the fluctuations in the threshold voltage of a formed device were much greater for pulses at the higher repetition rate.

So far the results have been restricted to observations made on point-contact and sandwich devices. Forming in gap devices, both thin film and bulk devices, was not attained until after 500 operations, during which the threshold voltage exhibited extremely large fluctuations and, unlike point-contact and sandwich devices, the first-fire threshold voltage was not necessarily larger than those for all the subsequent switching operations during the forming process. The threshold voltage of a formed gap-device with a gap width of $1.6 \mu\text{m}$ was about 14 V. The operational lifetime of a bulk gap-device was about 10^3 operations. Thin film gap devices, which had a chalcogenide glass film of $2 \mu\text{m}$ thickness deposited, had a lifetime of about 5×10^4 operations. Device failure in thin film gap devices was always of the short-circuit type but in bulk gap devices the failure was of the open-circuit type. This latter type of failure was also found in sandwich devices but only when the top electrode was thinner than $0.3 \mu\text{m}$. Devices with thicker top electrodes always failed in the short-circuit mode.

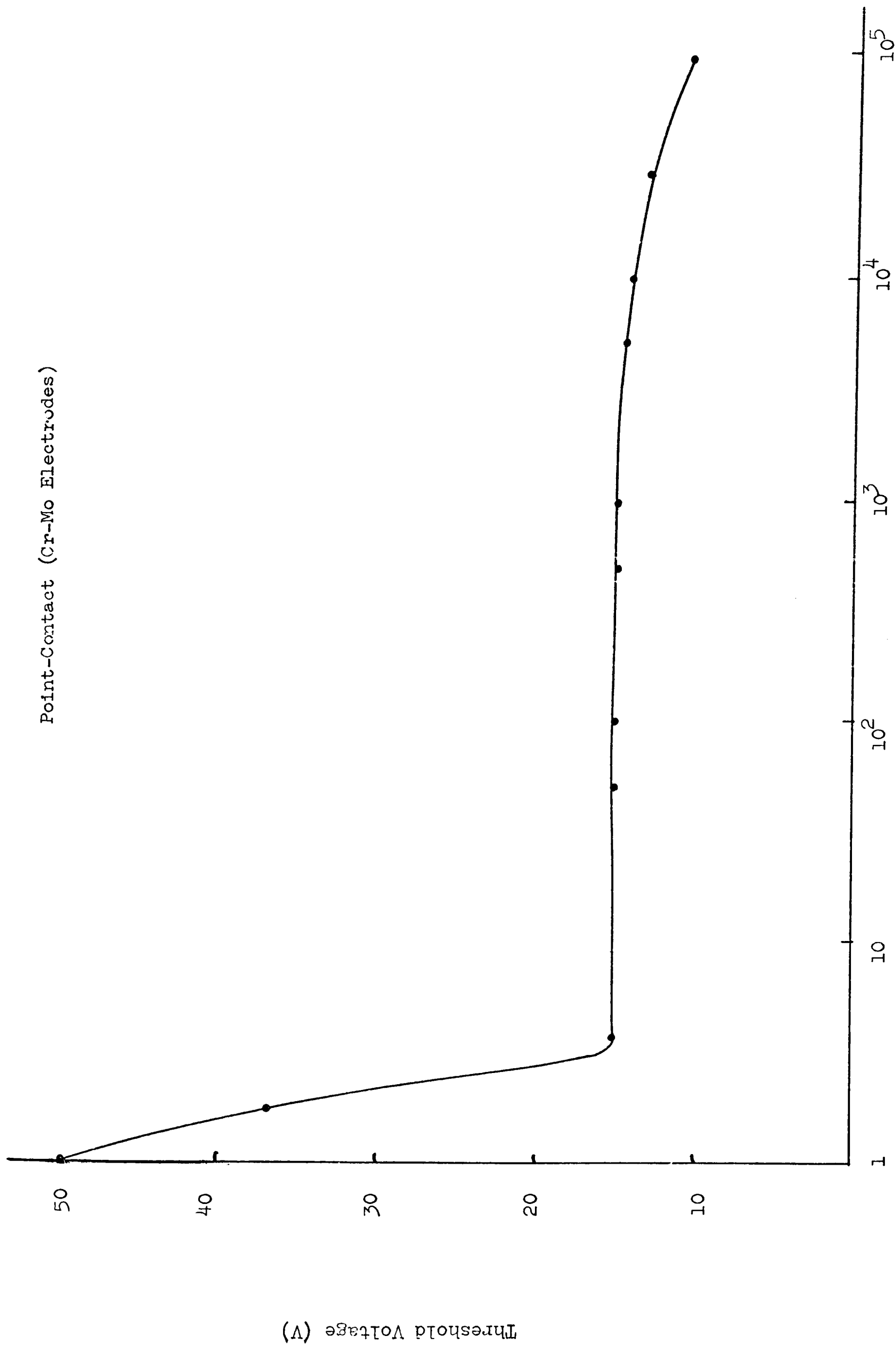


Fig. 4.2 Number of Operations

Fig. 4.2

Sandwich Device (Cr-Mo electrodes)

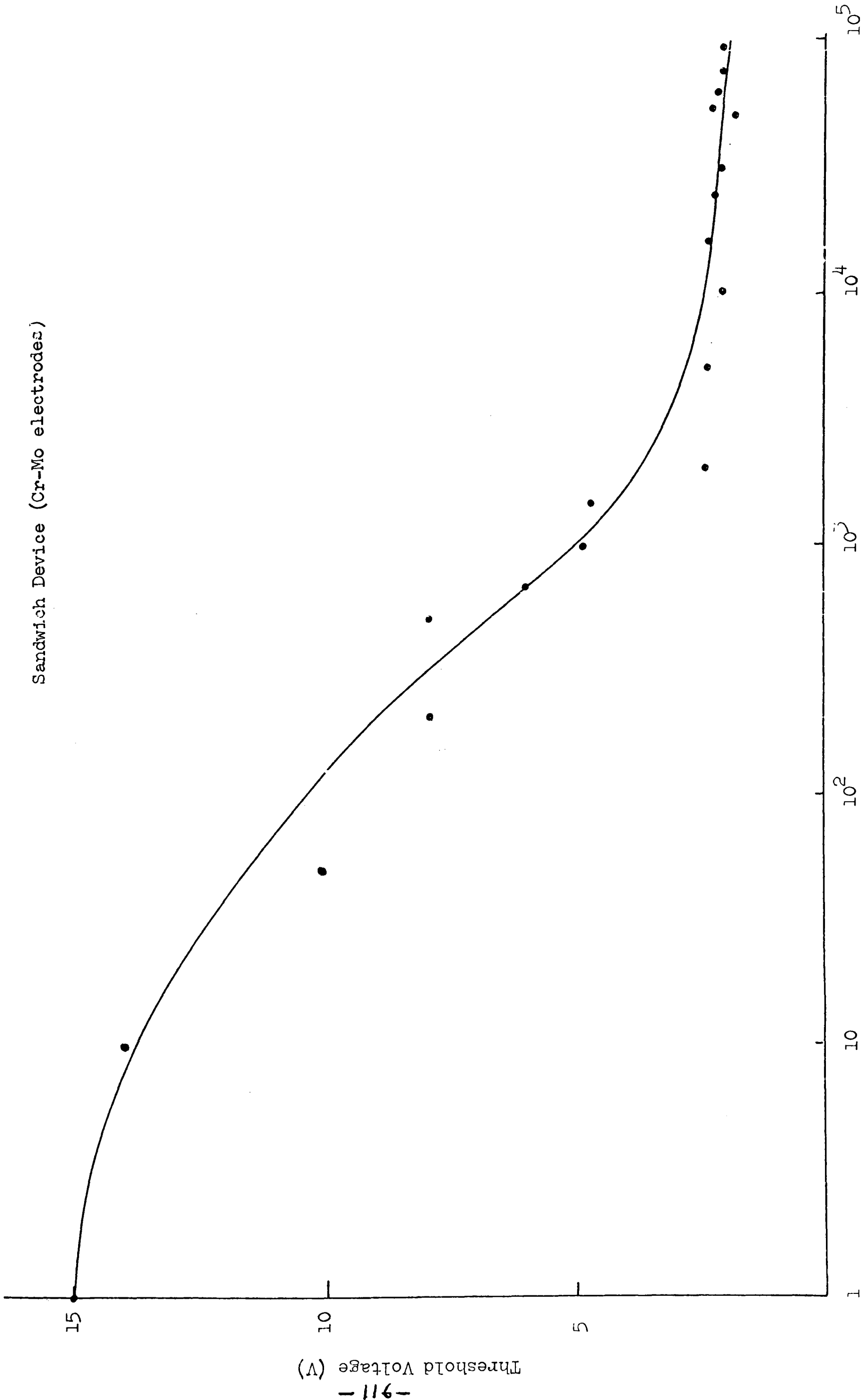


Fig. 4.3

Point-Contact Device (Cr-Mo electrodes)

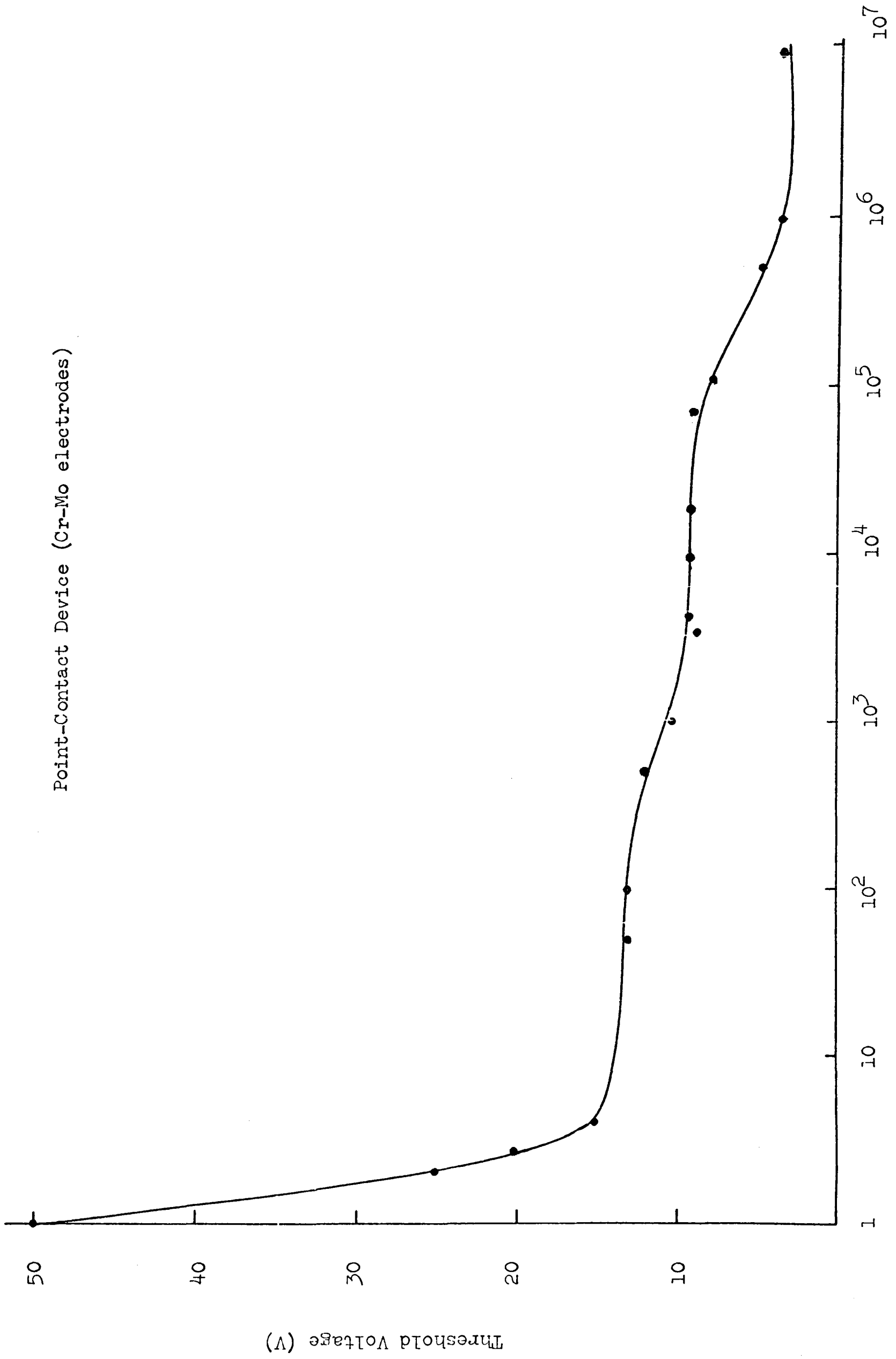


Fig. 4.4

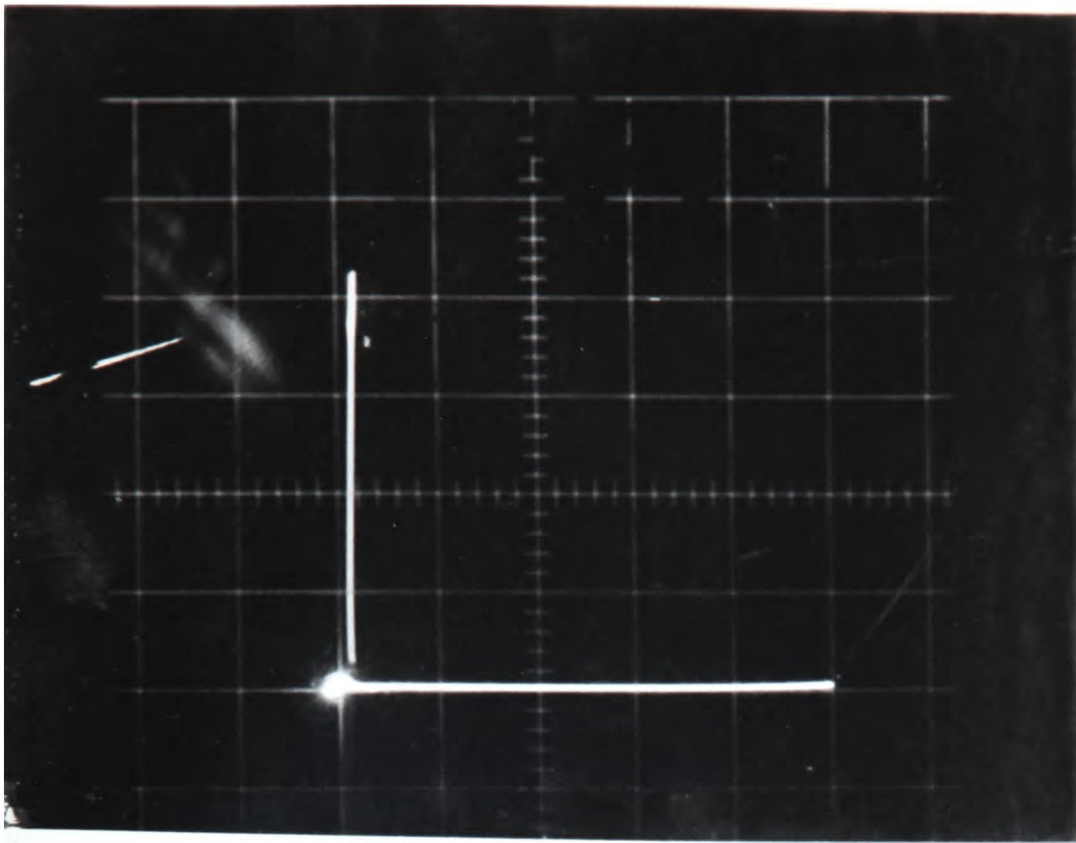
Finally, referring to figures 4.6, 4.8 and 4.9 it can be seen that the non-ohmic region which occurs prior to switching in these devices showed very distinctly during the first fire operation but became less apparent in the operations that followed. However, at a much later state in the device lifetime as the threshold voltage became closer to the holding voltage the non-ohmic region was enhanced and formed a considerable part of the off-state characteristics

(b) On-state characteristic

Figures 4.5 - 4.9 show photographs which were taken to display the current-voltage characteristics of two point-contact devices on the same thin film. Figures 4.5 and 4.6 shows the I-V characteristics for first-fire without and with the use of the logarithmic amplifier. Figures 4.7 and 4.8 show the I-V characteristics for the two point-contact devices after 10^3 switching operations and again without and with the use of the logarithmic amplifier. Finally, figure 4.9 shows the I-V characteristics of one device after 10^6 operations.

A thorough examination of the recorded current-voltage characteristics of both point-contact and sandwich virgin, unformed, devices showed that the on-state was a single trace with a negative-resistance portion near the end of the switching cycle as shown in the typical photograph in figure 4.6. After the devices were formed, the on-state characteristics eventually broke up into two (figure 4.8) or more branches (figure 4.10). The multiple-branching of the on-state did not always occur as soon as a device was formed and with some point-contact devices having Mo top contacts did not appear until after 10^4 switching operations. No definite or systematic relationship was found between the occurrence of branching and the number of switching operations. However, more branches generally appeared in the on-state as the number of switches increased and as many as five or more branches were observed in some devices after 10^6 operations, figure 4.9. In some cases, the nature of the branched characteristic, say two branches in the on-state, remained stable for 10^2 to 10^3 switching operations. The current-voltage characteristic of the on-state of a formed device can be described as a series of voltage steps which occur with very little change in current across the device. It can be seen from figure 4.10 that after the ramp pulse has exceeded the threshold (A) the

1.2 mA/div.



10 V/div.

Fig. 4.5.

Above: I-V characteristics for the first-fire switching operation of a point-contact device with 3 mm diameter tip Mo top contact and Cr film bottom electrode. The logarithmic amplifier was not used.

Below: I-V characteristics of a similar device as in fig. 4.8. The logarithmic amplifier was used and the voltage scale is logarithmic.

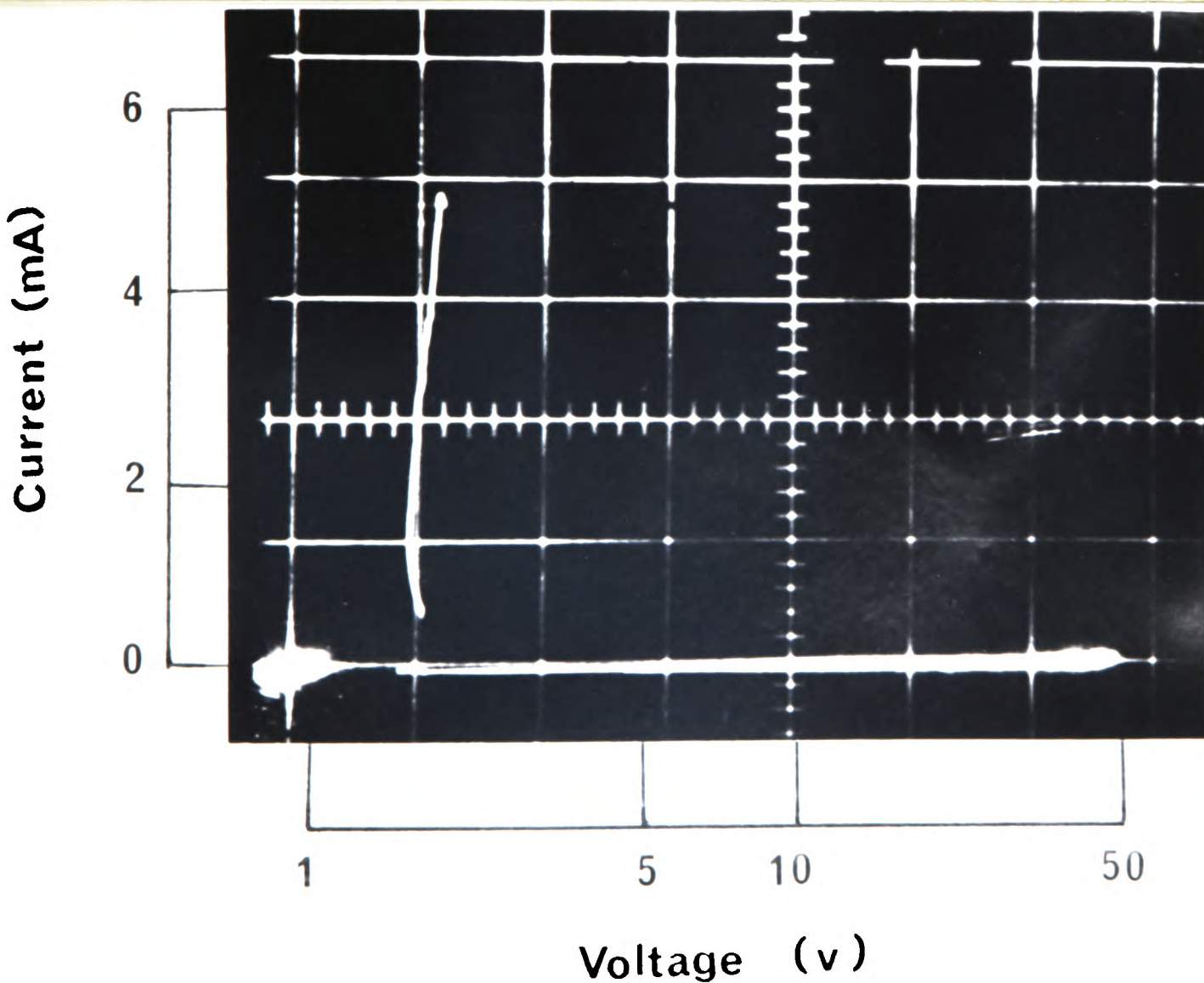
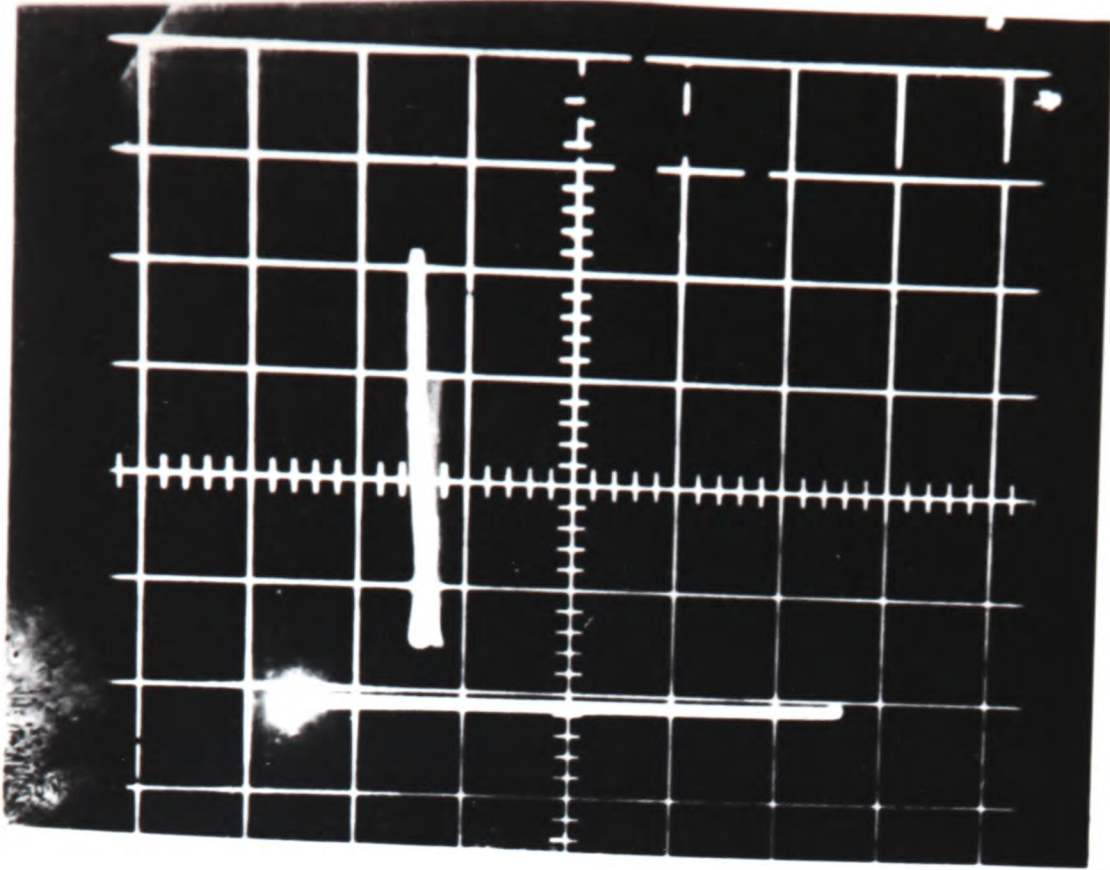


Fig. 4.6

0.6 mA/div.

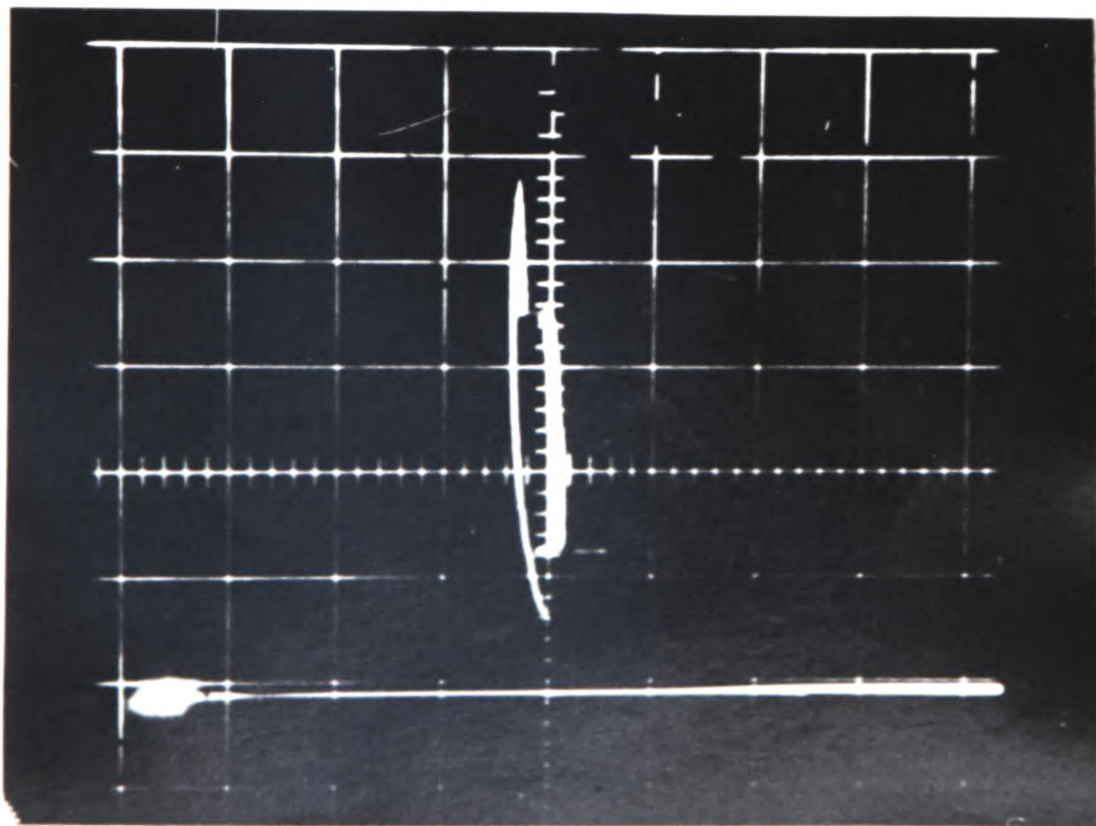


2V/div.

Fig. 4.7.

Above: I-V characteristics of a point-contact device after 10^3 switching operations obtained without the use of the logarithmic amplifier.
Below: I-V characteristics of a point-contact device after 10^7 operations obtained with the use of the logarithmic amplifier. The devices in figures 4.5-4.12 are all point-contact devices of the same geometry and electrode materials.

0.6 mA/div.



Logarithmic voltage scale

Fig. 4.8.

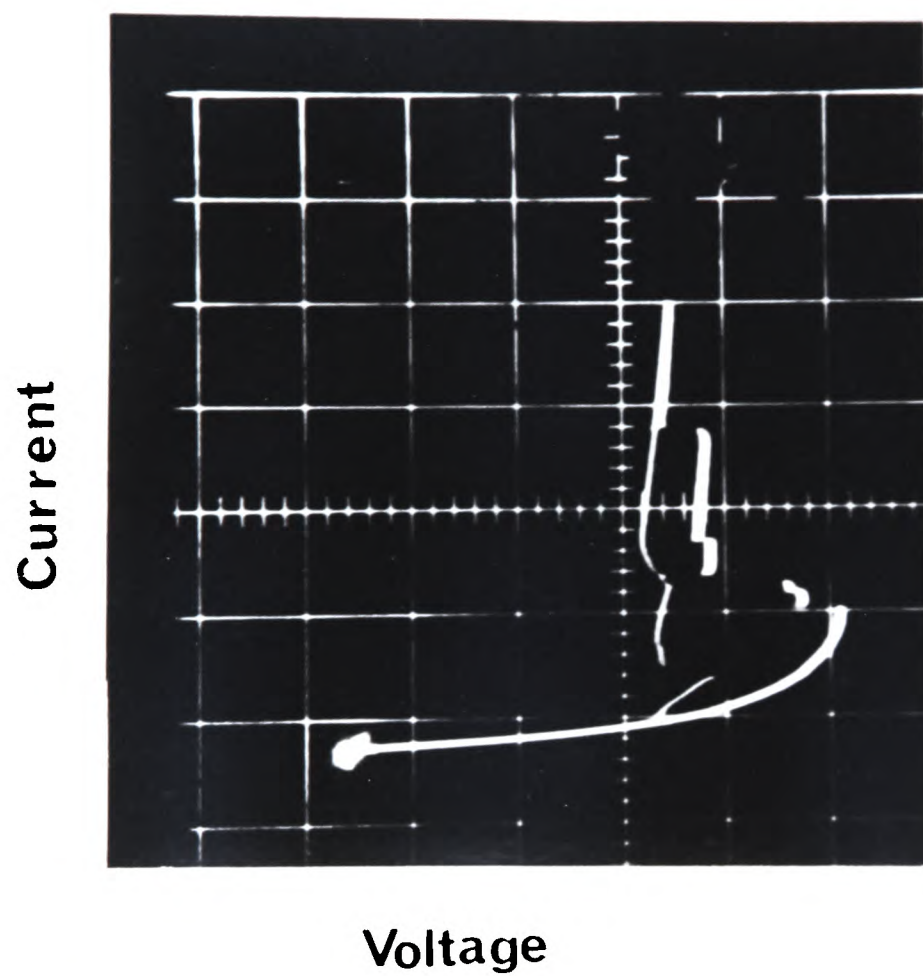


Figure 4.9
The I-V characteristics of a point-contact device after 10^6 switching operations.

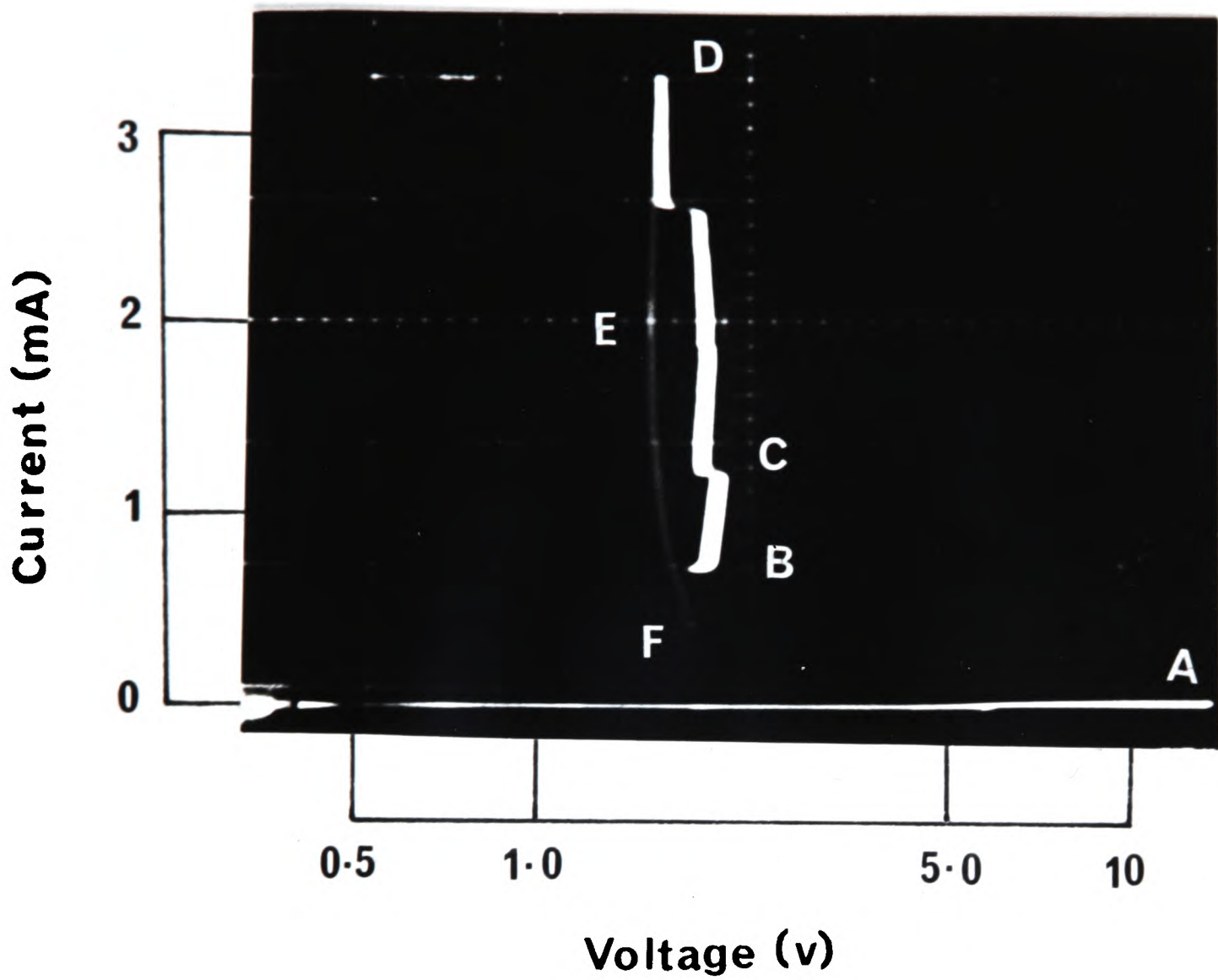


Figure 4.10

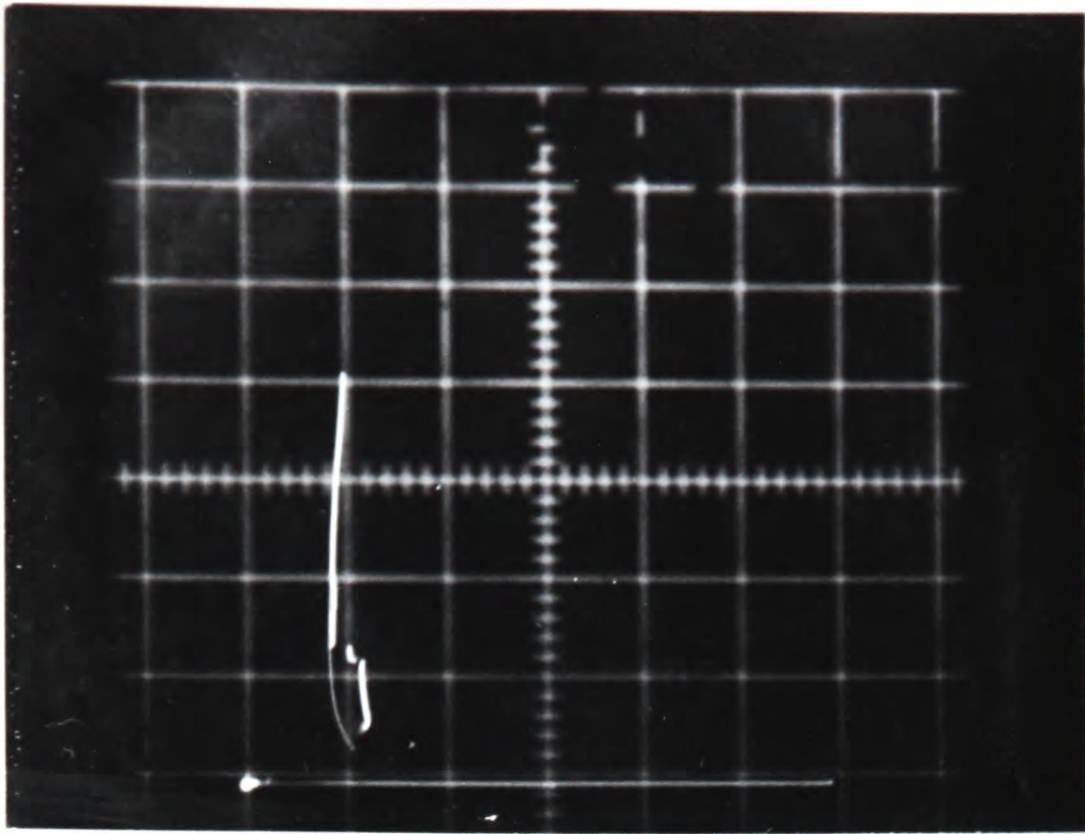
I-V characteristics of a point-contact device showing several current branches in the on-state. The characteristics were obtained with the use of the logarithmic amplifier.

device switches to a state at the lower end of the first branch (B) in the on-state. As the source voltage increases the current rises steeply until another critical point (C) is reached whereon the device conductance increases rapidly until the lower end of the next branch is reached and the current increases steeply again. Finally, the ramp pulse reaches its peak and the current in the on-state attains a maximum (D). The source voltage then drops rapidly and the on-state current also decreases rapidly, as shown by the fainter trace (E) in figure 4.10. The threshold switch reverts to its original state at a particular holding current with a corresponding holding voltage (F).

The logarithmic amplifier was particularly useful in revealing the fine detail of the on-state when the threshold voltage of a device, say an unformed device, was relatively large. It has also helped to establish beyond doubt that the on-state characteristic for the first-fire operation was always a single trace. However, at lower threshold voltages multiple branching of the on-state could be seen without the use of the logarithmic amplifier provided the branches were not extremely close to one another as shown in figure 4.11. The photograph in figure 4.11 was taken without the use of the logarithmic amplifier.

Apart from the relatively more stable behaviour of point-contact devices there were no basic differences between the current-voltage characteristics of sandwich and point-contact devices. They had comparable holding currents and voltages and there were very small differences, 0.1 - 0.2 V, between their minimum holding voltages, V_{mh} and their holding voltages, i.e. V_h at I_h (see Chapter One). In addition, the gradients of their on-state characteristics above the minimum holding voltage point, see figure 1.5, were similar, see figures 4.12 - 4.13. Gap devices, on the other hand, showed a somewhat different behaviour. The gradient of the on-state trace of a thin-film gap device was greater than that of either a point-contact or sandwich device, as shown in figure 4.14. Branching was also observed in gap devices but the branched pattern of the on-state was rather different from a typical branched pattern of a point-contact device in that a horizontal trace was observed, see figure 4.14. In addition, the holding current in gap devices, figure 4.14, was extremely small and a large difference existed between the holding voltage at I_h and the minimum holding voltage, i.e. the negative resistance region at the lower end of the on-state

1.2 mA/div.



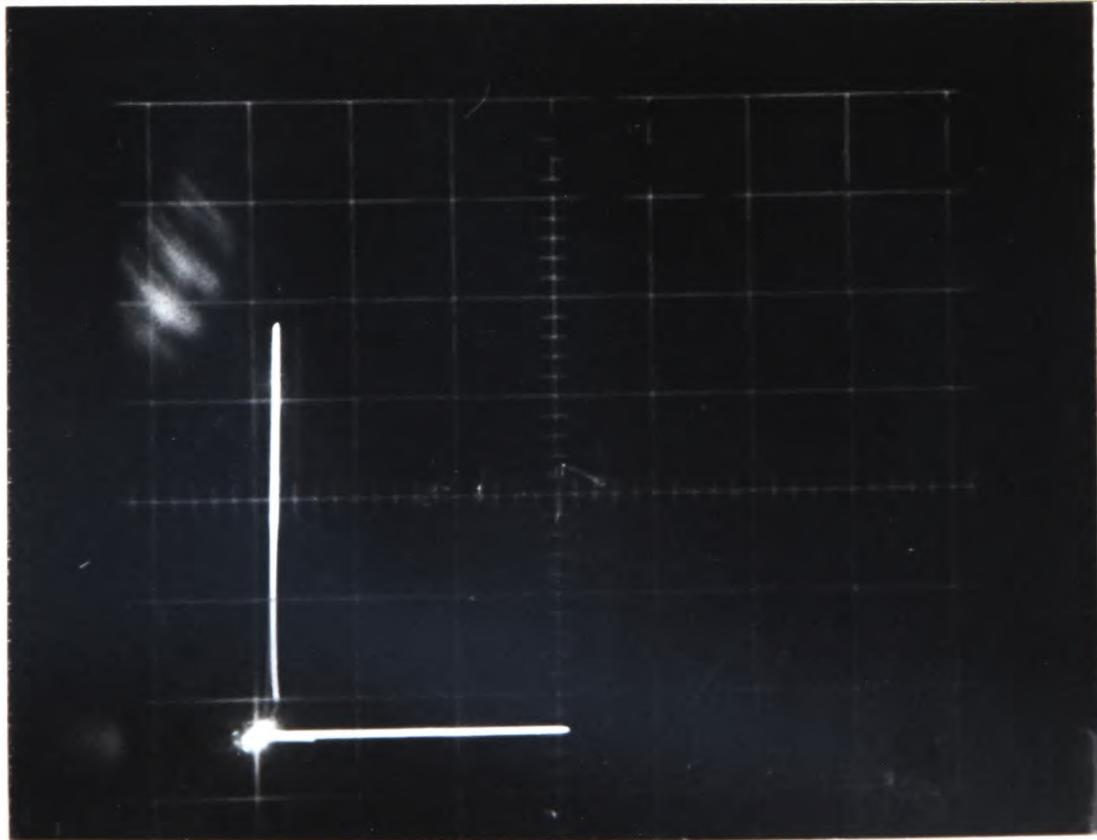
2V/div

Fig. 4.11.

Above: I-V characteristics of a point-contact device showing multiple branching in the on-state without the use of the logarithmic amplifier.

Below: The I-V characteristic of a point-contact device.

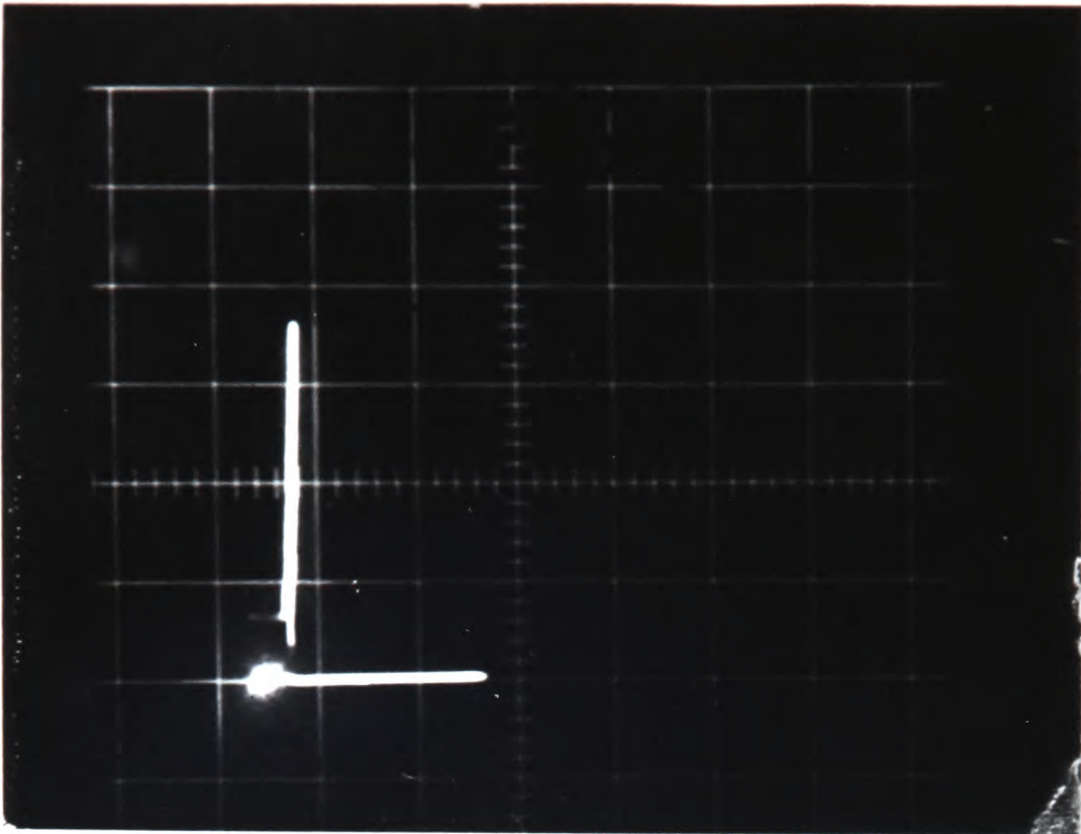
1.2 mA/div.



5V/div.

Fig 4.12.

1.2 mA/div



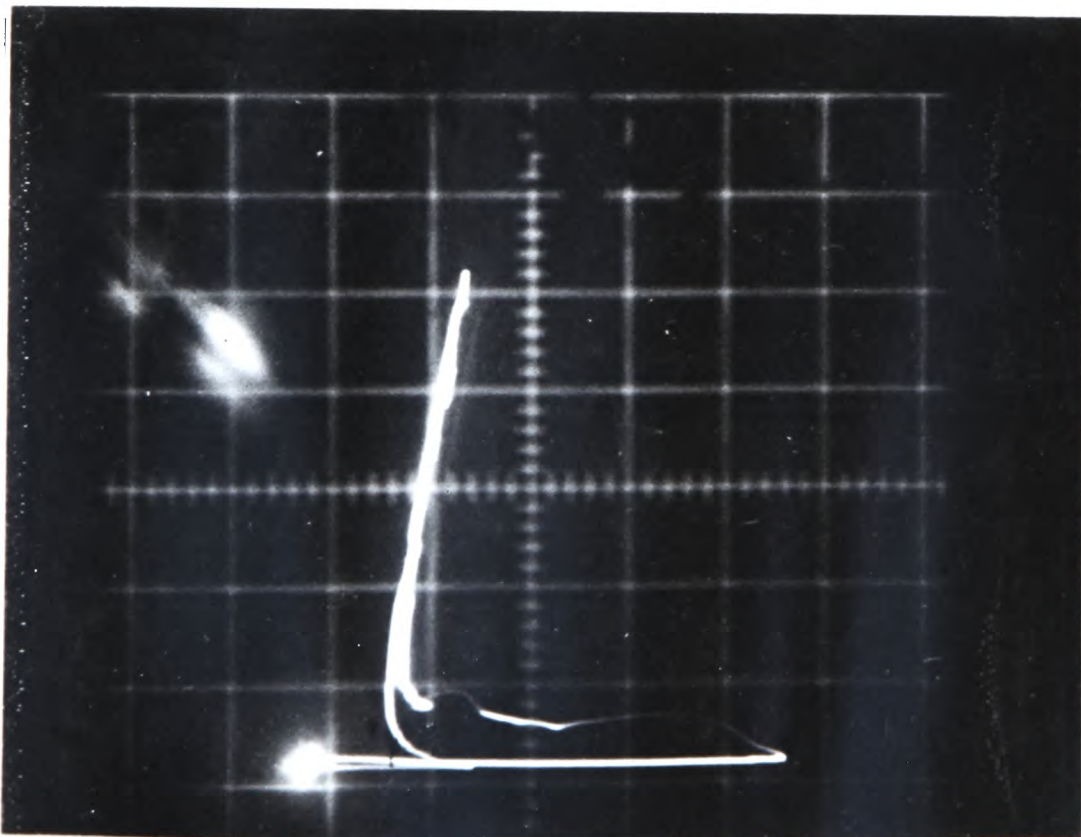
5 V/div.

Figure 4.13.

Above: I-V characteristics of a sandwich device with Al/Cr crossover electrodes.

Below: I-V characteristics of a gap device with Au electrodes.

1.2 mA/div.



5 V/div.

Figure 4.14.

trace for a gap device was large. This can also be seen from a photograph of current-voltage characteristics of a gap device published by Neale (1970) and similar observations reported by Hughes (1973).

(c) Nature of the on-state

All the observations discussed above indicated that there were some definite differences, particularly in the on-state between the behaviour of a virgin device and a formed device. These differences may have been caused by structural changes of the kind reported by Bosnell et al (1973). A formed device was reported to contain a filament of different composition from its surroundings and embedded in this filament were large single crystallites of tellurium. Therefore, in order to examine to what extent this model was compatible with observations made in this work and to acquire further information about the nature of the on-state, it was essential to carry out experiments to explore the occurrence of structural changes and the way in which they affect the on-state characteristic. These experiments were:

- (i) Comparison of devices of varying film thicknesses in order to examine the influence of fewer tellurium crystallites between electrodes as devices become thinner.
- (ii) Investigation of the effect of different electrode materials on the on-state parameters, the holding current and voltage, in order to gain information on the part played by the glass-electrode interface and the influence of electro-migration in the formation of the crystallite.
- (iii) Measurement of the a.c. conductivity of the channel for a range of frequencies. Again, the measurements were made before and after the forming process.
- (iv) Application of uniaxial stress to examine the effect on the conductivity of the channel and on device lifetimes. This experiment was carried out before and after the forming process.
- (v) Examination of the effect of a dramatic change in the ambient temperature of the device, say a change from room to liquid nitrogen temperature, in order to explore its possible influence on the growth of the crystallites and device characteristics.
- (vi) Investigation of the effect of device contact area on its characteristics.

- (vii) Investigation of the effect of varying the external load resistor and device capacitance.
- (viii) Examination of occurrence of multiple branching in the on-state characteristics with different switching sequences, for example, altering the pulse repetition rate and width considerably.
- (ix) Examination of the effect of pulse polarity on multiple branching, and on-state parameters.
- (x) Finally, an attempt was made to alter the composition of STAG by adding a fifth component, thallium, at the expense of some of the tellurium content in the alloy.

In addition, to make certain that the observations that have been mentioned were not specifically caused by the methods used to prepare the devices, it was decided to examine the current-voltage characteristics of a commercially-made device (Energy Conversion Devices, DO-7 package) and point-contact devices in which the thin films were prepared by r.f. sputtering. Such films were kindly supplied by Dr. A.J. Hughes of R.R.E., Malvern. The films were prepared on four substrates pre-coated with thin films of chromium. The target composition was $\text{Si}_{21}\text{Te}_{43}\text{As}_{27}\text{Ge}_9$ and the films had a thickness of about 2 μm .

Multiple branching in the on-state was observed in the DO.7 device. This device had already been switched many times before it was acquired and therefore it was difficult to estimate the number of switching operations the device had to go through before branching occurred.

Point-contact devices, fabricated from the r.f. sputtered film and with Mo probe top contacts, behaved in a similar manner to those fabricated from flash evaporated films. They had first-fire threshold voltages of about 110 V and, after forming, these dropped to about 14 - 15 V. Multiple branching appeared after about 10^4 operations. The operations lifetimes were about $10^5 - 10^6$ operations. However, not all devices fabricated on any one film had the same lifetimes or first-fire threshold voltages. This was attributed to the possible presence of argon gas inclusions at various parts of the r.f. sputtered film.

The rest of this chapter is devoted to describing the results of the experiments listed earlier. All measurements, unless otherwise stated were carried out on point-contact devices because of their stable behaviour.

IT IS VERY IMPORTANT TO NOTICE THAT, ALTHOUGH IT IS NOT MADE VERY CLEAR, IN THE FIGURES OF CHAPTER FOUR WHERE THE HOLDING VOLTAGE IS PLOTTED AGAINST SOME QUANTITY SUCH AS TEMPERATURE OR NUMBER OF SWITCHING OPERATIONS, THE HOLDING VOLTAGE REFERS TO THE MINIMUM HOLDING VOLTAGE V_{mh} AND NOT THE HOLDING VOLTAGE V_h AT I_h . THIS APPLIES TO ALL FIGURES WITH EXCEPTION OF FIGURE 4.61 WHERE ONE CURVE IS A PLOT OF THE HOLDING VOLTAGE V_h at I_h AGAINST THE LOAD RESISTOR.

4.2. Effect of film thickness

When investigating the effect of film thickness on the on-state behaviour using devices of different film thicknesses, it was considered essential that all other device parameters, such as (i) film composition, (ii) device geometry, e.g. gap type or point-contact type, (iii) electrode contact area, (iv) electrode material (v) external circuit parameters e.g. load resistor, should be the same for each device. To minimise the possibility of the devices having thin films of different compositions, batches of devices were prepared on one substrate. The thin film on the substrate had a staircase-like thickness profile as shown in figure 4.15. The heights of the steps from the Cr surface were 2.5, 1.5, 1, 0.75, 0.5, and 0.25 μm . Such a film was prepared by drawing the sliding mask, with the aid of the rotary shaft as shown in figure 1.3 at certain intervals and by the same distance while the chalcogenide glass film was being deposited. This resulted in different sections of the substrate, pre-coated with a thin film of Cr, being exposed for different deposition periods and the formation of a staircase-like profile. The width of each step was 4.5 mm and its height, or thickness, was monitored by the quartz crystal thickness monitor.

Owen (1973) has shown that the composition of flash evaporated films could vary with increasing thickness, but it was not made clear whether the films of different thicknesses were prepared in single or several evaporations.

The thin film was fitted in the point-contact jig and a molybdenum probe, 3 mm diameter tip, was used as top contact. Devices of different film thickness were obtained by simply placing the Mo probe on various parts of the film.

The current-voltage characteristics of the devices were displayed

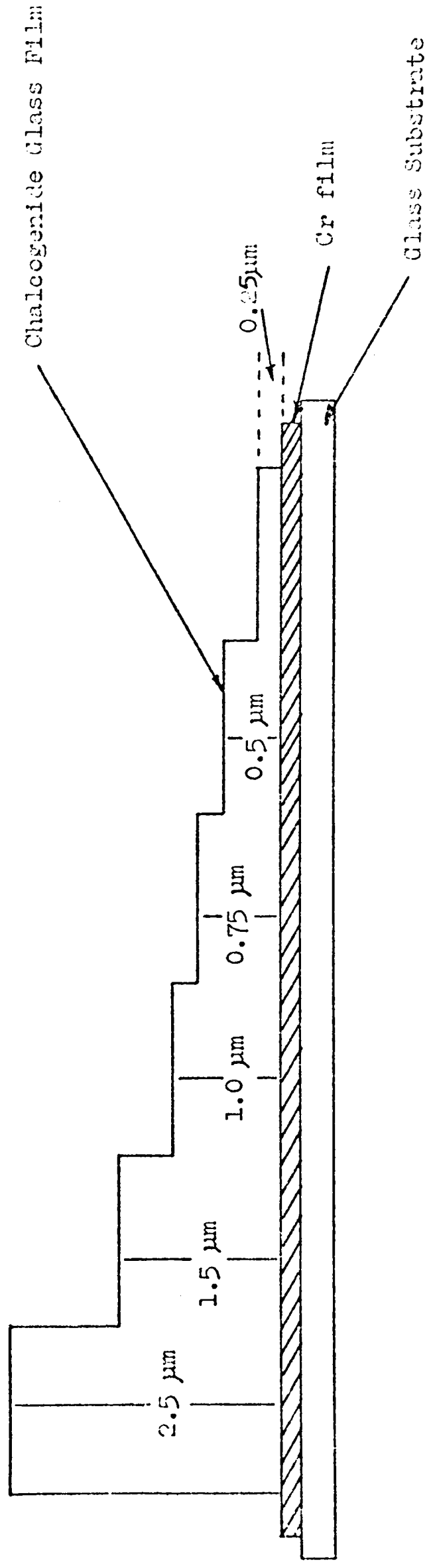


Fig. 4.15. A staircase-like STAG glass film deposited on substrate pre-coated with Cr film as bottom electrode. A Mo probe was used as top electrode.

by using positive ramp pulses of 1.3 ms width. The pulse height was initially 80 V but was reduced to 40 V when the devices had been formed.

Figure 4.16 shows a plot of the first-fire threshold voltage versus film thickness and shows that the threshold voltage increases with film thickness. The slope of the line is ~ 0.7 and this gives the relationship between the first-fire threshold and the film thickness d as:

$$V_{th} = k d^{0.7}$$

where k is a constant. Figure 4.17 shows a plot of threshold voltage for formed devices versus the corresponding film thickness. The slope of this curve is slightly less than half and the relationship between the threshold voltage and film thickness can be written as:

$$V_{th} = k d^{\frac{1}{2}}$$

This is in good agreement with the predictions of several authors. Main (1974) presented calculations which showed that in the case of purely thermal breakdown the threshold voltage and film thickness have the following relationship:

$$V_{th} \propto d^{\frac{1}{2}}$$

whereas in the case of electro-thermal breakdown they are related by the expression:

$$V_{th} \propto d.$$

Therefore, it is possible that switching in these devices, in the formed ones at any rate, is of thermal nature. Although there is a certain amount of difference between the dependence of the first-fire threshold voltage on film thickness and the dependence of threshold voltage in formed devices on film thickness, this difference is not strong enough to suggest that the switching mechanisms in formed and virgin devices are of different nature, say one electro-thermal and the second electronic.

In figures 4.18 - 4.23 the threshold voltages are plotted against the number of switching operations for devices of various thicknesses. The pulse repetition rate in every case was 10 pulse/sec. For devices with various chalcogenide film thicknesses in the range from 0.5 μm to 2.5 μm , the operational lifetimes, $\sim 10^7$ operations, were similar.

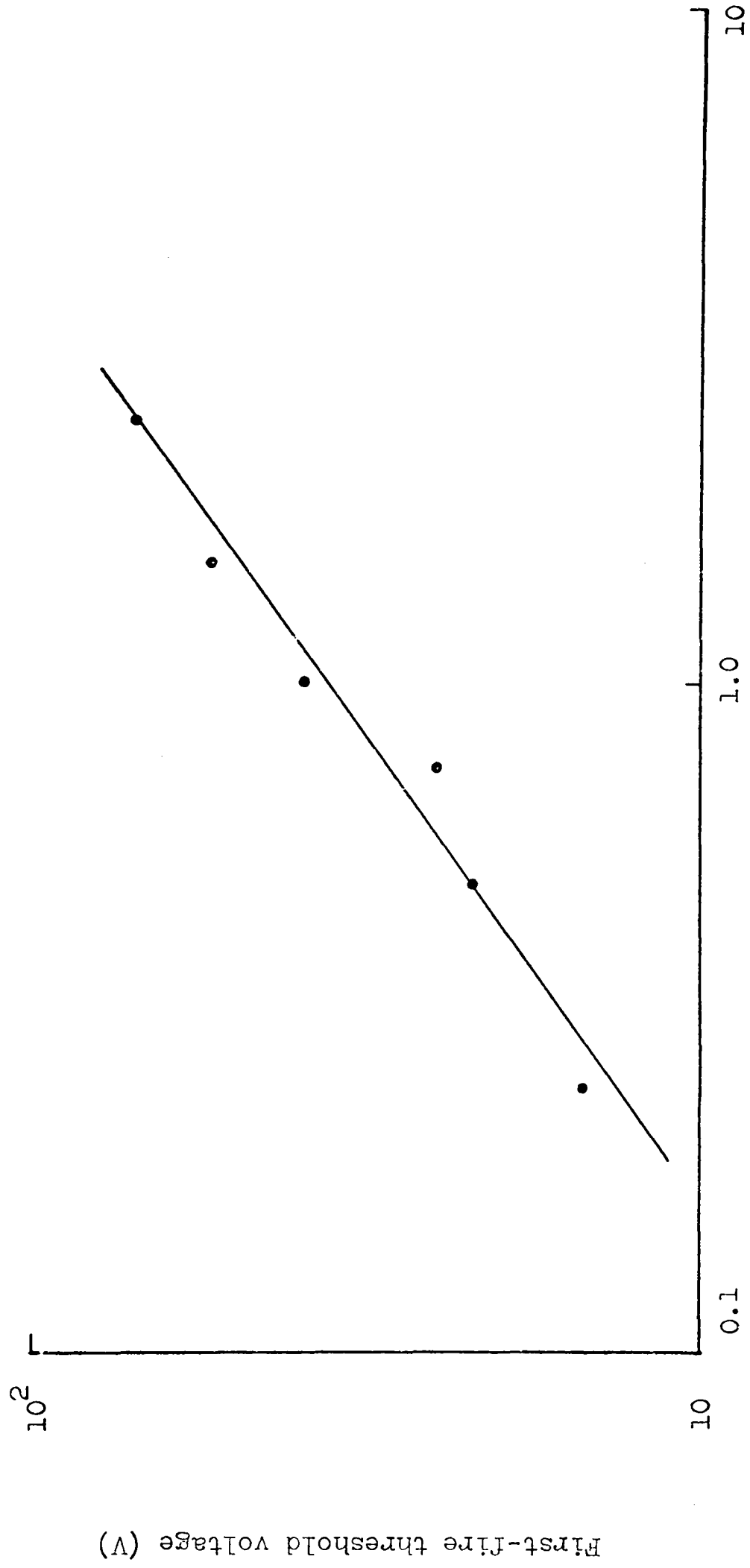


Fig. 4.16 Film thickness (μm)
 Threshold voltage vs. film thickness for virgin point-contact devices.

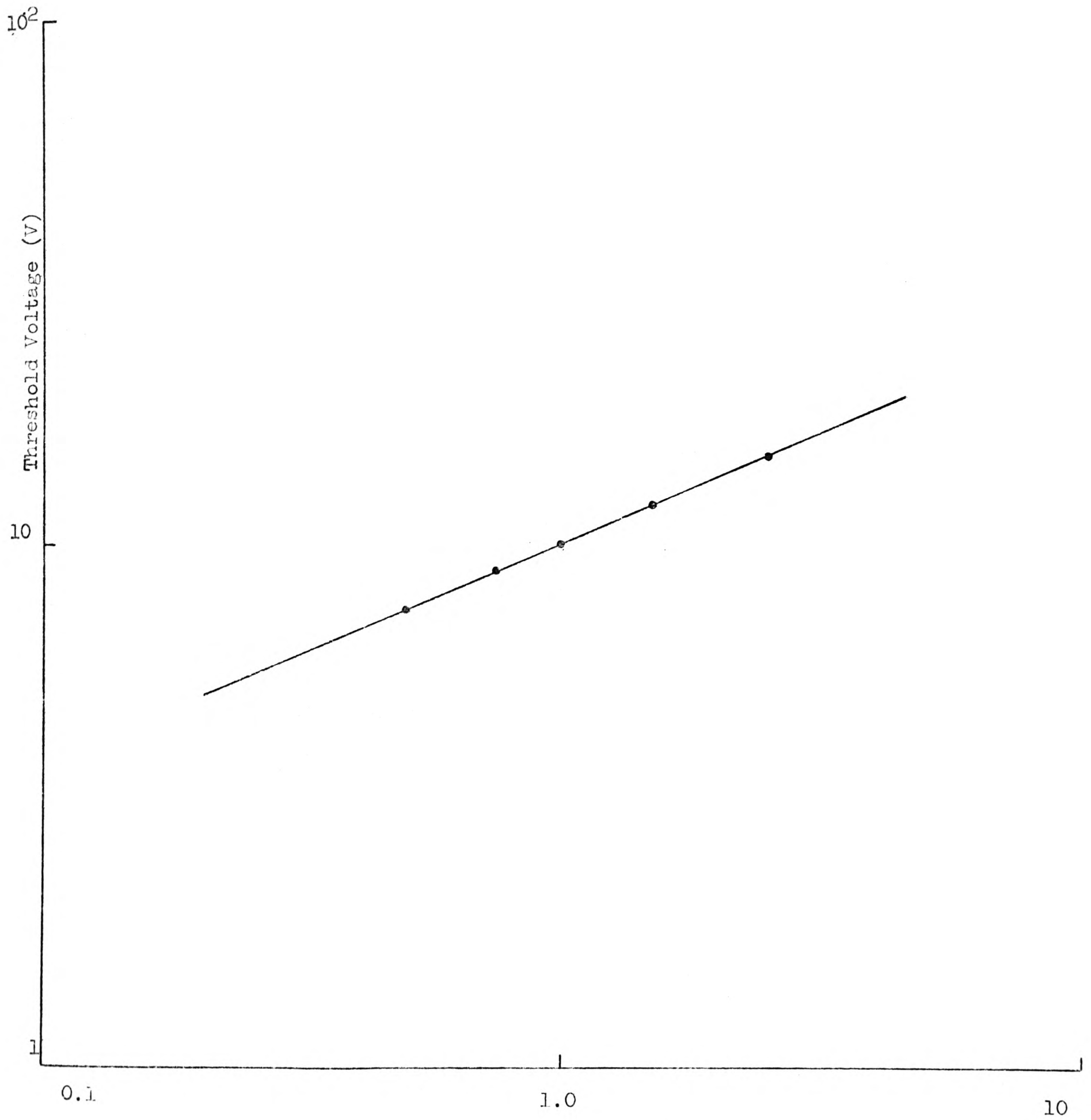


Fig. 4.17

Film thickness (μm)

Threshold voltage vs. film thickness for formed point-contact devices.

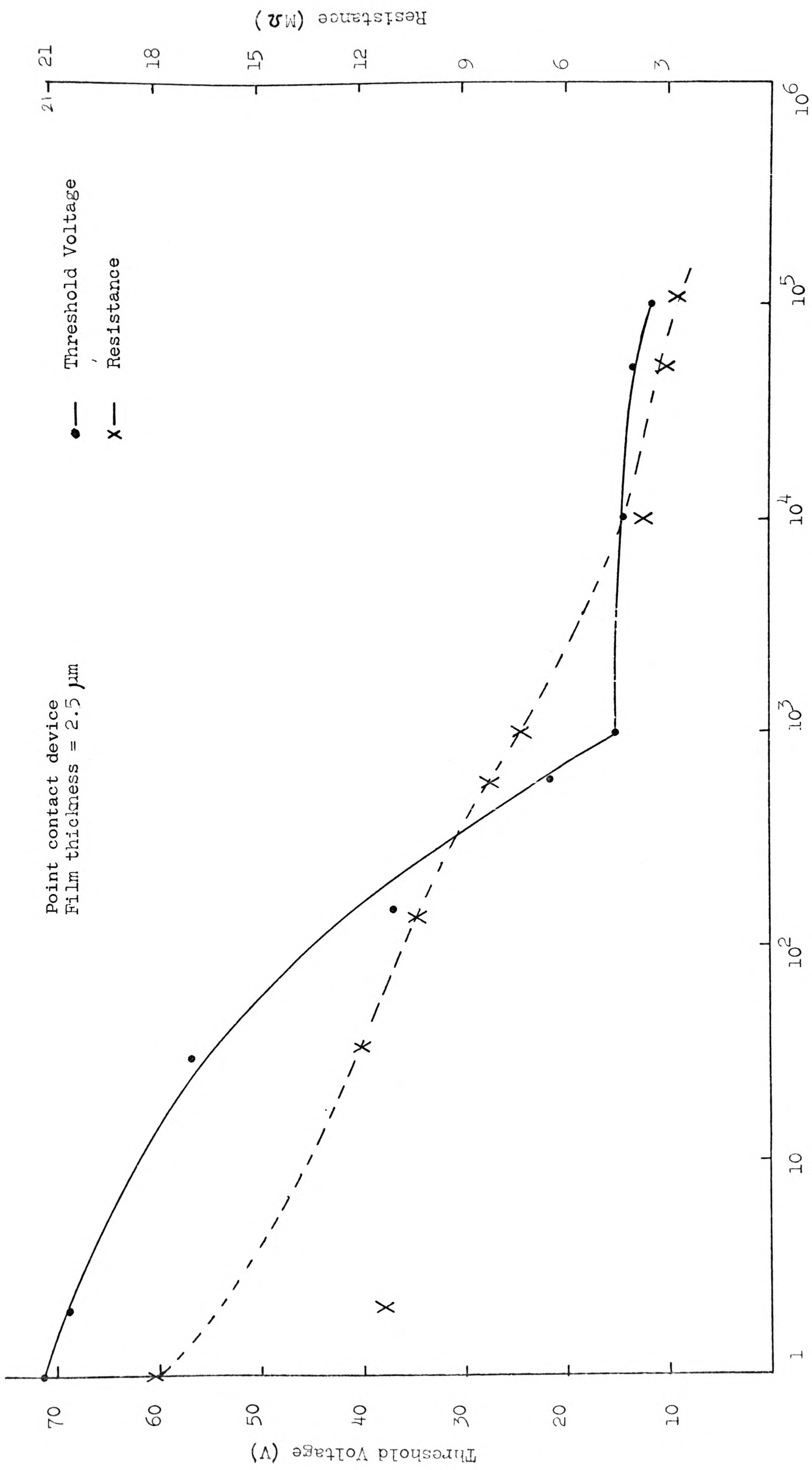


Fig. 4.18

Number of Operations

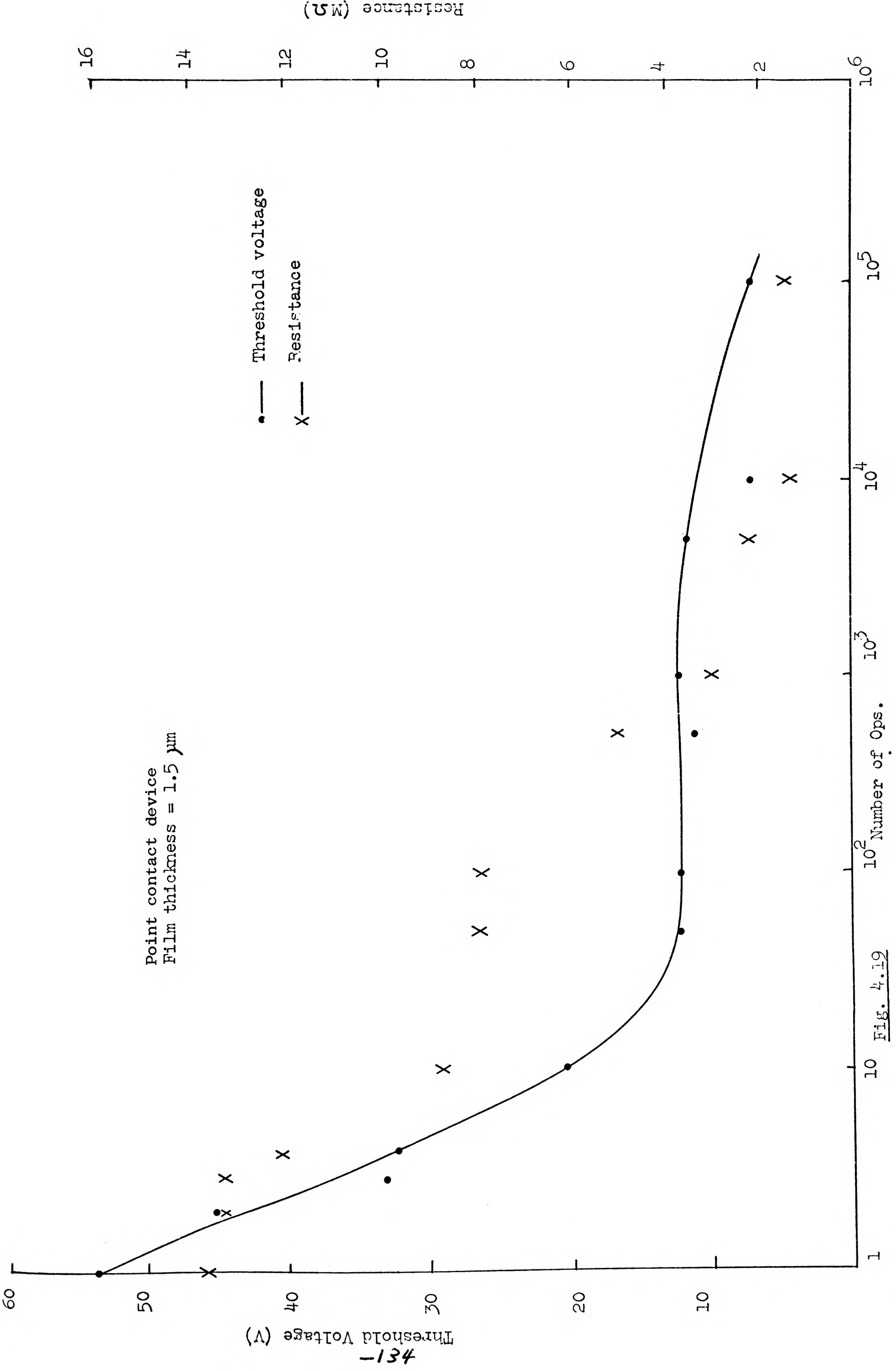


Fig. 4.19

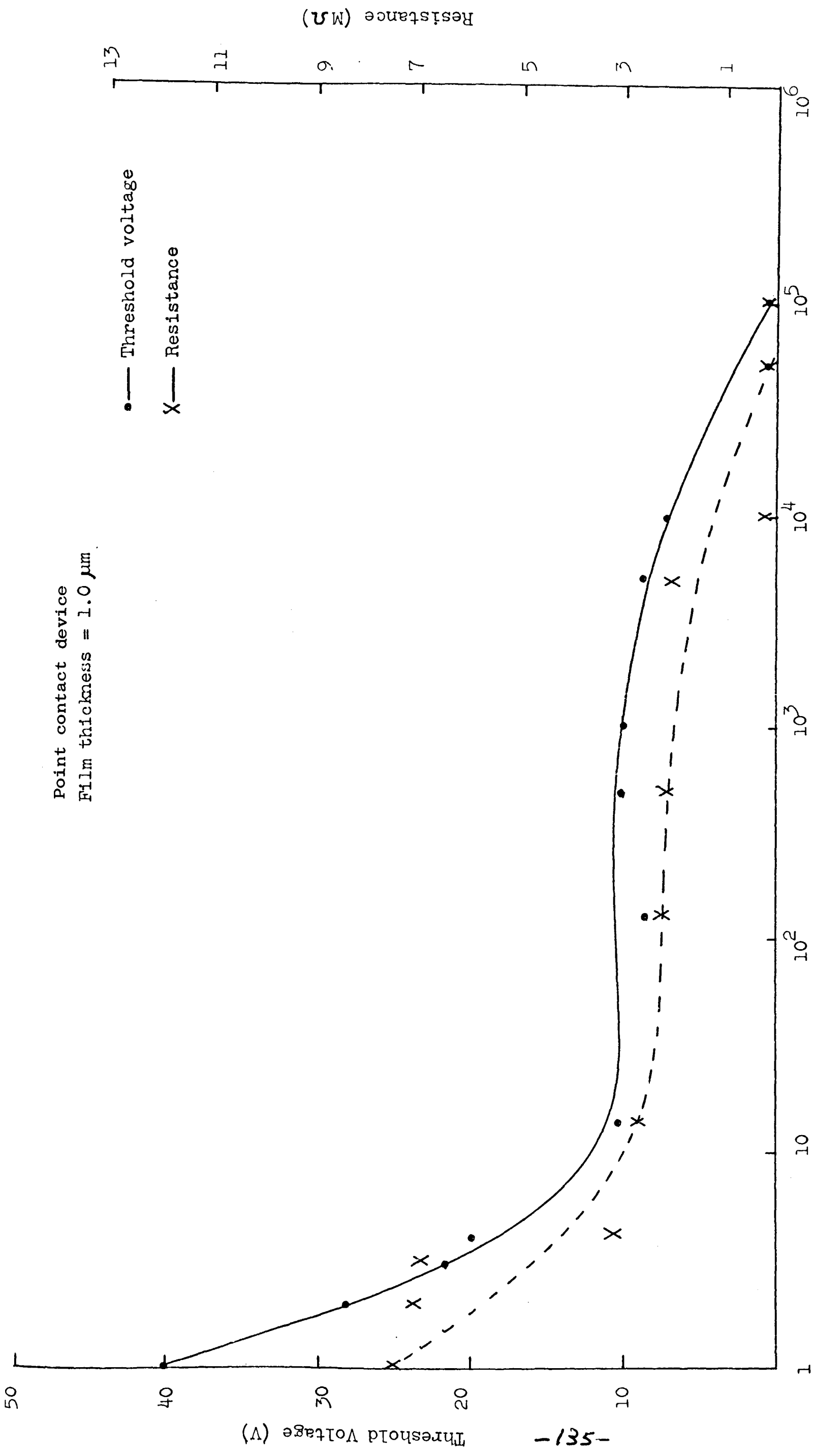


Fig. 4.20

Number of Operations

Point contact device
 Film thickness = 0.75 μm

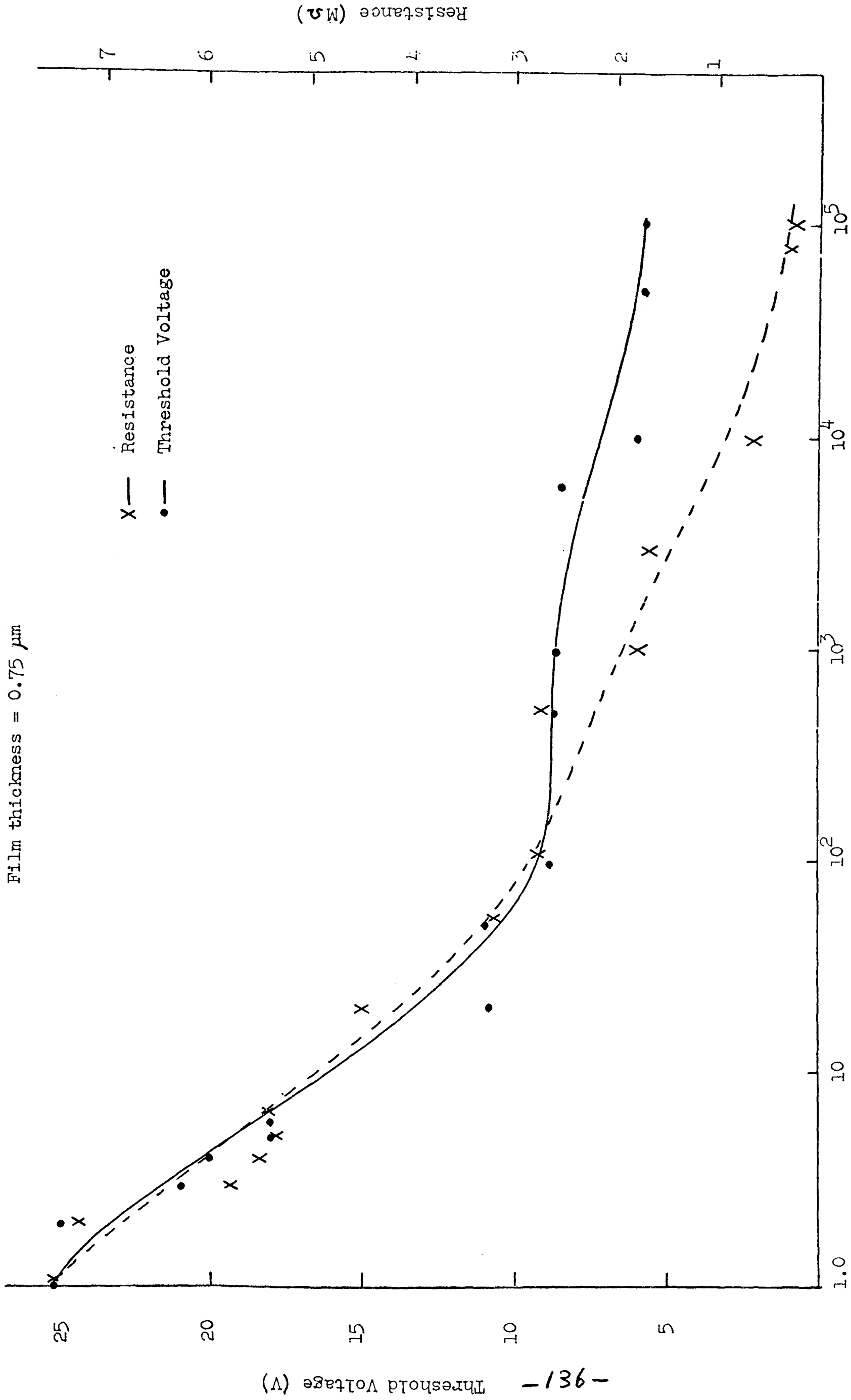


Fig. 4.21

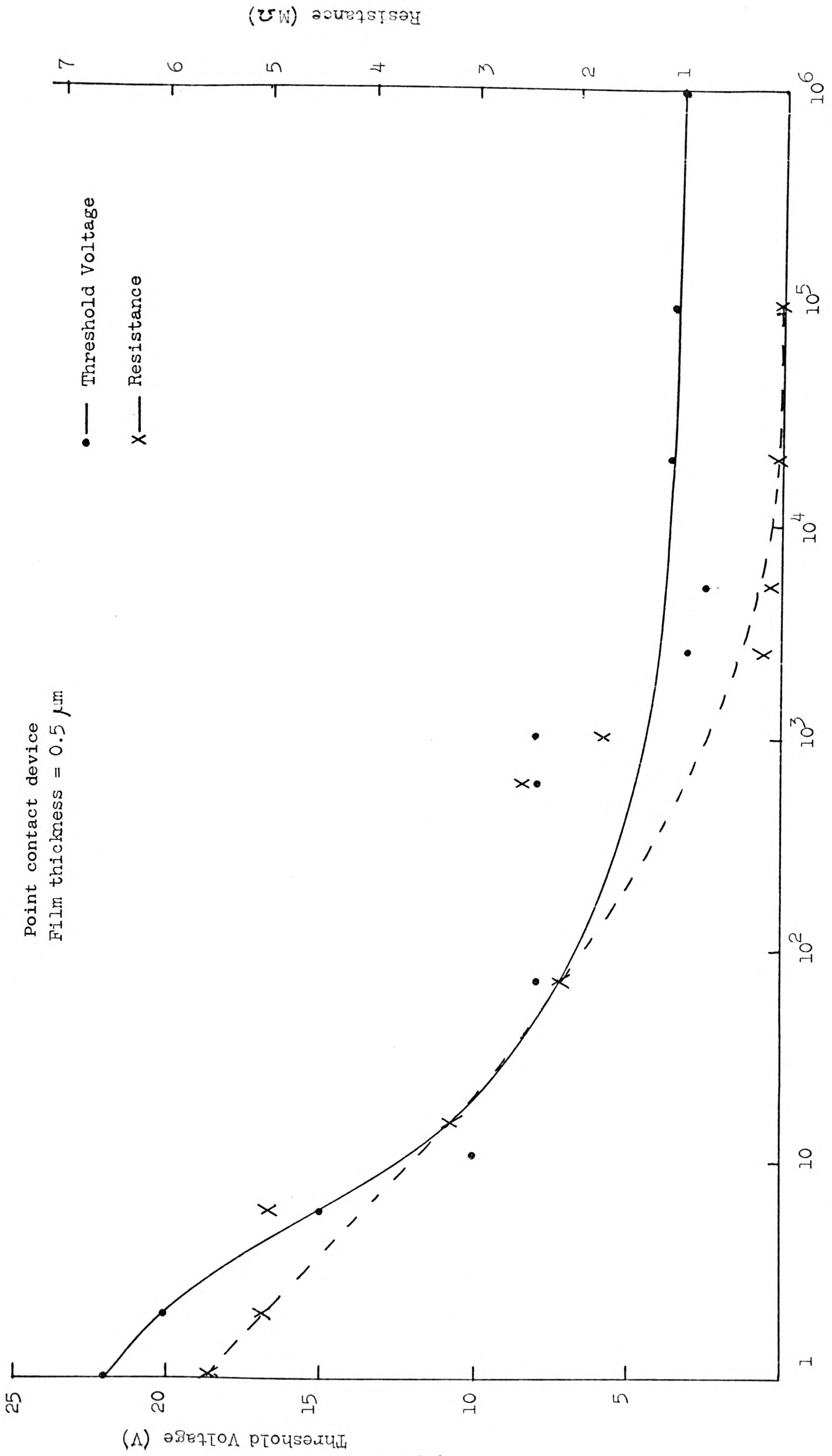


Fig. 4.22

Number of Operations

Point contact device
 Film thickness = 0.25 μm

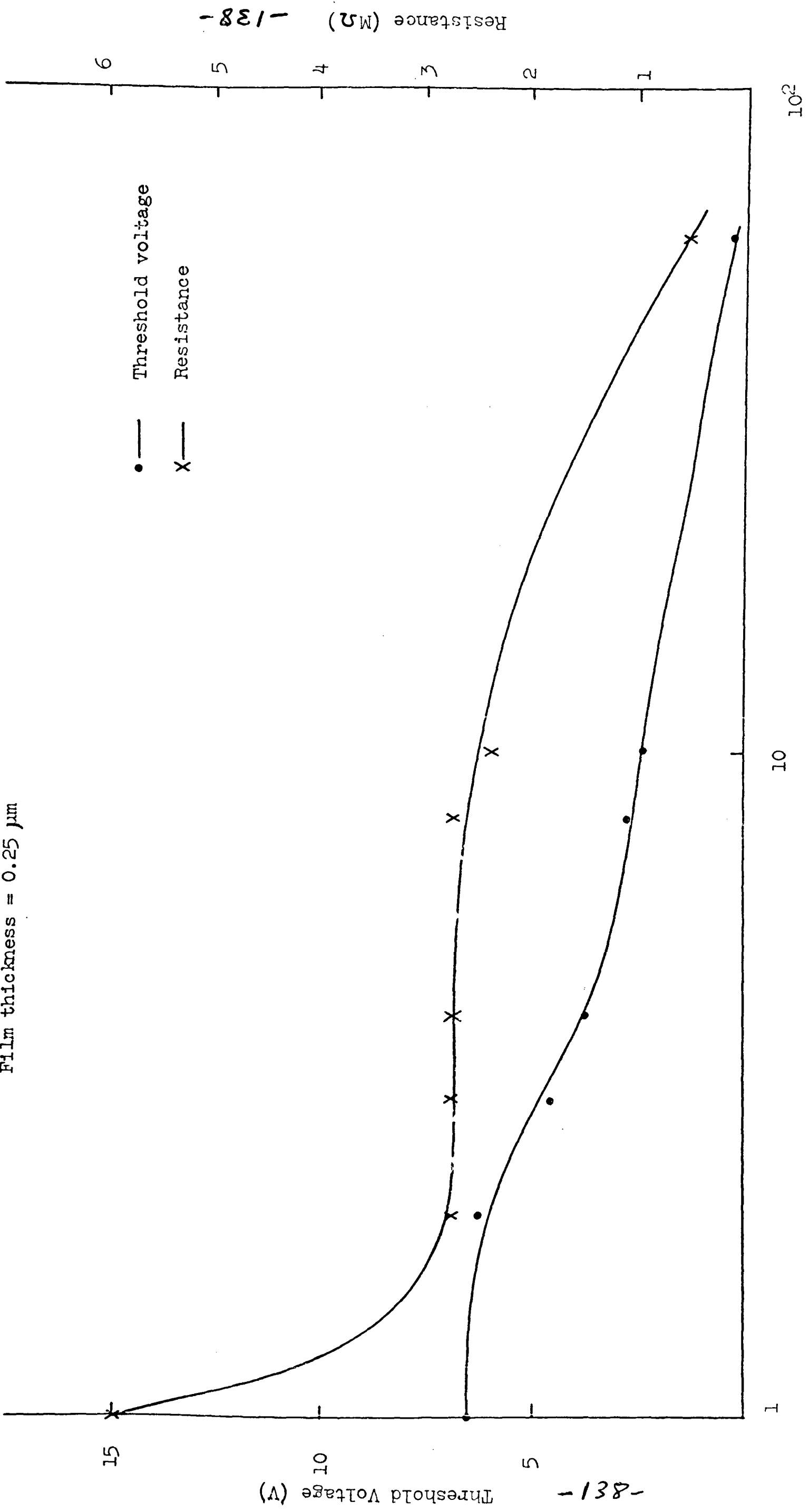


Fig. 4.23

Number of Operations

Resistance (M Ω) -138-

Threshold Voltage (V) -138-

However, devices with film thickness of 0.25 μm switched very erratically and had an operational lifetime of about 60 operations. Also plotted in figures 4.18 - 4.23 are the off-state resistances of the devices as functions of the number of switching operations. The off-state resistance of a switched device was found to increase with time. All measurements of resistances were carried out 10 seconds after switch-off. The resistance was measured using a Keithley 602 solid-state electrometer connected in series with the device and a variable low voltage power supply. The electrometer measured the current through the device and a Weir Mk III digital voltmeter measured the voltage across the power supply. The current through the device was restricted to 10^{-8} amp so that the measured resistance was essentially in the ohmic region of the preswitching current-voltage characteristic.

It can be seen from figures 4.18 - 4.23 that the threshold voltage versus number of operation curves and the off-state resistance versus number of operation curves have similar profiles. There seemed to be a definite relationship in any device between the threshold voltage and the off-state resistance. The threshold voltage dropped as the device resistance became smaller with increasing number of switching operations. This relationship is shown clearly in figure 4.24 where the threshold voltage after a certain number of operations is plotted against the device resistance after the corresponding number of operations.

No definite relationship between film thickness and the occurrence of multiple branching in the on-state could be established. In devices with film thicknesses in the range of 0.5 μm to 2.5 μm multiple branching appeared after 10^3 - 10^4 operations, but in devices of thickness 0.25 μm branching appeared after the first-fire operation.

The holding minimum voltage, measured from the photographically recorded current-voltage characteristics, was independent of device film thickness and had a value of about 1.7 V. In order to examine the effect of the number of switching operations on the minimum holding voltage, its value was measured and plotted against the corresponding number of operations in figures 4.25 - 4.30. It can be seen that, apart from the 0.25 μm thick device, the minimum holding voltage remained stable for at least the first 3×10^4 operations but showed fluctuation for larger numbers of operations. Also plotted in figures 4.25 - 4.30

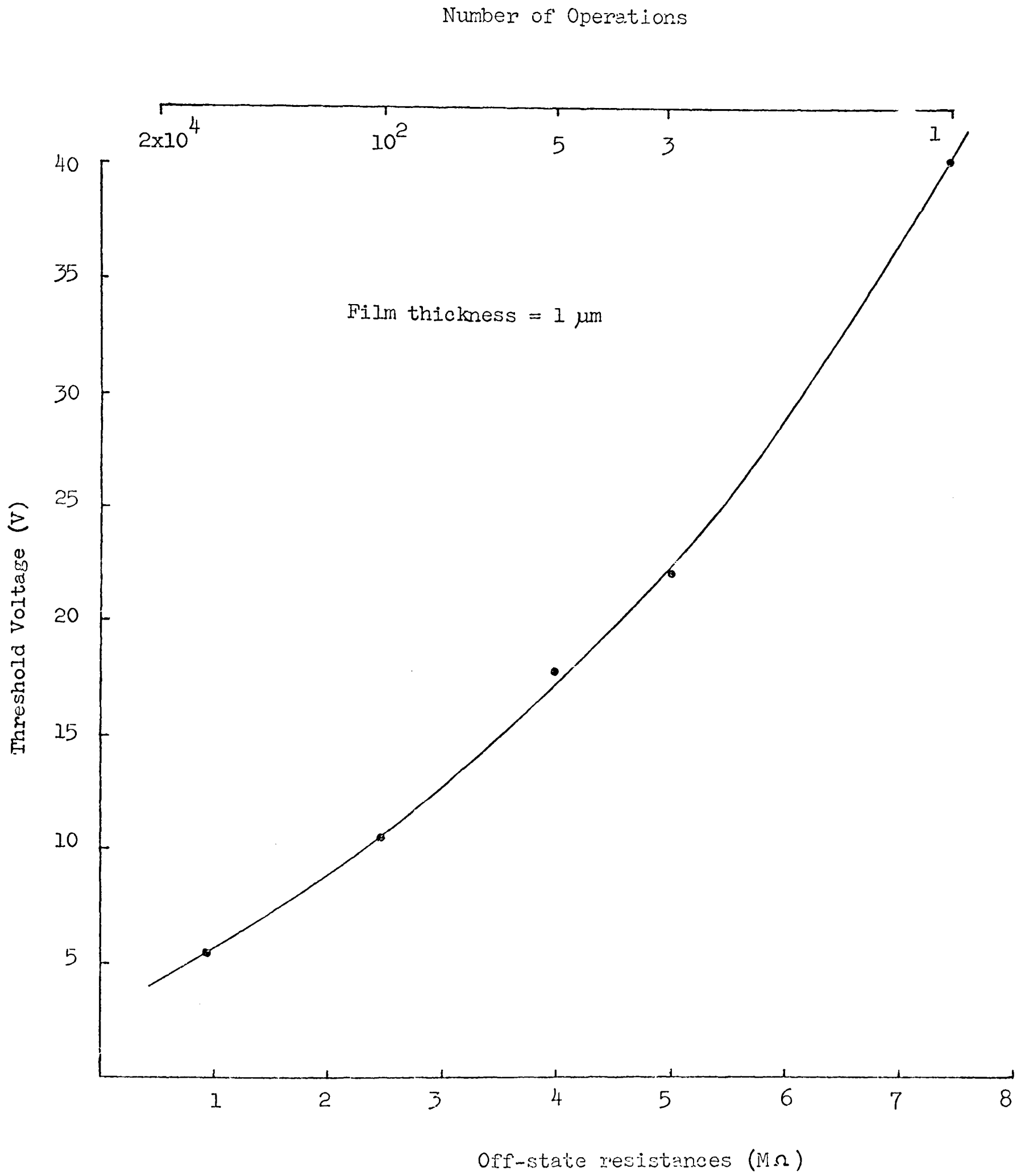


Fig. 4.24 Off-state resistance of a point-contact device vs. threshold voltage.

Film thickness = 2.5 μm

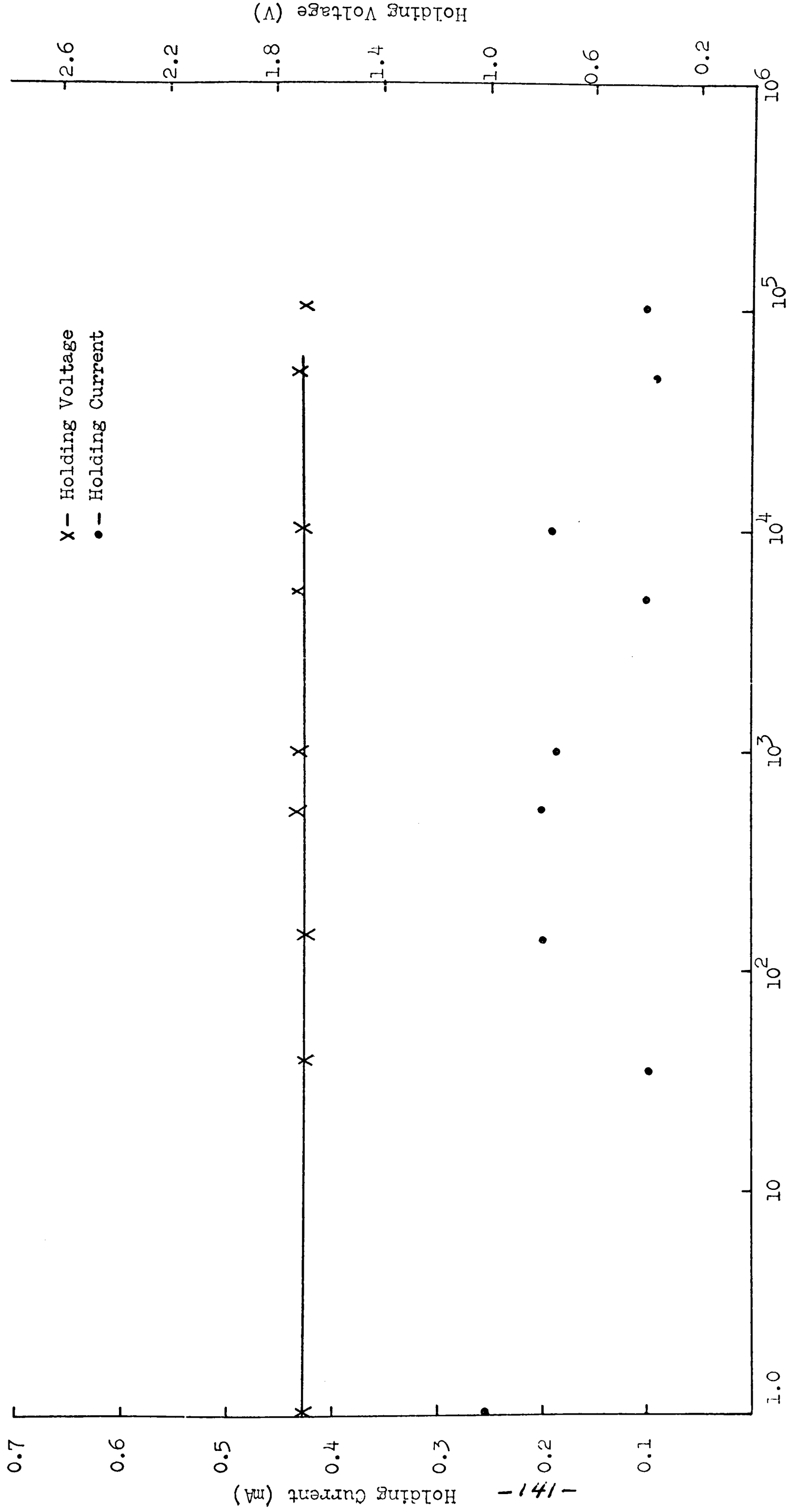


Fig. 4.25 Holding current and holding voltage vs. number of switching operations.

Number of Operations

Film Thickness = 1.5 μm

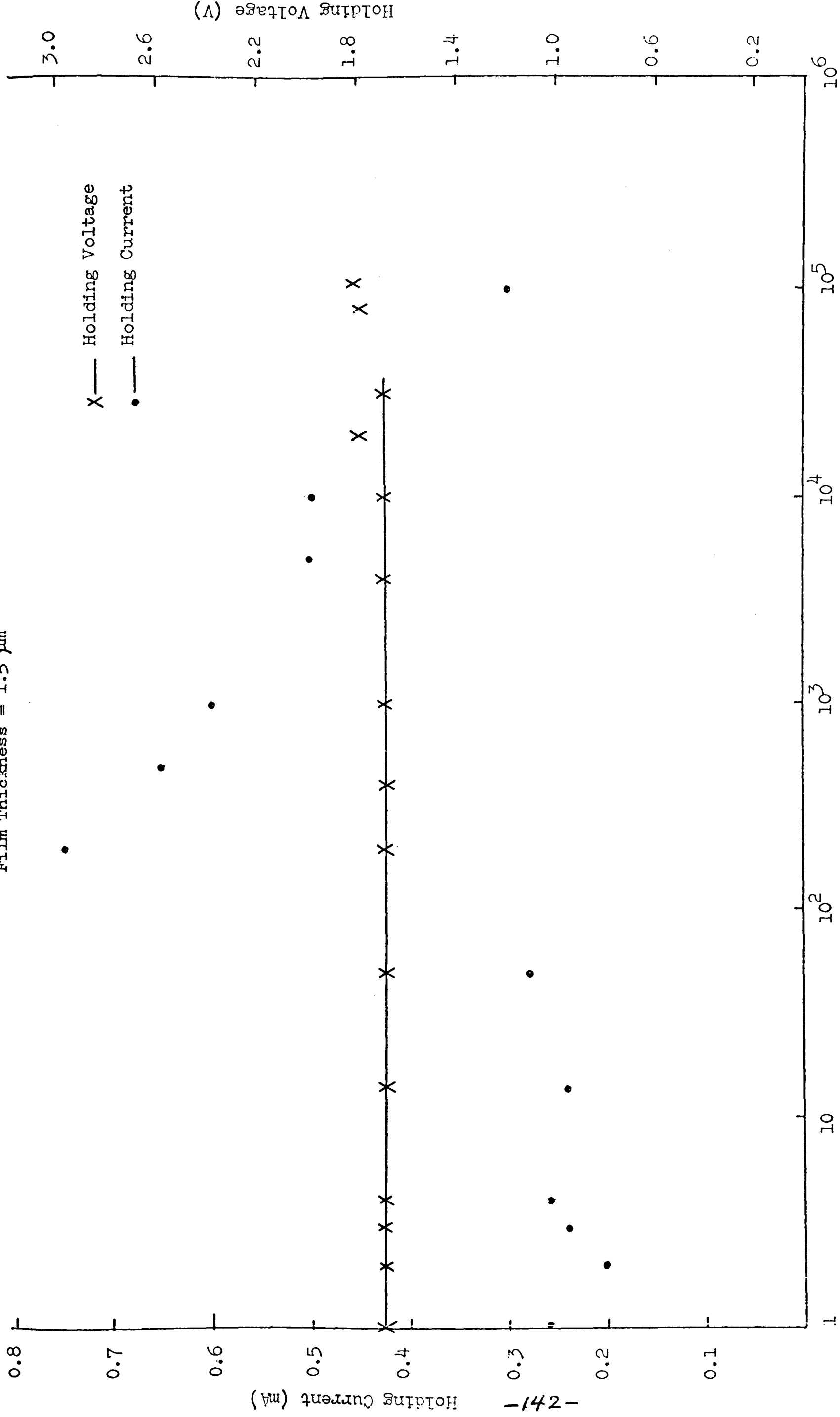


Fig. 4.26 Holding current and holding voltage vs. number of switching operations.

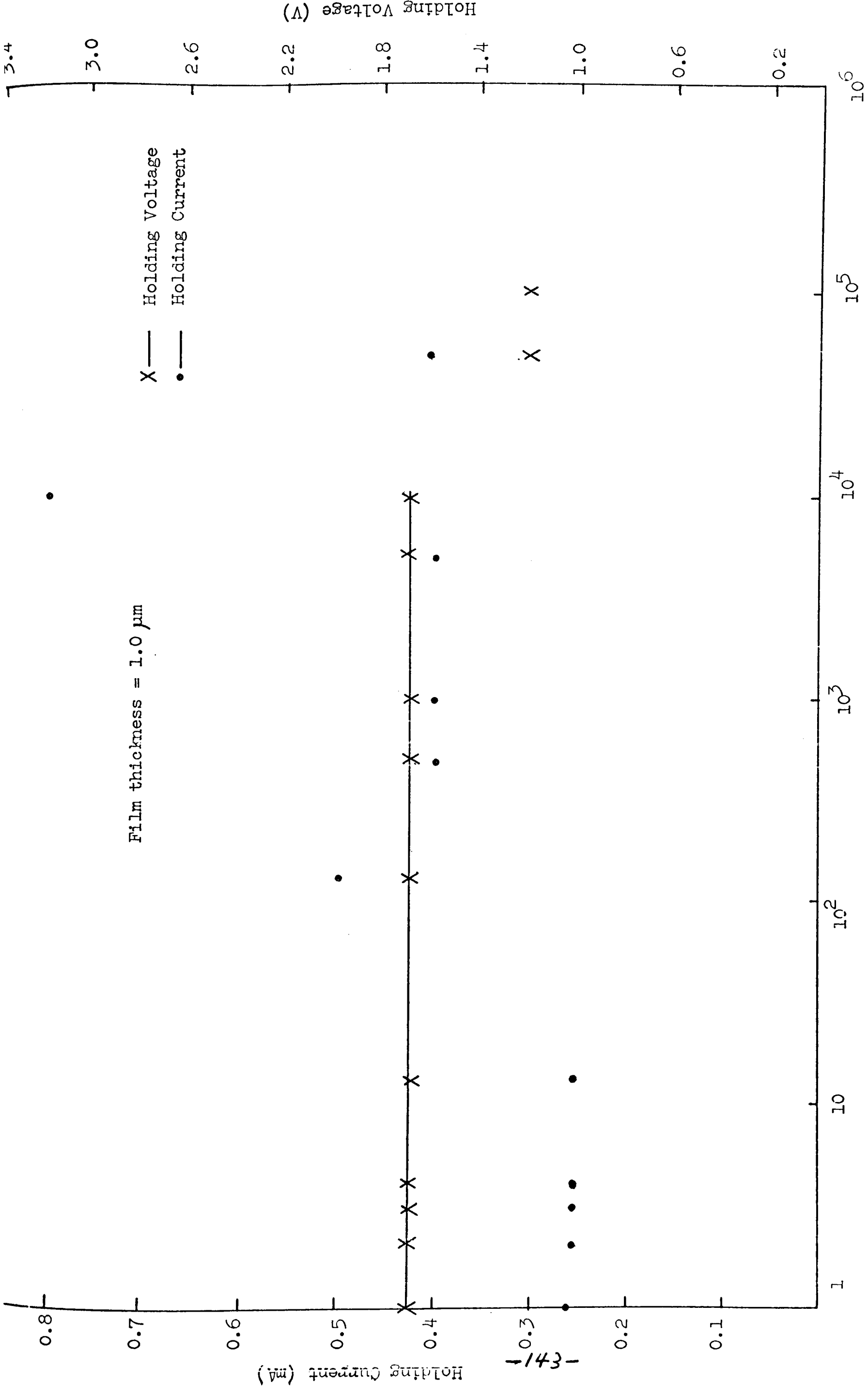


Fig. 4.27 Holding current and holding voltage vs. number of switching operations.

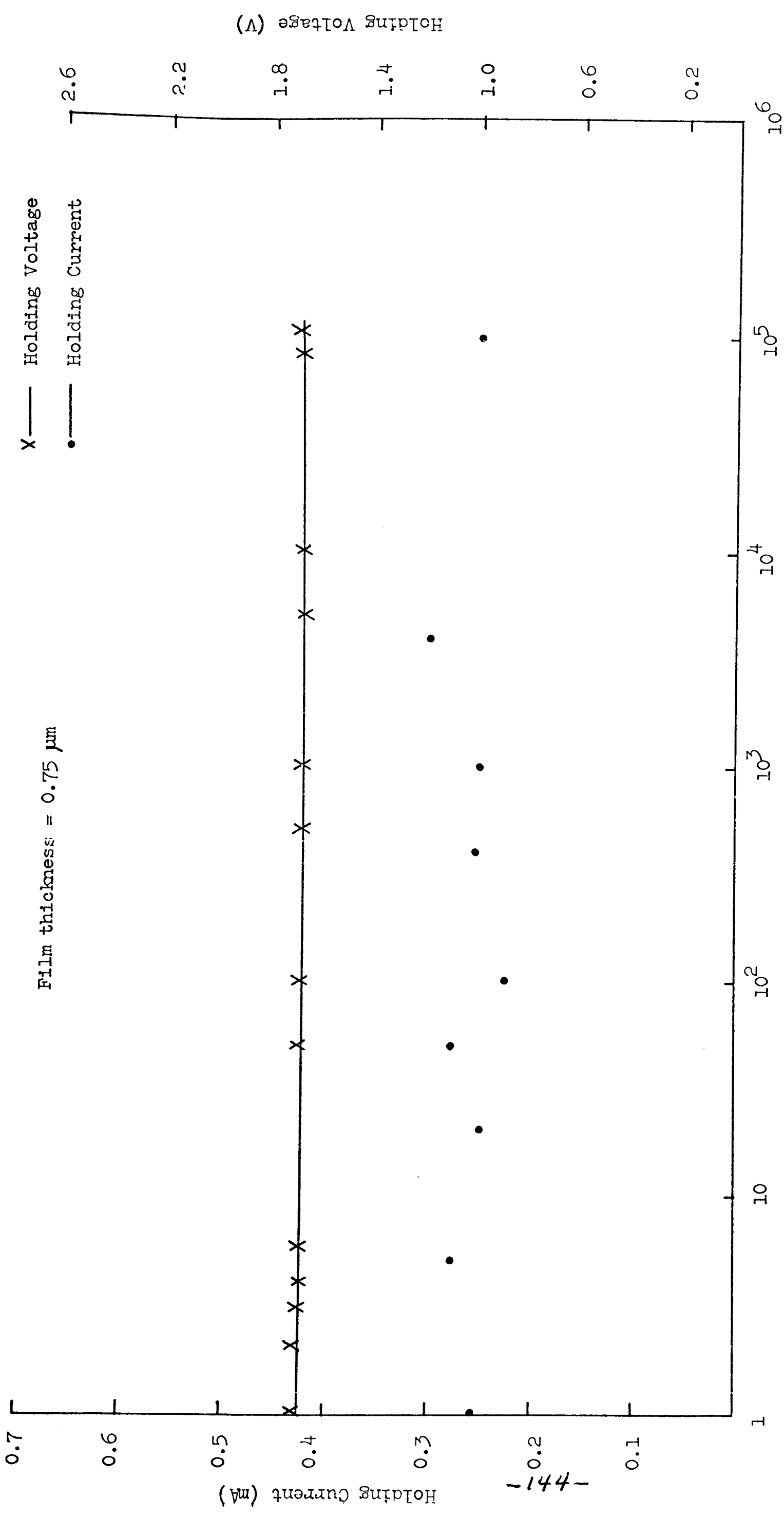


Fig. 4.28 Holding current and holding voltage vs. number of switching operations.

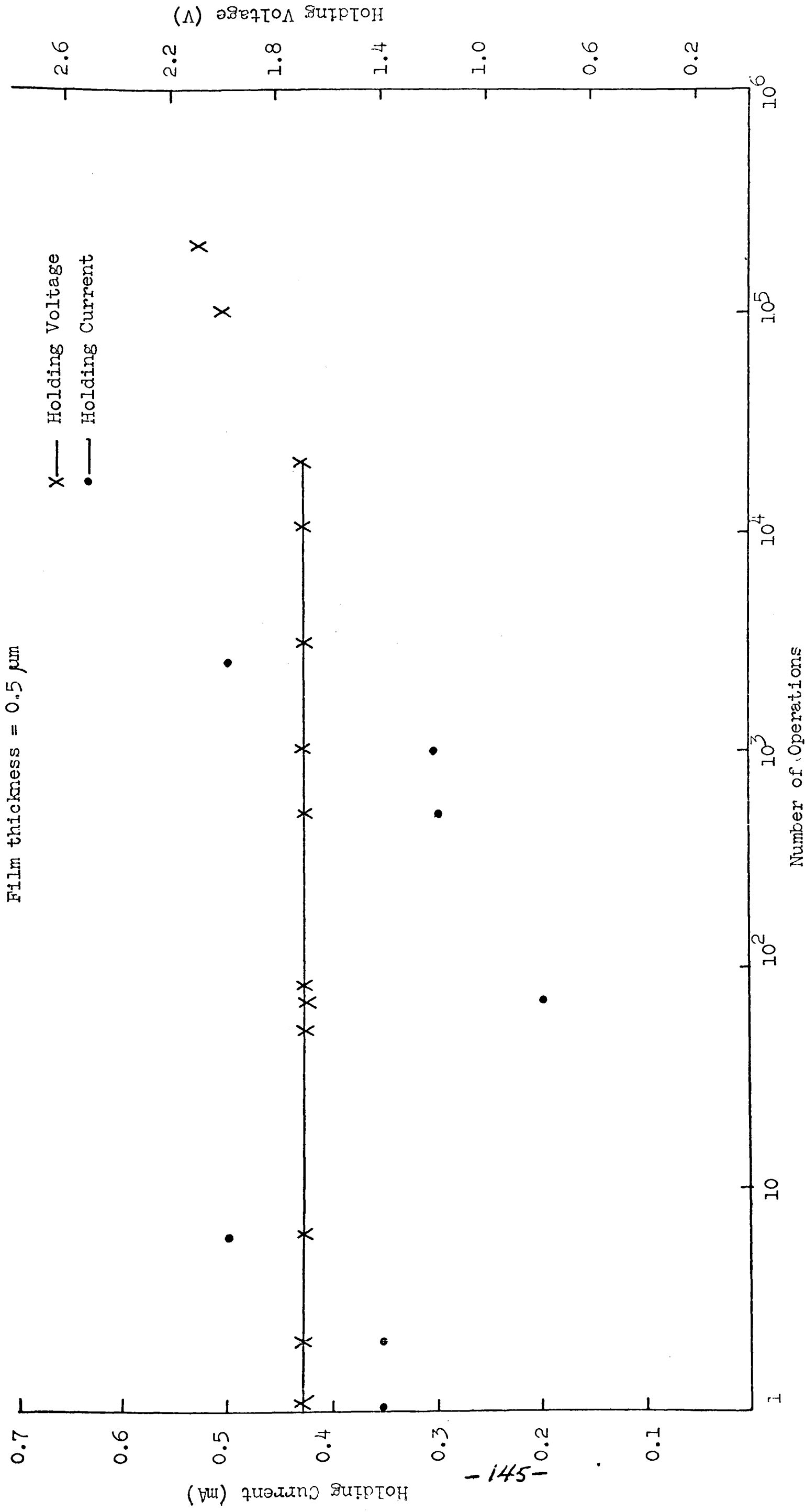


Fig. 4.29 Holding current and holding voltage vs. number of switching operations.

Film thickness = 0.25 μm

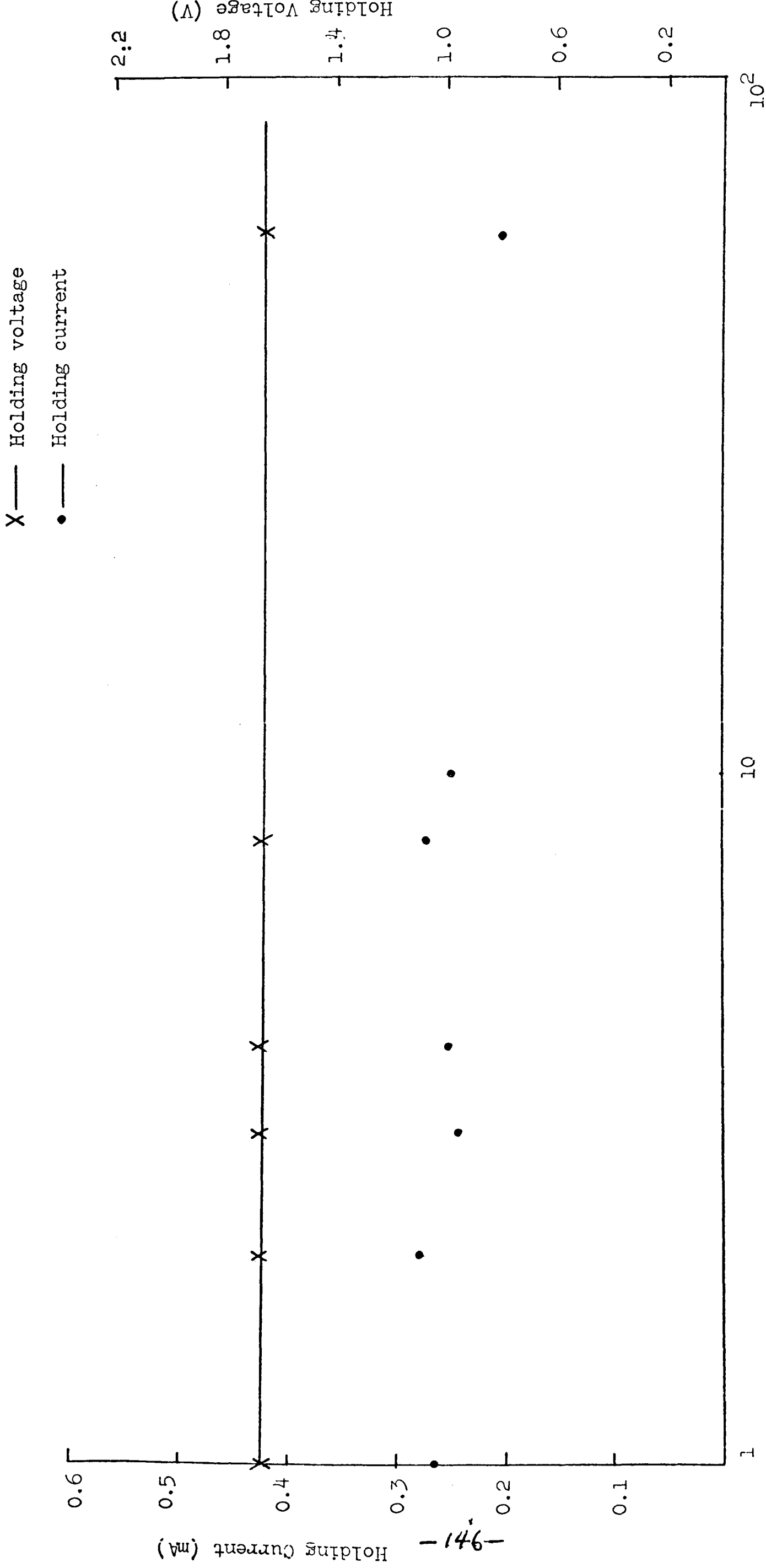


Fig. 4.30 Holding current and holding voltage vs. number of switching operations

are the holding currents against the corresponding numbers of operations. It can be seen that the holding current for all devices was the same, 0.26 mA, for the first-fire operations but showed very large fluctuations for subsequent operations. If a device was operated at a higher pulse repetition rate, > 100 pulse/sec, the fluctuations in the holding current could be observed on the displayed I-V characteristic in the form of small wriggling elliptical loops at the lower end of the on-state trace as shown in figure 4.31. Similar observations have been reported by Thomas (1972).

4.3 Effects of electrode materials

The investigation of electrode effects has so far been mainly concerned with the choice of electrode materials which improve the operational lifetime of these switching devices (Pearson, 1970, Neal, 1970, Pinto, 1971). The most successful device reported has been the DC-7 package where graphite electrodes have been used. In other types of devices, molybdenum electrodes were stated (Neal, 1970) to give the most stable characteristics.

In this work the effects of molybdenum, tungsten, chromium, gold, aluminium and titanium electrodes on device characteristics were investigated. Again, it was considered important to keep all other device parameters, such as geometry and film composition, the same in all devices having the different electrode materials. The substrates used were 1 x 2 x 0.2 cm polished rectangular pieces of Mo, W and Ti. The Mo substrate was placed in the electron-beam evaporation plant, had half of its polished surface area masked and a 3 μm thick film of gold was evaporated on the unmasked part. The same procedure was repeated with the W and Ti substrates but with 3 μm thick aluminium film deposited on part of the Ti substrate and ^achromium film on part of the W substrate. The three substrates were then transferred to the flash-evaporation plant where a 1.2 μm film of STAG glass was deposited. The top contacts were polished rods of Mo, W and Ti and each had a hemispherical tip diameter of 3 mm. Three other similar Mo rods were also constructed. The first was coated with a thick film of aluminium, the second with a 3 μm thick film of chromium and the third with a 3 μm thick film of gold. Suitable substrates and top contacts were then selected to provide matched pairs of electrode materials for the devices.

The following measurements were made on the point-contact devices:

1. The operational lifetimes and threshold voltages

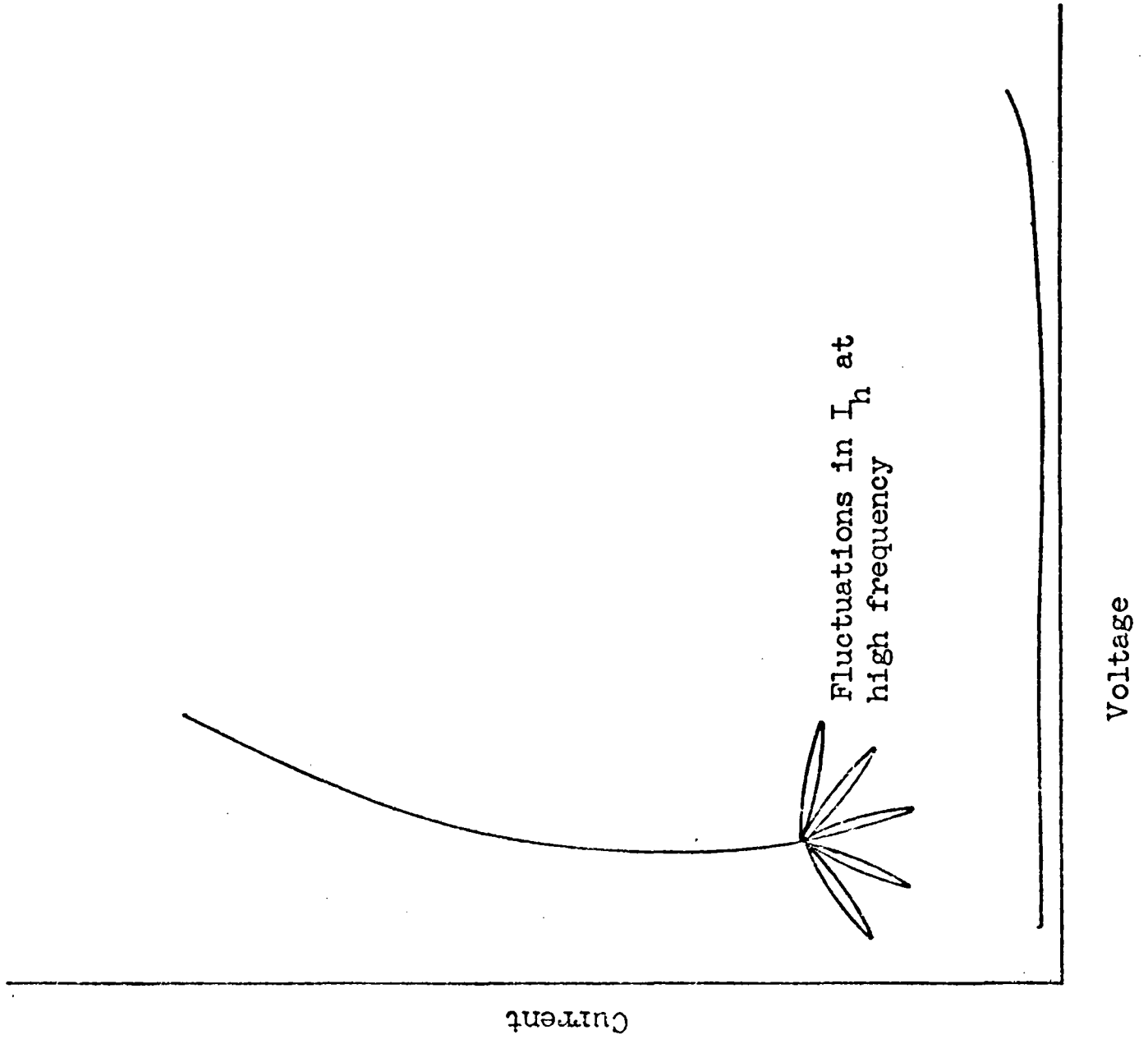


Fig. 4.31 The fluctuations in the holding current I_h observed when the device was operated at a pulse repetition rate greater than 100 pulse/sec.

2. The off-state resistance of the device as a function of the number of switching operations. The method used for measuring the resistances was the same as described in the previous section.
3. The holding current and voltages were measured as functions of the number of switching operations.

The operational lifetime of a threshold switch and the occurrence of multiple branching in the on-state were found to be considerably affected by the use of different electrode materials. The total number of operations, i.e. the operational lifetime, was about 10^8 for devices with Mo electrodes, 10^7 for Al, 5×10^6 for W, 10^6 for Cr and Au, 10^5 for Ti. These results compare very well with other workers' results (Pinto, 1971, Bosnell et al, 1972a). Bunton et al (1971) have reported an operational lifetime of 10^9 operations for devices with Au electrodes. Such a long lifetime was certainly not observed in the devices with Au electrodes. The first-fire threshold voltages were nearly the same in all devices, 75V for Ti, 70 V for Cr, Au and Al, and 60 V for W and Mo as shown in figures 4.32 - 4.37. The most stable device behaviour was obtained with Mo and W electrodes. With Al electrodes forming was not achieved until after about 500 switching operations, whereas with all other electrodes forming was achieved after a few operations and these results were consistent for a large number of tested devices. The threshold voltages in formed devices with Al, Mo and W electrodes were in the range of 10 V to 20 V, and less than 10 V for devices with Cr, Ti and Au electrodes. The off-state resistances after the first-fire operations were generally higher in devices which had larger operational lifetimes but not necessarily the highest in devices with Mo electrodes which had the longest operational lifetime. Also, the off-state resistance after the first-fire operation for Cr devices was comparable to that of Mo devices. It is important to note at this stage that the off-state resistances of all virgin devices with the different electrode materials were of the same magnitude, 24-26 M Ω , and all the changes occurred immediately after the first-fire operations. The decay in the off-state resistance with increasing number of operations was similar to that described in the previous section, see figures 4.18 - 4.23.

Multiple branching in the on-state appeared after 10^4 switching operations for Mo, 2×10^3 for W and Al, 2×10^2 for Au and after only a few operations with Cr and Ti.

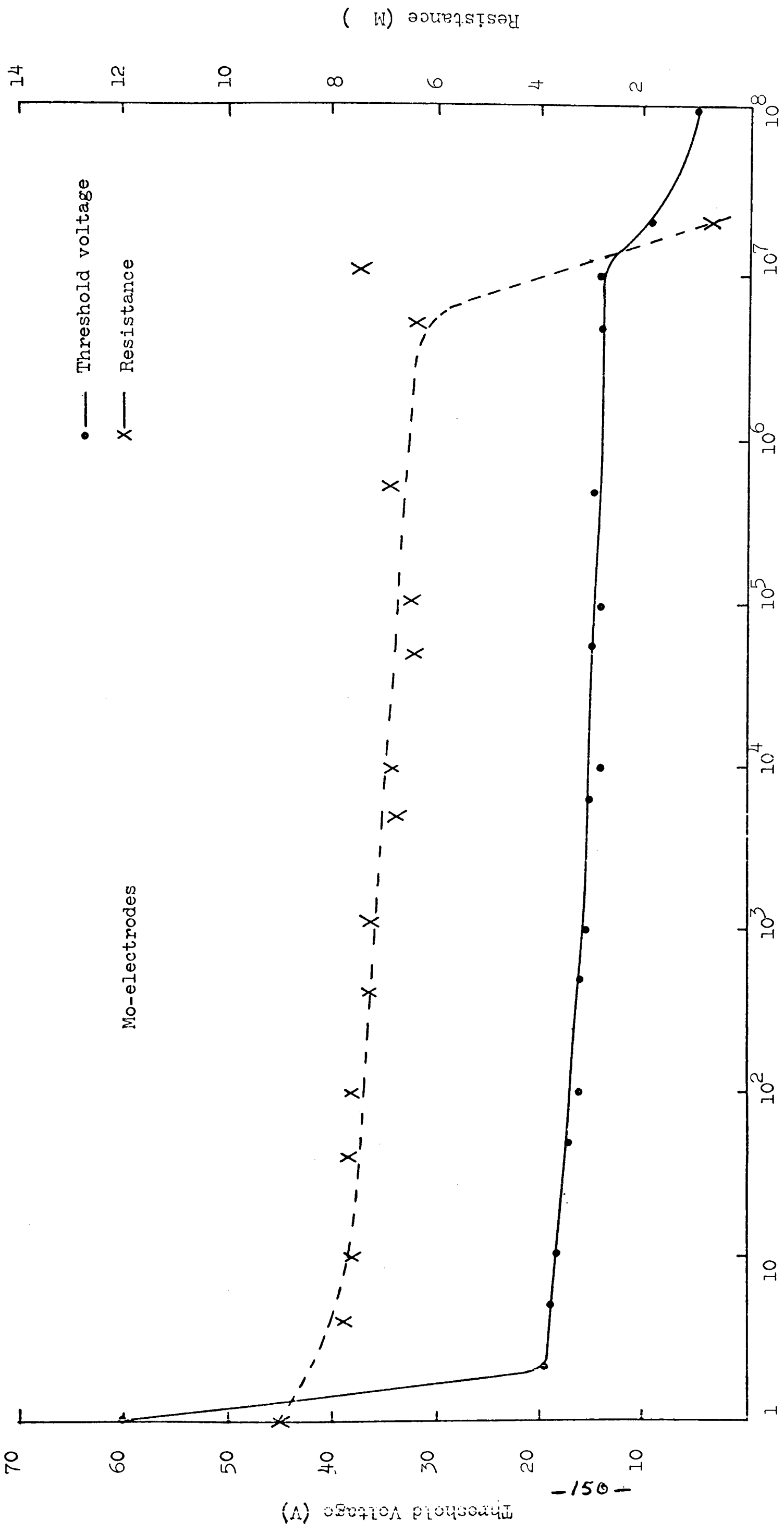


Fig. 4.32 Threshold voltage and off-state resistance vs. number of switching operations.

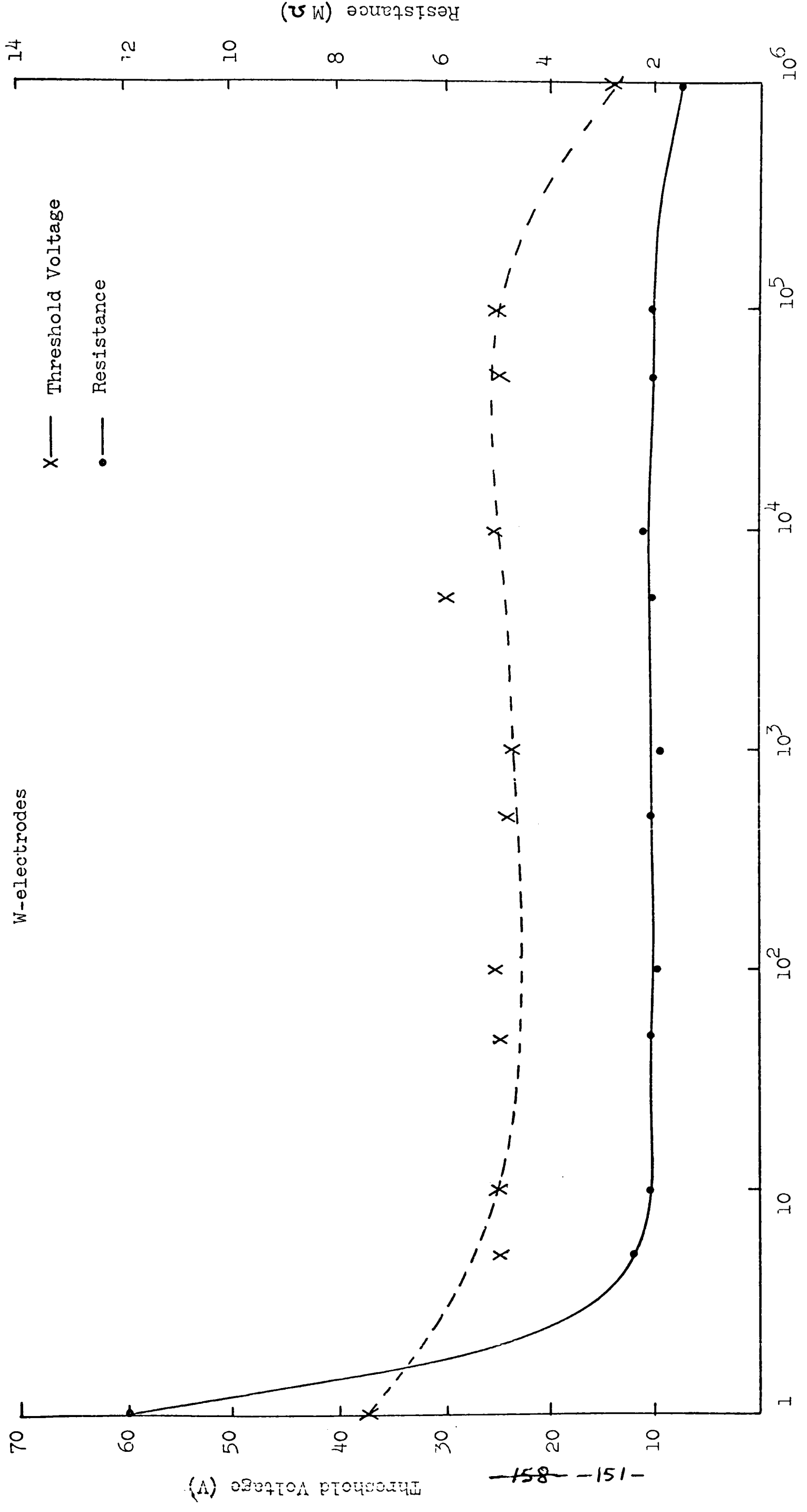
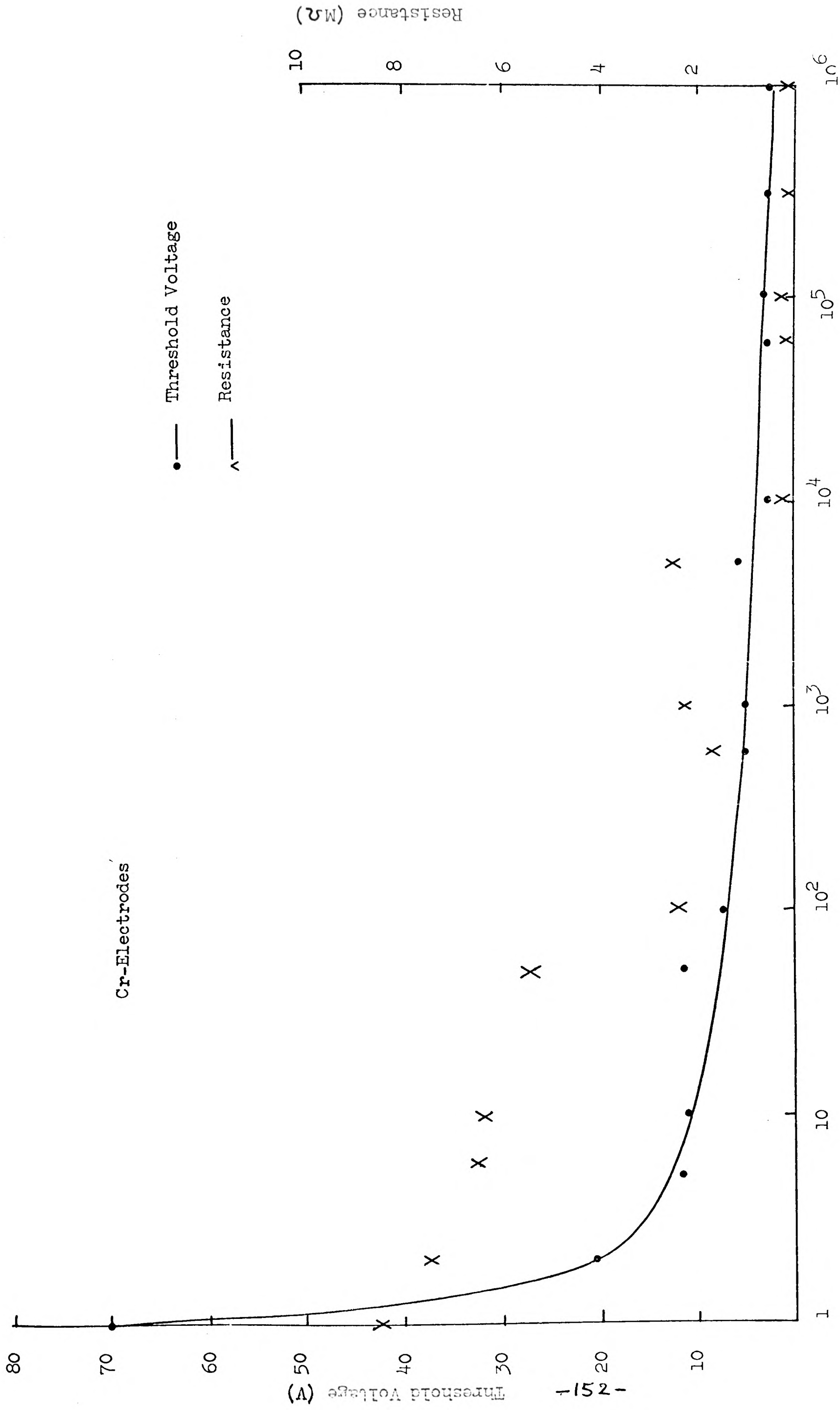


Fig. 4.33 Threshold voltage and off-state resistance vs. number of switching operations. Number of Operations

Cr-Electrodes



Number of Operations

Fig. 4.34 Threshold voltage and off-state resistance vs. number of switching operations.

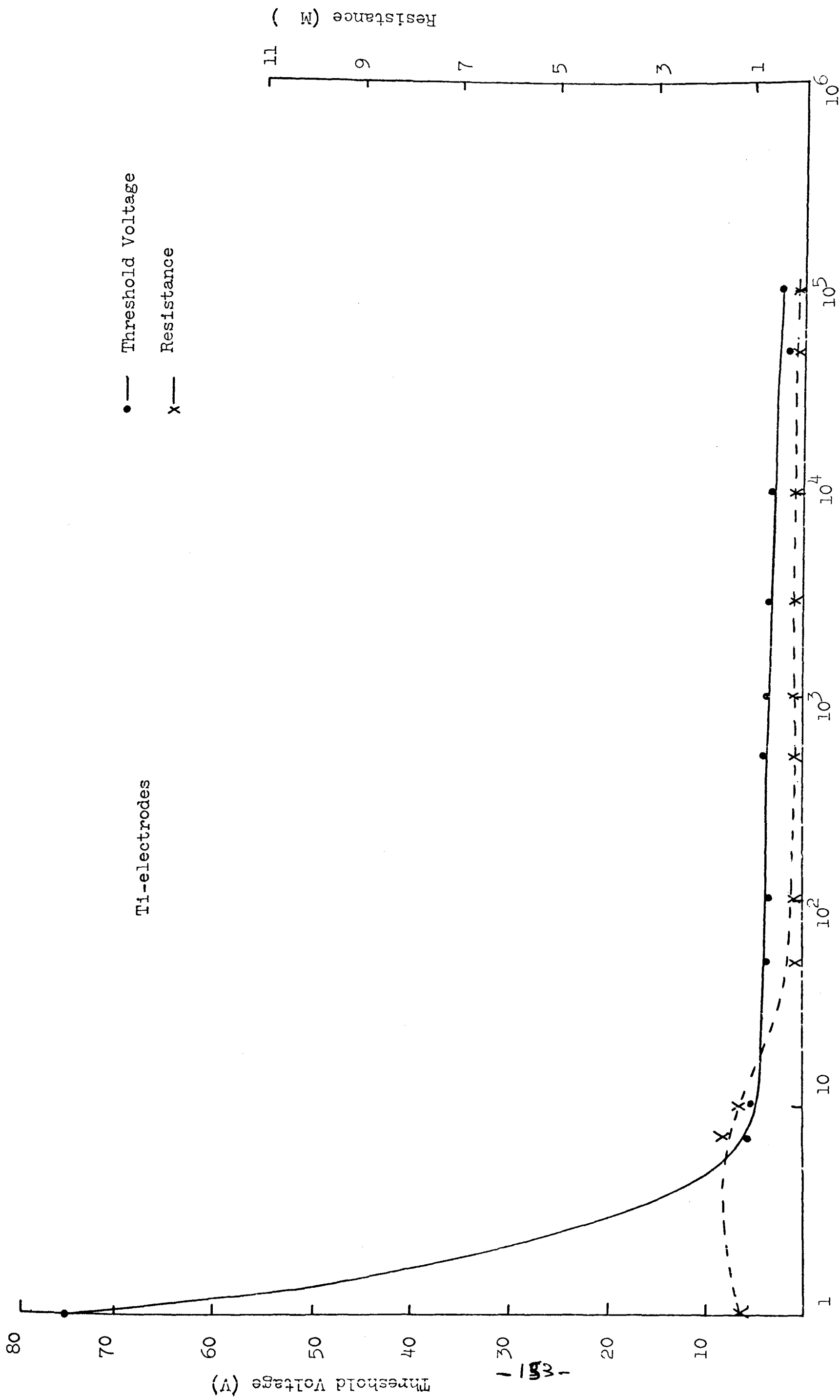
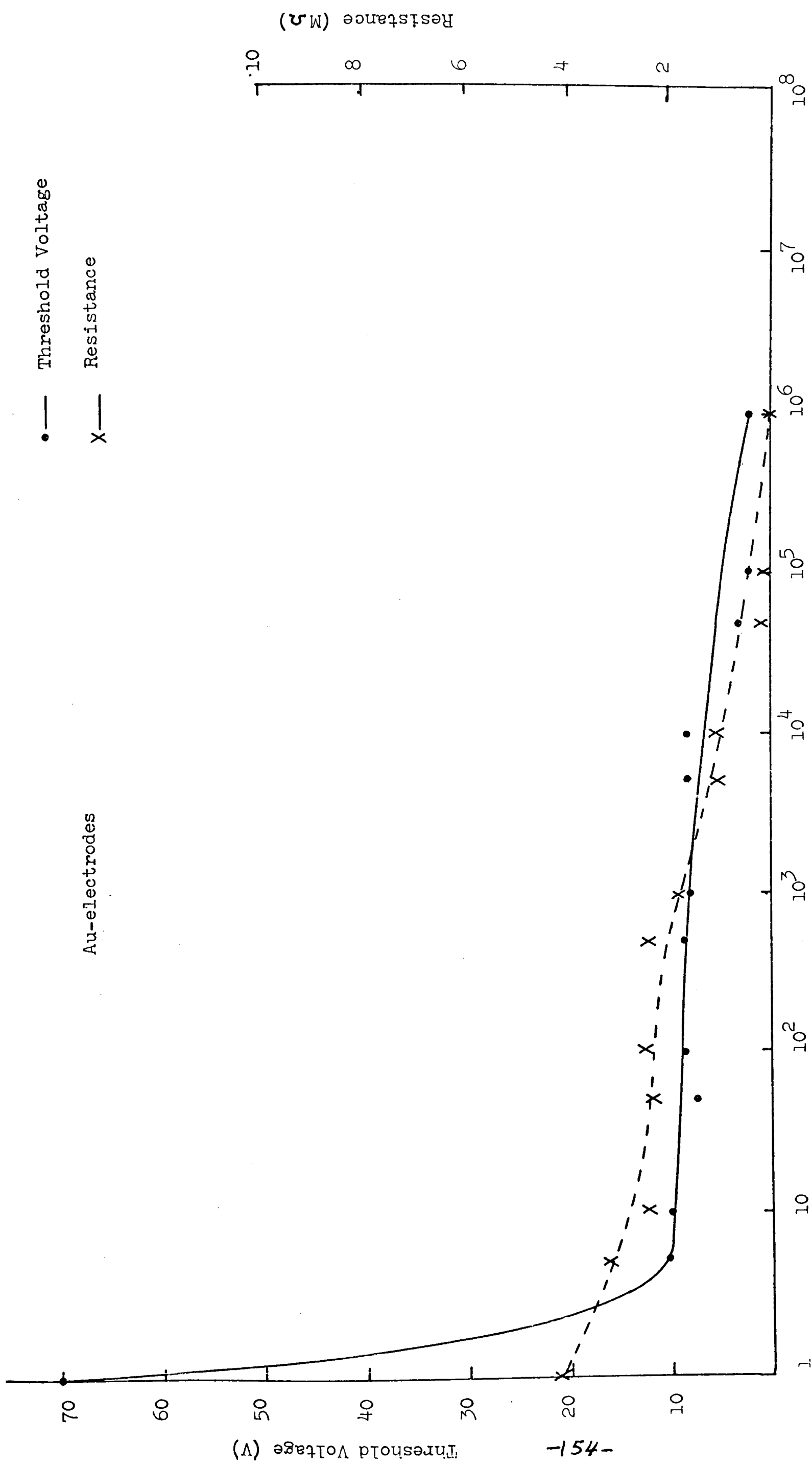


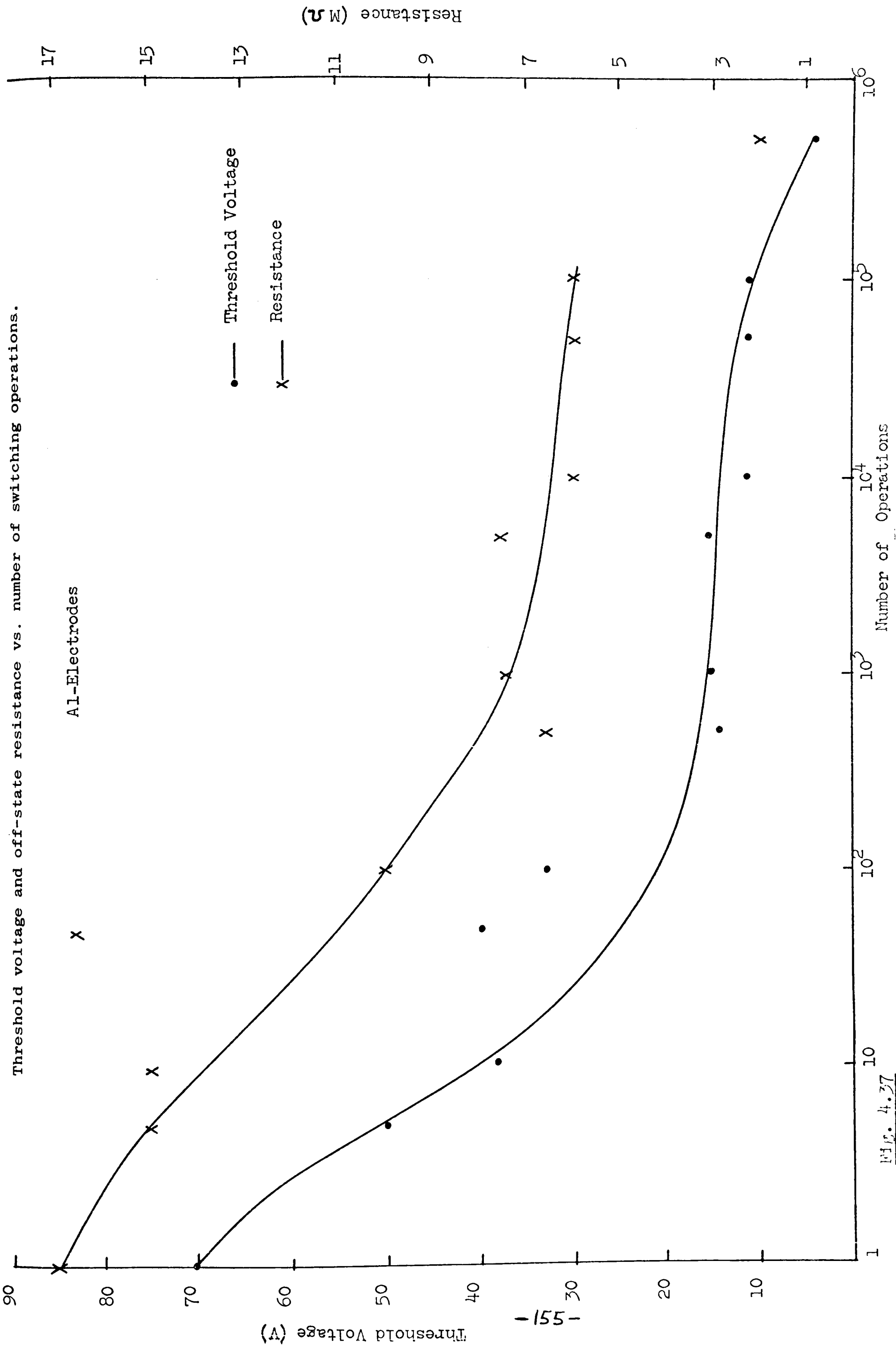
Fig. 4.35 Threshold voltage and off-state resistance vs. number of switching operations. Number of Operations



Number of Operations

Fig. 4.36 Threshold voltage and off-state resistance vs. number of switching operations.

Threshold voltage and off-state resistance vs. number of switching operations.



In figures 4.38 - 4.43 the holding currents and minimum holding voltages are plotted against the corresponding number of operations. It can be seen that the holding currents showed the usual large fluctuations even in the most stable devices, those with Mo and W electrodes. The fluctuations in minimum holding voltages for Mo and W devices were negligible for almost the entire operational lifetime of the devices. In Au devices, fluctuations in minimum holding voltage appeared after 4×10^3 operations, and after about 500 operations in Cr and Ti devices. Aluminium devices had a minimum holding voltage of about 2.8 V but it dropped to about 1.9 V after 100 operations. The magnitude of the minimum holding voltage in the rest of the devices was 1.7 V for Mo, 1.8 V for W, 2.0 V for Au, 1.3 V for Cr, and 1.2 V for Ti. These values were taken from the most stable parts of the minimum holding voltage versus number of operations plots.

4.4. Measurement of a.c. conductance of switching devices

These measurements were primarily carried out to investigate the degree of clustering of the tellurium crystallites in a formed device. As mentioned earlier, the measurements were carried out first on virgin devices then the devices were switched until they were formed and the same measurements were repeated on them. To avoid large stray capacitances associated with the long leads needed to connect a point-contact device to the Q-meter, these measurements were carried out on sandwich devices.

Two substrates were used, one had a chalcogenide glass film of 1.5 μm thickness and the other a 0.6 μm thick film. Both substrates had an array of eight sandwich devices with aluminium electrodes.

It was originally intended to carry out the a.c. conductance measurements with a Wayne-Kerr Radio Frequency Bridge B601. This instrument had an accuracy of 1%. However, it had a maximum impedance range of 10 M Ω which was not quite adequate to measure the off-state resistance of the virgin or unformed devices. Therefore, comparison of the a.c. conductances of a virgin and formed devices was not possible with this instrument. To overcome this problem, a Marconi TF 1245 Q-meter was used. The two quantities that were measured with the Q-meter were the device capacitance and the Q value. From these quantities the device conductance and the dissipation factor, $\tan \xi$ were calculated for a frequency range from 4×10^4 Hz to 4×10^7 Hz.

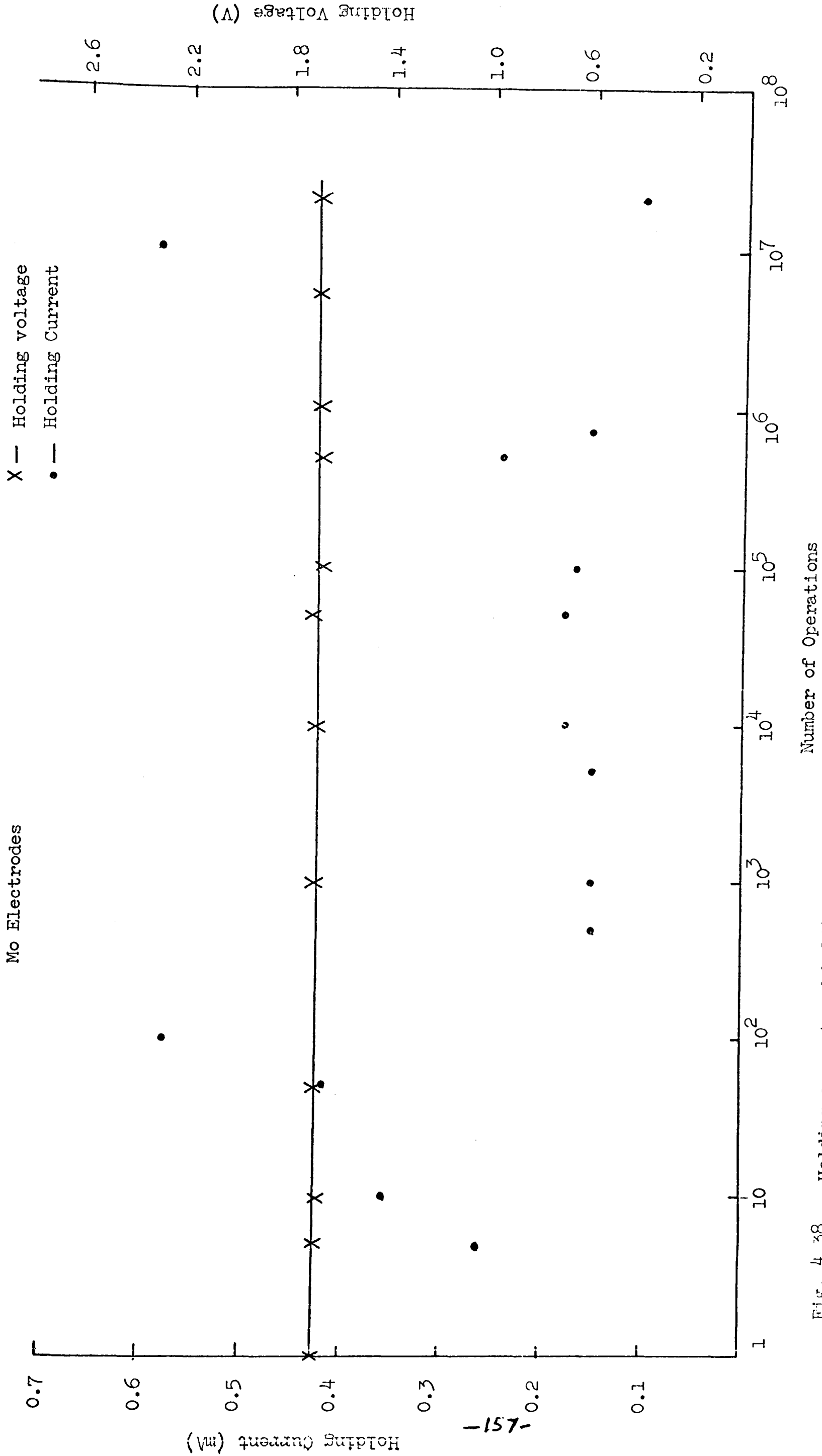


Fig. 4.38 Holding current and holding voltage vs. number of switching operations.

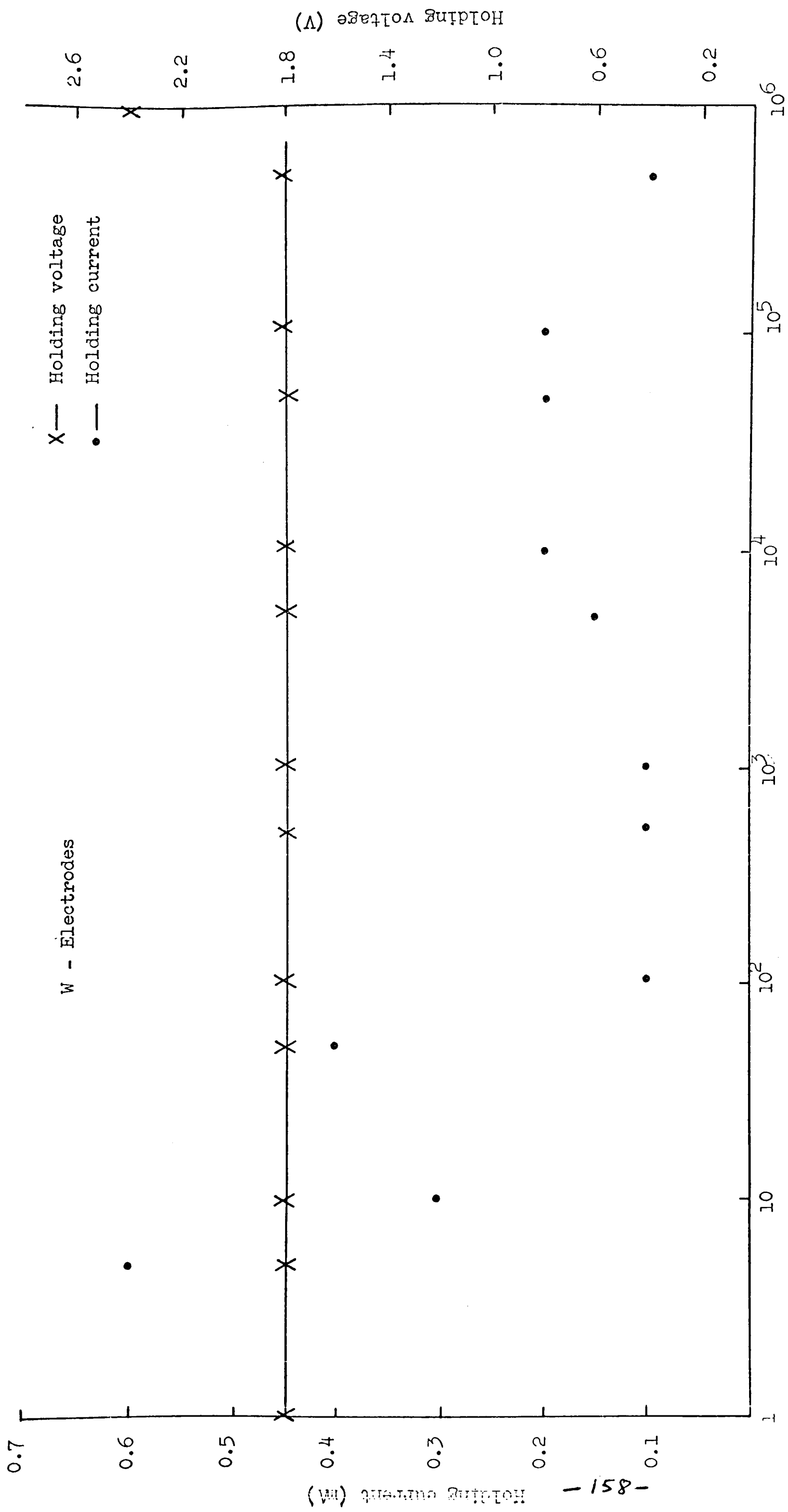
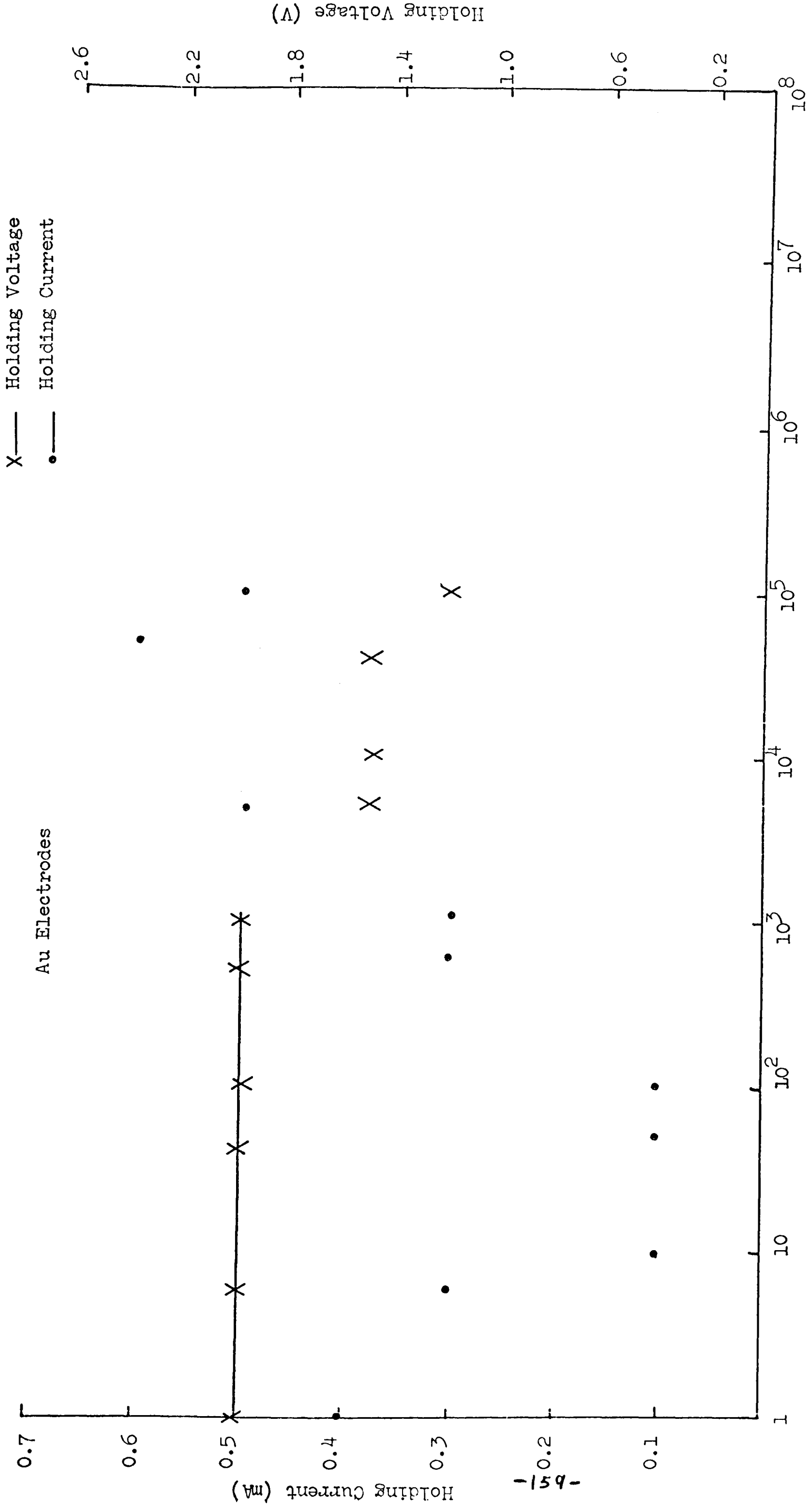


Fig. 4.39 Holding current and holding voltage vs. number of switching operations.



Number of Operations

Fig. 4.40 Holding current and holding voltage vs. number of switching operations.

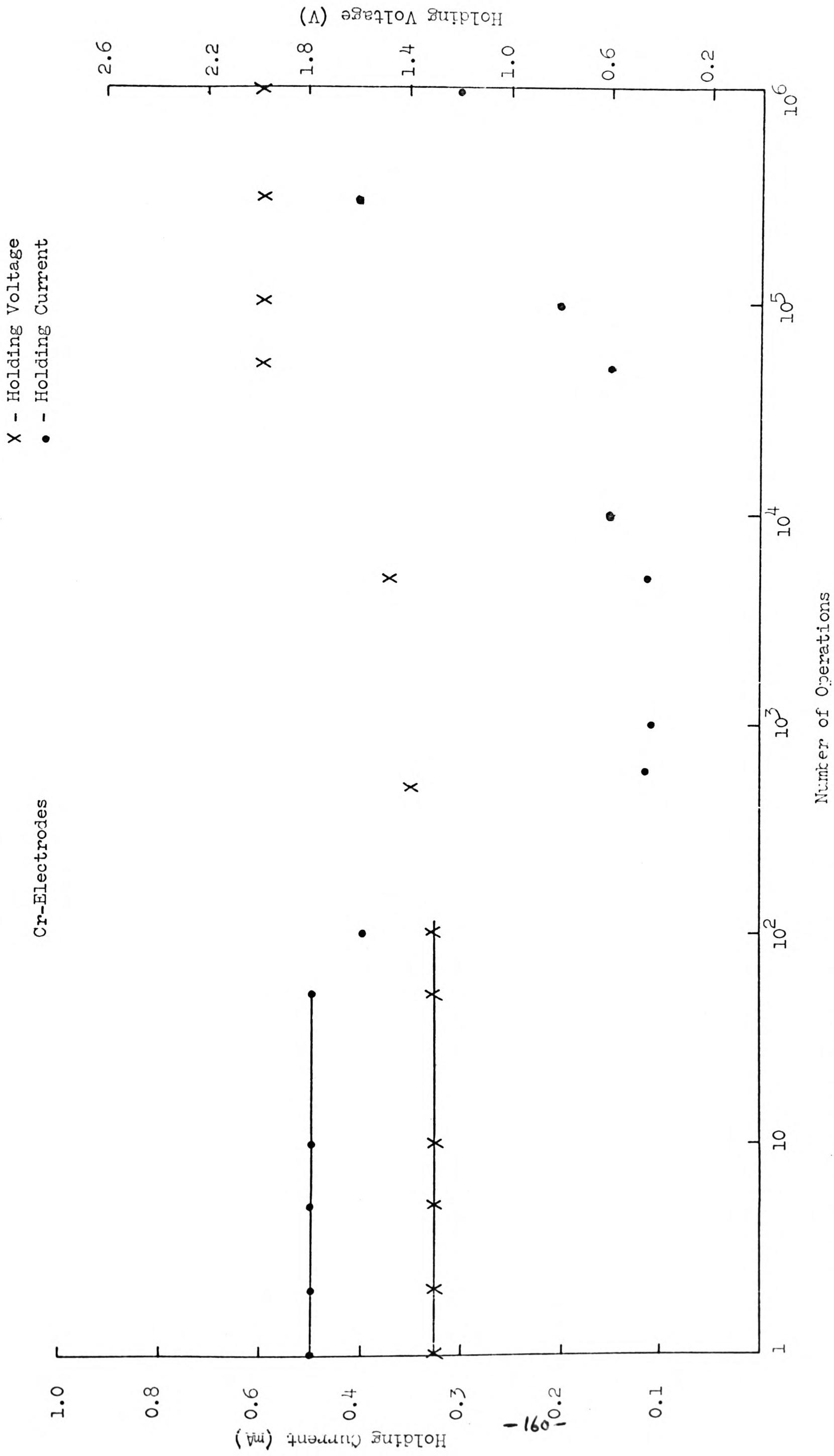
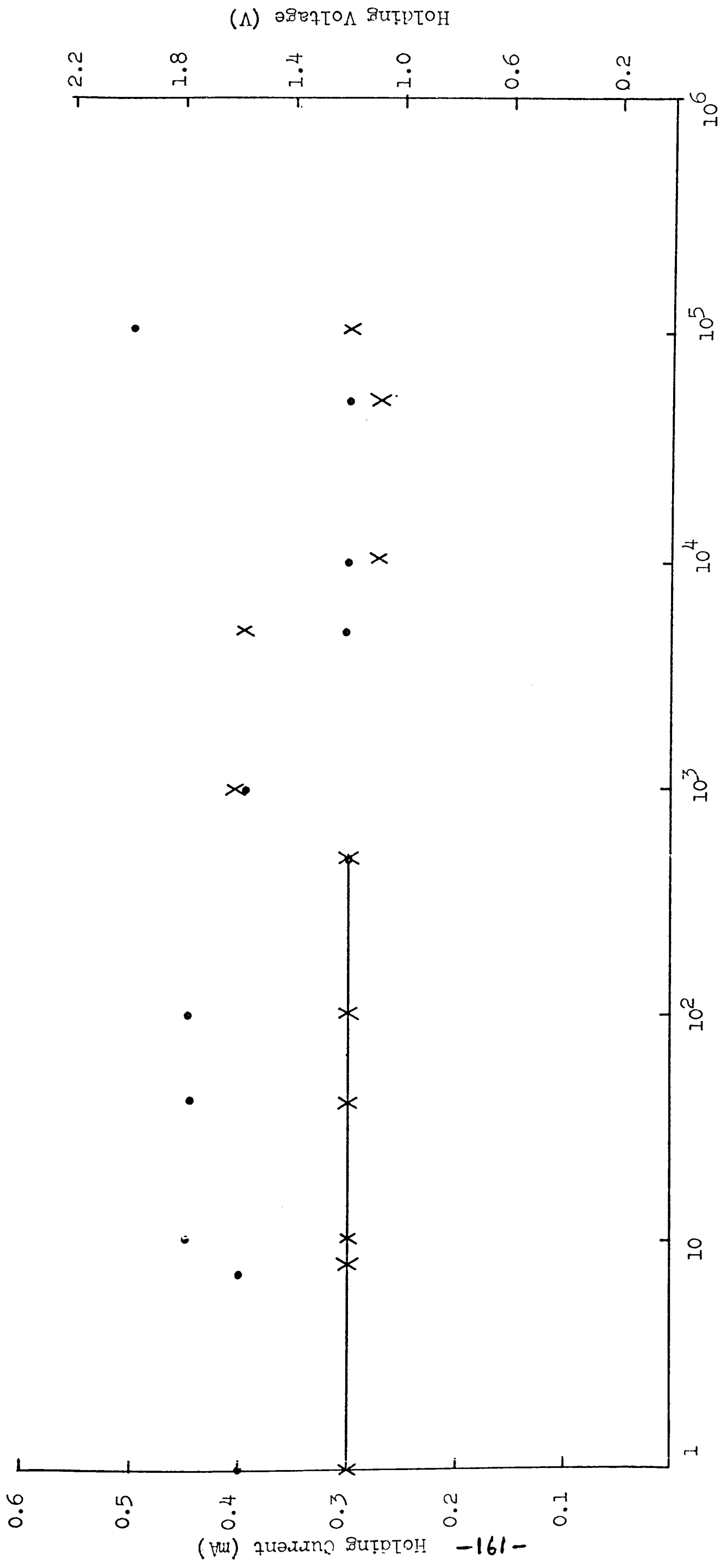


FIG. 4.41 Holding current and holding voltage vs. number of switching operations.

Ti Electrodes

X — Holding Voltage
 • — Holding Current



Number of Operations

Fig. 4.42 Holding current and holding voltage vs. number of switching operations.

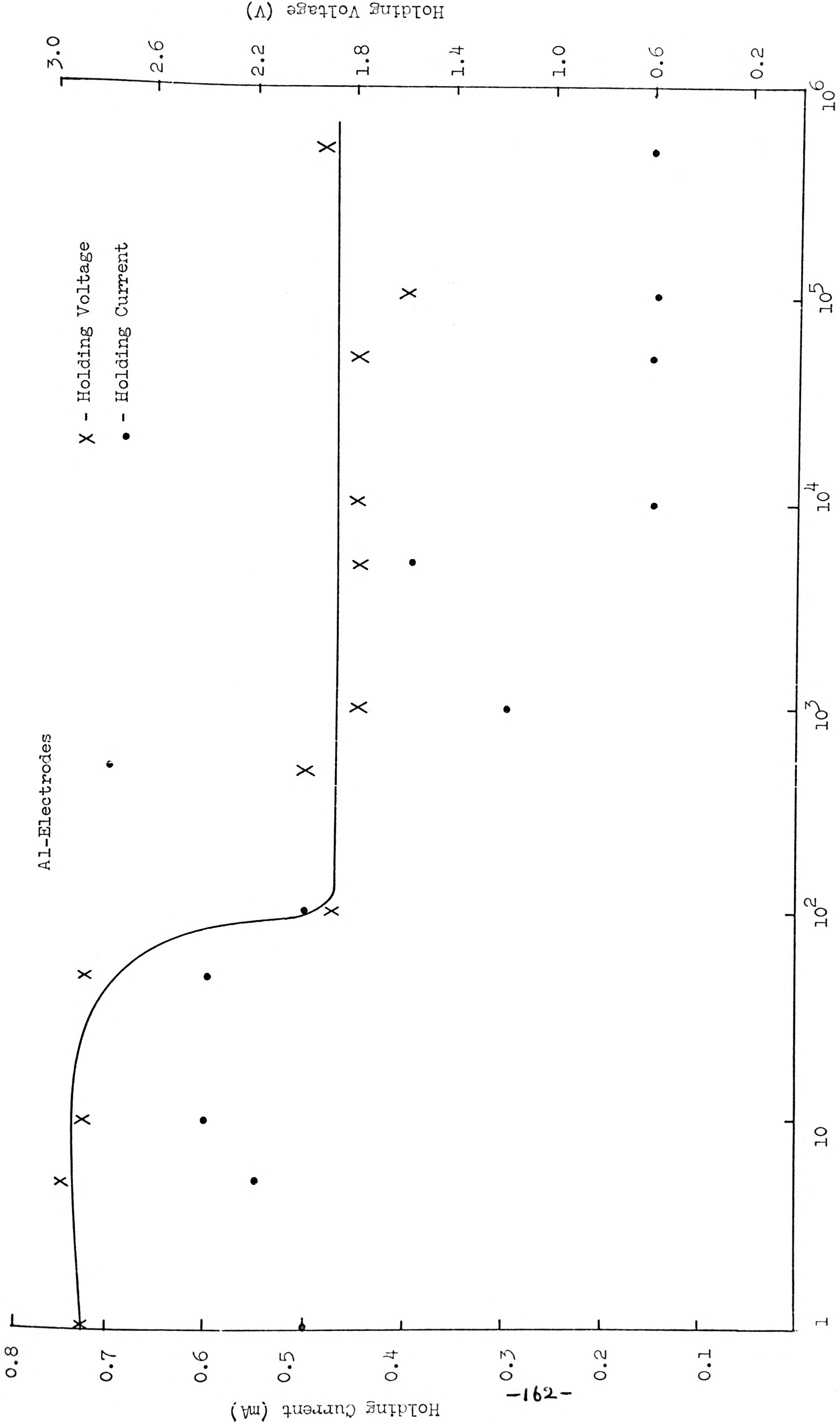


Fig. 4.43 Holding current and holding voltage vs. number of switching operations.

Number of Operations

The capacitance of a 1.5 μm thick virgin device was found to be 5.0 pf, and that of a 0.6 μm thick virgin device was 10.0 pf. No change in device capacitance, for either film thickness, was observed after the devices were switched and formed. All devices were switched under the same electrical conditions, i.e. pulse width, polarity, repetition rate and for the same number of operations, which was 10^3 . In figure 4.44, device capacitances are plotted against frequency and it can be seen that the capacitance remained independent of the frequency for the frequency range used.

The loss factor, $\tan \delta$, describes the quality of a dielectric and for a good dielectric it has an extremely small value, e.g. 10^{-4} for quartz, and should be independent of frequency. However, because of the presence of impurities, a very small frequency-dependence is often observed in non-polar dielectrics. Pearson et al (1963) have measured the loss factor for several glasses in the As-S-Br system and showed that the variations in $\tan \delta$ as a function of frequency were quite small, although certain increases in $\tan \delta$ at low frequencies were observed. The values of $\tan \delta$ for the STAG films examined in this work are plotted against frequency in figure 4.45, for the 0.6 μm devices, and in figure 4.46 for the 1.5 μm thick devices. In all the devices $\tan \delta$ decreased initially with increasing frequency, but increased beyond 10^7 Hz. It can also be seen that from a comparison of $\tan \delta$ for virgin devices of different thickness there was a considerable numerical difference at a specific frequency. However, $\tan \delta$ had more or less the same value at a given frequency for the formed devices. These results will be further discussed in Chapter Five. The conductances of the devices, as functions of frequency, are shown in figure 4.47. As would be expected, the conductances are higher in formed devices than those in virgin devices. The conductance of the 0.6 μm thick virgin devices is independent of frequency for lower frequencies but increases sharply at higher frequencies, $\sim 2 \times 10^5$ Hz.

4.5. Uniaxial Pressure Effects

The uniaxial pressure experiments were carried out on point-contact devices fabricated on a substrate where the chalcogenide thin film had been prepared by r.f. sputtering. The uniaxial pressure was provided by standard laboratory balance weights placed on top of the point-contact jig arm, see figure 3.16b which accommodated the top contact probe of a point-contact device. The diameter of the tip of the probe was 3 mm. The weights were placed close to the upper part of

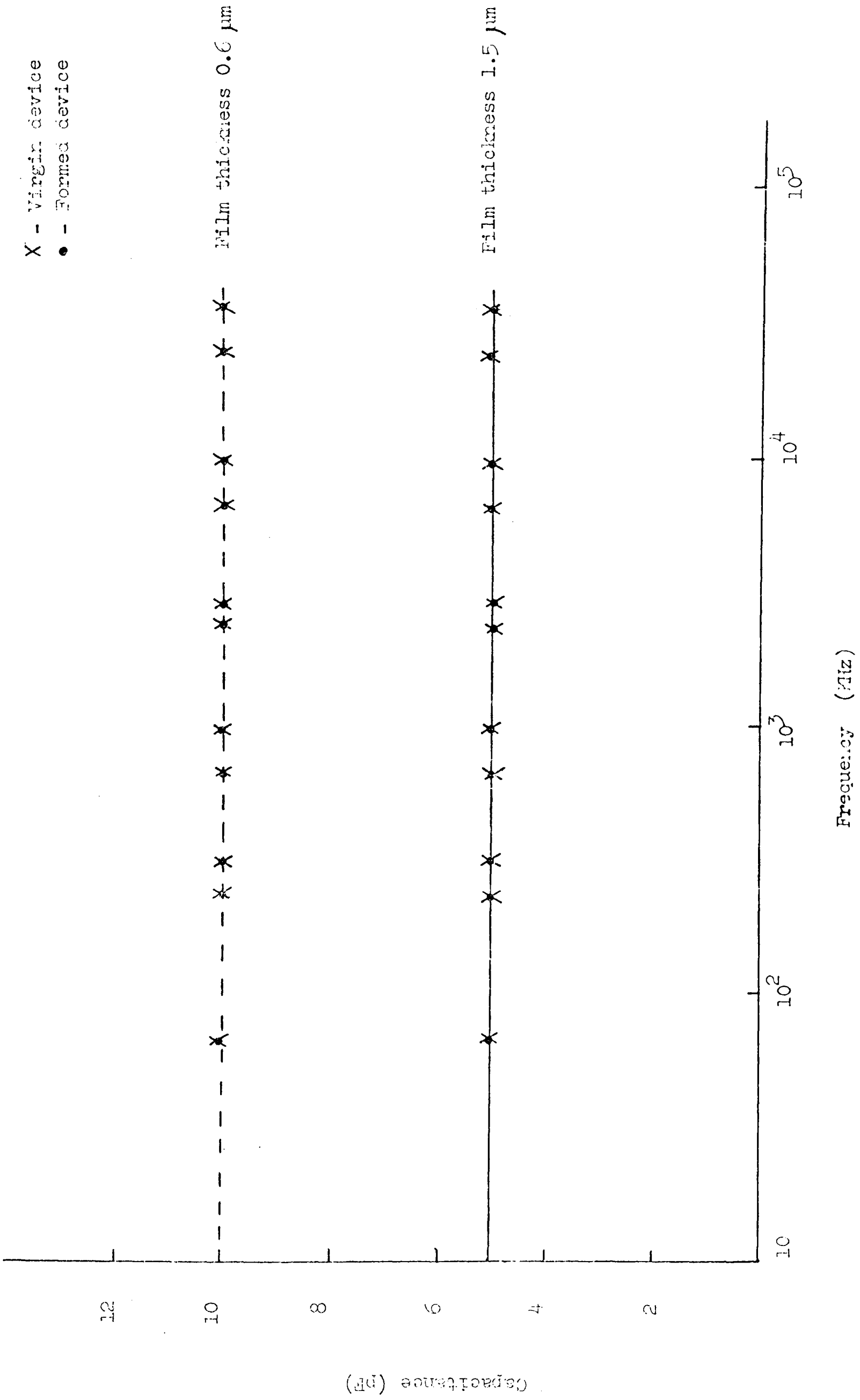


Figure 4.44 Capacitance of a sandwich device with Al electrodes versus frequency.

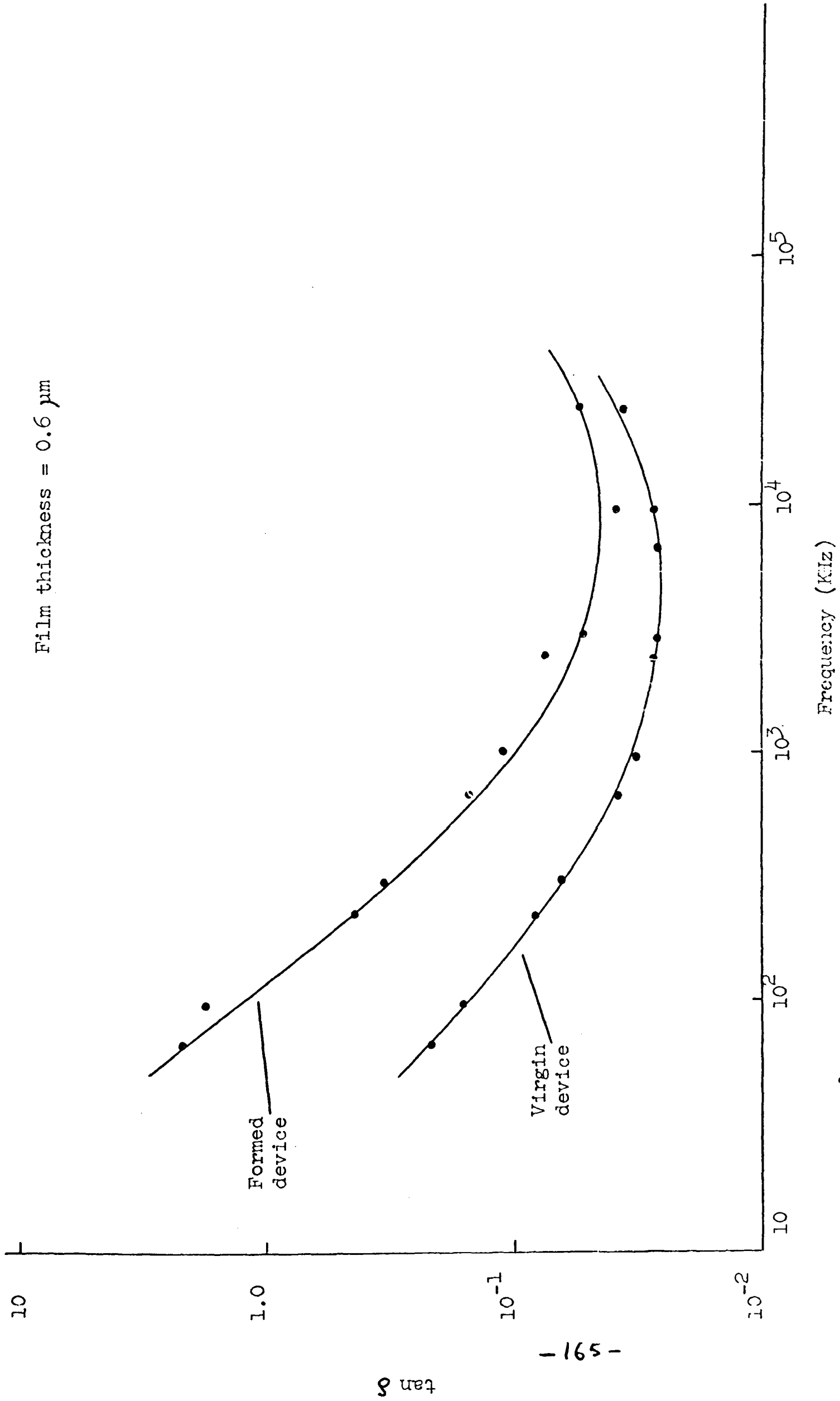
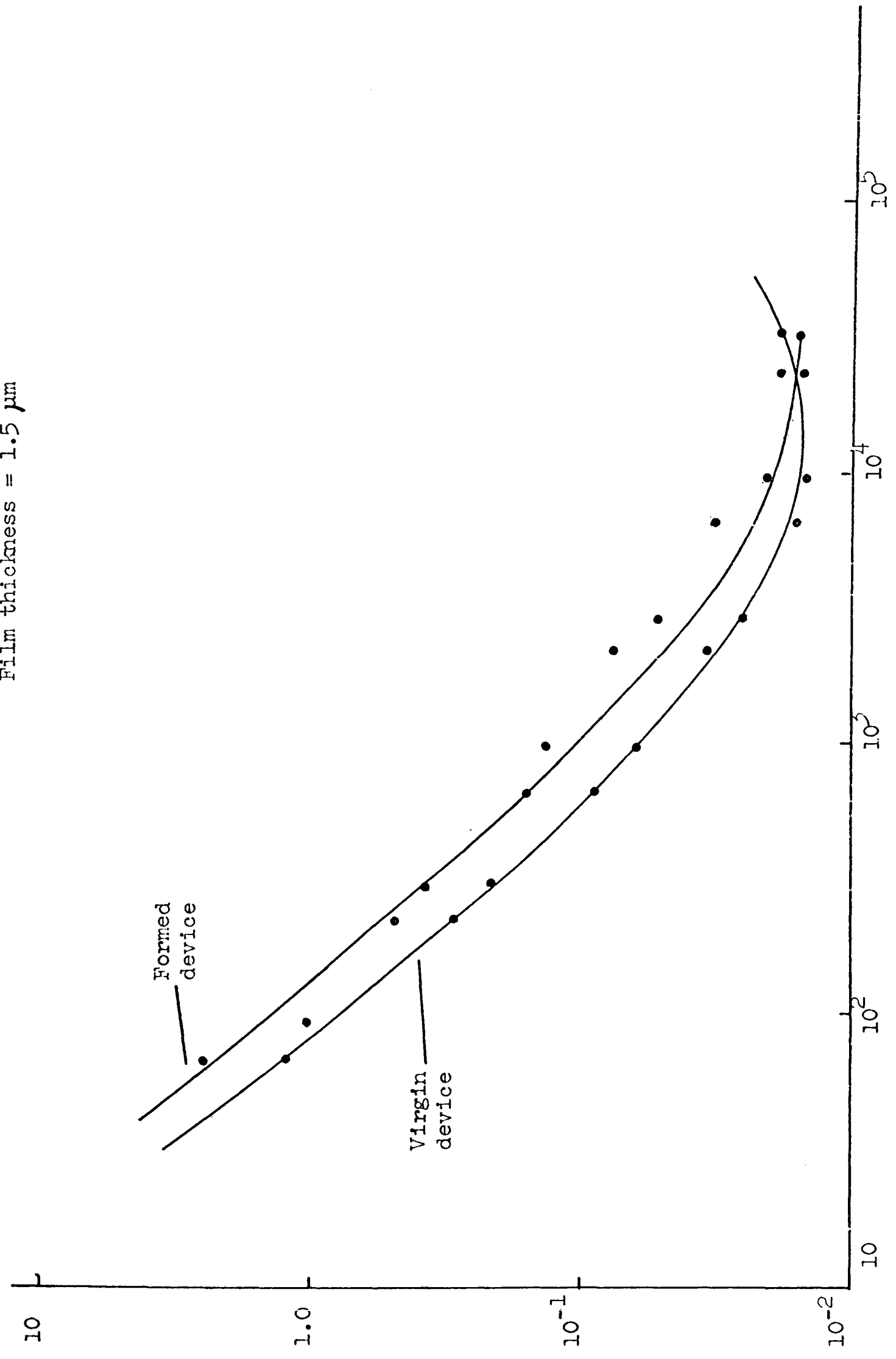


FIG. 4.45 $\tan \delta$ vs. frequency for a sandwich device with Al electrodes.

Tan δ vs. frequency of a sandwich device with Al electrodes.

Film thickness = 1.5 μm



Frequency (KHz)

Fig. 4.46

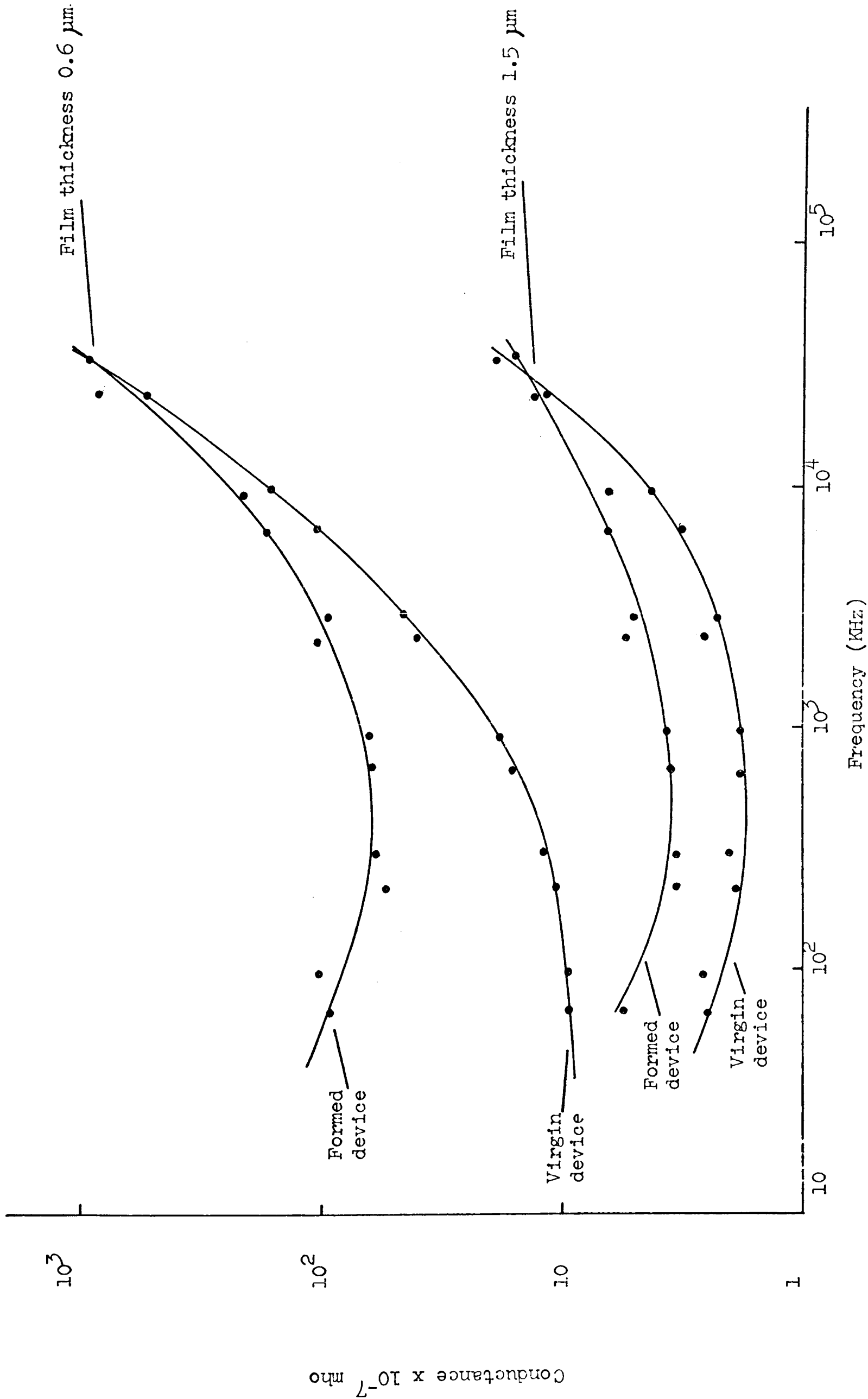


FIG. 4.47 Plots of conductance vs. frequency for virgin and formed sandwich devices with Al electrodes.

Mo probe. It was first necessary to find the maximum load that could be used without causing plastic deformation of the thin film material. This was achieved by applying a small voltage, \sim one V, across the device and measuring the current passing through it. A small load, say 2 g, was then placed on the arm and the increase in current was recorded and the load removed. If no plastic deformation occurred the current reverted to its previous load-free value. It was found that the maximum load the thin film material could tolerate without damage was 100 g.

To examine the effect of uniaxial pressure on a virgin and a formed device, various loads were placed on the arm and the percentage increase in current was calculated and plotted against the load as shown in figure 4.48, curve A for the virgin device. The device was then switched and formed. The total number of switching operations was 10^3 . Similar measurements were repeated on the formed device and the results are plotted in figure 4.48, curve B. It can be seen that there are several distinct differences between curves A and B. Firstly, the percentage increase in current for the same load was greater for the formed device, and secondly when the maximum load, 100 g, was removed, the current reverted to its original load-free value when the device was virgin but this did not occur in the formed device. Removal of the 100 g load caused the current to drop to a value around point X. However, for loads less than 70 g, and prior to placing the 100 g load, the current did drop to its original load-free value. Other important features of the two curves are the nature of the current increases in the two cases. In curve A, the percentage increase in current with applied load was smooth and gradual although non-linear. In curve B the current increased in somewhat similar manner up to a load of 70 g, but when 100 g load was placed a massive increase in current was recorded.

The effect of uniaxial pressure on device switching performance was also investigated using three different loads, 20, 50 and 100 g. The devices, initially virgin, were then switched until switching ceased, i.e. they remained in the conductive state. The results were also compared with those for a load-free device. The decay in threshold voltages for the various loads are shown in figure 4.49, where the threshold voltages of the devices are plotted against the number of switching operations. The first-fire threshold voltage in all the devices was the same, about 130 V. However, the threshold voltage dropped sharply after only a few

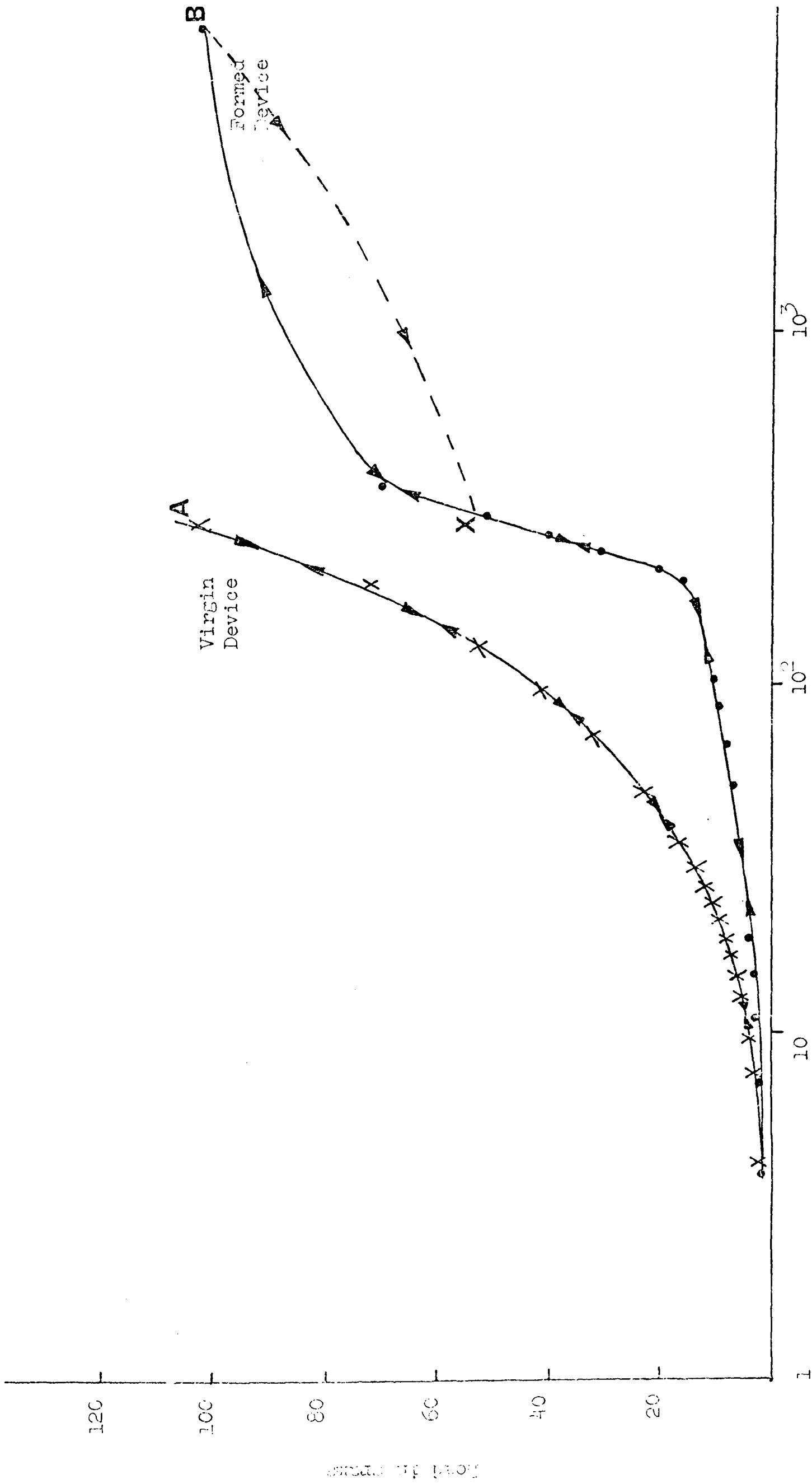


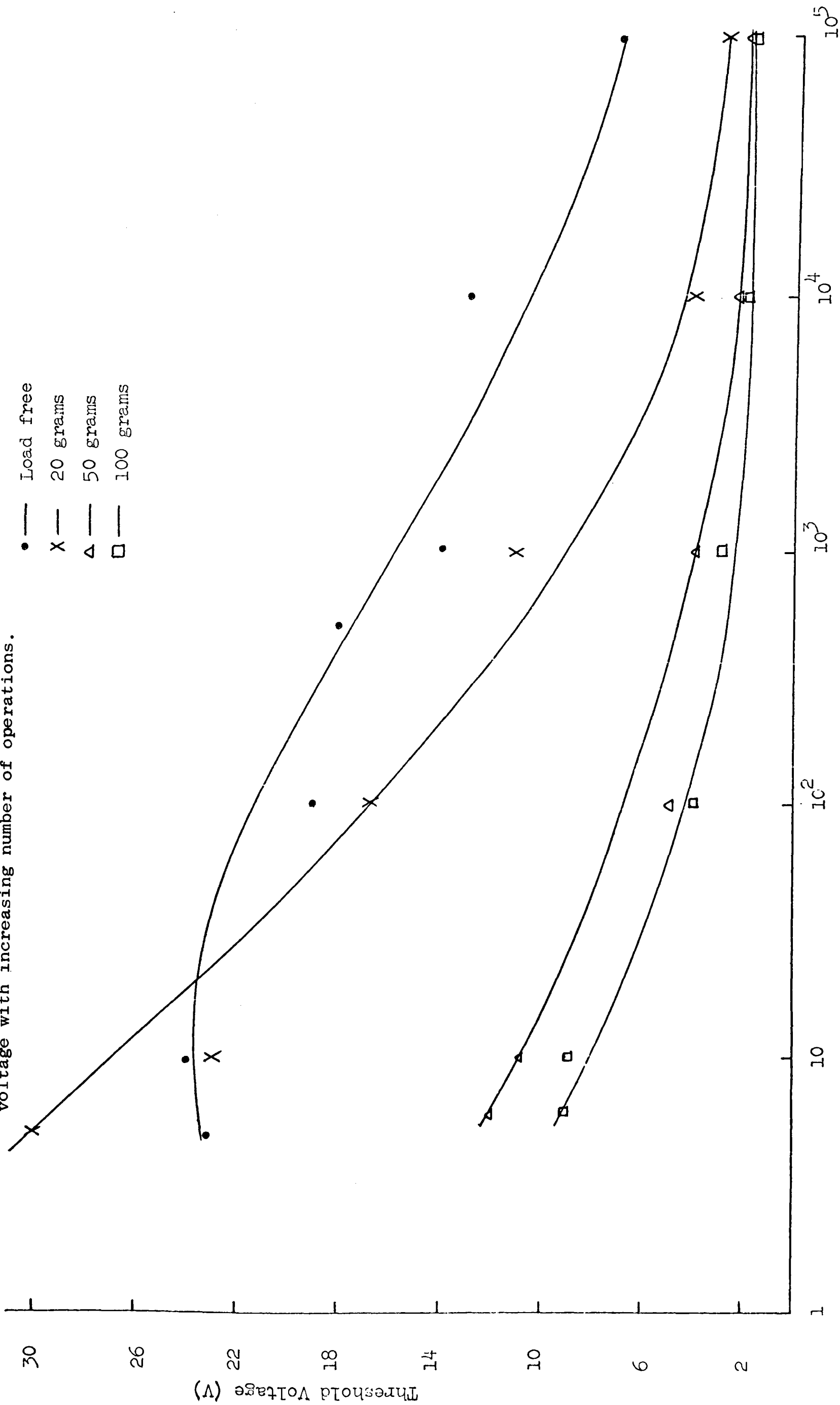
Fig. 4.48 The effect of uniaxial pressure, i.e. a load placed on the top contact of a point-contact device, on the current. The voltage bias across the device was kept constant.

Fig. 4.48

The effect of uniaxial pressure on the threshold voltage with increasing number of operations.

Device Load

- Load free
- X 20 grams
- △ 50 grams
- 100 grams



Number of Operations

operations in the loaded devices and the greater the load the larger was the drop. The behaviour of the off-state resistances of the devices were also similar as shown in figure 4.50. The occurrence of multiple branching in the on-state was strongly affected by the magnitude of the applied load. In the load-free device multiple branching did not appear until after 7×10^3 operations but after 10^2 operations in the device with 20 g load, and after only a few operations in the devices with the 50 and 100 g loads. The minimum holding voltage was not affected at all by the application of uniaxial pressure and had the same magnitude in all the devices.

4.6. Effect of Ambient Temperature

The investigation of the effect of a large change in device ambient temperature on the device characteristics was carried out at several selected temperature points below room temperature. These temperatures were 197K, 132K and 78K. The apparatus used is shown in figure 4.51. To obtain an ambient temperature of 197K, a mixture of solid CO_2 and acetone was used as a coolant and dry argon gas was passed through the metal box to avoid ice formation from atmospheric water vapour. The rate of gas flow was adjusted until a steady-temperature situation was achieved. The temperature was measured by a chromel/alumel thermocouple. Substrate 1 was used for the point-contact devices, whereas substrate 2 was used for monitoring the temperature. The two substrates were placed very close to one another so that they had the same ambient temperature. The temperatures 132K and 78K were achieved in a similar manner as for 197K but the coolant was liquid nitrogen and dry helium gas injected into the metal box at two different rates, higher for the higher temperature.

The investigation was carried out on devices having two different pairs of electrode materials, gold and molybdenum. The effect of a temperature change on the threshold voltage and preswitching conditions has been investigated by several workers (Walsh et al, 1970, Buckley and Holmberg, 1972, Vezzoli and Pratt, 1972). Walsh et al (1970) pointed out that V_t became zero close to the glass transition temperature. Buckley and Holmberg showed that the threshold voltage of a device made from $\text{Te}_{81}\text{Ge}_{15}\text{Sb}_2\text{S}_2$ glass with an electrode separation of $1.5 \mu\text{m}$ increased with decreasing temperature, but for temperatures below room temperature the threshold voltage became temperature independent. Attention in the present work was more concerned with the effect of

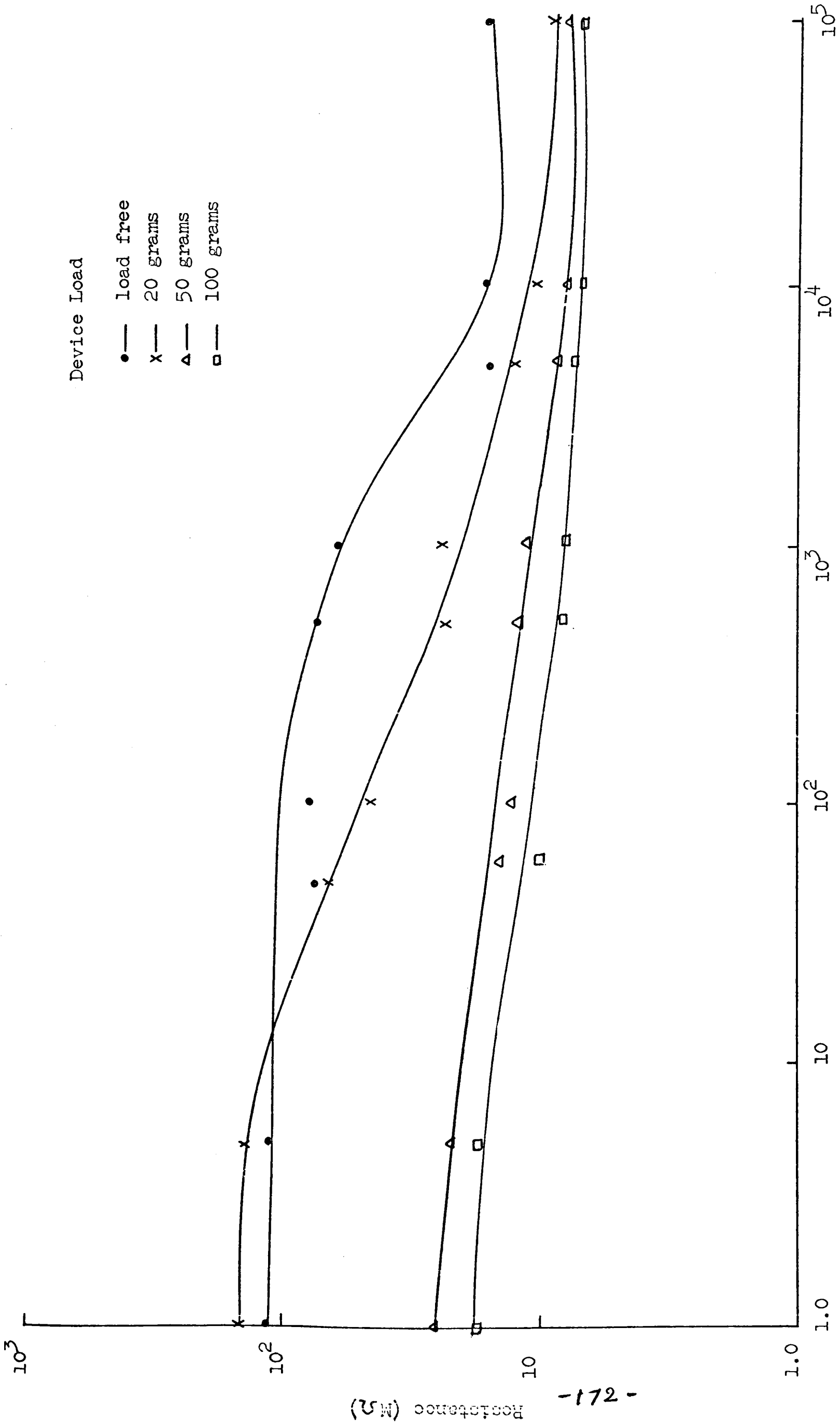
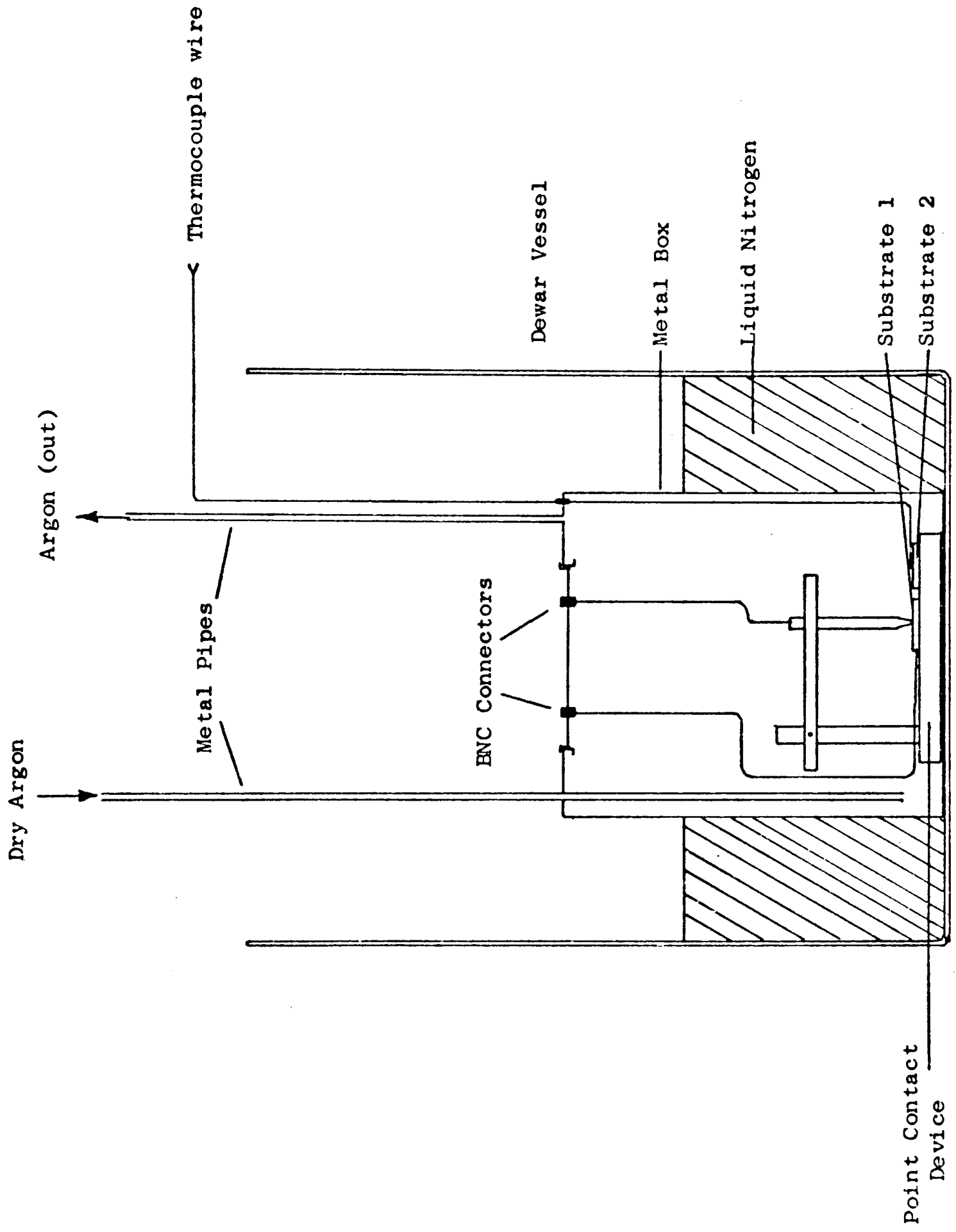


Fig. 4.50 The effect of uniaxial pressure on the off-state resistance of a device with increasing number of operations. Number of Operations



EXPERIMENTAL ARRANGEMENT FOR LOW-TEMPERATURE MEASUREMENT

Fig. 4.51

temperature change on the on-state parameters and the occurrence of multiple branching in the on-state. However, the threshold voltages of the devices at low temperatures were measured and are plotted against the number of operations in figure 4.52 and 4.53 for a device with gold electrodes and another with molybdenum electrodes. It can be seen that the behaviour of the threshold voltages of the devices at the lowest temperature, 78K, and at 132K for the device with molybdenum electrodes was rather erratic. The operational lifetime of the devices were prolonged when the devices were operated at low temperatures, and at a temperature of 78K the lifetime of the device with gold electrodes was greater than 10^7 operations and for those with molybdenum electrodes the lifetime was about 10^9 operations.

The holding currents were far more stable at low temperatures and showed very small fluctuations as the number of operations increased. This is shown in figures 4.54 - 4.55. However, there are relatively large fluctuations in holding current at room temperature. The holding current was found to increase linearly with decrease in ambient temperature, figure 4.56.

No effect on the minimum holding voltage was observed with changes in ambient temperature, see figures 4.57 - 4.58. A definite influence on the occurrence of multiple branching was observed with a decrease in ambient temperature. At 78K branching did not appear until after 10^5 operations in the devices with gold electrodes and about 4×10^5 in the devices with molybdenum electrodes. Therefore, the occurrence of multiple branching in the on-state appears at a much later stage when the devices are operated at low temperature. At room temperature multiple branching appeared after about 2×10^2 operations and 10^4 operations for devices with gold and molybdenum electrodes respectively.

4.7. Effect of Electrode Contact Area

This experiment was similar to the one reported by Coward (1971) with the exception that the devices used in this project were point-contact devices. The bottom electrode was a Cr thin film and the top contact was selected from a set of molybdenum rods with hemispherical tips of various diameters. The diameters used were between 1 and 50 mm. The devices were tested with 1.3 ms width positive ramp pulses at a repetition rate of 10 pulse/sec. The results are tabulated overleaf.

Device Ambient Temperature

- 78°K
- X 132°K
- Δ Room temperature

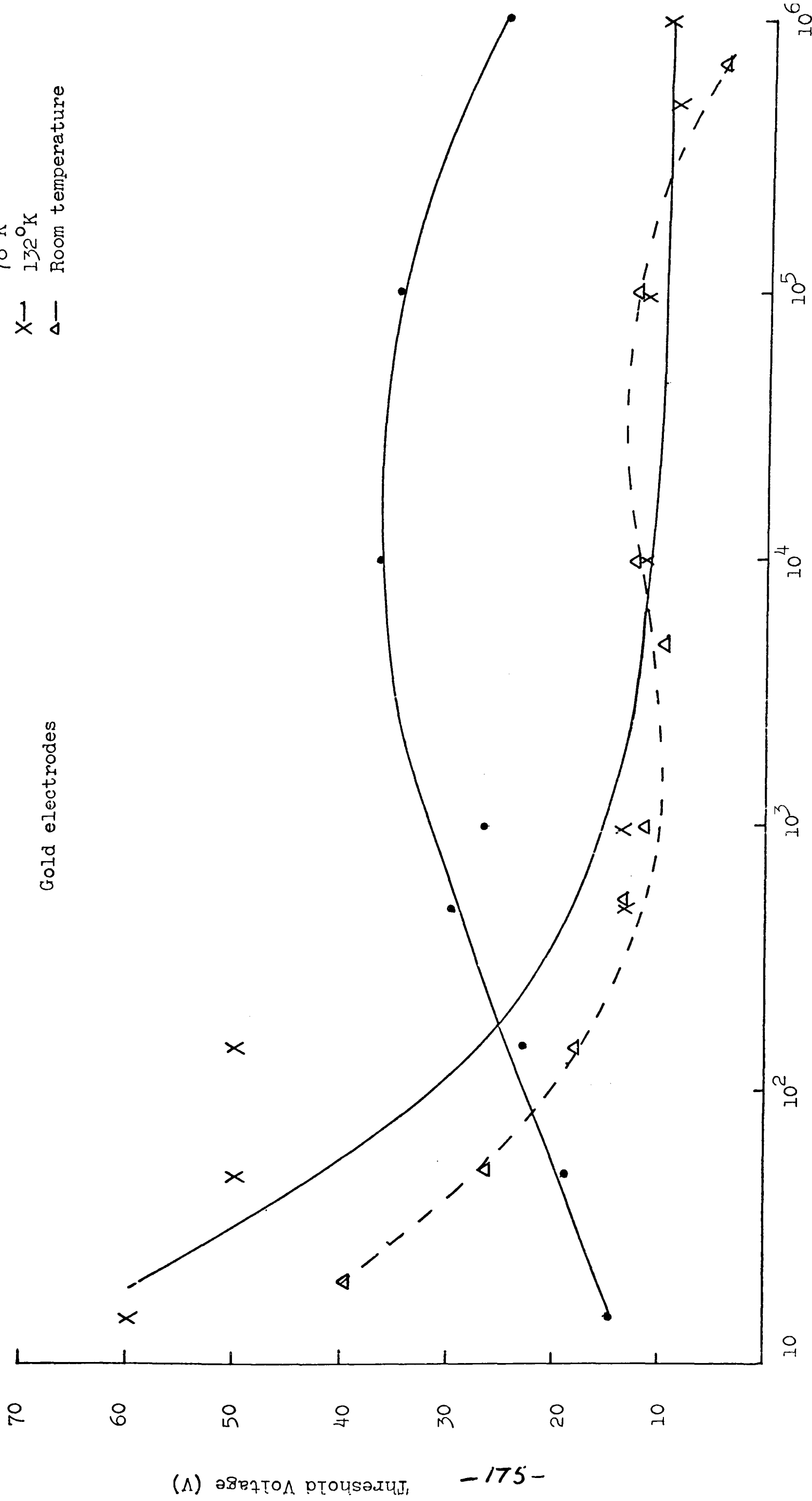
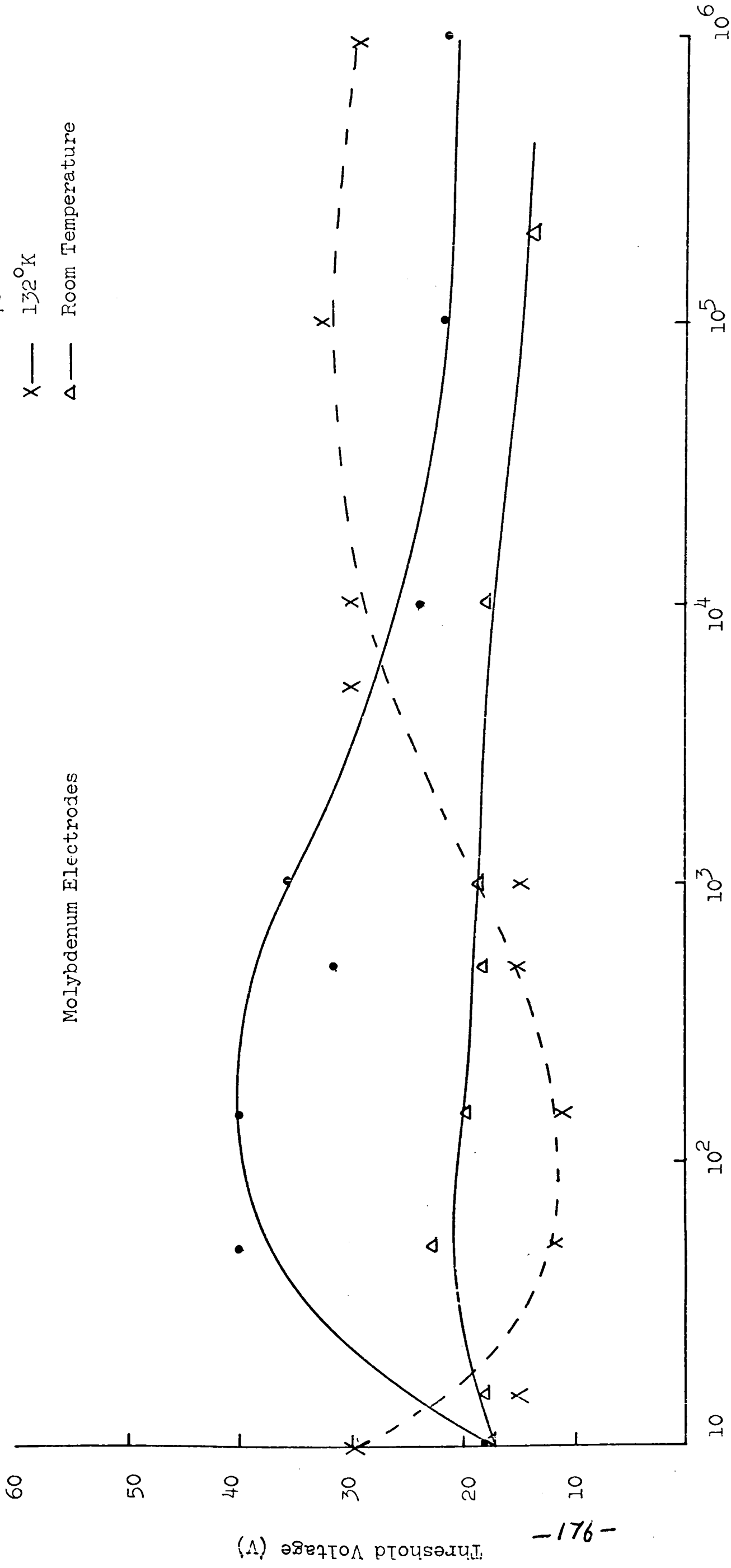


Fig. 4.52 Effect of different ambient temperatures on the threshold voltage with increasing number of operations.

Device Ambient Temperature

- 78°K
- X 132°K
- Δ Room Temperature



Molybdenum Electrodes

Number of Operations

Fig. 4.53

Effect of different ambient temperatures on the threshold voltage with increasing number of operations.

Gold Electrodes

Device ambient temperatures.

• — 78°K

X — 132°K

Δ — Room temperature

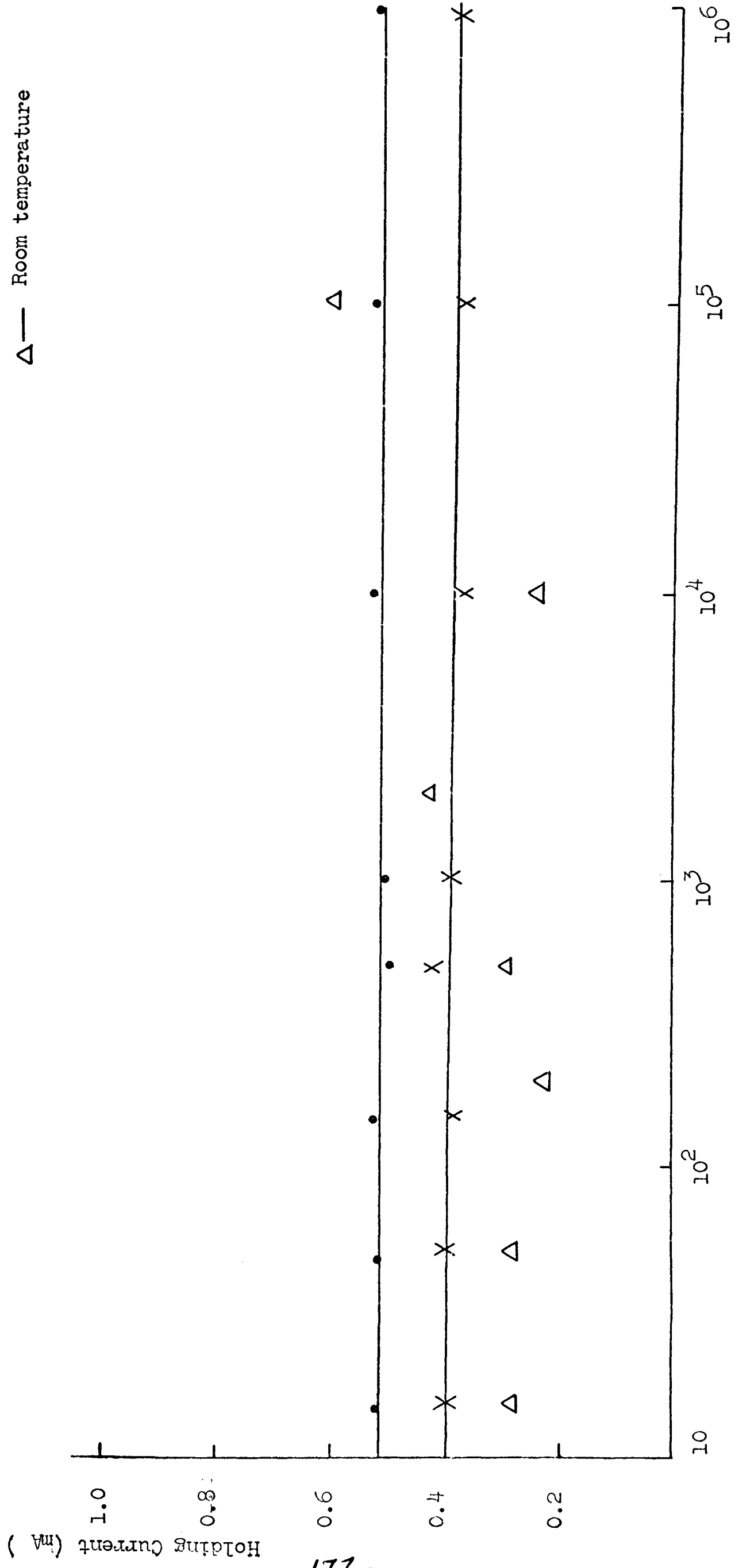
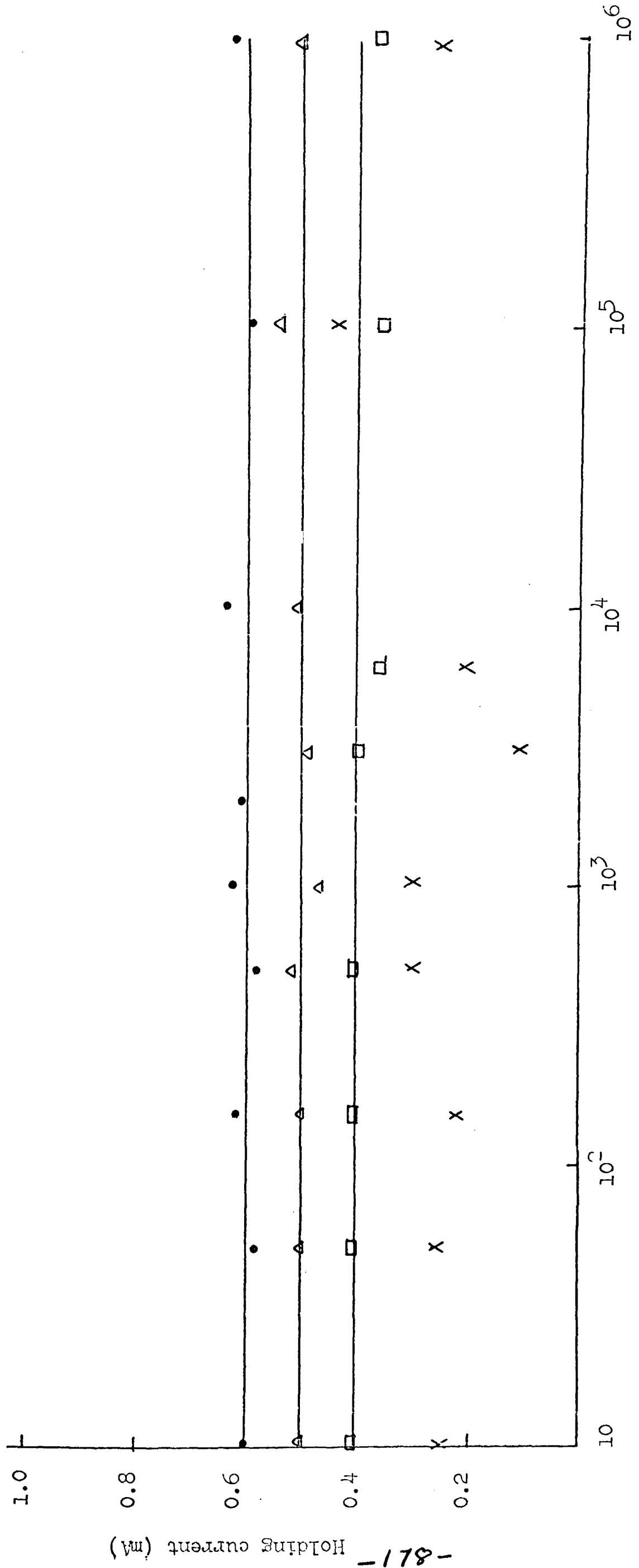


Fig. 4.54 Effect of different ambient temperatures on the holding current with increasing number of operations. Number of Operations

Device ambient temperature

- — 78°K
- △ — 132°K
- — 197°K
- X — Room temperature

Molybdenum electrodes



Number of Operations

Fig. 4.55 Effect of different ambient temperatures on the holding current with increasing number of operations.

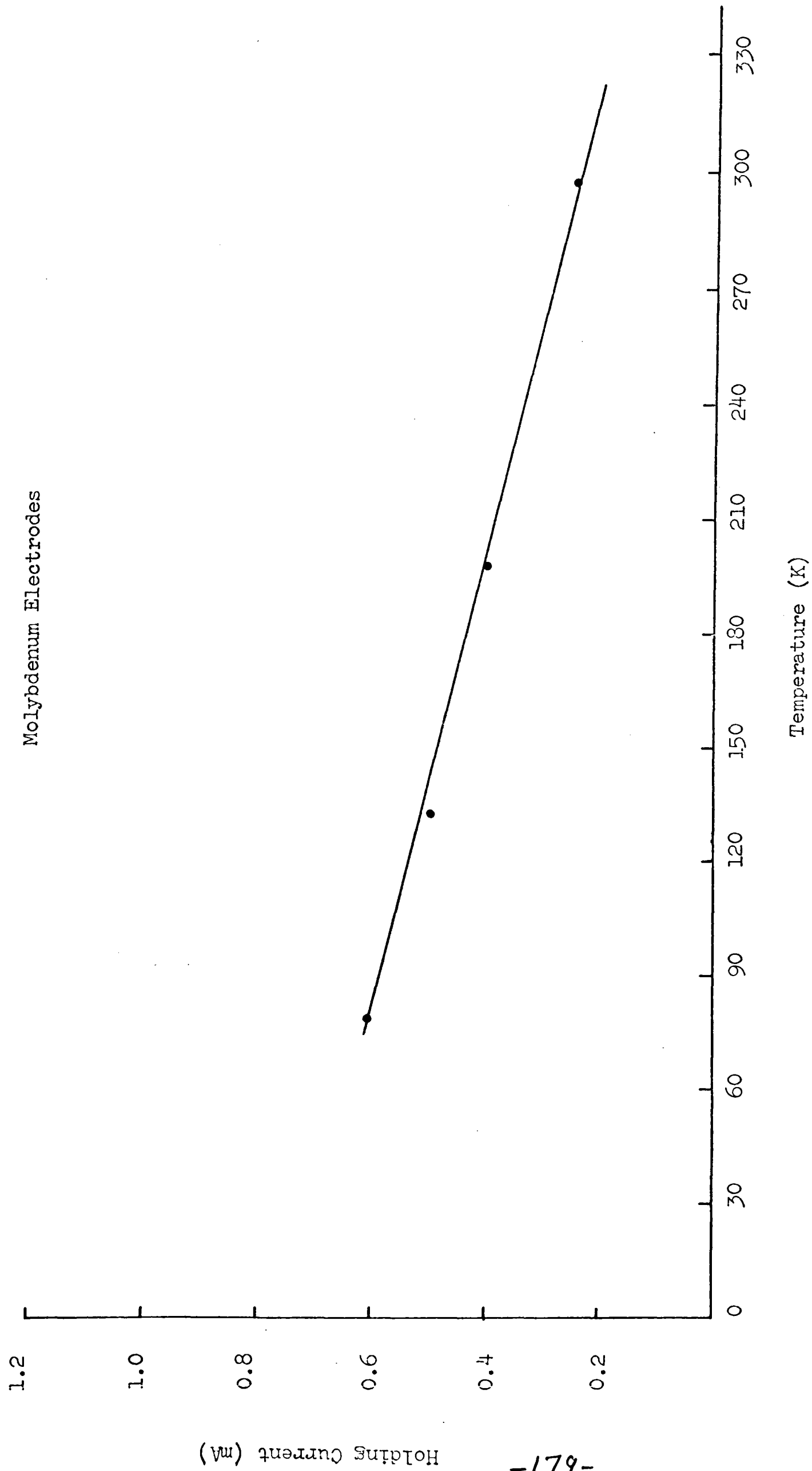


Fig. 4.56 The effect of ambient temperature on the magnitude of the holding current.

Device Ambient Temperature

- — 78°K
- △ — 132°K
- — 197°K
- X — Room temperature

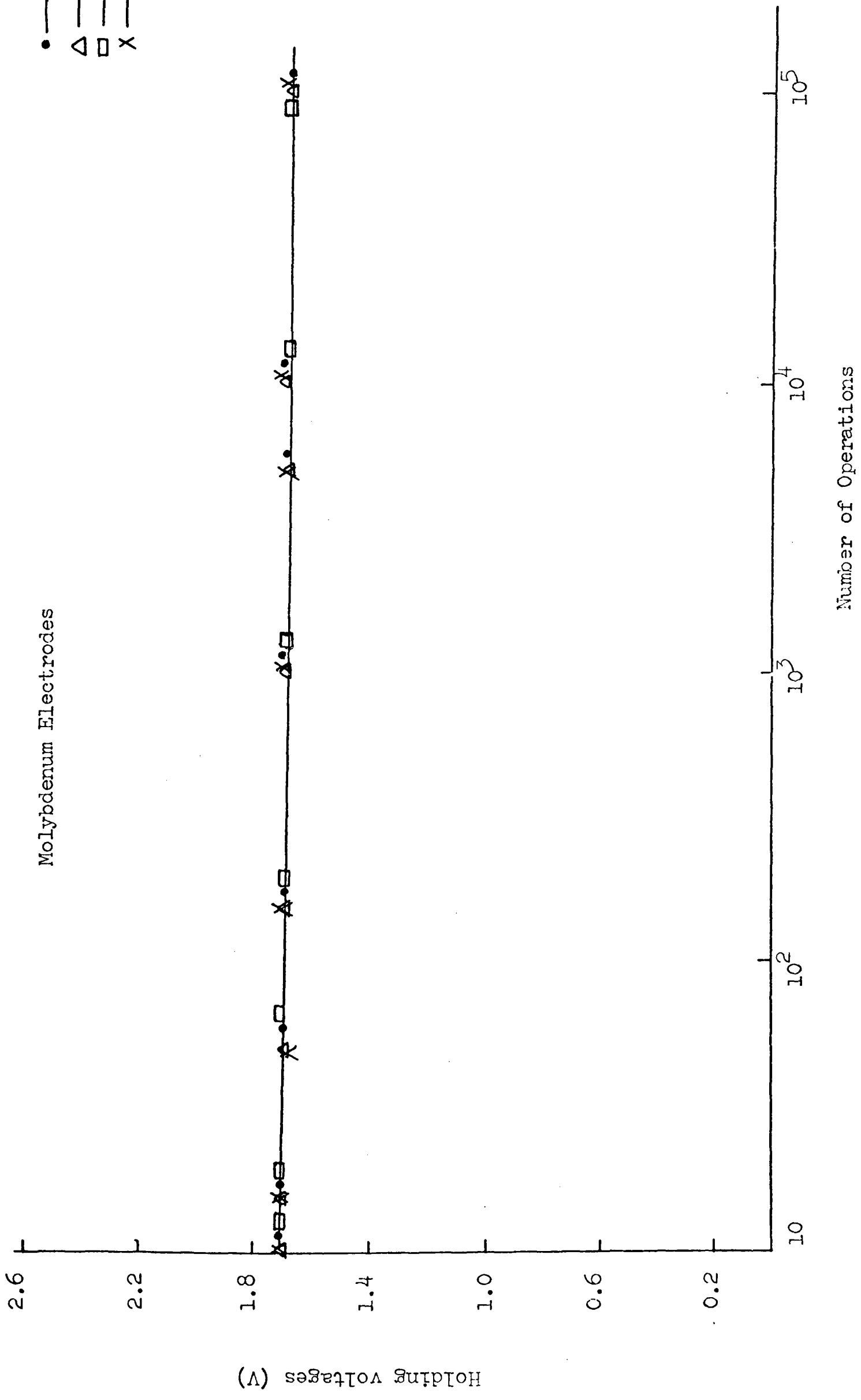
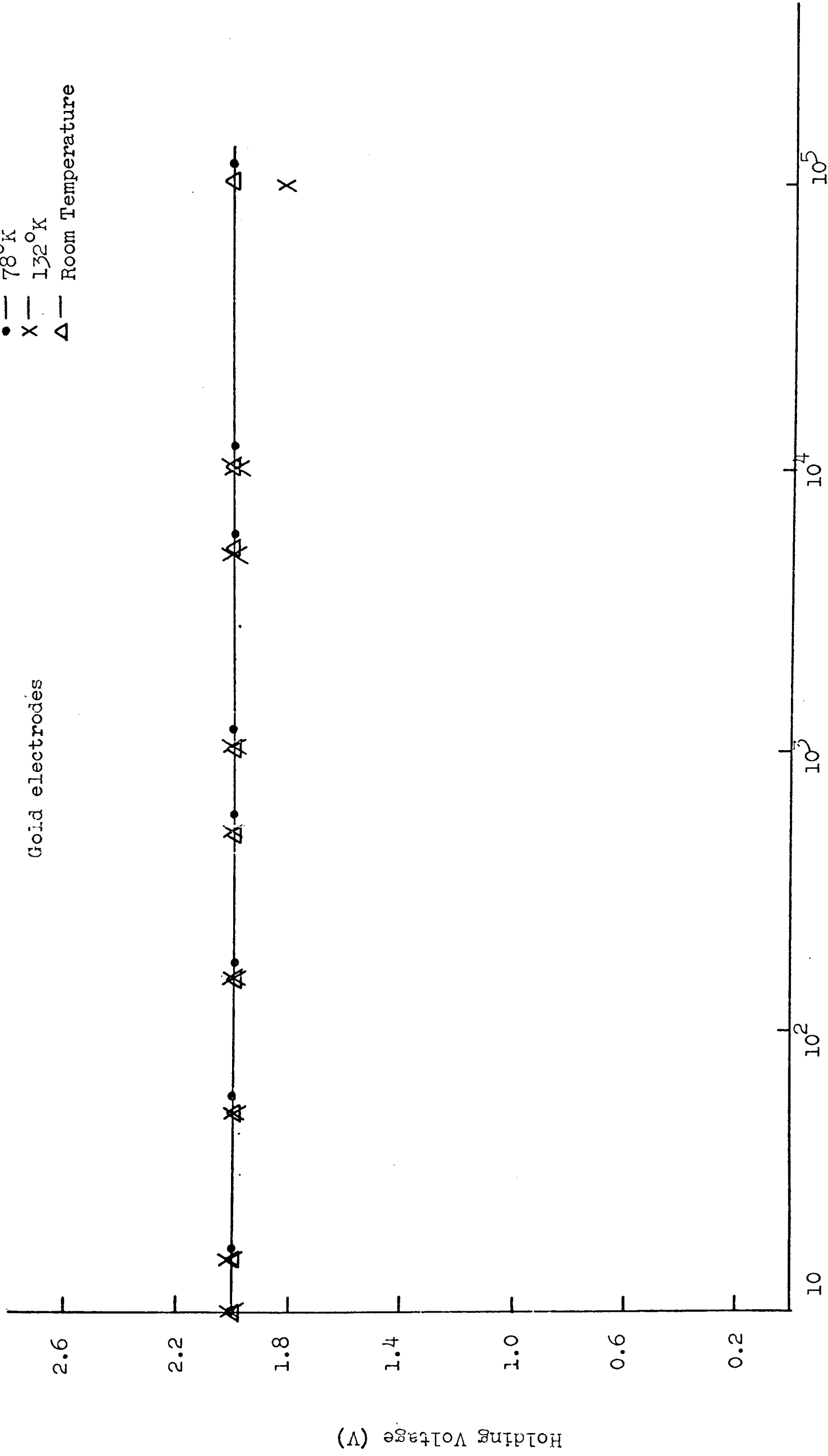


Fig. 4.57 Effect of different ambient temperatures on the holding voltage with increasing number of operations.

Device Ambient Temperature

- — 78°K
- X — 132°K
- Δ — Room Temperature

Gold electrodes



Number of Operations

Fig. 4.58 Effect of different ambient temperatures on the holding voltage with increasing number of operations.

Table 4.1

Top electrode diameter (mm)	No of switching operations		Minimum holding Voltage (V)
	Device Lifetime	Occurrence of branching	
1	2×10^3	500	1.7
3	10^7	5×10^3	1.7
5	10^7	5×10^5	1.7
7	10^6	10^3	1.7
10			1.7
15	Few hundred operations	After several operations	1.7
20			1.7
30			1.7
40	Few operations	After the first-fire operation	1.7
50			1.7

The short lifetimes of devices with large diameter top electrodes are interpreted as due to the large self-capacitances of the devices. The off-state resistances of the devices were also measured both before the devices were switched and then after they were switched and formed. Because of the large differences in the operational lifetimes of the devices, the off-state resistance of any device was measured as soon as the threshold voltage dropped to about 14 V irrespective of the number of switching operations. These results are plotted against the corresponding electrode-contact areas in figures 4.59 - 4.60. The electrode contact areas were calculated using Hertz's ^(Williams, 1967) equation:

$$r = R \left\{ \frac{FR}{2} \left(\frac{1}{E_1} + \frac{1}{E_2} \right) \right\}^{1/3}$$

where r is the radius of the circle of contact area made by the top contact probe with the thin film surface, R is the probe radius, F is the applied force and E_1 and E_2 are Young's moduli for molybdenum and STAG glass. For simplicity this equation is reduced to

$$r = R^{1/3} A$$

where A is a constant, and the contact area is $R^{2/3} B$, where B is another constant. The units of area in figure 4.59 and 4.60 are arbitrary. The off-state resistance of a virgin device decreased as the electrode-contact area increased, figure 4.59, but in formed devices the off-state resistance of a formed device was independent of the electrode contact area as shown in figure 4.60.

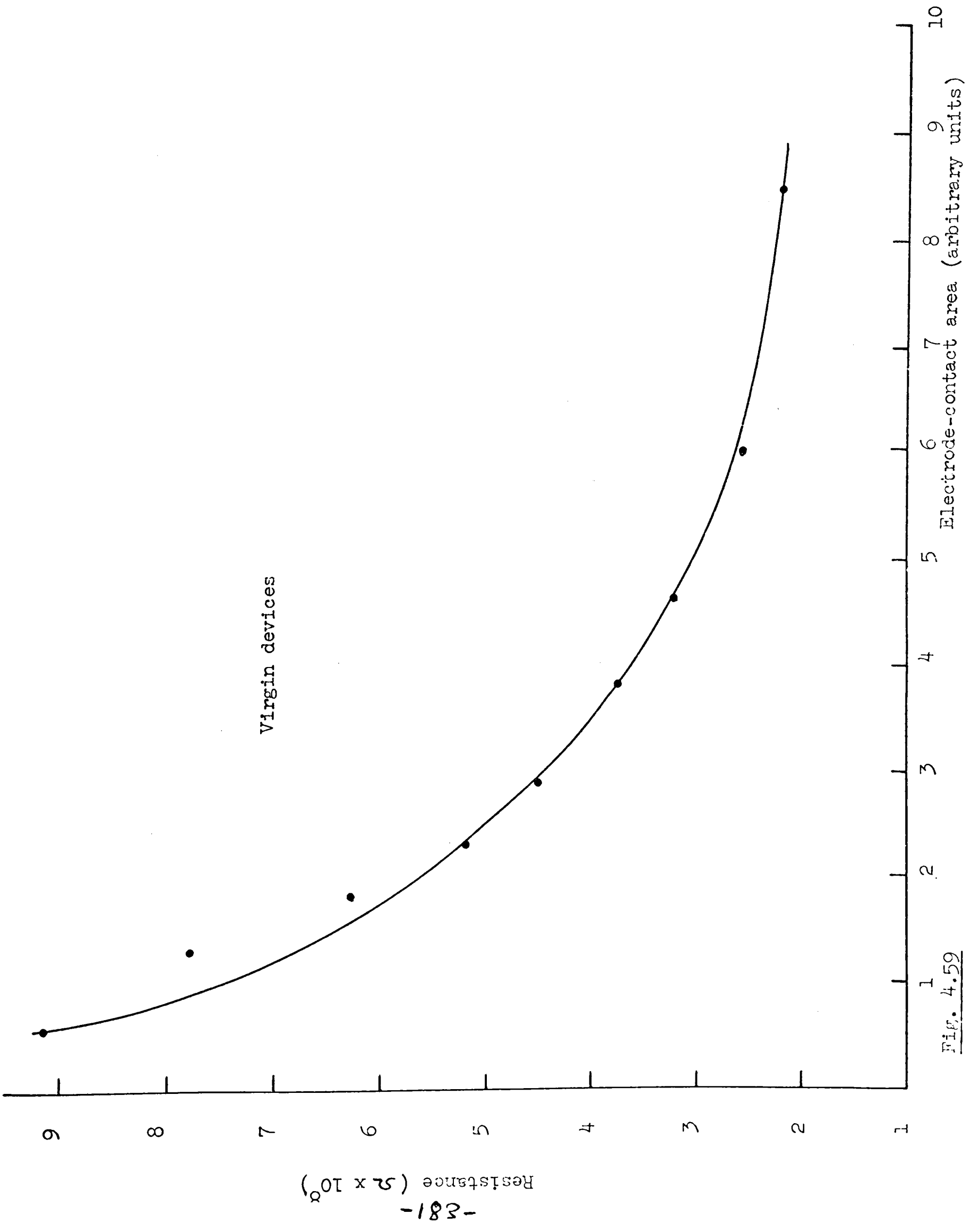


Fig. 4.59

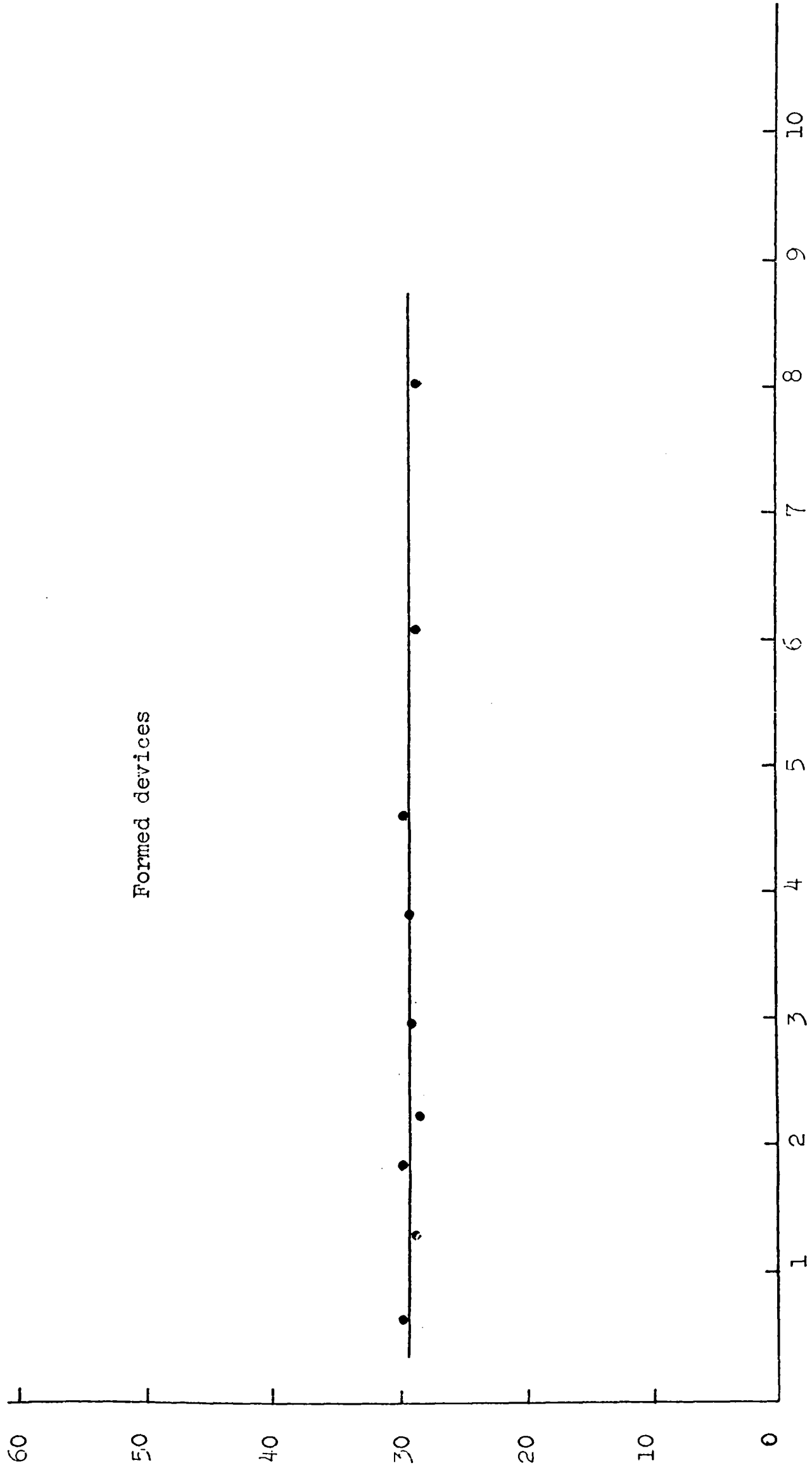


Fig. 4.60 Electrode-contact area (arbitrary units)

Fig. 4.60

4.8. Effect of device external circuit parameters

The results reported in previous sections were obtained with a constant external load resistor of $10\text{ K}\Omega$. Attempts were made to study the effects of varying the magnitudes of (a) the external load resistor, and (b) the device self capacitance on the holding voltage and current. The external load resistor, R_L , was varied by simply using resistors of different values in the range $0.5 - 82\text{ K}\Omega$. The results are shown in figure 4.61 where the holding voltages, i.e. the minimum holding voltage, V_{mh} , and the holding voltage at I_h , are plotted against the load resistor. The holding voltages in both cases increased with increasing value of the load resistor but became independent of the load resistor for values approaching $10\text{ K}\Omega$ and higher. No effect on the holding current could be detected with variation in R_L . Hughes (1974) observed a strong dependence of I_h on R_L .

If the value of the load resistor was such that $V_{th}/R_L < I_h$ the result was the on-state branch of the current-voltage characteristic was set into relaxation oscillations as shown in figure 4.62. This photograph was taken for a load resistor of $100\text{ K}\Omega$. A somewhat surprising result was the extremely short operational lifetime of the device < 200 operations, when operated under such a condition.

The self-capacitance of a point-contact device, with Mo top contacts of 3 mm diameter tip and film thickness of about $1.5\ \mu\text{m}$, was found to be $\sim 2.5\text{ pf}$ when measured with a Wayne-Kerr B601 bridge. To examine the effect of device self-capacitance on the on-state characteristic the external load resistor R_L was kept constant at $10\text{ K}\Omega$ and the device capacitance was varied by connecting external capacitors across the device. The magnitude of these capacitors was in the range of 3.3 pf to 100 pf . Their effects on the holding currents and voltages are listed below in Table 4.2.

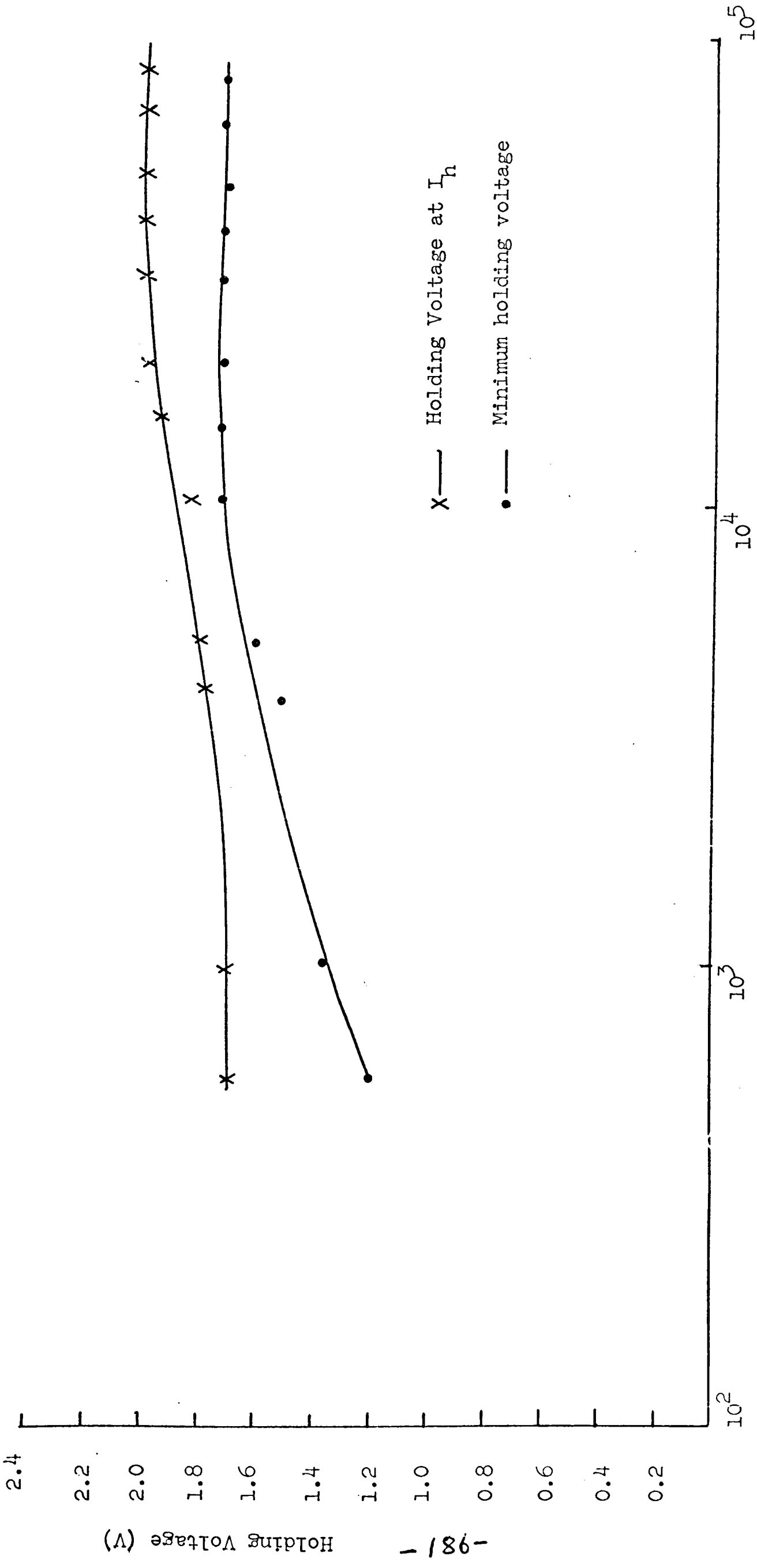
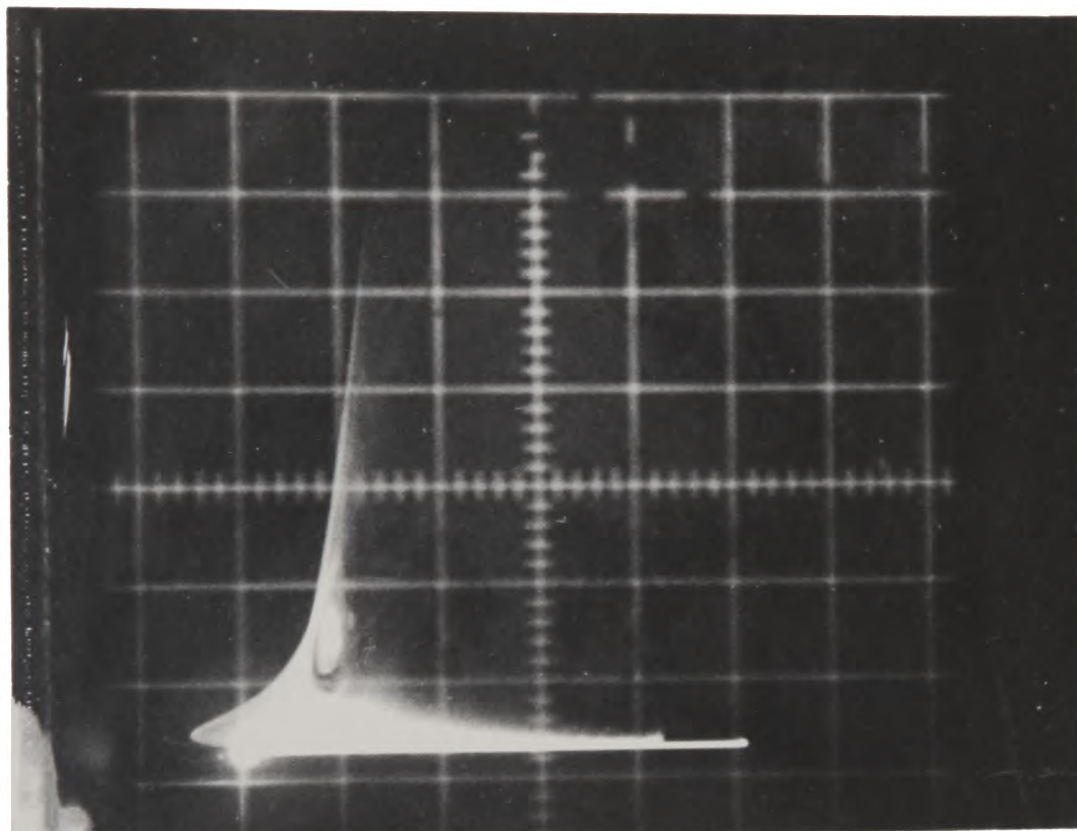


Fig. 4.61 Effect of the external load resistor on the magnitudes of the holding voltages.



2V/div.

Figure 4.62

The I-V characteristics of a device operated with a load resistor R_L such that $V_{th}/R_L \ll I_h$.

Table 4.2

External Capacitor (pf)	Holding Current (mA)	Minimum Holding Voltage (V)	Holding Voltage at I_h (V)
33	0.39	1.7	1.8
5	0.5	1.7	1.9
10	0.5	1.7	1.95
20	5.1	1.7	2.1
50	5.1	1.7	2.2
100	4.0	1.7	2.0

Because of the large fluctuations in holding currents, the measurements were restricted to first-fire switching operations, i.e. a fresh virgin device was used every time a larger capacitor was employed. This was also necessary because the operational lifetimes of the devices, with the larger external capacitors connected across them, were very short. The minimum holding voltage was unaffected by the device capacitance and it remained constant, 1.7V, regardless of the magnitude of the device capacitance. However, the holding voltage at I_h showed an increase but no systematic relationship between this increase and the increase in device capacitance could be established.

Finally, it was found that with large device capacitances, > 10 pf, forming was always achieved after one switching operation only.

4.9. Effect of Pulse Width and Repetition Rate

All the results reported so far were obtained with pulses of 1.3 ms width. In order to carry out a systematic investigation of the effect of pulse width and repetition rate on device lifetime and the occurrence of multiple branching in the on-state, three pulses, 1.3 ms, 0.3 ms and 0.1 ms were used to switch the devices. All these pulses were ramp pulses and had a height of 80 V and the load resistor was kept constant at $10\text{ K}\Omega$. For each pulse width, the devices were operated at three different repetition rates, 1 pulse/sec, 10 pulse/sec and 100 pulse/sec. Point-contact devices were used and all fabricated on the same substrate, with Cr film as a bottom electrode and Mo probe as top contact. The results are tabulated overleaf in Table 4.3.

Table 4.3

Pulse width (ms)	Pulse rate (pulse/sec)	Number of switching operations	
		Occurrence of multiple branching	lifetime
1.3	1	5×10^4	10^7
	10	2.5×10^4	10^7
	100	1×10^4	10^7
0.3	1	1×10^5	1×10^6
	10	1.5×10^5	1.5×10^5
	100	1.2×10^4	2×10^5
0.1	1	1×10^5	1×10^5
	10	1×10^5	1×10^5
	100	8×10^4	8×10^5

It can be seen that for the largest width pulses the operational lifetimes of the devices were longest and unaffected by the pulse repetition rates. The occurrence of branching was affected by the pulse repetition rate and multiple branching occurred earlier when the highest repetition rate, 100 pulse/sec was used. The operational lifetimes for the other pulse widths, 0.3 ms and 0.1 ms, were similar and shorter than those for 1.3 ms pulses.

There was a small difference in number of operations between the occurrence of multiple branching and the operational lifetime. In some devices, the difference was only a few switching operations.

4.10. Effect of pulse polarity

All the results reported in previous sections were obtained with positive pulses. Polarity effects on device characteristics, particularly the on-state characteristics, were investigated by first switching the device with a positive pulse and then, five seconds after switch off, applying a negative pulse of the same pulse width. This investigation was carried out at room temperature and on point-contact devices. Several electrode materials were used and no polarity effects on threshold voltage, holding voltage and device lifetime were observed in devices with symmetric electrodes, i.e. same material used for top and bottom electrodes. The absence of polarity effects at room temperature in devices with symmetric electrodes is well known (Balberg, 1970) but because of the asymmetric geometry of a point-contact device

it was necessary to ensure that this geometrical asymmetry did not make any significant contribution to polarity effects. In general, for devices with either symmetric or asymmetric electrodes the threshold voltage was not seriously affected by reversal of pulse polarity but fluctuations in its magnitude were observed. The operational lifetime was also unaffected by pulse polarity, except in devices with Te-Cr electrodes and these results will be described later.

Polarity effects in the on-state, however, were observed in devices with asymmetric electrodes. These effects were rather weak compared to those observed by Hensich et al (1972) who used semi-conducting electrodes. The electrode materials used were Cr, Mo, Te and Au and in the combinations given below. The first electrode material in each case represents the top contact of the point-contact device. The pulse polarity refers to that applied to the top contact.

(i) Mo-Mo electrodes

As mentioned earlier, no polarity effects were observed for threshold voltage and device lifetime. The effect of reversal of pulse polarity on multiple branching in the on-state will be mentioned at the end of this section.

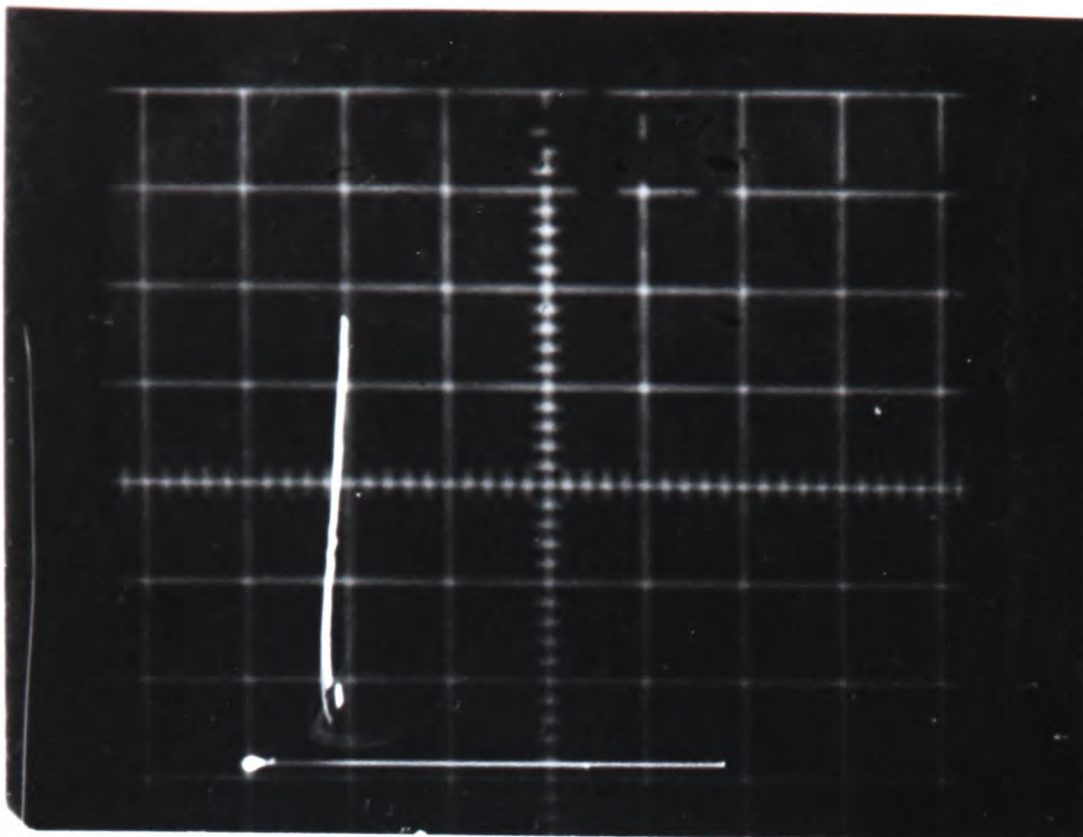
(ii) Au-Cr electrodes

The current-voltage characteristics for this device when actuated first by a positive pulse and then by a negative pulse are shown in figures 4.63 and 4.64 respectively. For a positive pulse the minimum holding voltage, V_{mh} , was 1.55 V and 1.3 V for the negative pulse. In addition, the slope of the on-state trace was slightly steeper for the negative pulse input. No effect on the holding current was detected.

(iii) Mo-Cr electrodes

The minimum holding voltage was 1.7 V for a positive pulse, figure 4.65, and 1.5 V for a negative pulse, figure 4.66. The negative resistance region at the lower end of the on-state trace was larger with a positive pulse input. The holding current was greater for the negative pulse, 0.7 mA compared to 0.4 mA for a positive pulse.

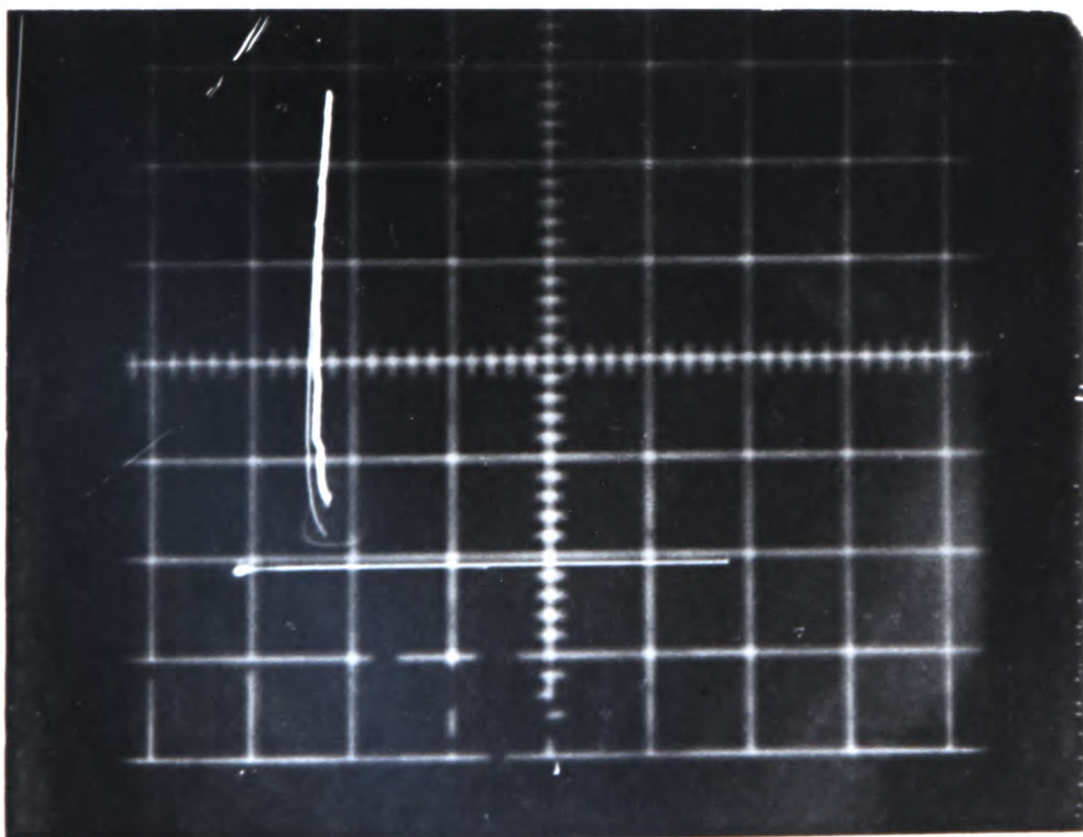
1.2 mA/div



2 V/div.

Fig. 4.63. Au-Cr electrodes

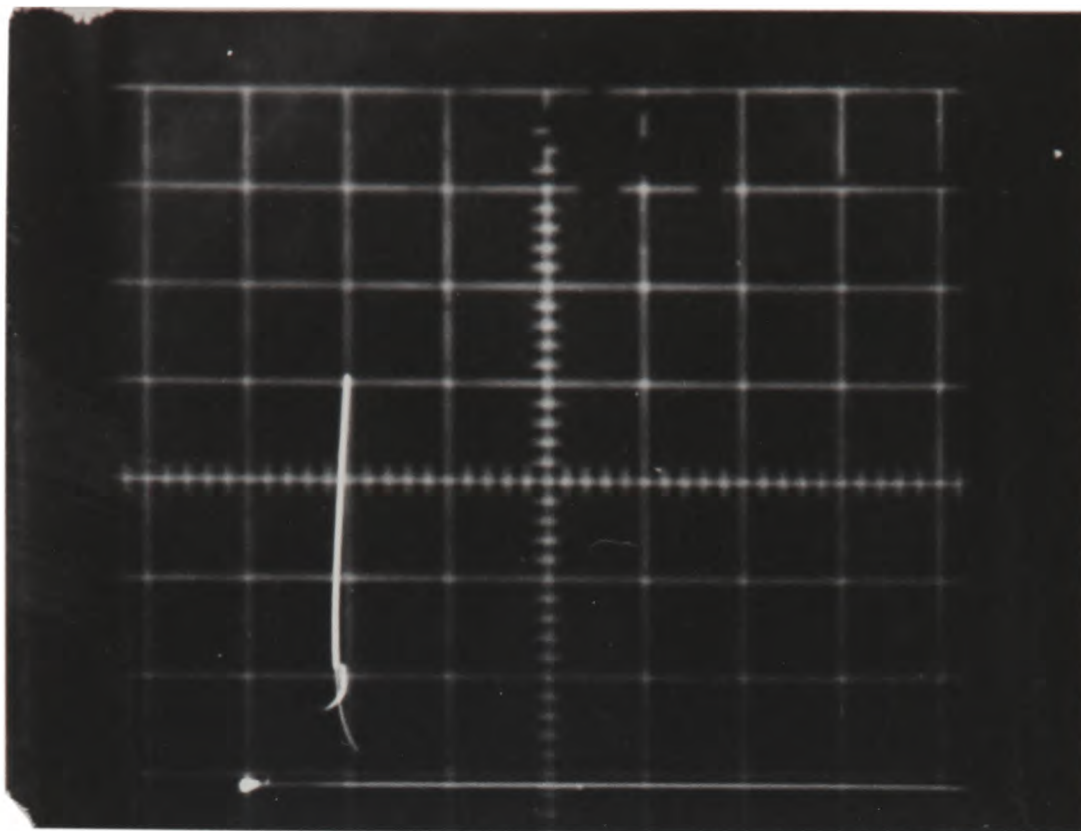
1.2 mA/div.



2 V/div.

Figure. 4.64. Au-Cr electrodes

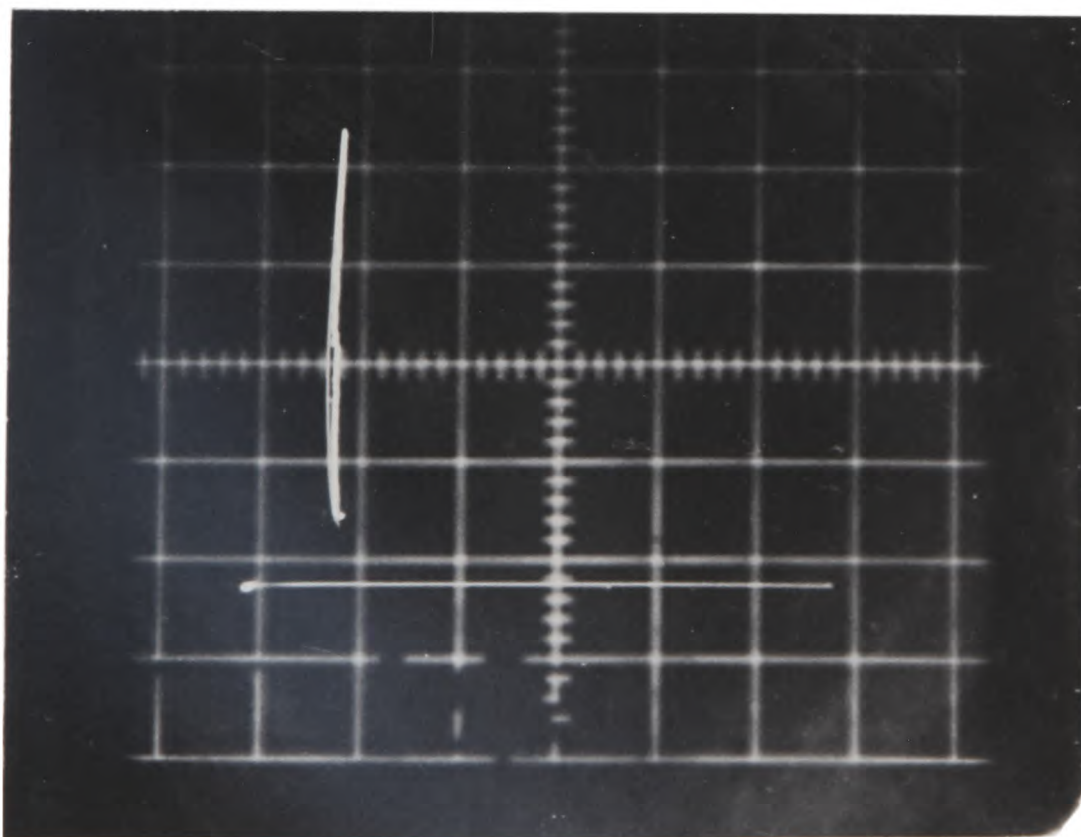
1.2 mA/div.



2V/div

Fig. 4.65. Mo-Cr electrodes

1.2 mA/div



2V/div.

Fig. 4.66. Mo-Cr electrodes.

(iv) Te-Cr electrodes

A Te rod, supplied by Hopkins and Williams Ltd., with a polished hemispherical tip of 3 mm diameter was used as top contact. The minimum holding voltage had the same magnitude, 0.85 V, regardless of pulse polarity. This can be seen from figure 4.67 which shows the current-voltage characteristics for a positive pulse and figure 4.68 which shows the characteristic for a negative pulse. The operational lifetime of the device was seriously affected by the reversal of the pulse polarity. With a positive pulse the lifetime was about 10^6 operations and multiple branching in the on-state appeared after about 10^4 operations. On the other hand with a negative pulse the lifetime was only a few operations, but if the positive pulse was reapplied the device recovered and operated well. This experiment was repeated with Cr as the top contact and a polished Te disc, sliced from a Specpure grade Te ingot, was used as the substrate on which a thin film of STAG glass was deposited. The minimum holding voltage was slightly higher, 1.1 V, in this arrangement and independent of pulse polarity, but the effect associated with the lifetime was not observed and the device operated reasonably well irrespective of the pulse polarity.

(v) Te-Te electrodes

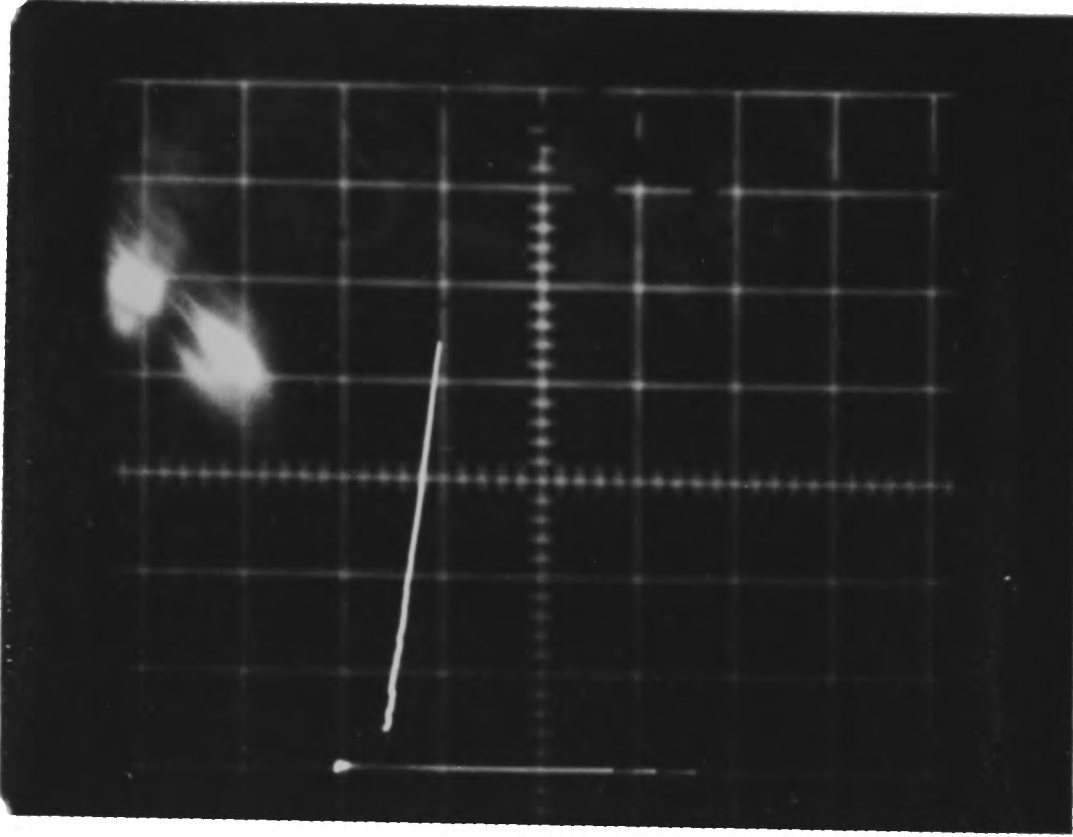
These devices had an operational lifetime of about 10^3 operations, a minimum holding voltage of about 0.9 V and these properties were independent of pulse polarity. Multiple branching in the on-state appeared after a few switching operations only.

(vi) Mo-Te electrodes

This device operated well and had an operational lifetime of 10^6 operations regardless of the applied pulse polarity. The minimum holding voltage was 1.5 V when the pulse polarity was positive and 1.1 V for a negative pulse.

Finally, the effect of pulse polarity on the form of multiple branching in the on-state will be described. Reversal of pulse polarity had no effect on the occurrence of branching but it had an effect on the form of the multiply-branched pattern. The pattern usually changed

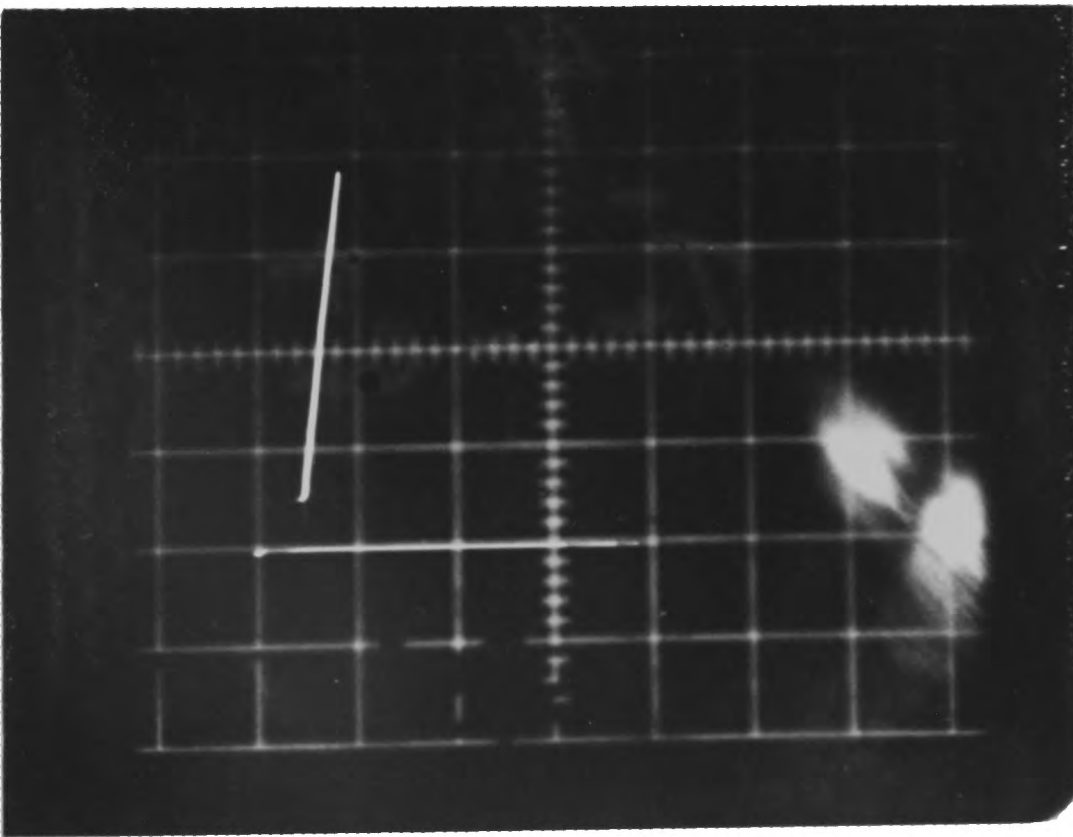
1.2mA/div.



2V/div.

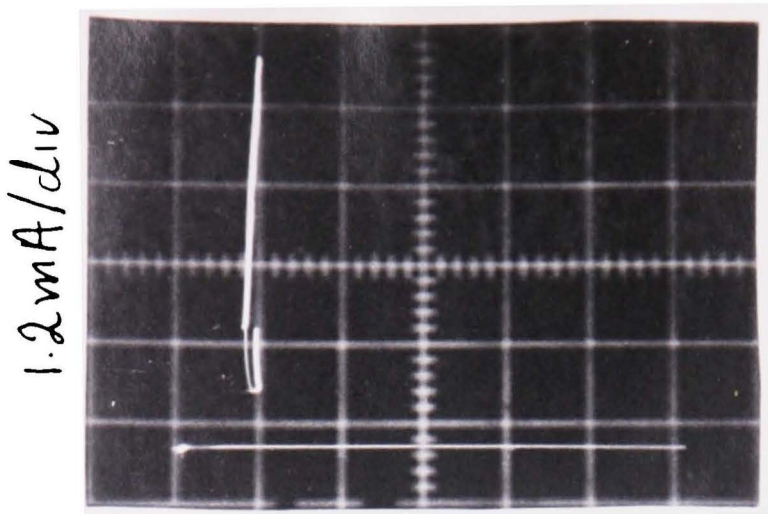
Fig 4.67. Te-Cr electrodes

1.2mA/div.



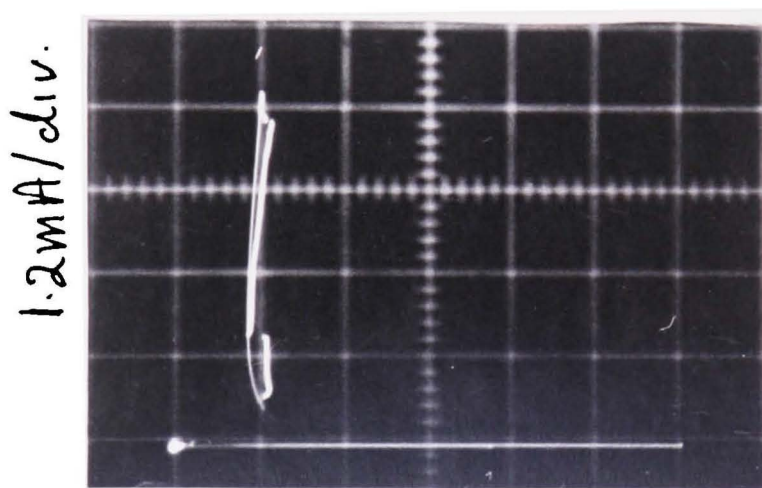
2V/div.

Fig. 4.68 Te-Cr electrodes.



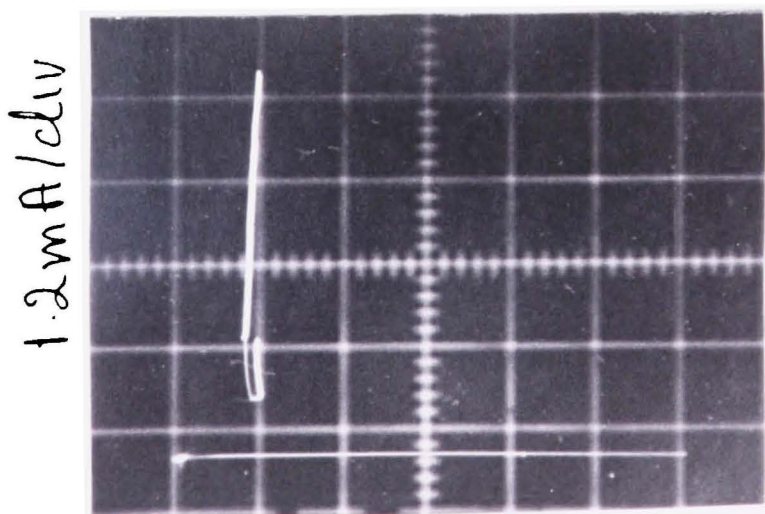
2V/div.

Fig. 4.69 Mo-Cr electrodes.



2V/div.

Fig 4.70. Mo-Cr electrodes



2V/div

Fig 4.71 Mo-Cr electrodes

on reversal of pulse polarity as can be seen from figures 4.69 - 4.71. In figure 4.69 a negative pulse was applied to the Mo electrode giving the pattern shown in figure 4.69. When the pulse polarity was reversed to positive, the pattern was as shown in figure 4.70. On reapplying a negative pulse the original pattern was recovered as shown in figure 4.71. The recovery of the original pattern was only possible if the number of switching operations with the pulse of opposite polarity was restricted to a few operations. However, if the number of operations was relatively large, say 500 operations, the original pattern was destroyed and could not be recovered on reapplying a pulse of the original polarity. This effect was observed in all devices regardless of the electrode material used.

4.11. Characteristics of devices fabricated from $\text{Si}_{12}\text{Ge}_{10}\text{As}_{30}\text{Te}_{40}\text{Tl}_8$ glass

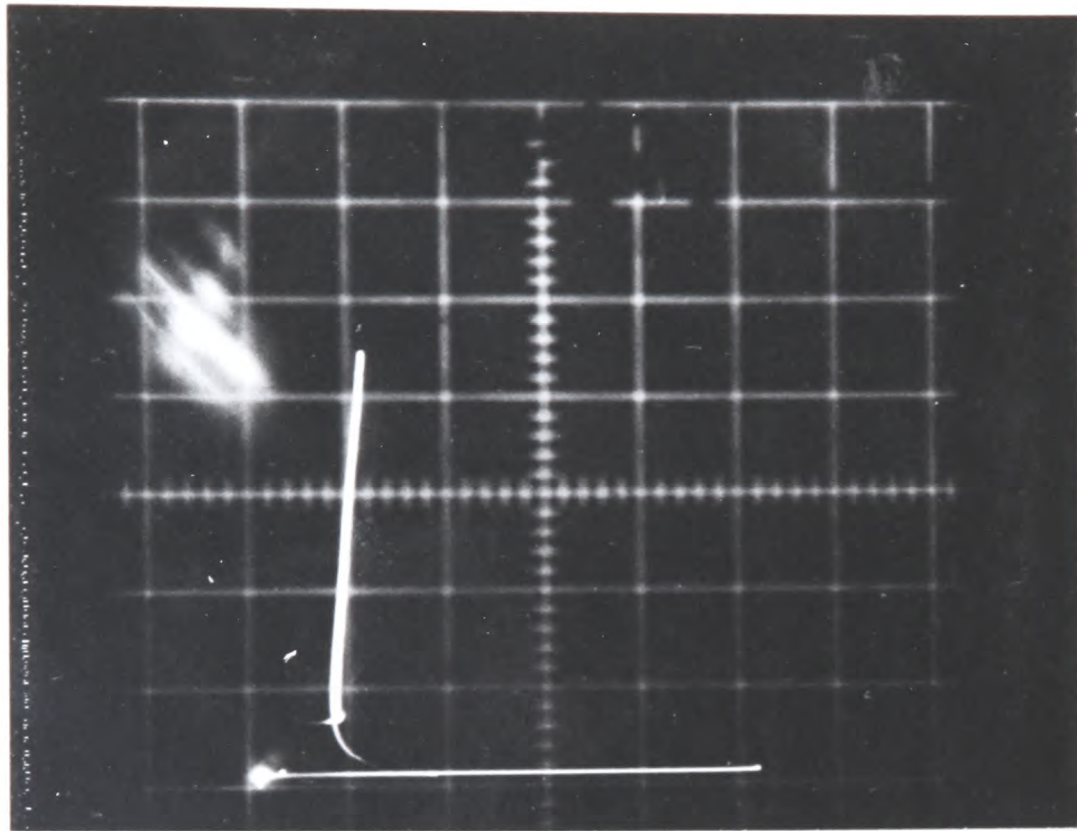
The effect of adding thallium to amorphous semiconductors is generally to lower the viscosity (Pearson, 1964) of the material melt. $\text{Si}_{12}\text{Ge}_{10}\text{As}_{30}\text{Te}_{40}\text{Tl}_8$ glass was mechanically much harder than STAG glass and more difficult to grind. Shanefield (1970a, 1970b) has reported that the addition of thallium to telluride glass switching devices increases the off-state resistance of the device but contributes to the device conductance in the on-state.

Figure 4.72 shows the current-voltage characteristics of a thin film device made from $\text{Si}_{12}\text{Ge}_{10}\text{As}_{30}\text{Te}_{40}\text{Tl}_8$ glass and with Cr thin film bottom electrode and Mo probe as top contact. It can be seen that the characteristics are similar to those of devices fabricated from STAG glass. Forming and multiple branching in the on-state were also exhibited by these devices. Multiple branching in the on-state, however, did not occur until after 10^6 switching operations. The operational lifetime of these devices was about 5×10^7 switching operations.

4.12. Analysis of chemical composition of the thin films

The analysis was carried out at Fulmer Research Institute on two flash evaporated films. The preparation of these films was made in separate evaporations and each film had a thickness of 2 μm . The analysis results ($\pm 10\%$) are as follows:

1.2 mA/div.



2V/div.

Figure 4.72

The I-V characteristics of a thin film device from $\text{Si}_{12}\text{Ge}_{10}\text{As}_{30}\text{Te}_{40}\text{Tl}_8$ glass with Cr thin film bottom electrode and Mo probe as top contact.

% Wt	As	Si	Te	Ge
Sample 1	23.5	3.5	65.5	7.5
Sample 2	26.5	3.5	62.7	7.3
thus % atom	As	Si	Te	Ge
Sample 1	16.4	0.9	77.7	5.1
Sample 2	18.7	0.9	75.7	5.0

It can be appreciated that the chemical composition of the two films prepared in two separate evaporations are almost identical. The composition of the r.f. sputtered films was $\text{Si}_8\text{Te}_{39}\text{As}_{40}\text{Ge}_{13}$ (private communication with Dr. A. J. Hughes of RRE). The higher Si content could explain the higher off-state resistance of the r.f. sputtered films as compared with that of the flash evaporated films (Robertson et al, 1972). Apart from this higher resistance, and also higher first-fire threshold voltage, there was no difference in the characteristics of devices fabricated from r.f. sputtered films and those of devices fabricated from flash evaporated films.

CHAPTER FIVE

Discussion

The results obtained in this project can be split into three major groups so that each group provides certain information about one particular aspect of switching in thin film chalcogenide devices. These groups are:

1. results which indicate that structural changes in the device material have occurred after switching of virgin devices; it has been shown that the electrical properties of formed devices are different from those of virgin devices,
2. results which give evidence of the nature of the on-state in terms of measured quantities which also have been investigated elsewhere; these include the effects of different electrode materials on device life-times and minimum holding voltages,
3. observations which describe a previously unreported on-state phenomenon called "multiple branching". (Williams and Irfan, 1974).

This chapter discusses each group of results in turn.

5.1. Structural changes in switching devices

Although no direct study - such as the use of electron microscopy - was made to investigate structural changes in the chalcogenide switching devices, comparisons of electrical measurements made first on virgin devices and then on the same devices after forming indicated beyond doubt that structural changes had taken place in formed devices. The nature of the changes is similar to those described by Bosnell et al (1972a, 1973).

(a) Off-state resistance and forming

Measurement of the off-state resistance of a chalcogenide switching device as a function of number of operations can provide useful information about possible structural changes and their distribution within the device material. The off-state resistance of a virgin device can be ten times greater than that of a formed device e.g. see figures 4.18 - 4.28. Similar observations have been recently reported by Ormondroyd et al (1974). This drop in resistance can be accounted for by structural changes in the material

and these are believed to occur in two stages (a) a rapid structural change which takes place during the forming process and this takes the form of material phase separation within the current filament region, and (b) a slower process which takes the form of formation and growth of tellurium crystallites in the filament. Both stages of structural change could be strongly dependent on the composition of the alloy and its tendency to phase separate as a result of the heat dissipated in the device during a switching cycle. It is possible that the applied electric field can also play a certain part in the phase separation and crystallisation processes. The influence of electric field on crystal growth in STAG glass has not yet been investigated but it is worth remembering that in differential thermal analysis experiments no crystallisation peaks are observed, but electron-microscopy examination of formed devices does reveal the presence of tellurium crystallites. Moreover, the field-enhancement of crystal growth in oxide glasses has been demonstrated by de Vekey and Majumdar (1970) as mentioned in Chapter Two. Roy et al (1969) have shown that the structure of several chalcogenide bulk glasses is diaphasic and the two phases can both be amorphous. In some cases crystalline inclusions are present. This may not be true of the evaporated or sputtered chalcogenide virgin thin films because their method of preparation leads to a thermal history very different from that of bulk glasses. But such phase separation and partial crystallization has been found to accompany switching cycles in these devices. This explains why forming is not observed in thick devices fabricated from bulk samples. Therefore, it is possible that forming is essentially a process which alters the thermal history of the thin film material and changes the structure of certain regions of the device material so that its structure becomes similar to that of bulk glass. This is the result of heating of the device material, or a certain region of the material, say a filament between the electrodes, taking place during switching, and particularly while the device is in the on-state (Male, 1974). After switch-off the cooling or quench rate is likely to be more comparable to the quench rate of bulk glasses rather than of

evaporated thin films especially in the central part of the filament surrounded by cooler glass which is a poor thermal conductor. Annealing studies on thin films show phase separation and sometimes crystallisation (Thomas et al, 1972) are caused by heat treatment and it was suggested that the first-fire process has similar effects to annealing.

The threshold voltage was found to decrease as the device off-state resistance decreased e.g. see figure 4.20. A log-log plot of threshold voltage versus off-state resistance is shown in figure 5.1. from data given in figure 4.24. The points in this plot are obtained from the curves in figure 4.24 and not all of them represent experimentally obtained measurements. It would seem that the threshold voltage dependence on the off-state resistance falls into two regions. The first region may be described by the relationship:

$$V_{th} \propto R_{off}^{1.6}$$

where R_{off} is the off-state resistance, and the second region given by:

$$V_{th} \propto R_{off}^{0.5}$$

Over a wide range of temperatures, the glass conductivity versus reciprocal-temperature plot has a single slope (Ormondroyd et al, 1974) which implies that the conductivity of the glass satisfies the expression:

$$\sigma = \sigma_0 \exp(-E/kT).$$

The conductance of a device is therefore:

$$G \propto \exp(-E/kT)$$

and the resistance is:

$$R \propto \exp(E/kT) \tag{5.1}$$

In the thermal theory of switching (O'Dwyer, 1964) the threshold voltage V_{th} fits the relation:

$$V_{th} \propto \exp(E/2kT) \tag{5.2}$$

where E is the conductivity activation energy.

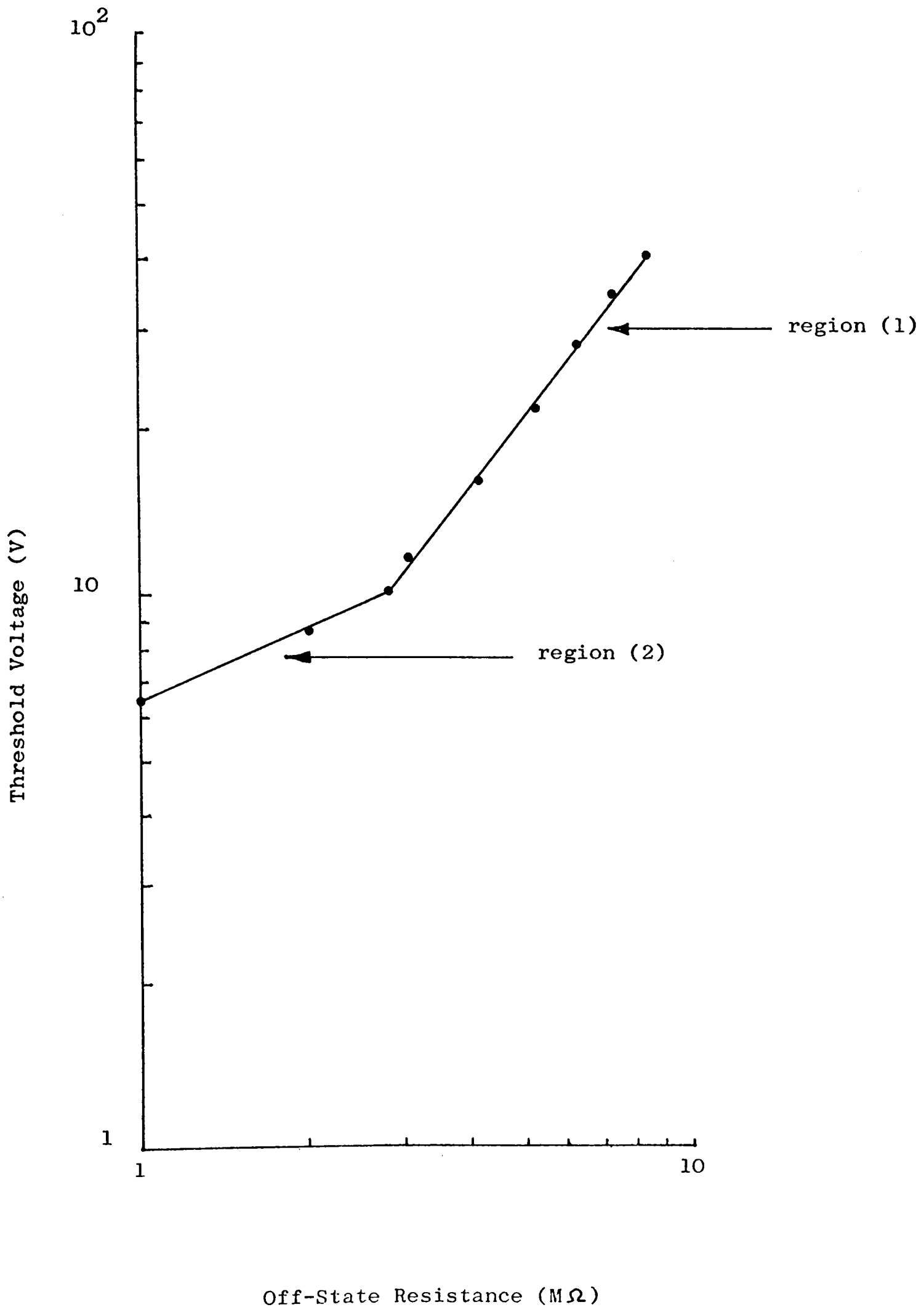


Figure 5.1

Threshold voltage vs. off-state resistance of a point-contact device.

Let $V_{th} \propto \exp(E'/kT)$

5.3

From region 1 in figure 5.1. we have

$$V_{th} \propto R_{off}^{1.6}$$

comparing this with (5.3) we obtain

$$E' = 1.6E$$

Similarly, from region 2 in figure 5.1

$$V_{th} \propto R_{off}^{0.5}$$

and $E' = 0.5E$.

Therefore, the behaviour of region 1 is not in agreement with the predictions of the thermal theory of switching, whereas region 2 - which represents the well-formed condition of the device - is in very good agreement with the theory and suggests that the switching mechanism could be thermal.

It is suggested that the first region represents the fast structural changes during the forming process. During this process the electronic and thermal properties of the material are changing continuously. For the particular device on which the results were taken, this region terminates after about the first fifty operations. The second region represents the growth of the tellurium crystallites embedded in the filament and this has the effect of reducing the effective thickness of the active material between the electrodes. Nesvadba (1973) has related fluctuations in the threshold voltage to the volume fraction of Te crystallites and postulated that

$$\Delta V_{th} \propto \Delta X$$

where ΔX is the volume fraction of the crystallites.

It was shown in Chapter Four that there is some difference between the dependence of threshold voltage on film thickness for virgin and well-formed devices. This, in addition to the relation between V_{th} and resistance, suggests that the breakdown mechanism in virgin devices could be different from that in wellformed devices.

It is not claimed that figure 5.1 represents the behaviour

of all switching devices. The device in figure 5.1 did not have a very stable formed threshold voltage or off-state resistance, i.e. after forming the threshold voltage remained relatively stable for only 10^3 operations and then dropped rapidly for larger numbers of operations. In more stable devices, such as those with Mo or W electrodes, the formed threshold voltage and off-state resistance can remain stable for 10^6 operations. In such cases, region 1 should terminate as soon as the threshold voltage becomes stable, for it would be meaningless to plot V_{th} vs. R_{off} when both quantities remain unchanged. Region 2, on the other hand, starts when the threshold voltage, and off-state resistance, starts to decay. It is found that there are great variations in the slopes of region 1 for different devices, in some devices the slope is ~ 8 , and this suggests that phase separation could be influenced by the type of electrode material used and its ability to conduct heat away. The effects of electrode materials on device behaviour are discussed in the next section. The slopes of region 2 for different devices, however, are 0.5 or very close to this value. The exact power dependence of the threshold voltage on the off-state resistance, particularly for region 1, has to be determined experimentally for each device.

Phase separation is also exhibited by some oxide glasses (Drake et al, 1972) and some workers consider phase separation to be a universal property of all switching devices. Milne and Anderson (1973), however, have reported that switching in gallium telluride single crystals was not accompanied by forming and stoichiometric changes could not be detected in the filamentary region of the switch. Moreover, "forming" in zinc sulphide crystals (Hargreaves et al, 1974) was found to be confined to the electrode regions of the device and did not extend completely through the crystal.

(b) Evidence of structural change from uniaxial pressure experiments

The effect of hydrostatic pressure on chalcogenide threshold devices was investigated by Walsh et al (1970) who showed that the threshold voltage decreased with increasing pressure. Mathur et al (1972) have reported that the delay time decreased with increasing pressure and the threshold voltage decreased at the

rate of 1.2 mV per atmosphere. Arai et al (1973) have demonstrated that the conductivities of chalcogenide glasses were enhanced by the application of hydrostatic pressure. Thomas and Warren (1970) used the results of Walsh and Callela (1969) to show that there is a reasonable correlation between a thermal model of switching and the experimental results on the effect of hydrostatic pressure on the preswitching current-voltage characteristic. Reports on the effect of uniaxial pressure on conduction in amorphous chalcogenide glasses are very few. Callela et al (1970) reported that a threshold device could be put into its conducting on-state by the application of a sufficiently large uniaxial pressure even when the applied field was extremely small.

It was shown in Chapter Four that the application of uniaxial pressure on a thin film of STAG glass which had a small voltage bias across it, caused an increase in the current flowing through the device, i.e. the uniaxial pressure enhanced the conductance of the device. A sketch of figure 4.48 is shown in figure 5.2. Because of the difficulty associated with calculating the pressure the percentage increase in current was plotted against the load. Moreover, the pressure pattern under a hemispherical tip on a flat surface is very complex. The central region of the tip is expected to give different contributions to the conductance than the remainder. Referring first to curve A which represents the percentage increase in current in a virgin device with increasing load, the uniaxial pressure could be cycled up and down this curve with excellent repeatability. This indicates that no permanent change or damage occurred in the material. This was true provided the applied load was not greater than 100 grams as stated in Chapter Four. The increase in current can be explained in terms of (a) geometrical effects and (b) bulk effects. In the former case this may involve a small reduction in the film thickness, an increase in the effective contact area between the hemispherically shaped probe tip and the film surface. In case (b) bulk effects such as a possible decrease in the distance between hopping sites may be involved. In crystalline semiconductors the increase in current with increasing uniaxial pressure for a constant applied voltage bias

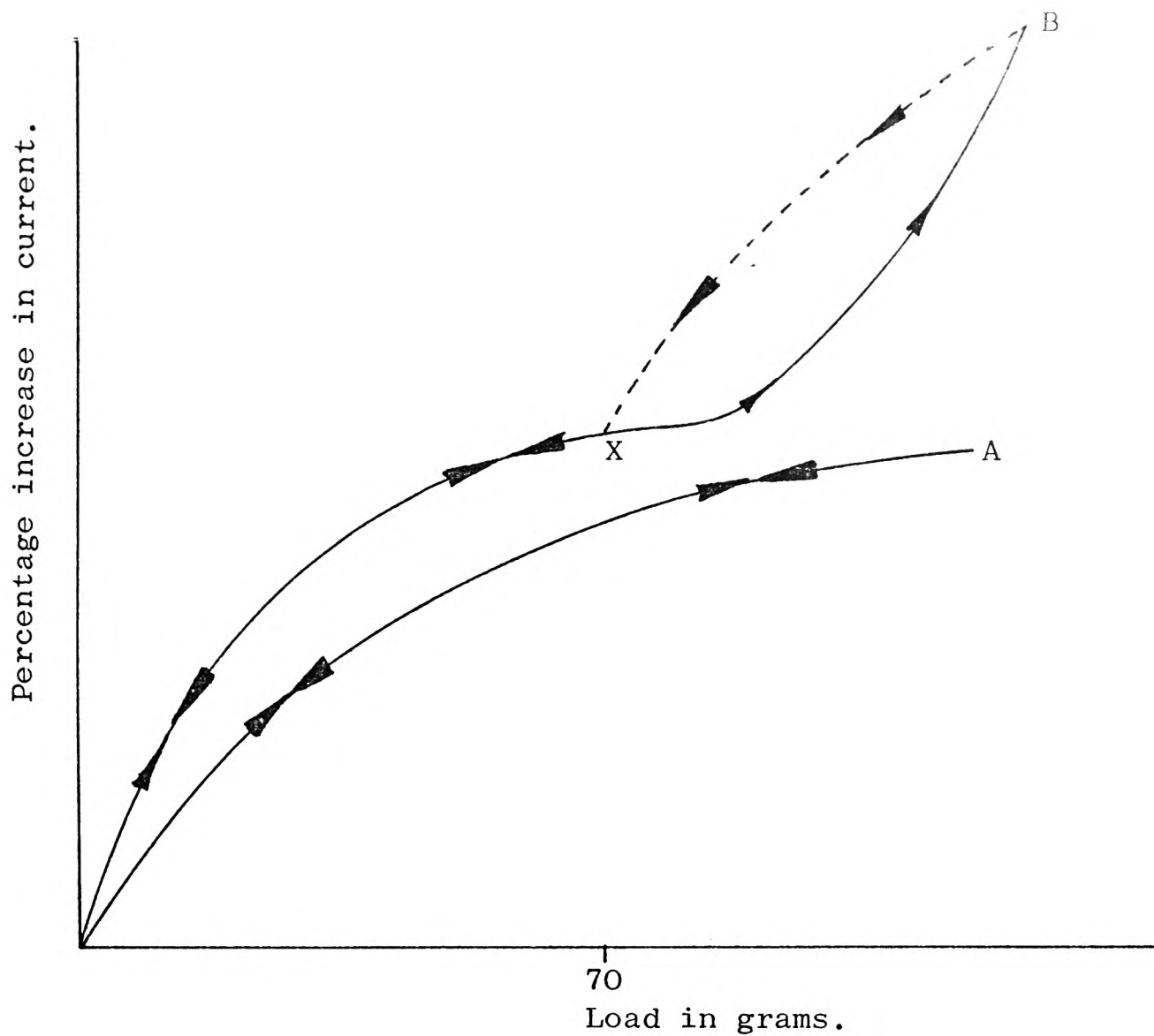


Figure 5.2.

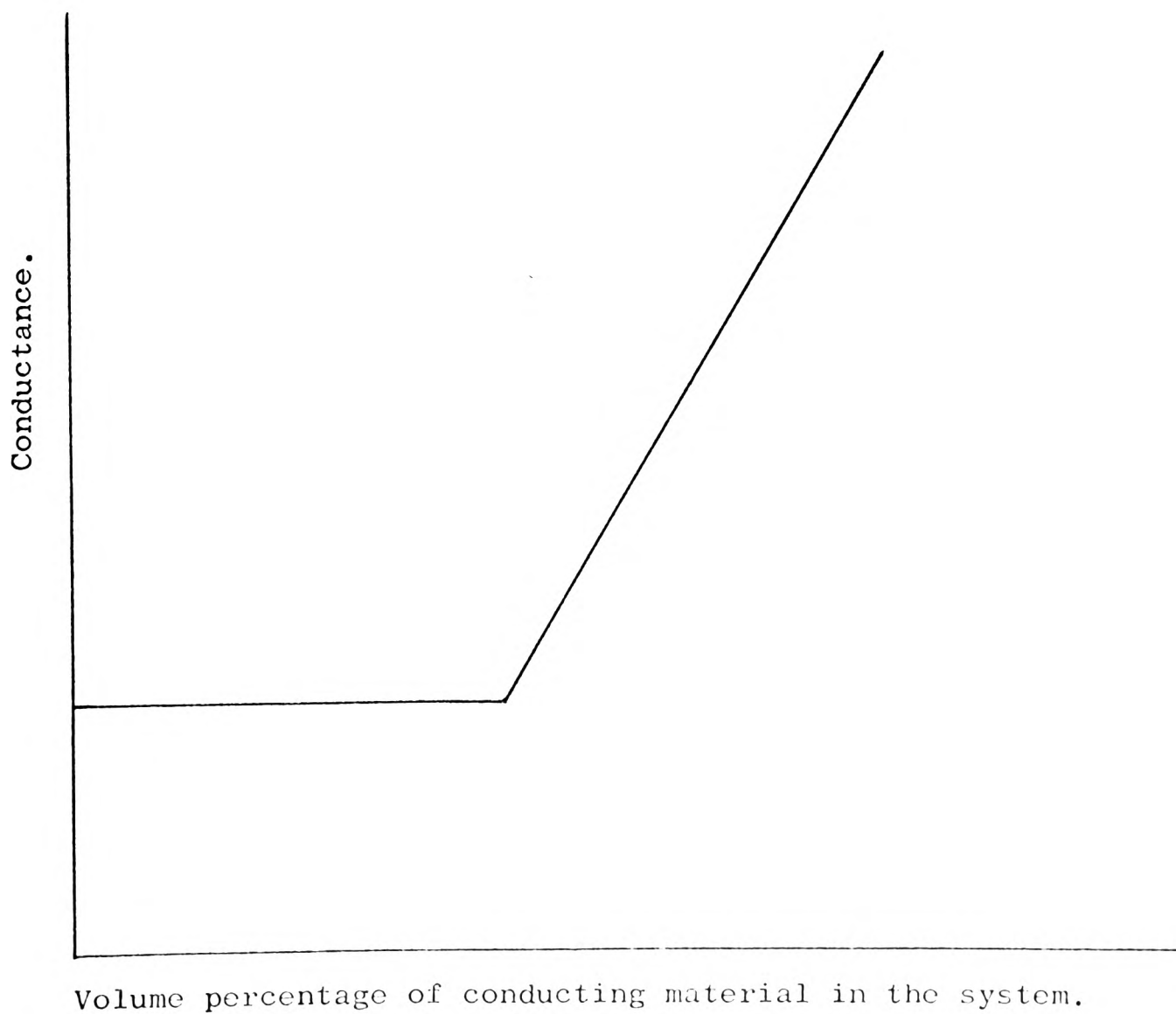


Figure 5.3

has been explained by Bulthuis (1966) and Williams (1967) to be due to a change in the semiconductor band-gap energy. The physical mechanisms operating for the formed device, curve B, may be similar to those for the virgin device for loads less than a critical load of about 70 grams. For greater loads, different mechanisms operate and the stress behaviour of the device material resembles that of an insulating matrix containing conducting particles. It has been shown by several workers (Milliaris et al, 1971, Aharoni, 1972, Bueche, 1972, Springett, 1973) that the conductivity of a system consisting of metallic particles in a non-conducting matrix remains unchanged until the ratio of the volume of the conducting particles to the volume of the non-conducting matrix approaches a critical value whereupon the conductivity increases sharply and abruptly. The behaviour is sketched in figure 5.3. Springett (1973) pointed out that this effect could also be achieved by the application of pressure to the system. It is suggested that the massive increase in current beyond point X in the formed device, curve B, is attributed to the presence of tellurium crystallites in the device material and these play the same role as the conducting particles in an insulating matrix. In a virgin device such crystallites are not present and this effect is not observed. The hysteresis effect observed in a formed device when the load is removed could be due to two crystallites, or more, coming into permanent contact with one another.

The drop in device off-state resistance and deterioration in device switching performance, see figures 4.49 - 4.50, with the application of uniaxial pressure could be explained in terms of stress-induced defects in the material which could act as nucleation centres for crystal growth. This may explain why the lifetime of a point-contact device with a top contact probe having a hemispherical tip of 1 mm diameter was only 2×10^3 operations, see table 4.1, compared to 10^7 operations, the lifetime of the device with probe of 3 mm diameter. The sizes of the top Mo probes were similar (a Mo rod 10 cm long with a diameter of 4 mm), but the pressure on the device film which had

the contact with the smaller tip diameter could have been several times greater than that on the device film with the larger diameter tip. The extent of the stress-induced crystallisation is expected to be greater in the former case and hence produce a shorter operational lifetime.

(c) Evidence of structural change from a.c. conductance measurements

The a.c. conductivity of chalcogenide glasses has been measured by several workers and over a large range of frequency the conductivity exhibits a dependence on frequency expressed by the empirical relationship

$$\sigma(\omega) \propto \omega^n$$

where ω is the angular frequency and the exponent has been found to have a value close to 0.8 (Rockstad, 1970). This power law dependence is often taken as evidence of a hopping conduction mechanism. The subject was reviewed by Jonscher (1972, 1973) who pointed out that this type of frequency dependence is found not only in amorphous materials, but also in ordered molecular solids. Attention was also drawn to the fact that the exponent n is not a constant for all systems but a function of temperature approaching unity at low temperature and decreasing to ~ 0.5 or less at higher temperatures. For $n \simeq 1$ the dielectric loss is almost frequency independent and this is exhibited in a wide range of dielectric materials. A value of $n = 2$ has also been reported (Owen and Robertson, 1970) and it was suggested that this ω^2 -dependence could be due to inhomogeneities in the material. Jonscher (1972) has pointed out that ω^2 results are suspect on the grounds of possible spurious effects of even very small series resistances and inductances, which may be due to the leads external to the device or may be caused by thin oxide layers on the electrodes giving rise to Maxwell-Wagner effects. A.c. conductance measurements in the present work were carried out on sandwich devices with Al electrodes and it is very likely that thin oxide layers were present at the electrodes. The slopes of the conductance vs. frequency curves in figure 4.47 for frequencies greater than 1 MHz are 1.4 and 1.1 for the 0.6 μm thick virgin and formed devices respectively and 1.2 and 0.6 for the 1.5 μm thick virgin and formed devices respectively. In each case the slope is greater for the virgin device.

The difference in slopes at high frequencies of conductance against frequency plots for virgin and formed devices implies different conduction mechanisms, which may be caused by the structural changes. The nature of these structural changes are not easy to determine from these measurements but from the discussions in the previous two sections in this chapter and the work of Bosnell et al (1973) and Ormondroyd et al (1974), who reported different activation energies for virgin and formed devices, these structural changes are considered to take the form of a filamentary region of different composition from its surrounding material and also containing conducting Te crystallites. These crystallites could also grow and group together to form Te clusters. On examination of the plot of conductance against frequency for formed and virgin devices in figure 4.47, we find that the two curves for the 0.6 μm thick device are widely separated at low frequencies, whereas the difference between the curves for the 1.5 μm thick device is much smaller and the two curves are almost parallel for frequencies less than 0.1 MHz. This difference in conductance between that of a formed device and virgin device for the 0.6 μm and 1.5 μm thick devices could be due to greater tellurium clustering in the thinner devices. If the degree of clustering is the same in both cases, it is bound to have a larger effect on the conductance of the thinner device because of greater proportional reduction in the thickness of the glassy material between the electrodes.

The $\tan \delta$ vs. frequency plots (figures 4.45 and 4.46) show no loss peaks for the frequency range considered. Such peaks are frequently observed in inhomogeneous systems (van Beek, 1967) over a very large frequency range -- $10 - 10^{15}$ Hz. For formed devices of 0.6 μm and 1.5 μm thickness $\tan \delta$'s have about the same magnitude up to a frequency of about 7 MHz, and from the relationship $\tan \delta \propto \sigma$ the conductivities must be about the same in formed devices. At higher frequencies differences in $\tan \delta$'s begin to appear and, again, this may be due to differences in the degree of clustering of the tellurium crystallites whose effect becomes greater at higher frequency (Volger, 1960, van Beek, 1967).

5.2 On-state current filament

It was shown in section 4.7 that the off-state resistance of

virgin devices with different electrode contact areas was inversely proportional to the contact area. Formed devices, on the other hand, had off-state resistances which were totally independent of the electrode contact areas. This result suggests that in a formed device there is a filament formed between the electrodes which has a higher conductivity than its surrounding material. This filament is a material filament and not a current filament (Coward, 1971), but its presence implies that current flow through a formed device - even off-state currents - is of a filamentary nature. The high temperature of this region in the on-state could be the cause of the structural and compositional changes that follow. Therefore, whichever mechanism initiates switching in virgin devices the current flow in the on-state is confined to a narrow hot filamentary region, and as far as the structural changes are concerned it is not important whether the current filament forms before or during switching in the device. Eckels et al (1974) have observed filament formation in a wide gap chalcogenide device before switching took place and suggested that in cases where the off-state current starts to flow into a filament before switching has occurred, the switching mechanism is predominantly thermal. It is interesting to notice that in formed devices containing a material filament the off-state current flow will always be filamentary and the current density, and local heat dissipation, are high.

The width of the material filament depends on the thermal boundary conditions in a complex manner (Kroll and Cohen, 1972). The point-contact devices tested in the present work are expected to have similar thermal boundary conditions, ^{to one another} and thus have material filaments of the same width when operated under similar electrical conditions. In figures 4.18 - 4.22 the off-state resistances of devices in the thickness range 0.5 - 2.5 μm are plotted against the corresponding number of operations. If the value of the off-state resistance after 10^3 operations is divided by the corresponding film thickness, a numerical value of $\sim 2 \text{ M}\Omega/\mu\text{m}$ is obtained and this suggests that the filament diameter in each device is more or less the same.

So far nothing has been said of the cooling effect of the electrode. It is a common belief among some researchers that the temperature of the filament near the electrodes is the lowest and the temperature in the device centre is highest. The opposite view has recently been expressed by Male and Thomas (1974) who proposed

a model which describes a thermally controlled on-state current filament. In this model, the on-state current flows through a hot filament which is severely constricted at the electrodes due to the large cooling effect of the electrode material. The voltage drop across the device in the on-state is mainly due to that across the two constricted regions of the filament. The constriction resistance may be written as,

$$R = \frac{l}{4\sigma_{sc}r}$$

(Holm, 1967) where σ_{sc} is the electrical conductivity of the chalcogenide glass within the constricted region, and r is the constriction radius. The current i through the constriction may be expressed as

$$i = 4 \sigma_{sc} r \frac{V}{2}$$

where V is the total voltage drop across the device.

In an analogous way, the heat flow into the electrode from each constriction is given by:

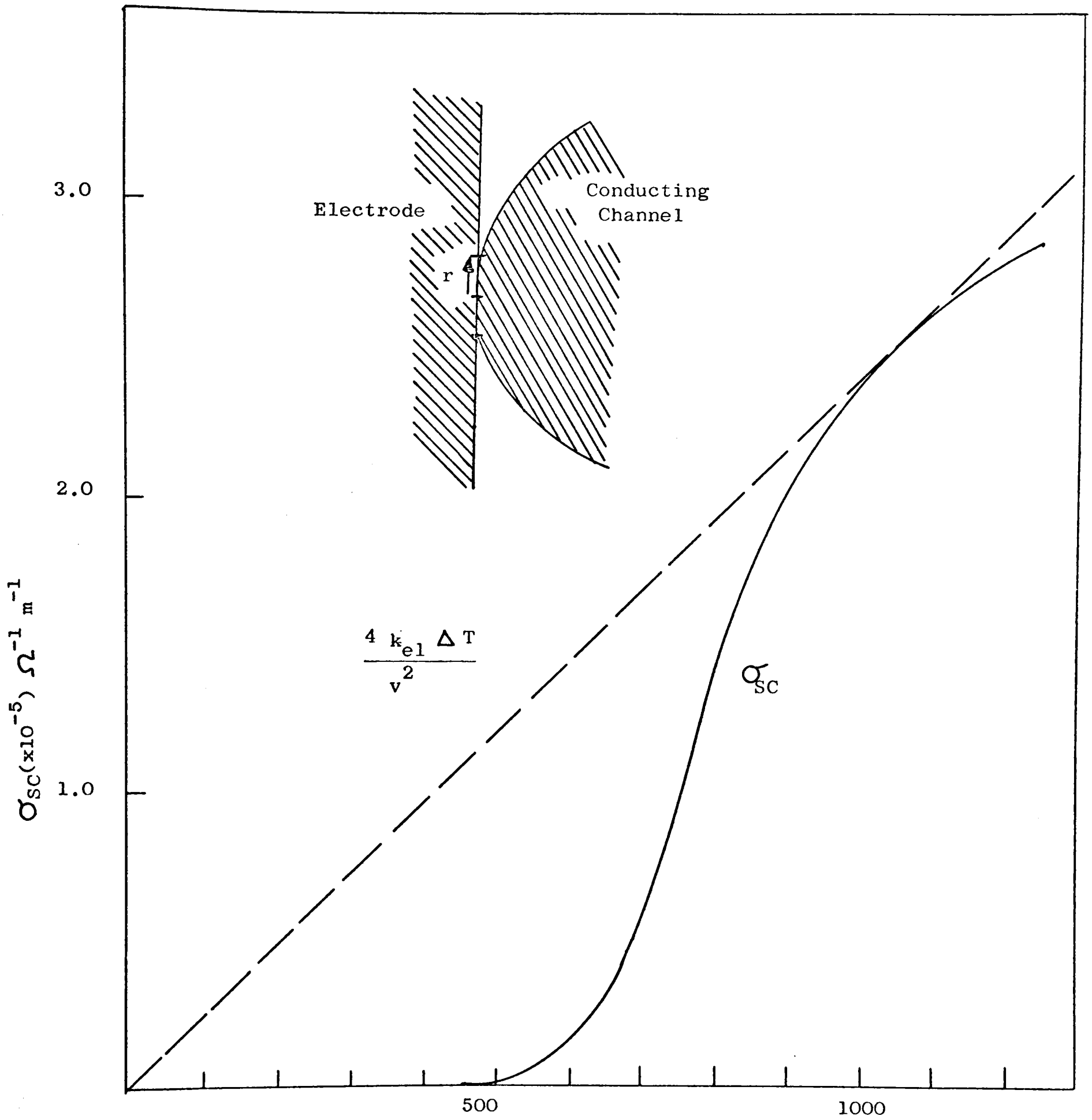
$$\frac{Vi}{2} = 4k_e r \Delta T$$

where k_e is the thermal conductivity of the electrode material and ΔT is the temperature difference between the constriction region and ambient. Combining these two relations gives:

$$V^2 \approx 4 k_e \Delta T / \sigma_{sc}.$$

The equation was solved graphically and the solution is shown in figure 5.4, where σ_{sc} is taken from the experimentally measured electrical conductivity of $As_{30}Te_{48}Ge_{10}Si_{12}$ up to 1500 K (Baker and Webb, 1974). A minimum (holding) voltage solution appears, corresponding to a constriction temperature close to 1400 K, where the ambient temperature is taken as 300 K. With an electrode material of thermal conductivity $10^2 \text{ W m}^{-1} \text{ K}^{-1}$, the minimum voltage is found to be 1.3 V. For slightly larger voltages two solutions exist, corresponding to lesser and greater temperatures respectively. These results are rather insensitive to the choice of ambient temperature.

In summary, the model of Male and Thomas (1974) yields two important predictions (a) the minimum holding voltage is proportional to the square root of the thermal conductivity of the electrode material and (b) the magnitude of the minimum holding voltage is rather insensitive to ambient temperature change. The temperature at the



TEMPERATURE RISE (ΔT) ABOVE AMBIENT (ASSUMED 300K)

Graphical solution of $v^2 = 4 k_{el} \Delta T / \sigma_{sc}$, where σ_{sc} is the electrical conductivity of $As_{30}Te_{48}Ge_{10}Si_{12}$. Inset shows schematically the interface of the conducting channel with the electrode (Male and Thomas, 1971).

Figure 5.4

centre of the on-state filament is much lower than the temperature at the constrictions and the work of Kroll and Cohen (1972) suggests a temperature of ~ 700 K at an on-state current of ~ 1 A.

Some of the experimental results obtained in this work give support to these predictions. First, it was shown in figures 4.54 and 4.55 that no measurable change in the minimum holding voltage occurred when the devices were operated at temperatures well below the ambient temperature. This was found when two different electrode materials, Mo and Au were used. Male and Thomas (1974) predicted that a change of 300 K in ambient temperature causes a change of only 0.2 V in the minimum holding voltage. Second, it can be seen from figure 5.5 that a theoretical plot of V_{mh} against $k_e^{\frac{1}{2}}$ (k_e is the thermal conductivity of the electrode material) gives a good fit to the experimental points. In the case of aluminium two points are shown, one which represents the minimum holding voltage of the device for the first 10^2 operations, see figure 4.43, and a second point which represents the minimum holding voltage for a larger number of operations. Aluminium is known to acquire a thin film of oxide layer (Holland, 1963) which could grow to a thickness of $\sim 100 \text{ \AA}$. Such an oxide layer could also be present on Al film prepared in poor vacuum, $\sim 10^{-5}$ torr, and it is suggested that such an oxide layer was present on the aluminium electrodes and fritting of oxide layers at the electrodes could have occurred after some switching operations. Morgan et al (1973) have shown that thin films of aluminium oxides sandwiched between two metallic electrodes breakdown at local high field associated with irregularities at the metal-oxide interface. Therefore for the first few switching operations the minimum holding voltage is high and not in good agreement with the theoretical plot of $V_{mh} \propto k_e^{\frac{1}{2}}$ but after fritting of the oxide layer the value of the minimum holding voltage dropped to a value which fits the theoretical prediction. For devices with Ti, Cr and Au electrodes the values of the minimum holding voltages are those which correspond to the stable part of the minimum holding voltage versus number of operations plots shown in figures 4.40 - 4.42. These figures show that in the case of devices with Au and Ti electrodes larger fluctuations in V_{mh} occurred after 10^3 switching operations. For devices with Cr electrodes the minimum holding voltage started to show fluctuations after only 10^2 operations and after about 2×10^4 operations its value increased to about 2.0 V. Possible reasons for these observations will be mentioned later in this section, but first it must

Minimum holding voltage vs. thermal conductivity of the electrode material. (Williams and Irfan, 1974).

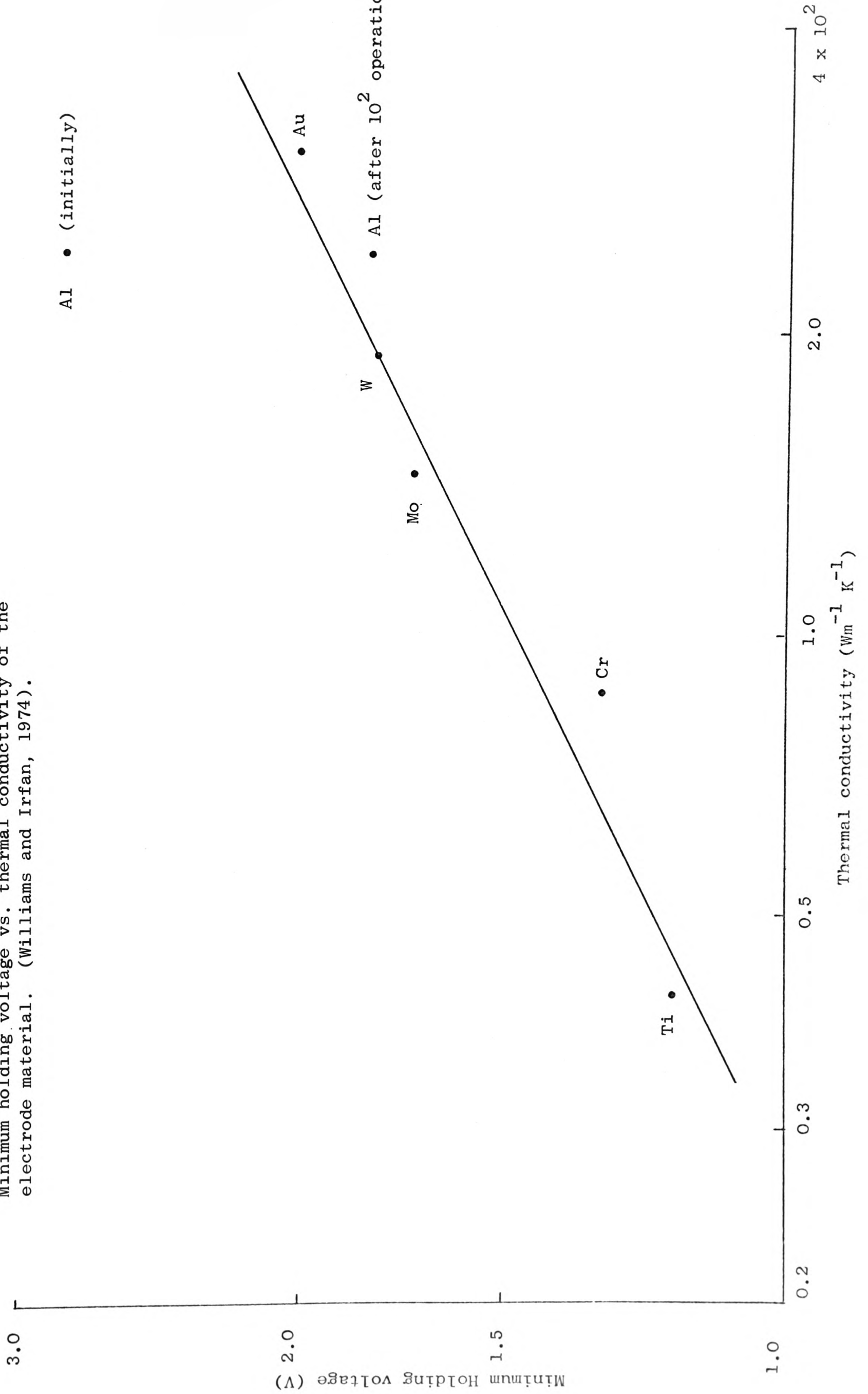


Figure 5.5

be pointed out that there are one or two experimental results which do not entirely support the prediction $V_{mh} \propto k_e^{\frac{1}{2}}$. The minimum holding voltage of a device with tellurium electrodes, see section 4.10, is about 0.9 V, whereas the predicted value of the minimum holding voltage obtained from a theoretical plot of $V_{mh} \propto k_e^{\frac{1}{2}}$ for an electrode material with thermal conductivity of $0.6 \text{ W m}^{-1}\text{K}^{-1}$, the value of k_e for Te (Cooper, 1971), is about 0.3 V, i.e. a much smaller voltage drop across the device in the on-state. In physical terms, a small voltage drop across the constriction would be expected from a material which has a thermal conductivity which is only ~ 50 times greater than that of STAG glass. With such a thermal conductivity the constriction of the filament would not be great at the electrodes and the constriction radius is much larger than for a constriction obtained when a material with a larger thermal conductivity is used, a larger constriction radius also implies a smaller amount of heat dissipation at the electrodes and a lower temperature. Therefore, the constriction temperature with Te electrodes could be considerably lower than that with Mo electrodes whose thermal conductivity is about three orders of magnitude greater than that of STAG glass.

The use of asymmetric electrode materials on chalcogenide switching devices was shown to give some polarity effects which were described in Chapter Four. It is interesting to examine the numerical values of the minimum holding voltages. For symmetric electrode devices using Mo and Cr, the minimum holding voltages were found to be 1.7 V and 1.2 V respectively. Therefore, the voltage drop at each constriction is 0.85 V for Mo and 0.60 V for Cr. Therefore, for an asymmetric electrode device with Mo/Cr electrodes one would expect a minimum holding voltage of 1.45 V. The experimental value is in fact, see 4.10, 1.5 V and 1.7 V for negative and positive pulses respectively. A value of 1.5 V is in good agreement with what one would expect if the minimum holding voltage is taken to be the sum of the voltage drop across the two filament constrictions. The polarity effect could be due to thermoelectric effects. According to Holm (1967), the absorption or rejection of Peltier heat can contribute significantly to the temperatures reached in intermetallic contacts. The direction of the flow of Peltier heat is dependent on the thermoelectric coefficients and direction of applied field and therefore with asymmetric electrodes the temperature at one particular electrode/glass film interface could change with a change in the direction of the applied field and give rise to polarity effects. Electronic effects are also feasible. Wey and Fritzsche (1972) studied the barrier photo-voltage, the light induced

change of the resistance as a function of wavelength, and the barrier capacitance of a chalcogenide alloy glass of composition $\text{Ge}_{16}\text{As}_{36}\text{Te}_{28}\text{S}_{21}$ sandwiched between semi-transparent electrodes. They found that Au, Al and Nichrome contacts produced a negative space charge and that Sb and Te produced a nearly neutral contact. The extent of the contribution of such space charges to polarity effects in the on-state is difficult to estimate but it must be pointed out that the value of the minimum holding voltage for a device with Cr/Te electrodes was unaffected by reversal of applied pulse polarity and had a value of ~ 0.85 V.

The discrepancy between the predicted and experimentally obtained values of the minimum holding voltages for devices with Te electrodes does not invalidate the relationship $V_{\text{mh}} \propto k_e^{\frac{1}{2}}$ but suggests that this simple relationship which holds extremely well for electrode materials whose thermal conductivities are two or three orders of magnitude greater than that of STAG glass, does not hold when the thermal conductivity of the electrode material is poor. In such a case the filament constrictions are very broad and the problem should not be treated as a constriction problem.

It is interesting to notice that the analysis of Kroll and Cohen (1972) predicted an on-state voltage drop of ~ 0.4 V for 1 μm - long axially uniform thermal on-state filament at a current of 10 mA. This is roughly the same value as is obtained from the relation $V_{\text{mh}} \propto k_e^{\frac{1}{2}}$ for a device with Te electrodes.

In the electronic model of switching (Mott, 1971) it is suggested that the holding voltage is slightly greater than the mobility gap, and electronic effects may have to be invoked to explain the discrepancy between the observed and predicted values of V_{mh} in devices with Te electrodes. Mott (1971) has also suggested that in cases where the holding voltage is much greater than one volt the possibility of a thermal on-state must be considered. It was also pointed out by Male (private communication) that when the electrode material is a relatively poor electrical conductor, constriction inside the electrode could occur and this gives rise to a higher voltage drop across the device in the on-state and this could explain the relatively high minimum holding voltage with Te electrodes.

Table 5.1 summarises measurements made on device lifetimes, multiple branching effects and holding voltages with various electrode materials.

Table 5.1

Electrode Material	No. of switching operations		Minimum holding Voltage (V)
	Device lifetime	Occurrence of multiple branching	
Mo	10^8	$>10^4$	1.7
Al	10^7	$>2 \times 10^3$	2.8 and 1.9
W	5×10^6	$>2 \times 10^3$	1.8
Au	10^6	$>2 \times 10^2$	2.0
Cr	10^6	<10	1.3
Ti	10^5	<10	1.2
Te	10^3	$>10^3$	0.9

The minimum holding voltage, and holding voltage at I_h , were found to vary with load resistor up to a resistance value of about $10 \text{ K}\Omega$ but remain stable for higher values, see figure 4.61. This seemed to be a departure from on-state current controlled conditions, but in fact this is nothing more than a loading effect. When a load resistor of 500Ω is used, its resistance is comparable to that of the on-state resistance of the device and such a loading effect occurs.

In all the devices operated at room temperature, the holding current was found to exhibit very large fluctuations and this makes it very difficult to draw any conclusions about its dependence on external circuit parameters. At temperatures well below room temperature I_h is stable with increasing number of operations, see figure 4.54. The holding current was also found to increase with decreasing ambient temperature (see figure 4.56) for temperatures below room temperature. Similar results were reported by Thomas et al (1972) for temperatures above room temperature. In both results the holding current extrapolates to zero at an ambient temperature of $\sim 450 - 500 \text{ K}$.

Referring to the analysis of Male and Thomas (1974), the heat flow into the electrode from each constriction is given by:

$$\frac{V_i}{2} = 4 k_e r \Delta T$$

where

$$T = T_c - T_a$$

and T_a is the ambient temperature and T_c is the constriction temperature.

The holding current is given by

$$I_h = \frac{\delta k_e r}{V_h} (T_c - T_a). \quad 5.4$$

If the expression $\frac{\delta k_e r}{V_h}$ is assumed to be constant then

$$I_h \propto \Delta T.$$

Therefore the holding current can be expressed as a linear function of ambient temperature and this is observed experimentally. At $I_h = 0$, $T_c = T_a$ and therefore the temperature of the constriction at zero holding current is about 450 K (the point at which the straight line in figure 4.56 meets the temperature axis. Finally if the temperature of the constriction is about 1400 K and the thermal conductivity of Mo is $\sim 1.7 \times 10^2 \text{ W m}^{-1} \text{ K}^{-1}$, then at a holding current of 0.75 mA (at $T_a = 0 \text{ K}$, see figure 4.56) and a holding voltage of 1.7 V these numerical values substituted into equation 5.4 give the constriction radius $r = 10^{-9} \text{ m}$. This radius is much smaller than expected. However in the above derivation the following assumptions have been made:

- (a) k_e is independent of temperature and this is not always the case. k_e for Au changes very little with change in ambient temperature over a very large range. For W, k_e is several times greater at a few degrees K than say, at room temperature. No data on variation of k_e for Mo could be found.
- (b) r is taken to be constant. However it was found that the slope of the on-state characteristics above V_{mh} , i.e. the positive differential resistance, was greater when the device was operated at room temperature than at liquid nitrogen temperature. So the on-state has a smaller differential resistance at low ambient temperature. At such temperatures, in order to maintain filament stability, more current is required and this increases the temperature at the constriction. This alters the thermal balance at the electrode-glass interface and to restore the original state an increase in constriction radius can be envisaged to give an effective decrease in differential resistance.

In figure 4.56 I_h extrapolates to zero at about 450 K. This is also about the same temperature at which the threshold voltage V_{th} has been reported to be extrapolate to zero (Thomas et al,

1972) i.e. switching ceases at such a temperature.

Discussion of multiple branching in the on-state will be deferred until the next section and the effect of electrode materials on the lifetime of the devices will be dealt with first. It can be seen that, in general, the lifetimes of the devices were shorter for those with electrode materials having a poor thermal conductivity or known to diffuse easily into the amorphous chalcogenide alloy. The properties of the interface layer between an electrode and the amorphous alloy are governed by the diffusion and alloying processes which are most likely to take place while the device is in the on-state. It was mentioned in Chapter Four that the off-state resistances of the virgin devices with different electrode materials were about the same, $\sim 25 M\Omega$. In formed devices, the off-state resistances dropped and this drop, say after 10^3 operations, was greatest for devices with Ti, Au and Cr electrodes. The off-state resistance of these devices after 10^3 operations was in the range of $0.3 - 2 M\Omega$, whereas the off-state resistance for devices which had the longer lifetimes and more stable characteristics - those with Al, W and Mo electrodes - was in the range of $5 - 7 M\Omega$. In the previous section the drop in off-state resistance was explained as due to phase separation and partial crystallization of the glass alloy. The extent of this phase separation could be largely influenced by the electrode materials through the processes of alloying or chemical reactions and diffusion into the glass. It was shown by several workers (Bunton et al, 1971, Vezzoli et al, 1972) that Mo, and possibly W, does not easily react or diffuse into the glass. Al is a soft metal and expected to react or diffuse easily into the glass. Nielsen (1973), however, has shown that the reaction between Al and Se is self-limiting and the selenide layer was only about 40 \AA thick. Moreover, Al is known to be glass forming (Bosnell et al, 1972a) with chalcogenide materials. Therefore, the relatively stable characteristics of devices with Mo, W, Al electrodes can be explained as being due to the lack of reactivity between the electrodes and the glass alloy. Au is known to diffuse easily into chalcogenide glasses (Freeman et al, 1969). It also reacts with chalcogenide glass to form AuTe (Cooper, 1971). Ti is also known to react with tellurium to produce a conducting compound known as titanium telluride (Cooper, 1971). The fluctuations in the minimum holding voltages, see figures 4.40 and 4.42, in devices with Au and Ti electrodes may be due to these reactions

which alter the thermal nature of the interfaces between the glass alloy and the material. In both cases it was found that the minimum holding voltage underwent large changes after 10^3 operations, and if one accepts that the voltage drop across the device in the on-state is mainly that across the filament constrictions, then these changes in V_{mh} are expected in view of the possibility that the thermal conductivities of Au and Ti are very different from those of their tellurides.

The lifetime of devices with Cr electrodes was found to be relatively low compared to that of devices with Mo. Devices with Cr electrodes have been reported to perform well (Dargan et al, 1974), but the properties of thin films of Cr are very sensitive to the conditions under which they are deposited. When deposited in poor vacuum conditions, say a pressure greater than 10^{-5} torr, which is the case in this work, Cr films contain chemisorbed oxygen (Walter, 1965). On switching, oxygen may react with Cr to produce an oxide. Oxygen could also react with the glass alloy and contribute to the deterioration in the device lifetime.

An important physical property that should be considered when choosing an electrode material is the melting point. Male and Thomas (1974) estimated the temperature of the filament constriction to be about 1400 K, depending on k_e of the material. Therefore materials with low melting points would melt and alloy with the chalcogenide glass. Refractory electrodes have higher melting points and, in addition to their lack of reactivity with chalcogenide glass, could be another reason for the relatively long operational lifetime of these devices.

Electromigration is also a process that could operate in these switching devices and cause device failure (Shaw et al, 1973). Male and Thomas (1974) argued that the vapour pressure of some glasses is sufficiently high to cause device destruction.

The short lifetime of a device with Te electrodes must be due to the poor heat dissipation after switch off. As mentioned earlier Te has a poor thermal conductivity and the device could be described as being well lagged. Such a condition is similar to a situation where the device is heated to a high temperature and then quenched very slowly allowing the crystallites in the filament to grow and interconnect.

5.3. The multiply branched on-state

As stated in Chapter Four, the phenomenon of multiple branching in the on-state was only observed in formed devices of all geometries. The on-state characteristics of virgin devices were always single traces. The occurrence of multiple branching is attributed to the structural changes that accompany switching of a virgin device. This structural change was described in section 5.1 to take place in two stages (a) a rapid process representing the phase separation of the material into two or more phases which are possibly both glassy, and (b) the formation and growth of Te crystallites in the filamentary region of the devices. The multiply branched on-state is interpreted in terms of the sequential formation of current channels between conducting Te crystallites, or clusters of crystallites, in a filamentary region between the electrodes.

It was also observed that multiple branching did not always appear as soon as the device was formed and in some cases - depending on the electrode material used and the pulsing conditions - it did not appear until after 10^5 switching operations. It is suggested that the Te crystallites are small immediately after the device has been formed. Nucleation centres, however, may be present and induce the growth of Te crystallites which increase in size as the number of switching operations increases and eventually produce Te crystallites which could be $0.2 \mu\text{m}$ long as reported by Bosnell and Thomas (1973).

Figure 5.6 is a sketch of the photograph given in figure 4.10 and figure 5.7 is a schematic of a well formed switching device having relatively large Te crystallites - or separate clusters of crystallites - between the electrodes. The attainment of the on-state represented by the trace E in figure 5.6 is described by first a "breakdown process" between electrode 1 and crystallite 1. In figure 5.6 this breakdown is the transition from A to B which occurs along the load line. This breakdown is then followed by a current channel forming between crystallites 1 and 2 and giving rise to a second current branch to the left of the first branch BC. A second current channel could develop between crystallite 2 and another crystallite to the left of it and giving rise to another current branch in the on-state and so on until finally a channel is formed between a crystallite and electrode 2. In figure 5.6 this final current channel formation

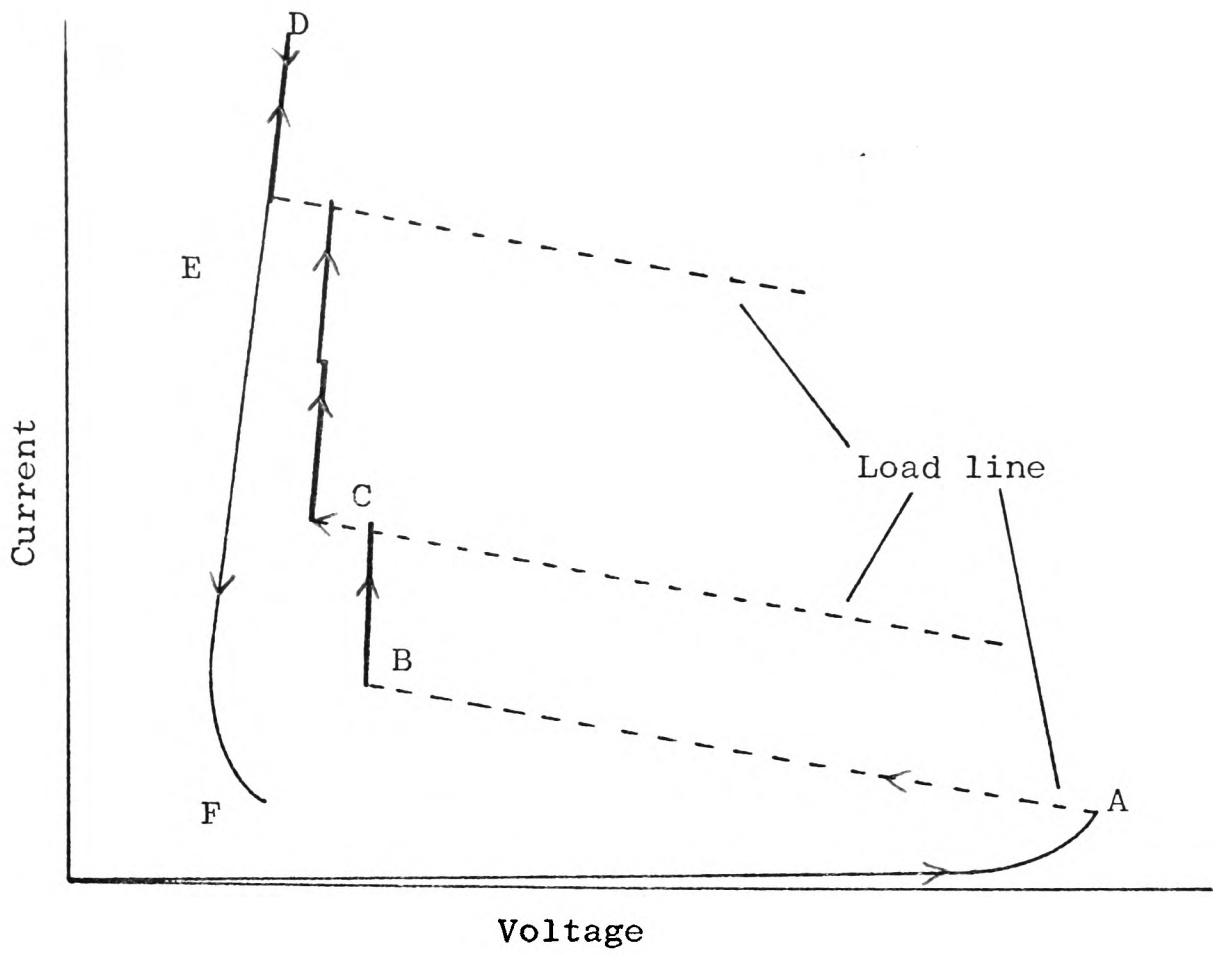


Figure 5.6

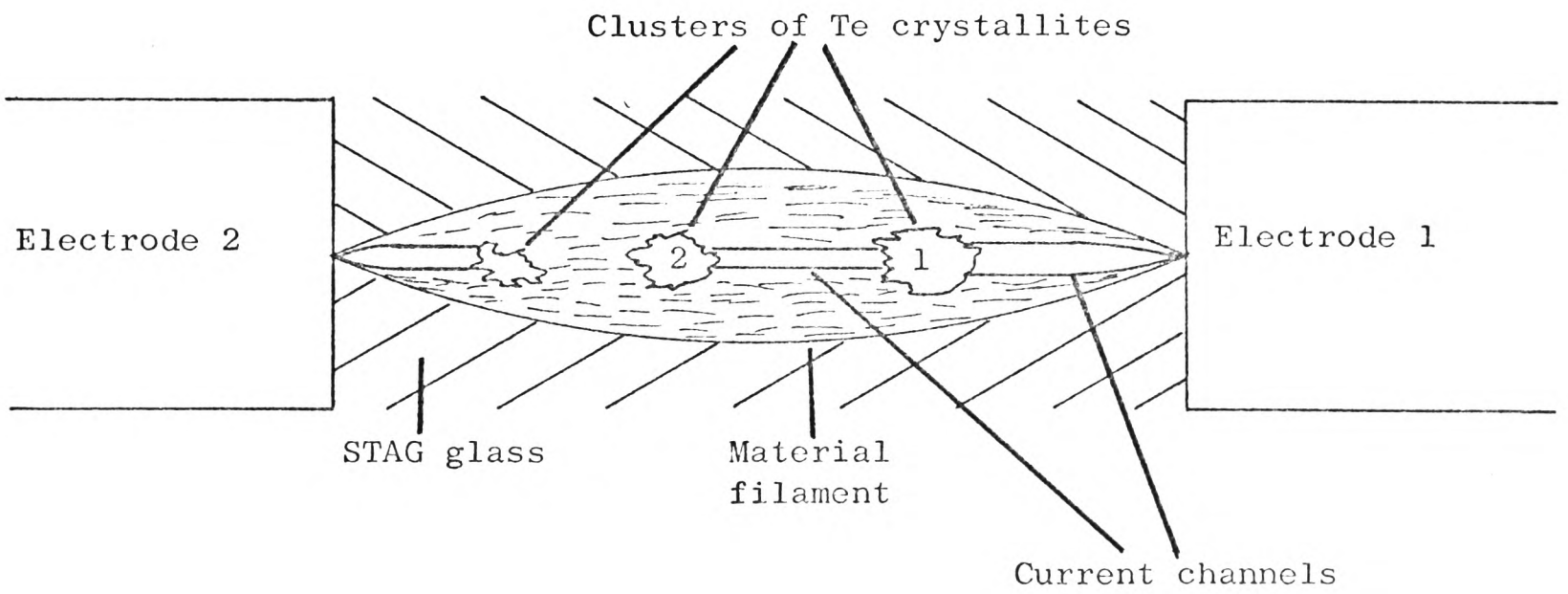


Figure 5.7

corresponds to the current branch terminating at D.

It must be emphasized that (a) the current branches in the multiply branched on-state always appeared to the right of the on-state trace E. In an extremely few cases and only in devices nearing the end of their lifetime very small branches did appear to the left of trace E, but these seemed very unstable and disappeared after a few number of operations only, (b) it was always possible to adjust the applied pulse height so that one current branch only, say BC in figure 5.6 would appear and further current branches, to the left of BC, could be made to appear by increasing the height of the applied pulse, and (c) the on-state trace E is in the same position as the single on-state trace of an unformed device which does not exhibit a multiply-branched on-state characteristic.

The nature of the breakdown process between A and B could be thermal or electronic, although in the previous two sections in this chapter and also in Chapter Four, some evidence has been presented for thermal switching in well-formed devices.

In deciding upon possible mechanisms responsible for the occurrence of multiple branching in the on-state the following mechanisms have been examined:

(i) Growth of dendrites from Te crystallites

Interconnection between two Te crystallites could take place as a result of dendrites growing from the surface of the two crystallites and interconnecting to form a current path as postulated by Thomas et al (1972). In such a situation the second current branch, the one to the left of BC in figure 5.6, would be due to interconnection taking place between the two crystallites which are closest to one another and not necessarily in the order envisaged in figure 5.7. Other branches occur when more crystallites interconnect. There are, however, some experimental observations which are not in favour of such an argument. First, it was observed that in some cases the nature of the branched characteristics, say two branches in the on-state, remained stable for $10^2 - 10^3$ switching operations. This would imply that interconnectivity between all crystallites is broken after switch off and the initial condition concerning the sizes and distances

between any two crystallites is immediately restored. Such a situation is difficult to envisage and it is unlikely that the initial situation could be restored in the short time between the switching pulses. Secondly, it was suggested (Bosnell and Thomas, 1972) that to satisfy the Gibb's Criterion for thermodynamic stability of the tips of the dendrites their volume free energy (ΔF_v) must be less than the surface energy (γ) (Brophy, Rose and Wulff, 1966). Therefore, unless the radius at overlap of two dendrites is greater than the critical radius ($r^* = -\frac{3\gamma}{\Delta F_v}$) for stability, interconnectivity is broken as the embryonic tips of the dendrites redissolve. This would lead to a continuous appearance and disappearance of current branches in the on-state. Again, this is incompatible with the observation of a very stable branched pattern for a large number of operations.

It is also difficult to explain the change in an on-state pattern that occurs when the pulse is reversed in terms of interconnection between crystallites due to dendritic growth.

In conclusion, growth of dendrites and interconnection of Te crystallites could take part in the formation of current paths and on-state current branches, but it is unlikely to be the dominant mechanism. Dendritic growth is very likely to play a significant part in forming current paths or channels in a device nearing the end of its operation lifetime and having a large number of crystallites or clusters which are very close to one another.

(ii) Sequential thermal breakdown between Te crystallites

This is a very likely mechanism. After the initial and possibly thermal breakdown between point A and B the current through the device is much greater than the off-state current and considerable local heating occurs in the filament. At point C the current is relatively larger and "thermal switching" causes a transition along the load line to the next on-state branch to

the left of BC and so on until point D is reached at the top of the current-branch and represents thermal breakdown between a Te crystallite and electrode 2, figure 5.7.

It must be emphasised that between points B and C there is hardly any increase in voltage or field while the current, also power, increases and produces an increase in the temperature of the material. Furthermore, the time interval between B and C when a switching pulse of 1.3 ms is applied is a fraction of a ms. Therefore, it is very reasonable to suggest that thermal breakdown is the origin of the current channels between the Te crystallites.

Constrictions similar to those that occur at the metal electrodes of the device are not likely to be present at the ends of a current channel between two Te crystallites. The thermal conductivity of Te is rather poor compared to that of metals like Mo as pointed out in the previous section, and if the device temperature at the centre is about 700 K (Kroll and Cohen, 1972) the thermal conductivity of the Te crystallites at such an "ambient" temperature is only $\sim 2.8 \text{ W m}^{-1} \text{ K}^{-1}$. Besides if such constrictions exist the voltage drop across a device in the on-state is the total sum of the voltage drop across the individual constrictions and this would lead to holding voltages greater than those across a device without a multiply branched on-state characteristic. This is not observed and the minimum holding voltage of an unformed or virgin device is normally similar to that of a well formed device.

A thermal current channel formed between two Te clusters would have two "hot spots" at the current channel/Te interfaces. The size of a Te crystallite must be large enough to sustain the hot spot and this is necessary for the stability of the current channel.

It is worth pointing out that the electrical conductivity of Te at 700 K is about two orders of magnitude greater than that of STAG glass at this temperature (Baker and Webb, 1974).

(iii) Localized avalanche breakdown in the region between two Te clusters

Owing to the presence of the Te crystallites in a medium of different electrical conductivity the field across the device is non-uniform and a situation could arise where the field between

two Te clusters is large enough to initiate electron avalanching and avalanche breakdown in that region. In dielectrics and industrial insulators, the phenomenon of internal discharges and "treeing" caused by inclusions and cavities is well known (Kreuger, 1964, Anderson, 1964, Klein, 1971).

In reverse-biased p-n junctions avalanche breakdown is localized and occurs at small regions across the junction (Chynoweth and Mackay, 1956). These regions are described as microplasmas. The reverse-bias current-voltage characteristics of some diodes exhibiting microplasma breakdown show slope discontinuities in the breakdown region (Kressel, 1967). The origin of these microplasmas are thought to be high field spots associated with inhomogeneities such as crystalline defects, inclusions and non-uniformities in impurity concentrations. The microplasmas emit light due to electron-hole recombination and the presence of light spots was reported by Chynoweth et al, (1956). Nesvadba (1973) observed light emission in bulk chalcogenide gap switches during switching to the on-state and it is possible that this light emission was associated with microplasma breakdown. Emission of light in the on-state has been recently reported by Vezzoli et al, (1974).

Although localized avalanche breakdown cannot be ruled out as a breakdown mechanism giving rise to current branches, it does not always stand up to critical inspection. Consider the breakdown or transition from branch BC to the next branch. As mentioned earlier there is very little increase in field between points B and C, yet the temperature at point C is greater due to more power dissipation in the material. As the breakdown field for avalanche breakdown increases with temperature, a more favourable condition for localized breakdown would be at point B and not C.

(iv) Formation of multiple filaments

An alternative and totally different approach to the interpretation of a multiply branched on-state is in terms of multiple filament formation. When a large electrode contact is used and the device is switched to ^{the} on-state with a wide pulse it is conceivable that more than one current filament could be

formed at various intervals during the on-state thus giving rise to a multiply branched on-state characteristic (I am indebted to Dr. A.H. Lettington for this suggestion). Such a formation of parallel multiple filaments has been observed in amorphous boron thin films and the phenomenon was described as multiple switching (Feldman and Moorjani, 1970). Barnett et al (1968) have also reported multiple filament formation in a crystalline semiconductor. In chalcogenide switching devices, however, there has been no reports of multiple filament formation. Also, multiple filament formation cannot give a feasible explanation to the change in the form of a branched on-state pattern with pulse polarity.

Armitage et al (1971) have observed that in a narrow, 1 μm , gap chalcogenide device switching operations occurred across several parallel breakdown paths or filaments; but this was caused by the electrodes being damaged at the ends of one filament with the result that there was a reduction in the magnitude of the applied field and the following switching operation took place between two points on the electrodes where the field was larger. Moreover, only one filament, and not several, were observed during a single switching operation. Burton et al (1972) have suggested that in a memory device, switching occurs through a series of low voltage memory switches distributed throughout the switching filament.

All the mechanisms discussed above involve a sequential formation of current channels. Alternatively one might envisage an "additive" mode of formation of current branches in which a current channel is formed between the device electrodes and then as the current through the filament increases the filament diameter broadens and comes into contact with inhomogeneities. The high temperature of the filament could cause distortion of field between such inhomogeneities and possible localized breakdowns which could give rise to current branches.

The effects of pulse polarity on the form of a multiply branched on-state can be explained in terms of absorption or rejection of Peltier heat at an electrode/glass interface. This can significantly affect the temperature at one interface in such a way that the conditions for breakdown between one electrode and a neighbouring Te cluster in the device material are more favourable than those at the other electrode. If the Te clusters are not uniformly distributed between the electrodes reversal of pulse polarity could give rise to different on-state branched

characteristics. In Chapter Four it was reported that if the pulse polarity was reversed and then the number of switching operations was limited to a few operations then on a further pulse reversal the original on-state was restored. If, however, the number of operations with the reversed pulse were large the original branched pattern was not restored. This effect can be explained by assuming that in a prolonged period of switching the sizes and shapes of the Te clusters could alter so that when the pulse was restored to its original polarity the branched pattern changes.

Referring to table 5.1 it can be seen that there is a correlation between the occurrence of multiple branching and device lifetime. Devices which had relatively short lifetimes exhibited multiple branching after a small number of operations and vice-versa. In the previous section it was argued that electrode materials which react with or diffuse into the glass or have poor thermal conductivities such as Te could encourage phase separation and crystallization of the glass alloy. Therefore, when such materials are used as electrodes, Te crystallites are expected to appear at very early stages of the device operational lifetime and multiple branching would also appear after a small number of operations as was observed. It was also observed that when a device was operated at low temperature, say liquid nitrogen temperature, the occurrence of multiple branching was delayed in comparison with its occurrence at room temperature. At low temperatures, and immediately after switch off, the cooling or quenching of the hot filament is faster than that at room temperature and electrode diffusion into the glass could also be inhibited or slowed down. Under such a condition the growth of Te crystallites could be slow and this may explain the delayed occurrence of multiple branching in the on-state.

Referring to table 4.3, the occurrence of multiple branching was not seriously affected by the width of the applied pulse for the pulse-width range examined, 0.3 - 1.3 ms, or the pulse repetition rate; although it would appear that multiple branching did appear after a fewer number of operations when the widest pulse, 1.3 ms, was used. It is suggested that if a device is left in the on-state for a relatively long period, electromigration, phase separation and growth of Te crystallites is likely to be enhanced. Thomas et al (1972) have shown that the recovery time of the off-state resistance is larger for longer on-time. Therefore, multiple branching appears after fewer operations when the widest pulse - 1.3 ms - is used.

Whichever mechanism is responsible for the formation of current

channels between the Te crystallites, it is thought that the current flows in a narrow channel between the crystallites. "Hot spots" are established at the channel/Te crystallite interfaces which cause local melting of the crystallites and possible re-dissolving. A prolonged on-time would therefore cause some considerable amount of melting and contribute towards a longer operational lifetime of the device. In fact, it was observed that, table 4.3, the lifetime of a device was the longest when the widest pulse - 1.3 ms - was used to switch the device.

Finally, the addition of some thallium to STAG glass delayed the appearance of multiple branching in the on-state. It is suggested that thallium is very likely to phase separate with tellurium and if the temperature of the centre of the device in the on-state is about 700 K this is much higher than the melting point of thallium. Tellurium is known to be glass forming with thallium (Cooper, 1971) and it is possible that the two elements alloy together to form a glass and thus inhibit the growth of Te crystallites.

CHAPTER SIX

Summary and Conclusions

A detailed investigation of the on-state characteristic has shown that electrical switching of chalcogenide glass thin film devices causes structural changes in the material. These structural changes have been explained in terms of two separate processes, a phase separation and then a growth of Te crystallites. Forming, which was observed in all tested devices of any geometry, is caused by phase separation. Measurements, carried out on virgin and formed devices, of (a) off-state resistance as a function of number of switching operations (b) off-state resistance as a function of ^{the} electrode contact area (c) a-c conductance and (d) the effect of uniaxial pressure on the current flowing through a device at constant voltage bias, have all confirmed that structural changes have taken place in a formed device. Some of these measurements also suggested that switching in well-formed devices is controlled by a thermal mechanism.

The photographically recorded current-voltage characteristics of an unformed device showed that in general the on-state current-voltage characteristic is continuous for increasing current. After forming, the on-state characteristic often consisted of two or more branches, separated by voltage steps - followed by a final on-state trace for decreasing current which was similar to the on-state trace of the unformed device. The current branches occurred in sequence and prior to the attainment of the final on-state. This has been explained in terms of sequential formation of current channels between the electrodes and Te clusters and between the Te clusters themselves. The origin of the current channels could be one or a combination of several mechanisms, namely (a) growth and interconnection of dendrites from the surfaces of Te crystallites, (b) thermal breakdown in the regions between either an electrode and a Te cluster or between two Te clusters, (c) localized avalanche breakdown in the region between Te cluster/electrode and a Te cluster. Mechanism (b) is thought to be the dominant one. The interpretation of multiple branching in terms of multiple filaments lacks experimental support.

The minimum holding voltage was found to be insensitive to changes in the ambient temperature. The minimum holding voltage was also found to be proportional to the square root of the thermal conductivity of the electrode material. This result is in agreement with a thermal constriction model where the minimum holding voltage is the sum of the

voltage drops across two filament constrictions at the electrode/glass interfaces. For a material with poor thermal conductivity such as Te this prediction did not hold and the observed minimum holding voltage was about three times greater than the calculated value. It is suggested that when the electrode material has a thermal or electrical conductivity comparable with that of the glass at high temperature, the concept of a simple filament constriction at the electrodes is no longer adequate and more general treatment of the problem is required.

The holding current was found to exhibit very large fluctuations with number of switching operations at room temperature. At low temperatures, however, the holding current was stable and linearly proportional to the ambient temperature. From a plot of holding current against ambient temperature, the holding current was found to extrapolate to zero at a temperature similar to that at which a plot of threshold voltage against temperature also extrapolates to zero as reported elsewhere. On the basis of the constriction model the radius of filament constriction was also calculated using experimentally obtained values of holding current and voltage and assuming filament constriction temperature of 1400 K, was found to be about 10^{-9} m.

Some weak polarity effects were observed and these took the form of a small change in the minimum holding voltage when asymmetrical electrodes were used, and a change in the structure of the multiply-branched on-state pattern. In both cases these polarity effects are attributed to thermoelectric effects.

The lifetime of a switching device was found to depend largely on the choice of electrode material. Devices with electrode materials which either reacted chemically, diffused or had poor thermal conductivity had relatively short operational lifetimes. The longest operational lifetime was obtained with Mo electrodes which is in agreement with the reports of other workers. There was also a correlation between the occurrence of multiple branching and lifetime. In devices with short operational lifetimes branching occurred at much earlier stages compared to devices with long operational lifetime. This correlation follows from the explanation that both effects are associated with structural changes and crystallization of the switching material which occurs faster in short-lived devices.

The addition of some thallium to STAG glass delayed the occurrence of multiple branching in the on-state and this was interpreted in terms

of the thallium having an inhibitive effect on the growth of Te crystallites.

Finally, the lifetime of a device exhibiting multiple branching in the on-state was longer when the device was switched with the widest pulse-of the pulse-width range examined 0.3 - 1.3 ms - and this is explained as being due to local melting of the Te crystallites by "hot spots" at the ends of a current channel between two crystallite clusters.

In conclusion, the observations of multiple branching may be explained in terms of a model in which the on-state properties are those of a hot filament from which crystallites of a highly conducting phase may be precipitated out of the glass. The occurrence of multiple branching in a threshold switch is influenced by the mode of pulsing, the number of switching operations, ambient temperature, glass composition and the electrode materials.

APPENDIX

Future Work

The phenomena of switching in chalcogenide glasses could only be fully explained when the physics of amorphous solids is better understood and when the three dimensional heat balance equation is solved mathematically. In both cases, the problems are formidable. Furthermore, structural changes and the ensuing inhomogeneities make the problem more complex.

STAG glass is relatively stable but not exactly suitable for the fabrication of fully stable devices. More stable devices have to be made from more stable materials and one which does not undergo phase separation or partial crystallization. Work of this kind is being carried out at RRE where sulphur is being added to STAG glass at the expense of some of the tellurium content in STAG glass. Such a material is reported to have a higher T_g and produce more stable devices. But it must be realized that the addition of S may also bring its own problems, particularly if it phase separates, as S is known to react with most elements, including C, at high temperatures and this makes the choice of suitable electrode material a more difficult task. The addition of thallium to STAG delays the occurrence of multiple branching in the on-state and this effect should be further investigated. The design of particular switching materials should involve a detailed study of the alloy phase diagram and other physical phenomena such as T_g . It is also worth bearing in mind that in the case of STAG glass DTA alone does not show crystallization peaks, whereas Te crystallites are detected in formed devices. Therefore, it may be useful to investigate crystal growth in the material under the influence of an applied electric field prior to its use in switching devices.

A wider range of electrode materials, particularly those with poor thermal conductivity, should be used to investigate the effect of electrode thermal conductivity on the minimum holding voltage. Possible thermo-electric effects at an electrode/glass interface is also another area where quantitative study is required.

The phenomenon of multiple branching in the on-state is new and offers ample scope of further research. As stated earlier, multiple branching did not always appear as soon as the device was formed.

Systematic electron microscopy examination should be carried out on two formed devices one with multiply branched on-state and the second without, to examine the sizes of the Te crystallites in each case. If the interpretation of multiple branching in terms of sequential formation of current channels between Te clusters is valid, one would expect the crystallites to be much larger in the formed devices with multiply branched on-state.

The effect of Te crystallites on the on-state characteristic could be usefully assessed by introducing a small quantity of very fine Te powder particles into a small tube containing switching semiconducting liquid. If the powder particles cause multiple branching in the on-state to occur, then agitation of the tube should cause a change in the powder particles clustering and also a change in the form of the on-state branched pattern.

Finally, careful electron-microscopic examination of the top contact of a point-contact device should give a good idea about the extent of electrode damage, if local melting of the electrode occurs at the filament constriction and the temperature of the filament constrictions. Such experiments should be repeated on electrode materials with different thermal conductivities and melting points. The examination of the top contact should be carried out after the very first switching operation and the on-state current should be restricted by means of a suitable load resistor to a value just above the holding current. Due to the very small size of the constriction radius the top contact must have an extremely fine surface finish and should be examined prior to its use as device top contact.

REFERENCES

- Adler D 1970 Electronics 28, 61.
Adler D 1972 Amorphous Semiconductors (London: Butterworth)
Adler D 1973 J.Vac.Sci.Technol. 10, 728.
Adler D et al 1967 Phys.Rev. 155, 826.
Aharoni SM 1972 J.Appl.Phys. 43, 2463.
Allison J 1972 Reported at IEE discussion meeting on Amorphous Switches
Altunyan SA et al 1971 Sov.Phys.Semicond. 5, 427.
Anderson JC 1964 Dielectrics (London: Chapman & Hall Ltd. and Science Paperbacks)
Anderson PW 1958 Phys.Rev. 109, 1492.
Andreeva LP et al 1971 Fiz.Tverdogo Tela 13, 2122.
Arai K et al 1973 J.Non-Cryst.Sol. 13, 131.
Armitage D et al 1971 Can.J.Phys. 49, 1662.
Baker FH and Webb LM 1974 J.Mater.Sci. 9, 1128.
Balberg I 1970 Appl.Phys.Lett. 16, 491.
Barnett AM and Jensen HA 1968 Appl.Phys.Lett. 12, 341.
Beam WR and Takahashi T 1964 Rev.Sci.Instrum. 35, 1623.
Beckman M et al 1962 Proc.Electron Components Conf. 53.
Boer KW 1970(a) Sol.Stat.Comm. 8, 1329.
Boer KW 1970(b) Phys.Stat.Solidi 1, K21.
Boer KW and Ovshinsky SR 1970 J.Appl.Phys. 41, 2675.
Boer KW, Bohler G and Ovshinsky SR 1970 J.Non-Cryst.Sol. 4, 573.
Bosnell JR et al 1972(a) J.Phys.D: Appl.Phys. 5, L29.
Bosnell JR et al 1972(b) Solid St.Electron 15, 1261.
Bosnell JR and Savage JA 1972 J.Mater.Sci. 7, 1235.
Bosnell JR et al 1973 Phil.Mag. 27, 665.
Brophy JH, Rose RM and Wulff J 1966 Thermodynamics of Structure (J. Wiley & Sons) P 100.
Buckley and Holmberg 1972, see Fritzsche 1974.
Bueche F 1972 J.Appl.Phys. 43, 4837.
Bultuis K 1966 Philips Res.Repts. 21, 85.
Bunton GV 1972 Thin Solid Films 14, 249.
Bunton GV et al 1971 J.Non-Cryst.Sol. 6, 251
Bunton GV and Quilliam RM 1973 IEEE Trans. on Electron Devices, ED.20, 140.
Burton P and Brander RW 1969 Int.J.Electron. 27, 517.
Burton P et al 1972 reported at the Solid State Device Conf. Inst. of Physics.
Calella P et al 1970 Technical Report 3935, Picatinny Arsenal, Dover, New Jersey, USA.
Chittick RC et al 1969 J.Electrochem.Soc. 116, 77.
Chopra KL 1965 J.Appl.Phys. 36, 184.
Chopra KL 1969 Thin Film Phenomena, McGraw Hill Book Co., New York.
Chen HS and Miller CE 1970 Rev.Sci.Instr. 41, 1237.
Chen HS and Wang TT 1970 Phys.Stat.Sol. a, 2, 79.
Chynoweth AG and Mackay K 1956 Phys.Rev. 102, 369.
Cohen MH 1970 J.Non-Cryst. Sol. 4, 391.
Cohen MH, Fritzsche H and Ovshinsky SR 1969 Phys.Rev.Lett. 22, 1065.
Collins FM 1970 J.Non-Cryst.Sol. 2, 469.
Cooper WC 1971 Tellurium (Van Nostrand Reinhold Company).
Coward LA 1971 J.Non-Cryst.Sol. 6, 107.
Croitoru N et al 1970(a) Phys.Stat.Sol. 3, 1047.
Croitoru N et al 1970(b) J.Non-Cryst.Sol. 4, 493.
Croitoru N et al 1973 J.Non-Cryst.Sol. 11, 377.

- Dalton J 1963 J.Chem.Ed. 40, 99.
- Dargan C et al 1974 Thin Solid Films, 23, 343.
- Deis DW et al 1970 J.Non-Cryst.Sol. 2, 141.
- Drake CF et al 1969 Phys.Stat.Sol. 32, 193.
- Drake CF et al 1972 Report at IEE Discussion Meeting on Amorphous Semiconductor Switches, 8 May.
- Duwez P et al 1963 Trans.Met.Soc. AIME 227, 362.
- Eaton DL 1964 J.Am.Ceram. 47, 553.
- Eckels DE et al 1974 J.Appl.Phys. 45, 3005.
- Ellis SG 1967 J.Appl.Phys. 38, 2906.
- Fagen E^A and Fritzsche H 1970 J.Non-Cryst.Sol. 12, 170.
- Feldman C and Moorjani K 1970 Thin Solid Films, 5, R₁ - R₄.
- Fourier JBJ Théorie Analytique de la Chaleur, Gauthier-Villars, Paris 1842.
- Freeman et al 1969 Thin Solid Films 3, 367.
- Fritzsche H 1969 IBM J.Res.Develop. 515.
- Fritzsche H 1971 Proc.Low Materials Conf. (London: Taylor and Francis) 279.
- Fritzsche H and Ovshinsky SR 1970(a) J.Non-Cryst. Sol. 2, 393.
- Fritzsche H and Ovshinsky SR 1970(b) J.Non-Cryst. Sol. 4, 464.
- Glang R et al 1967 Thin Solid Films 1, 151.
- Gorgunova NA and Kolomiets BT 1956 Zh.Tekh.Fiz. 25, 984.
- Haberland DR and Kehrer HP 1970 Sol.Stat.Electron 13, 451.
- Hall JE 1970 J.Non-Cryst.Sol. 2, 125.
- Hargreaves RL et al 1974 J.Phys.D.Appl.Phys. 7, 85.
- Henisch HK 1969 Sci.American 221, 30.
- Henisch HK et al 1970 J.Non-Cryst.Sol. 538.
- Henisch HK et al 1971 Sol.Stat.Electron 14, 765.
- Henisch HK and Vendura Jr GJ 1971 Appl.Phys.Lett. 19, 363.
- Heywang W and Haberland DR 1970 Sol.Stat.Electron. 13, 1077.
- Hindley NK 1970(a) J.Non-Cryst.Sol. 5, 17.
- Hindley NK 1970(b) J.Non-Cryst.Sol. 5, 31.
- Hilton AR 1970 J. Non-Cryst.Sol. 2, 28.
- Holland L 1963 Vacuum Deposition of Thin Films (Chapman and Hall).
- Holm 1967 Electric Contacts, 4th ed. (Springer, Berlin, Germany).
- Holmstrom R 1969 IEEE Proc. 57, 1451.
- Hughes AJ 1973 Reported at Chelsea College Meeting, December 19.
- Hughes AJ et al 1974 J.Non-Cryst.Sol. in press.
- Iida M and Hamada A 1971 Jap.J.Appl.Phys. 10, 224.
- Iizima S et al 1970 Sol.Stat.Comm. 8, 153.
- Ioffe AF and Regel AR 1960 Prog.Semicond.4, 237.
- Jones GO 1956 Glass (London: Methuen Monograph).
- Jonscher AK 1972 J.Non-Cryst.Sol. 8-10, 293.
- Jonscher AK 1973 Electronic and Structural Properties of Amorphous Semiconductors (London: Academic Press) p.329.
- Kaplan T and Adler D 1971 Appl.Phys.Lett. 19, 418.
- Kaplan T and Adler D 1972 J.Non-Cryst.Sol. 8-10, 538.
- Kashchiev D 1972 Phil.Mag. 25, 459.
- Klein N 1969 Advan.Electron and Electron.Phys. 25, 309.
- Kolomiets BT and Nazarov 1960 Sov.Phys.Sol.Stat. 2, 195.
- Kolomiets BT et al 1969 Sov.Phys.Semicond. 3, 267.
- Kressel H 1967 RCA Rev. 28, 175.
- Kreuger FH 1964 Discharge Detection in High Voltage Equipment (London A Heywood Book)
- Kroll DM and Cohen MH 1972 J.Non-Cryst.Sol. 8-10, 544.
- Lebedev AA 1926 Rev.Opt.Theor.Inst. 5, 4.

- Lee SH Henisch HK and Burgess WD 1972 J.Non-Cryst.Sol. 8-10, 422.
- Lee SH and Henisch HK 1973 Sol.Stat.Electron 16, 155.
- Lucas I 1971 J.Non-Cryst.Sol. 6, 136.
- MAB 67, see section on materials characterization in Fundamentals of Amorphous Semiconductors (Washington DC, National Acad. of Science 1972)
- Mackenzie RC (ed) 1970 Differential Thermal Analysis (London: Academic Press).
- Main C 1974 Reported at a Switching Meeting, Warwick University, March.
- Maissel LI and Glang R 1970 Handbook of Thin Film Technology (New York: McGraw Hill).
- Male JC 1970 Electron.Lett. 6, 91.
- Mathis DC 1969 Phys.Rev.Lett. 22, 936.
- Male JC and Thomas DL 1974 J.Non-Cryst.Sol. 13, 409.
- Mathur LF and Arntz FO 1972 J.Non-Cryst.Sol. 8-10, 445.
- Malliaris A et al 1971 J.Appl.Phys. 42, 614.
- Milne WI and Anderson JC 1973 J.Phys.D:Appl.Phys. 6, 2115.
- Morgan DV et al 1973 Thin Solid Films 15, 123.
- Mott NF 1967 Advances in Physics 16, 49.
- Mott NF 1969 Contemp.Phys. 10, 125.
- Mott NF Phil.Mag. 24, 911.
- Mott NF and Davies EA 1971 Electronic Processes in Non-Crystalline Material (London: Oxford University Press).
- Neale RG 1970 J.Non-Cryst.Sol. 2, 558.
- Nesvadbøda 1973 PhD Thesis, University of Warwick.
- Nielsen P 1973 Thin Solid Films, 15, 309.
- Nowick AS 1969 Comments on Solid State Physics 2, 155.
- O'Dwyer JJ 1964, The Theory of Dielectric Breakdown in Solids, Oxford.
- O'Dwyer JJ 1969 J.Electrochem.Soc. 116, 239.
- Onodera N et al 1969 J.Non-Cryst.Sol. 1, 331.
- Ormondroyd RF et al 1974 J.Non-Cryst.Sol. 15, 310.
- Ovshinsky SR 1958 and 1960 see J.Non-Cryst.Sol. 2, 100.
- Ovshinsky SR 1968 Phys.Rev.Lett. 21, 1450.
- Ovshinsky SR 1970 J.Non-Cryst.Sol. 2, 99.
- Ovshinsky SR and Fritzsche H 1973 IEEE Trans.on Elect.Devices ED-20, 91.
- Owen AE 1970 Contemp.Phys. 11, 227.
- Owen AE 1973 Electronic and Structural Properties of Amorphous Semiconductors (London: Academic Press) p. 161.
- Owen AE and Robertson JM 1970 J.Non-Cryst.Sol. 2, 40.
- Owen AE and Robertson JM 1973 IEEE Trans.on Electron.Devices ED-20, 105.
- Pamplin BR 1970 Contemp.Phys. 11, 1.
- Parsons JR Phil.Mag.12, 1159.
- Pearson AD 1964 Modern Aspects of the Vitreous State (London: Butterworth and Co.) Vo. 3, p.29.
- Pearson AD 1969 IBM J.Res.Develop. 510.
- Pearson AD 1970 J.Non-Cryst.Sol. 2, 1.
- Pearson AD et al 1962 J.Electrochem.Soc. 109, 243C.
- Pearson AD et al 1963 Advances in Glass Technology (New York: Plenum Press) p.357. Also Advances in Glass Technology, part 2, (Plenum Press) p.145.
- Pearson AD and Miller CE 1969 Appl.Phys.Lett. 14, 280.
- Pinto R 1971 Thin Solid Films 7, 391.
- Pinto R et al 1971 Appl.Phys.Lett. 19, 221.
- Popescu C and Croitoru N 1972 J.Non-Cryst.Sol. 8-10, 531.
- Poraj-Kosic EA 1959 Glast.Ber. 32, 450.

- Primak W 1958 Phys.Rev. 110, 1240.
- Puckle OS 1955 Time Bases (London: Chapman and Hall Ltd.) p.360.
- Rawson H 1967 Inorganic glass-forming systems (London: Academic Press).
- Richards JL 1966 The Use of Thin Films in Physical Investigations, ed: J.C. Anderson, Academic Press.
- Ridley BK 1963 Proc.Phys.Soc. London, 82, 954.
- Robertson JM et al 1972 J.Non-Cryst.Sol. 8-10, 439.
- Roy R 1970 J.Non-Cryst.Sol. 3, 33.
- Roy R et al 1969 Sol.Stat.Comm. 7, 1467.
- Sarjeant PT and Roy R 1968 Mat.Res.Bull. 3, 265.
- Savage JA 1971 J.Mater.Sci. 6, 964.
- Schmidlin FW 1970 Phys.Rev.B1, 158B.
- Secrist DR and Mackenzie JD 1964 Modern Aspects of the Vitreous State (London: Butterworth and Co.) Vo. 3, p.149.
- Sideris G 1966 Electronics 39, 19, 191.
- Siegel BM and Harris L 1948 J.Appl.Phys. 19; 739.
- Shanefield D 1970(a) J.Non-Cryst.Sol. 2, 210.
- Shanefield D 1970(b) J.Non-Cryst.Sol. 2, 382.
- Shanks RR 1970 J.Non-Cryst.Sol. 2, 504.
- Shaw MP et al 1973 Appl.Phys.Lett. 22, 114.
- Sheng WW and Westgate CR 1971 Sol.Stat.Comm. 9, 387.
- Shuocker D 1971 Appl.Phys.Lett. 19, 7.
- Shuocker D 1972 J.Non-Cryst.Sol. 8-10, 427.
- Shuocker D 1973 J.Appl.Phys. 44, 310.
- Springett BE 1973 J.Appl.Phys. 44, 2925.
- Stevens JM 1971 J.Non-Cryst.Sol. 6, 307.
- Stocker HJ 1969 Appl.Phys.Lett. 15, 55.
- Stocker HJ 1970 J.Non-Cryst.Sol. 2, 371.
- Stocker HJ et al 1970 J.Non-Cryst.Sol. 4, 523.
- Stratton R 1961 Progr.Dielect. 3, 235.
- Tauc J et al 1970 J.Non-Cryst.Sol. 4, 279.
- Thomas CB 1972 Reported at Inst.Phys.Meeting, Imperial College, 18th March.
- Thomas CR et al 1972 Phil.Mag. 26, 617.
- Thomas DL and Male JC 1972 J.Non-Cryst.Sol. 8-10, 522.
- Thomas DL and Warren AC 1970 Electron Lett. 6, 62.
- Turnbull D 1969 Comtemp.Phys. 10, 473.
- Van Beek LKH 1967 Progr.Dielect. 7, 69.
- Van Marum M 1799 Ann.Phys. (Leipzig) 1, 68.
- Van Roosbroeck W 1972 Phys.Rev.Lett. 28, 1120.
- De Vekey RC and Majundar AJ 1970 Nature, 225, 172.
- Vezzoli GC and Pratt IH 1972 Thin Solid Films 15, 161.
- Vezzoli GC et al 1974 J.Appl.Phys. 45, 4534.
- Vogel R and Walsh PJ Appl.Phys.Lett. 14, 216.
- Volgler J 1960 Progr.Semicond. 4, 205.
- Walsh PJ and Callela P 1969 "Pressure effects on thin films of amorphous chalcogenide semiconductors" Abstract in Bull.Amer. Phys.Soc. 14, 115 and in information report ESLIR 451.
- Walsh PJ et al 1969 Phys.Rev. 178, 1274.
- Walsh PJ et al 1970 J.Non-Cryst.Sol. 2, 107.
- Warren AC 1969(a) Electron.Lett. 5, 461.
- Warren AC 1969(b) Electron.Lett. 5, 609.
- Warren AC 1973 IEEE Trans. on Electron Devices, ED-20, 123.
- Warren AC and Male JC 1970 Electron.Lett. 6, 567.
- Weimer et al 1964 see chapter on mask fabrication in Handbook of Thin Film Technology 1970 ed: Maissel and Glang, McGraw Hill.
- Wey HY and Fritzsche H 1972 J.Non-Cryst. 8-10, 336.

Williams JL 1967 Brit.J.Appl.Phys. 18, 1699.
Williams JL and Irfan AY 1974 J.Phys.D. 7, 1287.
Wittels M et al 1954 Phys.Rev. 93, 1117.
Wolter AR 1965 J.Appl.Phys. 36, 2377.
Zachariasen WH 1932 J.Am.Chem.Soc. 54, 3841.
Ziman JM 1960 Electrons and Phonons (Oxford University Press).

THAMES POLYTECHNIC LIBRARY